# Seeing the Light:
# Synthesis of Luminescent Rhodacyclopentadienes and Investigations of their Optical Properties and Catalytic Activity

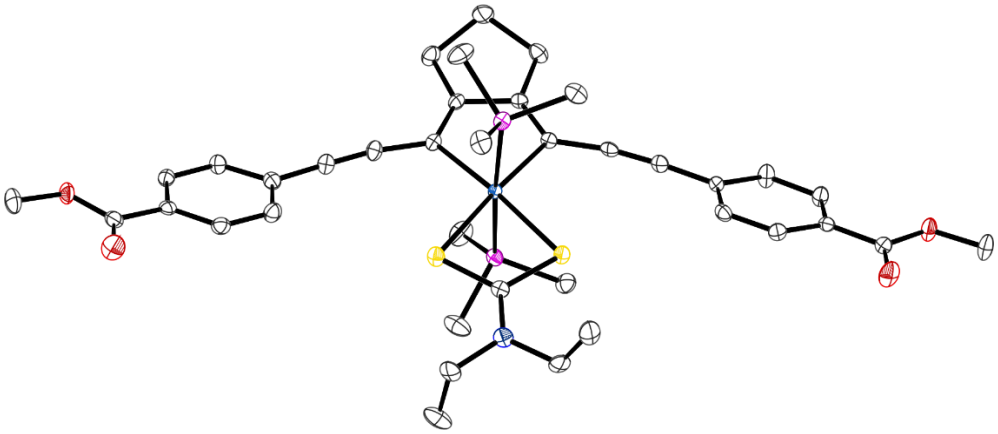

Dissertation zur Erlangung des naturwissenschaftlichen Doktorgrades

der Julius-Maximilians-Universität Würzburg

Nicola Schwenk

aus Kirchheim unter Teck

Würzburg, 2017

Eingereicht bei der Fakultät für Chemie und Pharmazie am:
_____

Gutachter der schriftlichen Arbeit
1. Gutachter: Prof. Dr. Todd B. Marder
2. Gutachter: Prof. Dr. Ulrich Schatzschneider

Prüfer des öffentlichen Promotionskolloquiums
1. Prüfer: Prof. Dr. Todd B. Marder
2. Prüfer: Prof. Dr. Ulrich Schatzschneider
3. Prüfer:_____

Datum des öffentlichen Promotionskolloquiums
am:_____

Doktorurkunde ausgehändigt
am:_____

***Start by doing what is necessary, then what is possible, and suddenly you are doing the impossible.***

Francis of Assisi

*Für meine Familie*

Die Experimente zur vorliegenden Arbeit wurden in der Zeit von Oktober 2012 bis März 2017 am Institut für Anorganische Chemie der Julius-Maximilians-Universität Würzburg unter der Aufsicht von Prof. Dr. Todd B. Marder durchgeführt.

# Content

# Abstract

Luminescent organotransition metal complexes are of much current interest. As the large spin-orbit coupling of 2nd and 3rd row transition metals usually leads to rapid intersystem crossing from $S_1$ to $T_1$, which enables phosphorescence, there is a special interest in using triplet-emitting materials in organic or organometallic light emitting diodes (OLEDs). Marder *et al.* have found that, reductive coupling of both *para*-R-substituted diarylbutadiynes and diaryldodecatetraynes on $Rh(PMe_3)_4X$ leads to quantitative yields of bis(arylethynyl)-rhodacyclopentadienes with complete regiospecificity (R = $BMes_2$, H, Me, OMe, SMe, $CF_3$, CN, $CO_2Me$, $NMe_2$, $NO_2$, C≡C-TMS and X = -C≡C-TMS, -C≡C-$C_6H_4$-4-$NMe_2$, -C≡C-C≡C-$C_6H_4$-4-$NPh_2$, Me, Cl).[47,49] Unexpectedly, these compounds show intense fluorescence rather than phosphorescence ($\phi_f$ = 0.33-0.69, $\tau$ = 1.2-3.0 ns). The substituent R has a significant influence on the photophysical properties, as absorption and emission are both bathochromically shifted compared to R = H, especially for R = $\pi$-acceptor.

To clarify the mechanism of the formation of the rhodacyclopentadienes, and to investigate further their unique photophysical properties, a series of novel, luminescent rhodacyclopentadienes with dithiocarbamate as a bidentate ligand at the rhodium centre has been synthesised and characterised (R = $NO_2$, $CO_2Me$, Me, $NMe_2$, SMe, Ar = $C_6F_4$-4-OMe). The rhodacyclopentadienes have been formed *via* reductive coupling of diaryl undecatetraynes with [Rh($\kappa^2$-*S*,*S*`-$S_2CNEt_2$)($PMe_3$)$_2$]. The structures of a series of such compounds were solved by single crystal X-ray diffraction and are discussed in this work. The compounds were fully characterised *via* NMR, UV/Vis and photoluminescence spectroscopy as well as by elemental analysis, high-resolution mass spectrometry (HRMS) and X-ray diffraction.
When heating the reactions, another isomer is formed to a certain extent. The so-called dibenzorhodacyclopentadienes already appeared during earlier studies of Marder *et al.*, when acetylacetonate (acac) was employed as the bidentate ligand at the Rh-centre. They are probably formed *via* a [4+2] cycloaddition reaction and C-H activation, followed by a $\beta$-H shift.

Use of the perfluorinated phenyl moiety Ar = $C_6F_4$-4-OMe provided a total new insight into the mechanism of formation of the rhodacyclopentadiene isomers and other reactions. Besides the formation of the expected rhodacyclopentadiene, a bimetallic compound was generated, isolated and characterised *via* X-ray crystallography and NMR spectroscopy, elemental analysis and high resolution mass spectrometry.

For further comparison, analogous reactions with [Rh($\kappa^2$-*S*,*S*`-$S_2CNEt_2$)($PPh_3$)$_2$] and a variety of diaryl undecatetraynes (R = $NO_2$ $CO_2Me$, Me, $NMe_2$, SMe, Ar = $C_6F_4$-4-OMe) were carried out. They also yield the expected rhodacyclopentadienes, but quickly react with a second or even third equivalent of the tetraynes to form, catalytically, alkyne cyclotrimerisation products, namely substituted benzene derivatives (dimers and trimers), which are highly luminescent. The rhodacyclopentadienes (R = $NO_2$, $CO_2Me$, Me, SMe, Ar = $C_6F_4$-4-OMe) are stable and were isolated. The structures of a series of these compounds were obtained *via* single crystal X-ray crystallography and the compounds were fully characterised *via* NMR, UV/Vis and photoluminescence spectroscopy as well as by elemental analysis and HRMS.

Another attempt to clarify the mechanism of formation of the rhodacyclopentadienes involved reacting a variety of diaryl 1,3-butadiynes (R = $CO_2Me$, Me, $NMe_2$, naphthyl) with [Rh($\kappa^2$-*S*,*S*`-$S_2CNEt_2$)($PMe_3$)$_2$]. The reactions stop at an intermediate step, yielding a 1:1 *trans* $\pi$-complex, confirmed by single crystal X-ray diffraction and NMR spectroscopy. Only after several weeks, or under forcing conditions ($\mu$w / 80 °C, 75 h), the formation of another major product occurs, having bound a second diaryl 1,3-butadiyne. Based on earlier results of Murata, the product is identified as an unusual [3+2] cycloaddition product, $\sigma$-bound to the rhodium centre.

# Chapter One

# Homo- and Cross-Coupling Reactions

# 1. Chapter One: Homo- and Cross-Coupling Reactions

## 1.1 Introduction

### 1.1.1 The Sonogashira Cross-Coupling Reaction

Probably the most commonly used reaction to couple terminal alkynes with vinyl or aryl halides is the C≡C cross-coupling reaction catalysed by palladium, initially reported by the groups of Cassar and Heck.[1] Shortly thereafter, Sonogashira and co-workers showed that this kind of cross-coupling could be improved by the addition of copper iodide to the reaction mixture.[2] This famous reaction, known as the Sonogashira cross-coupling reaction, works in the presence of catalytic amounts of bis(triphenylphosphine)palladium dichloride and triethylamine (and other amines) as base under very mild conditions. The following reaction (Scheme 1) gives a typical example:

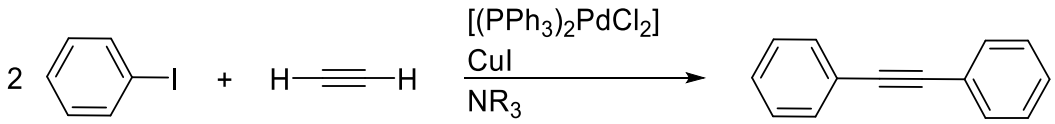


**Scheme 1** General cross-coupling reaction *via* Sonogashira.[2]

To a mixture of iodobenzene and a catalytic amount of bis(triphenylphosphine)palladium dichloride in degassed diethylamine under a nitrogen atmosphere copper iodide was added. During six hours, a slow current of acetylene was passed through the flask at room temperature. When the base was removed under reduced pressure, the residue was charged with water and the mixture was extracted with benzene. After concentrating the mixture, the benzene-extract was filtered through a short alumina column to remove the catalyst. The solvent was removed under reduced pressure and the crude diphenylacetylene was obtained. For purification, the diphenylacetylene was recrystallised from ethanol to give the product in 85% yield. In general, the reactions can be completed by stirring at room temperature for three to six hours.

The proposed mechanism for the catalytic cycle is the following (Scheme 2):

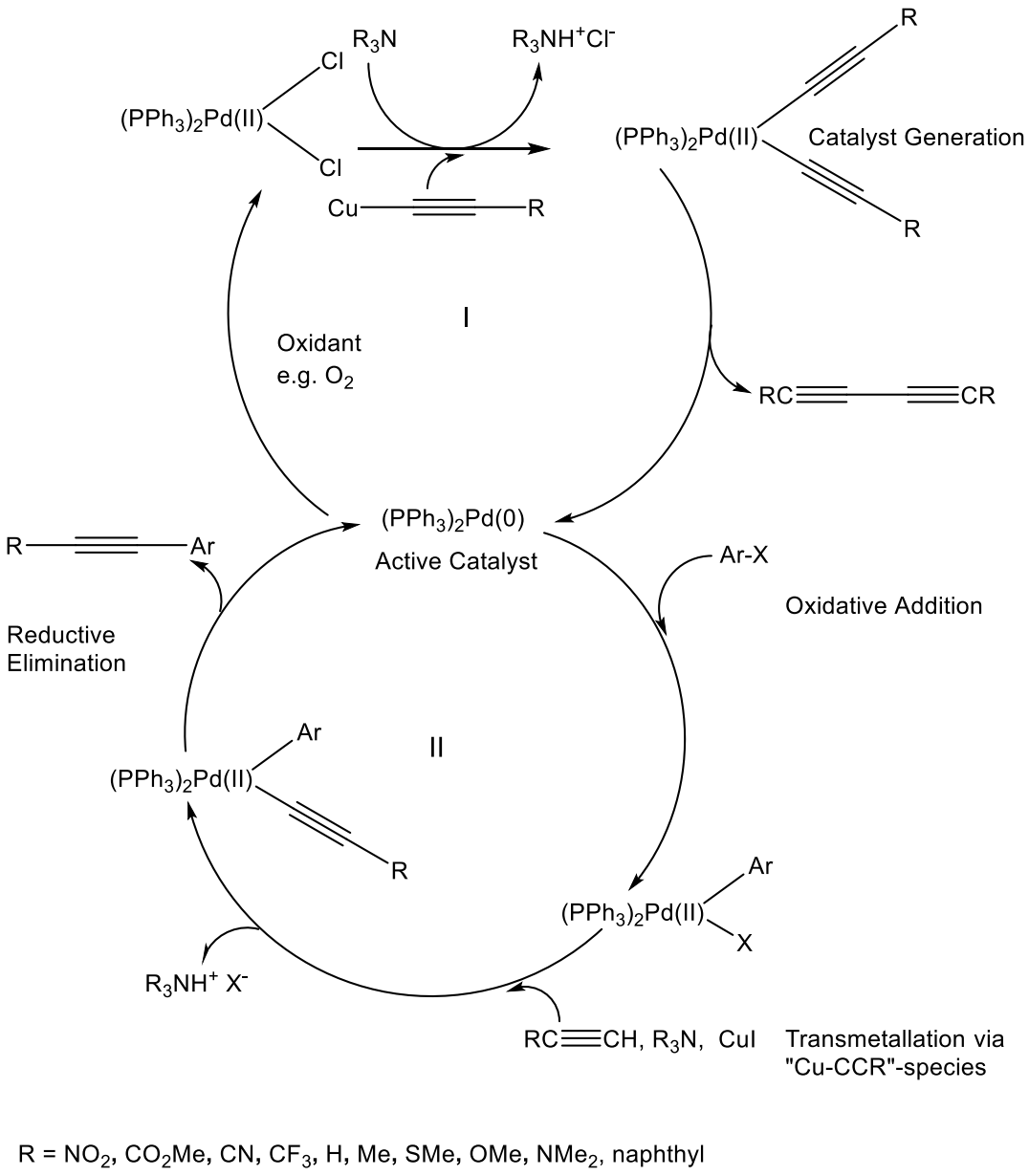


R = $NO_2$, $CO_2Me$, CN, $CF_3$, H, Me, SMe, OMe, $NMe_2$, naphthyl

**Scheme 2** Proposed mechanism for Sonogashira cross-coupling reaction.[2]

In general, for this type of coupling reaction there are two cycles. The first cycle generates, *in situ*, the active Pd(0) from the air stable Pd(II) species promoted by a copper-acetylide intermediate in the presence of an amine, acting as base. Once the active catalyst is generated, the actual catalytic cross-coupling cycle can take place. In an oxidative addition, the aryl or vinyl halide species is added to the palladium centre. In the next step, the alkyne is transferred to the palladium centre *via* transmetallation from the copper centre. The aryl- or vinyl-alkynyl derivative is formed *via* reductive elimination. Therefore, the coupling partners have to occupy positions *cis* to each other. The active catalyst species is recycled. Probably the most important

issue, besides the *in situ* generation of the active Pd(0)-catalyst, is the requirement for oxygen-free reaction conditions. As oxygen acts as strong oxidising agent, the inactive Pd(II)-species would be reformed which would lead to formation of significant amounts of the homocoupled diyne side-product.

There are two ways to improve the reaction rate. The first is to make the Pd centre more nucleophilic by using bulky, strongly donating phosphine or NHC ligands, which makes oxidative addition more favourable. The second way is to choose a more reactive aryl halide for oxidative addition to the Pd centre. It has been shown that Ar-I > Ar-Br >> Ar-Cl >> Ar-F. Substituting the functional group at the *para*-position of the aryl ring with an electron withdrawing group, also increases the reaction rate.[3]

### 1.1.2 Generation of Symmetric Diyne Derivatives

*Oxidative homocoupling*

For the dimerisation of terminal alkynes *via* oxidative homocoupling, copper-catalysed reactions are often used. The best known example is the Glaser coupling.[4] The reaction works via an oxidative homocoupling mediated by a copper(I)-acetate intermediate (Scheme 3). It takes place with copper(I)-chloride in air. This type of coupling was modified by Eglinton and Galbraith in 1959.[5]

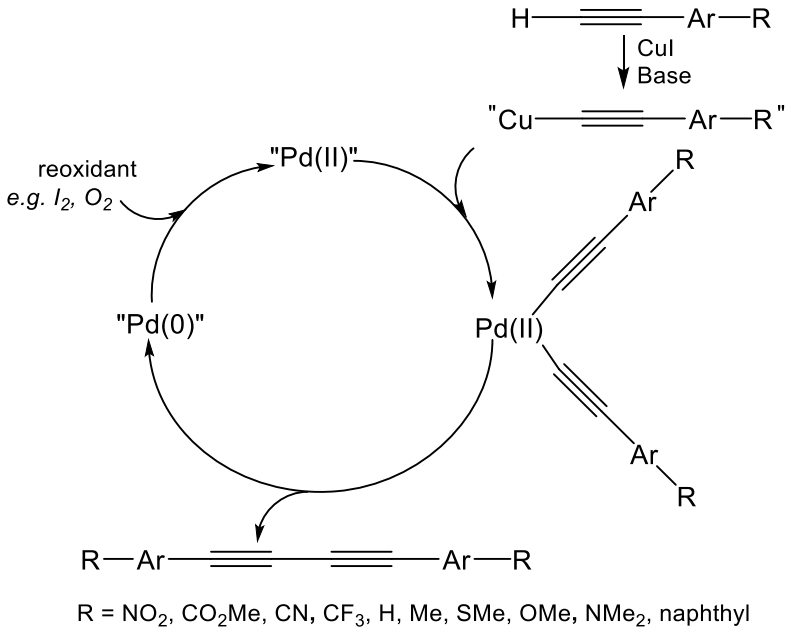


**Scheme 3** General mechanism of a Pd/Cu-catalysed alkyne homocoupling reaction.

Using copper(II)-acetate in methanol with pyridine as base, this reaction works quite well in combination with water-soluble compounds such as $HC{\equiv}CMe_2OH$. As the reaction runs rather slowly with water-insoluble compounds, copper(I)-acetate often has to be used in excess. Scheme 3 shows a modified version of the Glaser coupling, using a combination of Cu and Pd as catalysts.

In 2005, Marder and co-workers found that during the homocoupling reaction two isomeric side-products can be obtained (Scheme 4).[6]

The formation of the two enynes (**b**, **c**) can occur if there is not enough oxygen (or added oxidant in terms of $I_2$) present. However, the presence of excess $PPh_3$ supresses the formation of the side-products.

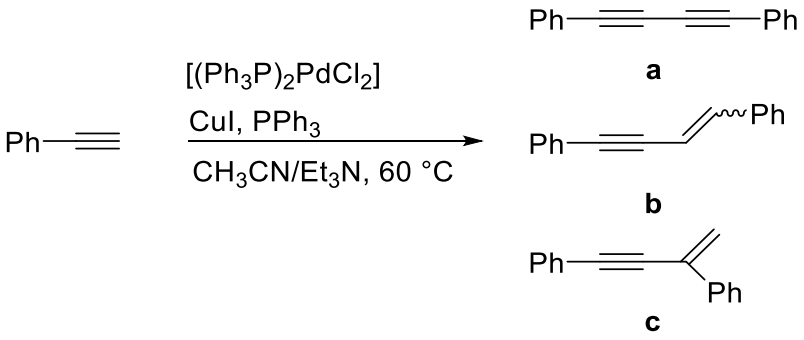


**Scheme 4** Formation of two isomeric enyne side-products during the homocoupling reaction.[6]

Another method for generating homocoupled alkynes was found when using organo stannane compounds,[7] which, besides their strong toxicity, unfortunately, also led to enyne side products **b**, that were difficult to separate from the desired diyne **a** (Scheme 5).

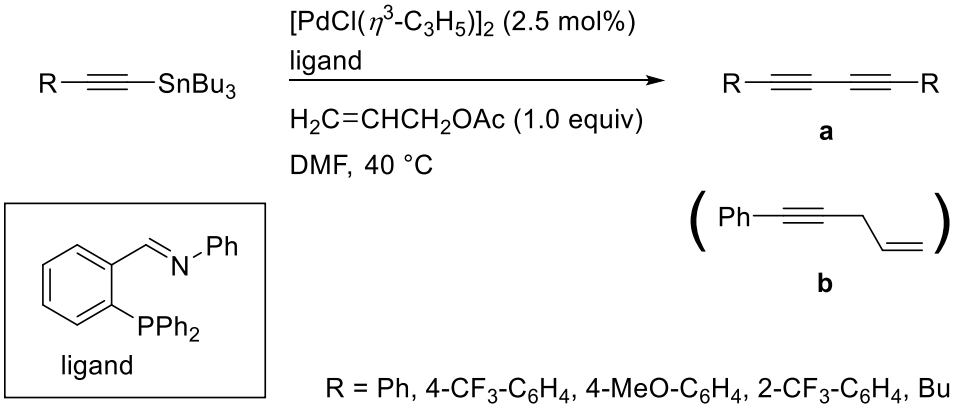


**Scheme 5** Synthesis of homocoupled alkynes *via* alkynylstannanes.[7]

Also organo stannanes, promoted by $BF_3{\cdot}Et_2O$ and *para*-trifluoromethylphenyl(difluoro)-$\lambda^3$-bromane, were used in uncatalysed Michael additions to obtain homocoupled alkynes in moderate yields (Scheme 6).[8]

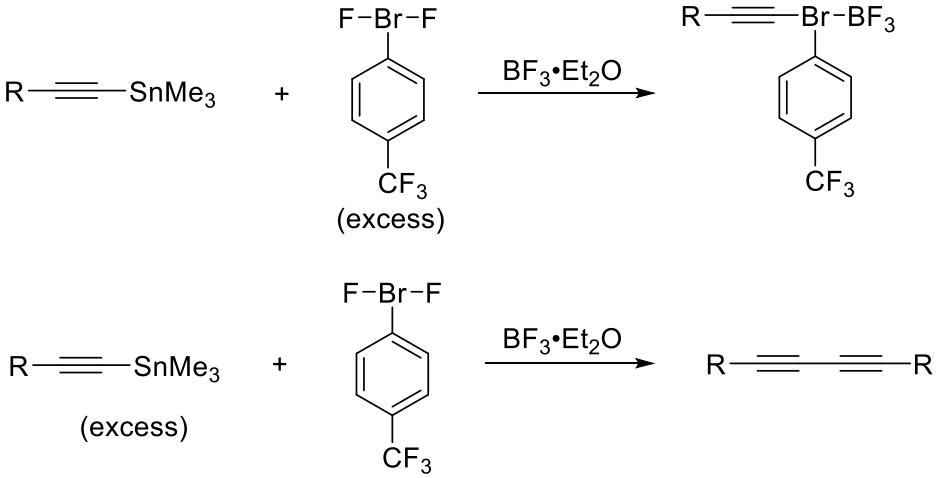


**Scheme 6** Synthesis of homocoupled alkynes promoted by $BF_3{\cdot}Et_2O$ and *para*-trifluoromethylphenyl(difluoro)-$\lambda^3$-bromane.[8]

Another method to homocouple terminal alkynes was developed by Hay in 1962.[9] He succeeded in the homocoupling of phenylacetylene, 1-ethynylcyclohexanol and 1-hexyne in acetone, using copper iodide, tetramethylethylendiamine and oxygen as oxidant. The high yields obtained when using this method, due to the very active copper-catalyst, made it possible to use a variety of organic solvents under mild conditions. A totally different approach, was developed by working with solid-state chemistry, whereby $Cu(OAc)_2$ was used as catalyst in combination with potassium fluoride/alumina at room temperature and with morpholine as base.[10] Similar techniques were used in combination with microwave irradiation to increase the reaction rate.[11]

As the excess of copper salt in the oxidative coupling reactions reported by Glaser and Eglinton is not favourable from an economic point of view, and as environmental consciousness has grown, systems employing palladium/copper catalysts have been developed. The reactions have been improved such that completion is achieved in shorter time, using smaller amounts of catalyst (1 – 5 mol %). Liu and Burton were among the first to report the synthesis of symmetrical butadiynes obtained from oxidative homo-coupling of two alkynes,[12] with iodine used as oxidant as well as $[(PPh_3)_2PdCl_2]$ and copper iodide in diisopropyl amine to give good to excellent yields of the products. Another improvement for working in air is the use of

hydrophobic [bmim]$PF_6$ (1-Butyl-3-methylimidazolium hexafluorophosphate) ionic liquids in combination with copper chloride-tetramethyl ethylendiamine catalyst systems. The recovery of the catalyst is promoted by the hydrophobic character of the ionic liquid.[13]

*Bis-acetylene derivatives via R-CC-X Systems*

To avoid the formation of E,Z-enyne side-products which may be generated with the use of Pd/Cu catalysts, it is possible to use R-C≡C-X (X = halide) species for the homocoupling of terminal alkynes. A variety of systems was investigated to improve the generation of bis-acetylenes *via* R-C≡C-X systems. At the beginning of research on this field, organosilicon compounds were used (Scheme 7).[14]

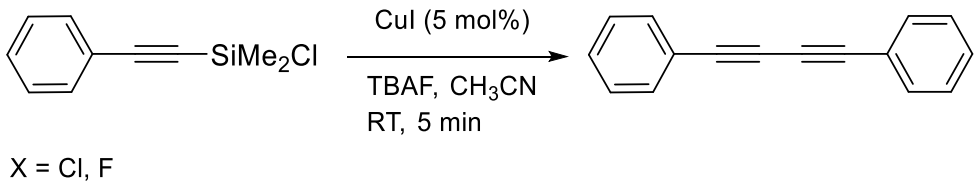


**Scheme 7** Homocoupling *via* organosilicon compounds. **[14]**

For a small variety of terminal alkynes, a homocoupling with lithium salts is possible. The reaction takes place with additional use of $NiCl_2(PPh_3)_2$, accompanied by two equivalents of $PPh_3$, tetramethylguanidine or substituted amidine bases.[15] At low temperature, a reductive elimination of the two alkynes from the Ni(II)-centre takes place, to form the diyne (Scheme 8).

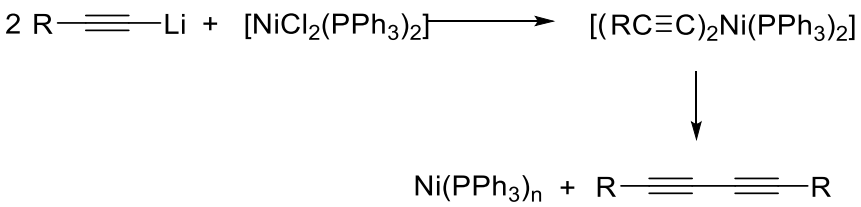


**Scheme 8** Homocoupling of a lithium acetylide promoted by $NiCl_2(PPh_3)_2$.[15]

Comparable reactions involving [Ni(CO)$_4$] are known. Indeed, a large amount of methyl phenylpropiolate can be obtained, depending on temperature and solvent (Scheme 9).[16]

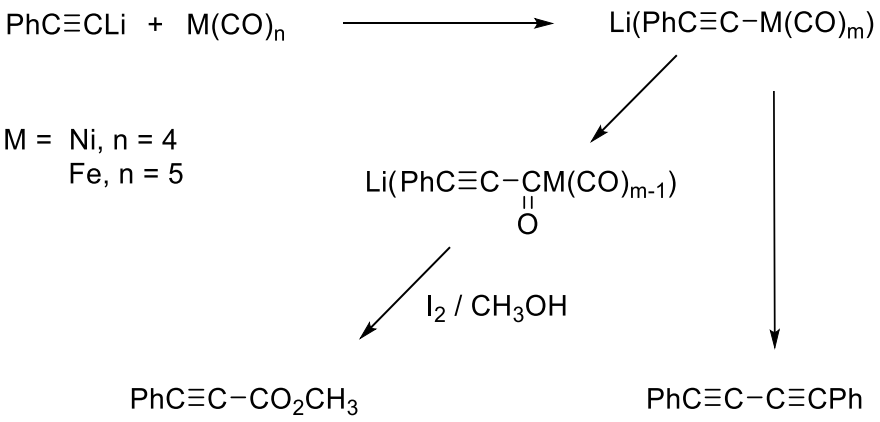


**Scheme 9** Reactions of [Ni(CO)$_4$] and [Fe(CO)$_4$] with lithium phenylacetylide.[16]

Other starting reagents, to obtain homocoupled diynes, are alkynyl boronates. In combination with Cu(I) or Cu(II) salts in aprotic solvents, they can be coupled to give 1,3-butadiynes in high yields. As an alternative, iodoalkynes can be used for butadiyne synthesis. With [Pd(PPh$_3$)$_4$] as catalyst and dimethylformamide as solvent, the homocoupling takes place with loss of iodine. A further advantage is that the reaction is quite simple and leads to high yields.[17]

*Synthesis of unsymmetrical bis-acetylene derivates*

For the successful formation of unsymmetrical diynes, the reaction reported by Cadiot and Chodkiewicz turned out to be the method of choice.[18] Glaser-type reactions and previously reported ones using palladium/copper co-catalysts give unfavourable results.[4] A mixture of diyne derivatives was obtained which turned out to be difficult to separate. In contrast, it was possible to obtain unsymmetrical diynes, free from symmetrical side-products, when using Cadiot's and Chodkiewicz' method (Scheme 10).

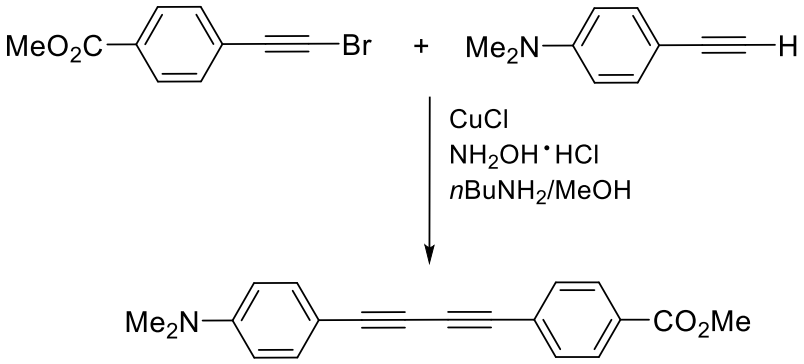


**Scheme 10** Example for a Cadiot-Chodkiewicz reaction.[18]

The unsymmetrical diynes are formed by coupling alkynyl halides with terminal alkynes promoted by copper catalysts. [18]

This type of coupling is also applicable for the synthesis of aryl-substituted bis(diyne) systems, which are connected by a $C_nH_{2n}$ bridge. Subsequently, the Cadiot-Chodkiewicz coupling was improved by using catalytic amounts of $[Pd(PPh_3)_2Cl_2]$ in pyrrolidine.

It was shown that R-Cl, R-Br and R-I alkynyl halides can be coupled successfully with terminal alkynes (Scheme 11).[19]

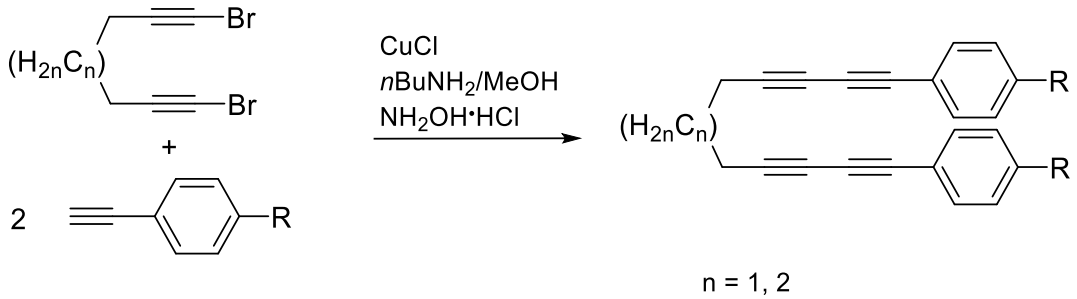


**Scheme 11** Formation of aryl-substituted tetraynes *via* the Cadiot-Chodkiewicz reaction.[19]

In 1998, Nishihara and co-workers introduced the coupling of alkynyl halides and alkynyl silanes promoted by copper(I) catalysis in dimethylformamide which also provides various unsymmetrical diynes in acceptable yields.[20]

A very different approach is provided by the modification of the already homocoupled diyne TMS-C≡C-C≡C-TMS (Scheme 12). With methyl lithium a stepwise desilylation can take place followed by a subsequent coupling of one butadiyne moiety with different aryl, vinyl or alkyl halides.[21]

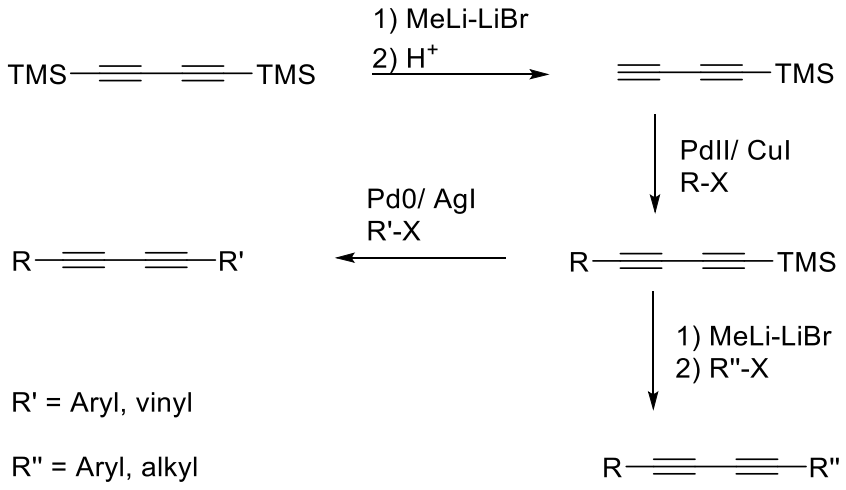


**Scheme 12** Modification of homocoupled diynes, substituted with TMS.[21]

## 1.2 Results and Discussion

### 1.2.1 Synthesis of Homocoupled 1,3-Butadiynes

The synthesis of the 1,3-butadiynes is a three step process starting from the TMS-protected ethynylbenzenes (R = $NO_2$, $CO_2Me$, Me, $NMe_2$, SMe, naphthyl, $CF_3$, Ar = $C_6F_5$, compounds **1a-h**), which are generated in the first step by a Pd-catalysed Sonogashira cross-coupling from either bromo- or iodobenzenes. The second step is the deprotection under basic conditions to obtain the terminal ethynylbenzenes. The last step to obtain the target compounds is a Glaser-type homocoupling (Scheme 13). All of the reactions were monitored by GCMS and the products were purified by filtration through a short silica gel column or by recrystallisation giving moderate to excellent yields. The products were characterised *via* $^1$H-NMR spectroscopy.

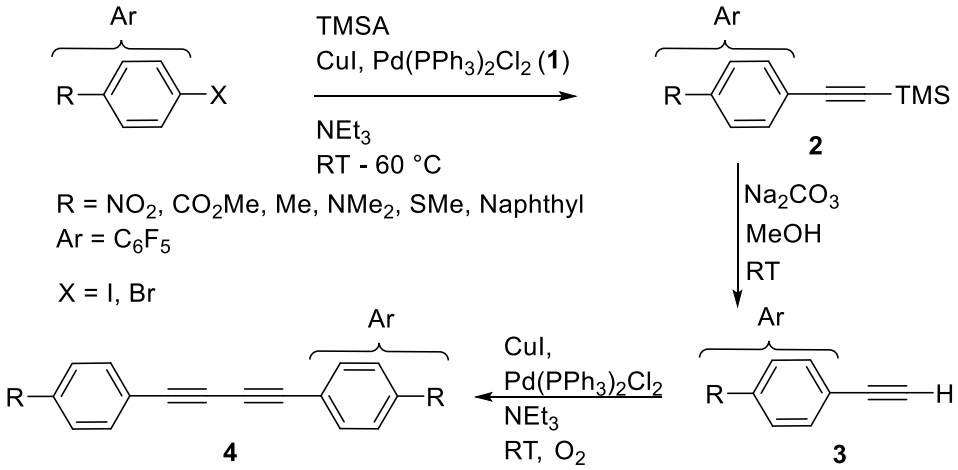


**Scheme 13** Stepwise reaction to homocoupled 1,3-butadiynes.

In general, iodobenzenes are more reactive than bromobenzenes, so while the coupling reactions with iodobenzenes takes place at room temperature within hours, for the same reactions with bromobenzenes higher temperatures and longer reaction times are needed to reach total conversion. A small excess of TMSA always has to be used during a Sonogashira cross-coupling as the active Pd(0)-species has to be generated *in situ* from $Pd(PPh_3)_2Cl_2$. This process is promoted by CuI (Chap. 1.1.1).

Usually, after the Sonogashira reaction has reached completion, the solvent is removed *in vacuo* and the residue is diluted in either $Et_2O$, hexane or a mixture of both and filtered through a short silica gel column to remove the catalysts and ammonium salts.

Table 1 shows an overview of the yields of the different substituted TMS-protected alkynes. All reactions give good to excellent yields. Reactions with $C_6F_5$ (**2f**) and with $CF_3$ (**2h**) as the substituent in the *para*-position give lower yields. The reason for the lower yield in the case of the $CF_3$ substituted product **2h** is that it is a liquid and, due to its volatility, some of the product was lost during the removal of the solvent *in vacuo*.

**Table 1** Yields of TMS-protected alkynes.

| Compound | Substituent | X | Yield (%) |
|---|---|---|---|
| **2a** | $NO_2$ | Br | 91 |
| **2b** | $CO_2Me$ | I | 96 |
| **2c** | Me | I | 84 |
| **2d** | $NMe_2$ | I | 94 |
| **2e** | SMe | Br | 98 |
| **2f** | $C_6F_5$ | I | 64 |
| **2g** | Naphthyl | I | 89 |
| **2h** | $CF_3$ | Br | 76 |

The synthesis and isolation of 4-(trimethylsilylethynyl)pentafluorobenzene **2f** is an exception from the standard procedure mentioned above. First, due to the five fluorine atoms at the phenyl ring, the starting compound, iodopentafluorobenzene can undergo hydrodehalogenation.[22] To avoid this, the reaction was carried out under moderate temperatures varying from room temperature to 50 °C. Furthermore, compound **2f** is quite volatile, which did not allow removal of the solvent *in vacuo* after the reaction was finished. This also explains the lower yield for compound **2f**. It was necessary to isolate the crude product *via* extraction. Therefore, the precipitated solid was removed from the solution by filtration and the solution was diluted with $Et_2O$. The mixture was then washed several times with diluted acetic acid to protonate the triethylamine, converting it to triethylammonium chloride, which then dissolved in the aqueous phase.

Additionally, a certain amount of homocoupled TMSA is always produced during a Sonogashira cross-coupling, which is an expected by-product. However, our group already reported that using fluorinated substrates in this reaction produces more homocoupled TMSA than usually observed due to the hydrodehalogenation side reaction.[22] To get rid of the homocoupled TMSA in this case, it had to be separated from the product *via* distillation. The conditions had to be chosen carefully, as residual homocoupled TMSA can also end up in the

product because of its relatively low melting point of 136-137 °C (Conditions chosen: 1-3 mbar, 104-108 °C). The residual homocoupled TMSA could be removed *via* precipitation in the refrigerator. This is a rather simple way to isolate the product as a colourless liquid with moderate yields. Nevertheless, it has to be noted that homocoupled TMSA is not a problem for the following deprotection of compound **2f**. It would also be deprotected, ending up as butadiyne, which is a gas, so it can be easily removed *in vacuo*.

To obtain the terminal ethynylbenzenes, a deprotection under basic conditions was carried out. Thus, the TMS-group was removed with $Na_2CO_3$, NaOH or KOH in methanol at room temperature and the reaction reached completion overnight. The reaction mixture was extracted into diethylether or dichloromethane, and washed with water to remove the residual base. Afterwards, the organic fractions were separated, dried over $MgSO_4$ and the solvent was removed *in vacuo*. The purity of the products was analysed by GCMS and $^1$H NMR spectroscopy, showing that most of the products were pure after the extraction. For some products, further purification *via* short silica gel column was necessary.
Table 2 shows an overview of the bases used for the deprotection and the different yields of the terminal alkynes **3a-h**. The deprotected ethynylperfluorobenzene **3f** was used without further purification as it is extremely volatile. It has to be noted that the purification was not the only challenging step during the synthesis of **3f**. As the fluorine atoms at the benzene ring can be easily substituted by nucleophiles, especially in the para position, the base was changed from $Na_2CO_3$ to TBAF.

**Table 2** Used bases and yields obtained for terminal alkynes **3a-h**.

| Compound | Substituent | Base | Yield |
|---|---|---|---|
| **3a** | $NO_2$ | $Na_2CO_3$ | 51 % |
| **3b** | $CO_2Me$ | $Na_2CO_3$ | 73 % |
| **3c** | Me | $Na_2CO_3$ | 95 % |
| **3d** | $NMe_2$ | $Na_2CO_3$ | 75 % |
| **3e** | SMe | $Na_2CO_3$ | 74 % |
| **3f** | $C_6F_5$ | TBAF | 43 % |
| **3f'** | OMe-4-$C_6F_4$ | $Na_2CO_3$ | 84 % |
| **3g** | Naphthyl | KOH | 84 % |
| **3h** | $CF_3$ | $Na_2CO_3$ | n.a. |

Usually this reaction takes place in THF, as TBAF is used as a 1 M solution in THF. Unfortunately, when doing this reaction in THF, there was no product left after removing the solvent, because of the volatility of **3f**. For this reason, the solvent was changed to $Et_2O$, which has a lower boiling point than THF, and this minimises the loss of product during the removal of the solvent *in vacuo*. Another problem, which occurred during the synthesis, was a black solid which appeared subsequently when adding TBAF to the reaction mixture (Scheme 14). Fortunately, the solid could be filtered-off easily, after the reaction, giving the product as a clear, dark liquid. To avoid the undesired black solid and the dark colour of the product, another attempt was made, using NaOH in THF (Scheme 14). When using this method, the reaction was finished within 30 min and the reaction mixture remained colourless. Fortunately, no impurity or by-product was evident in the GCMS, so the product was used *in situ* as a solution in THF for the final homocoupling reaction.

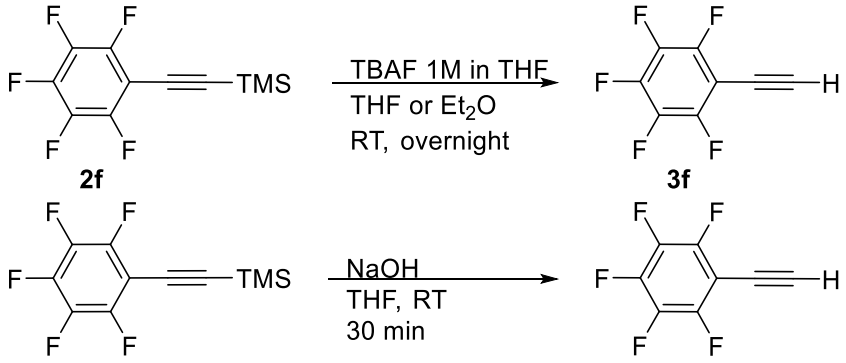


**Scheme 14** Deprotection routes to compound **3f**.

In another reaction, the reactivity of the *para*-substituted fluorine atom was used to substitute it for an OMe-group. This took place in one step along with the deprotection, starting from compound **2f**. Compound **2f** was thus added to a suspension of $Na_2CO_3$ in methanol and stirred at room temperature overnight (Scheme 15).

In contrast to the deprotection of **2f** to prepare the completely perfluorinated compound **3f**, no impurities were observed in the GCMS spectrum. As usual, the organic phase was extracted from $Et_2O$, washed with water and dried over $MgSO_4$. After the solvent was removed *in vacuo*, the product was obtained as a colourless solid in good yields.

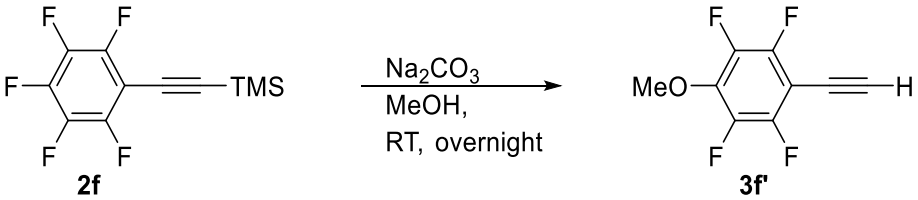


**Scheme 15** Synthetic route to alternative terminal alkyne **3f'**.

Due to the fact that 4-ethynylbenzo-trifluoromethane **3h** is at least as volatile as **3f**, it was not detected in the GCMS under the usual conditions. A $^{1}$H-NMR spectrum of **3h** diluted in $Et_2O$ showed no impurities, so it was used *in situ* as a solution in $Et_2O$ for the homocoupling reaction.

As already mentioned, the final step to obtain the 1,3-butadiynes was carried out by homocoupling of two terminal ethynylbenzenes (Chap. 1.2, Glaser coupling). In most cases, the reaction was carried out in triethylamine with CuI and $Pd(PPh_3)_2Cl_2$ as catalysts in air to use $O_2$ as the oxidant. As some of the homocoupling reactions did not reach completion, or gave low yields, $I_2$ was additionally used as an oxidising agent, which caused a more time consuming work-up as the crude product had to be washed with thiosulfate to remove the excess iodine. An alternative route to homocouple the ethynylbenzenes is the reaction with $Cu(OAc)_2$ as catalyst using pyridine as the base in MeOH solution.
Purification of the products was performed either *via* recrystallisation, washing, or silica gel column chromatography. All reactions were monitored by GCMS and the products were characterised by $^{1}$H NMR spectroscopy.
Table 3 shows an overview of the catalysts used for the homocoupling reaction and the yields of the different substituted buta-1,3-diynes.

**Table 3** Yields of homocoupled diynes.

| Compound | Substituent | Catalyst | Yield |
|---|---|---|---|
| **4b** | $CO_2Me$ | $Pd(PPh_3)_2Cl_2$ | 46 % |
| **4c** | Me | $Pd(PPh_3)_2Cl_2$ | 52 % |
| **4d** | $NMe_2$ | $Cu(OAc)_2$ | 81 % |
| **4e** | SMe | $Cu(OAc)_2$ | 93 % |
| **4f** | $C_6F_5$ | $Pd(PPh_3)_2Cl_2$ | 27 % |
| **4g** | Naphthyl | $Cu(OAc)_2$ | 87 % |
| **4h** | $CF_3$ | $Pd(PPh_3)_2Cl_2$ | 66 % |

All homocoupling reactions gave moderate to good yields. Reactions using $Cu(OAc)_2$ as the catalyst gave better yields. However, all of the reactions reached total conversion and for this reason, the lower yields using the standard Pd-catalysed reaction are rather a result of difficulties during the work-up.

### 1.2.2 Synthesis of Undecatetraynes

The synthesis of the different functionalised undecatetraynes was carried out using the terminal ethynylbenzenes mentioned above (R = $NO_2$, $CO_2Me$, Me, $NMe_2$, SMe, $CF_3$, Ar = $C_6F_4$-4-OMe). In contrast to the formation of the 1,3-butadiynes, undecatetraynes were not synthesised *via* the Glaser-type homocoupling, but *via* the Cadiot-Chodkiewicz cross-coupling with exclusion of $O_2$, to prevent the formation of homocoupled product (Chap. 1.2). Therefore, a degassed solution of CuCl in *n*-butylamine and methanol was charged with a small amount of hydroxylamine hydrochloride to prevent the oxidation of Cu(I) to Cu(II), which would deactivate the catalyst or lead to homocoupling. Afterwards, the deprotected ethynylarene was added, whereby a yellow suspension was formed. After stirring the mixture for a few minutes, 1,7-dibromo-hepta-1,6-diyne was added (Scheme 16). In some cases, the reaction was finished within hours, whereas others were stirred overnight at room temperature.

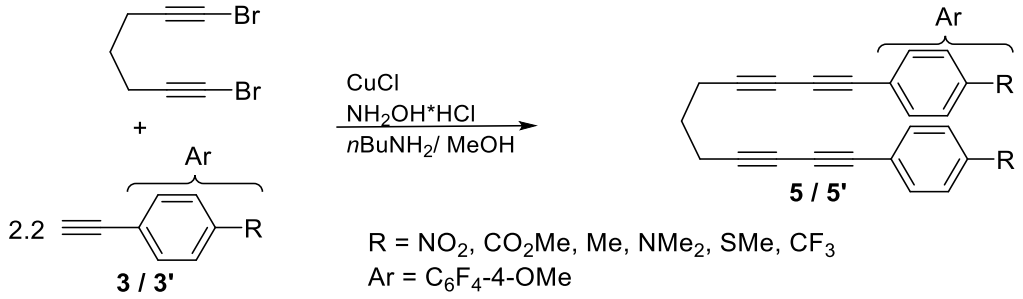


**Scheme 16** General reaction pathway to obtain undecatetraynes.

Monitoring the reactions by GCMS was not the method of choice, as the cross-coupling products cannot be detected, but at least the disappearance of the starting material could be monitored. In addition to the target compound, the formation of a mono-coupled by-product is possible. To prevent this, a small excess of terminal alkyne was always used in the reaction. When the reaction was finished, the solvent was removed *in vacuo* and the crude product was filtered through a short silica gel column chromatography, suspended in methanol and filtered or recrystallised from a hot methanol / dichloromethane mixture. The products were characterised *via* $^{1}H$, $^{13}C$ and $^{19}F$ NMR spectroscopy.

Table 4 shows an overview over the yields of the different substituted undecatetraynes **5 a-h**. All reactions gave moderate to good yields. The reaction to form **5e** gives the lowest yield. It is not clear why the cross-coupling reactions using these substrates gives yields only up to 72 %. One possibility might be the stability of the 1,7-dibromo-hepta-1,6-diyne during the reaction. It was observed that even GC-mass spectra taken directly after starting the reaction did not show

the bis-brominated bisdiyne but the terminal alkyne was still present in a large amount. It has to be noted that the isolated 1,7-dibromo-hepta-1,6-diyne is very easily detectable *via* GCMS. Therefore, a decomposition of it, during the catalytic reaction, is likely. On the other hand, the purification of the undecatetraynes is rather challenging, as most of them are very soluble in most of the common solvents and they are thus not easy to separate from impurities or catalysts. Often, the crude product had to be recrystallised or precipitated at low temperature (10 - −30 °C), causing an additional loss of yield, as some of the product stayed in the mother liquor and was not isolable without impurities.

**Table 4** Yields of cross-coupled undeca-tetraynes.

| Compound | Substituent | Yield |
|---|---|---|
| **5a** | $NO_2$ | 60 % |
| **5b** | $CO_2Me$ | 72 % |
| **5c** | Me | 62 % |
| **5d** | $NMe_2$ | 40 % |
| **5e** | SMe | 30 % |
| **5f'** | $C_6F_4$-4-OMe | 50 % |
| **5h** | $CF_3$ | 41 % |

The generation of an undecatetrayne with fluorinated benzene rings was a very important task in order to investigate the mechanism of formation of dibenzo rhodacyclopentadienes and will be discussed later in this work (Chap. 2.2.2). It has to be noted that using the perfluorinated substrate **3f** to generate an undecatetrayne *via* Cadiot-Chodkiewicz cross-coupling also posed a challenge.

As usual, the reaction was carried out in a mixture of methanol and *n*-butylamine (Scheme 16). When compound **3f** was added to the reaction mixture, a red precipitate subsequently appeared. After stirring the reaction overnight at 60 °C, no starting material was observed by GCMS.

Furthermore, neither homocoupled alkyne nor mono-substituted product was detected. However, some other peaks with a mass of 245 and 335 were detected, which could not be attributed to the desired undecatetrayne. Removing the solvent *in vacuo* left a blackish oil, which was undesired, because until then all the synthesised undecatetraynes were orange to colourless solids. This led to the conclusion that the reaction was unsuccessful. A mass spectrum of the crude product did not show any of the expected peaks, belonging to either homocoupled, mono-substituted product, or the expected undecatetrayne.

Finally, a $^{19}F$ NMR spectrum showed that only two, instead of three, expected fluorine peaks remained. This led to the conclusion that the *para* fluorine atom of compound **3f** must have been attacked by a nucleophile, as utilised for the generation of compound **3f'**. A possible nucleophile for this attack is *n*-butylamine (*n*-$BuNH_2$).

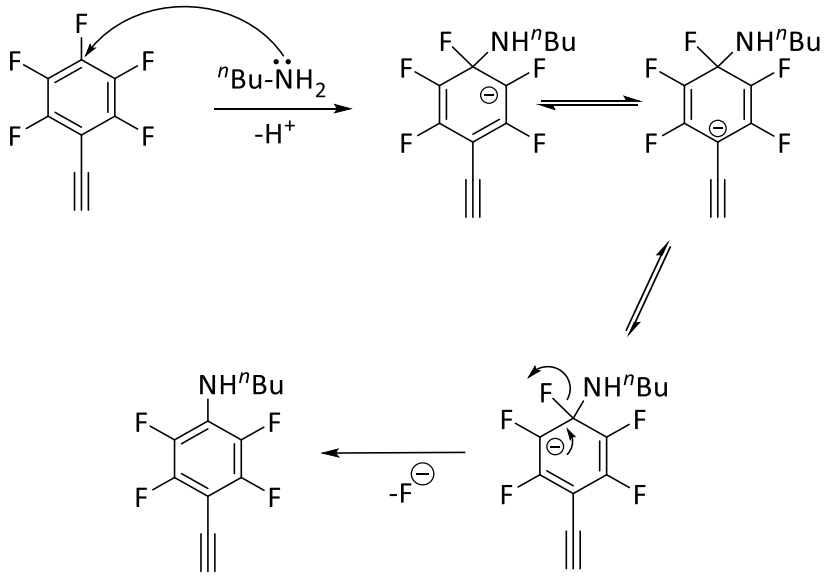


**Scheme 17** Suggested mechanism for nucleophilic attack at the *para* fluorine atom.[23]

Scheme 17 shows a possible mechanism for the substitution of the fluorine atom at the *para*-position by a nucleophile (here: OMe or $^nBuNH_2$).[23] Substitution reactions on benzene rings usually occur *via* an $S_NAr$ pathway. Due to the rigid geometry of a benzene ring, an $S_N2$ mechanism is not possible, because the backside cannot be attacked by any nucleophile. The first step of this reaction is the addition of the nucleophile to the *para*-carbon. This intermediate is stabilised by three resonance structures. In the next step, the fluoride is eliminated.

Having compound **3f'** in hand, in which the *para*-fluorine is already substituted by an OMe-group, a new attempt was made to obtain an undecatetrayne with four fluorines at each benzene ring. This substrate was expected to have comparable electronic and structural properties to the perfluorinated one. The reaction was carried out as usual, leading to a successful synthesis of **5f'**. The solid was purified by washing with cold MeOH and recrystallisation from a mixture of hot dichloromethane and MeOH.

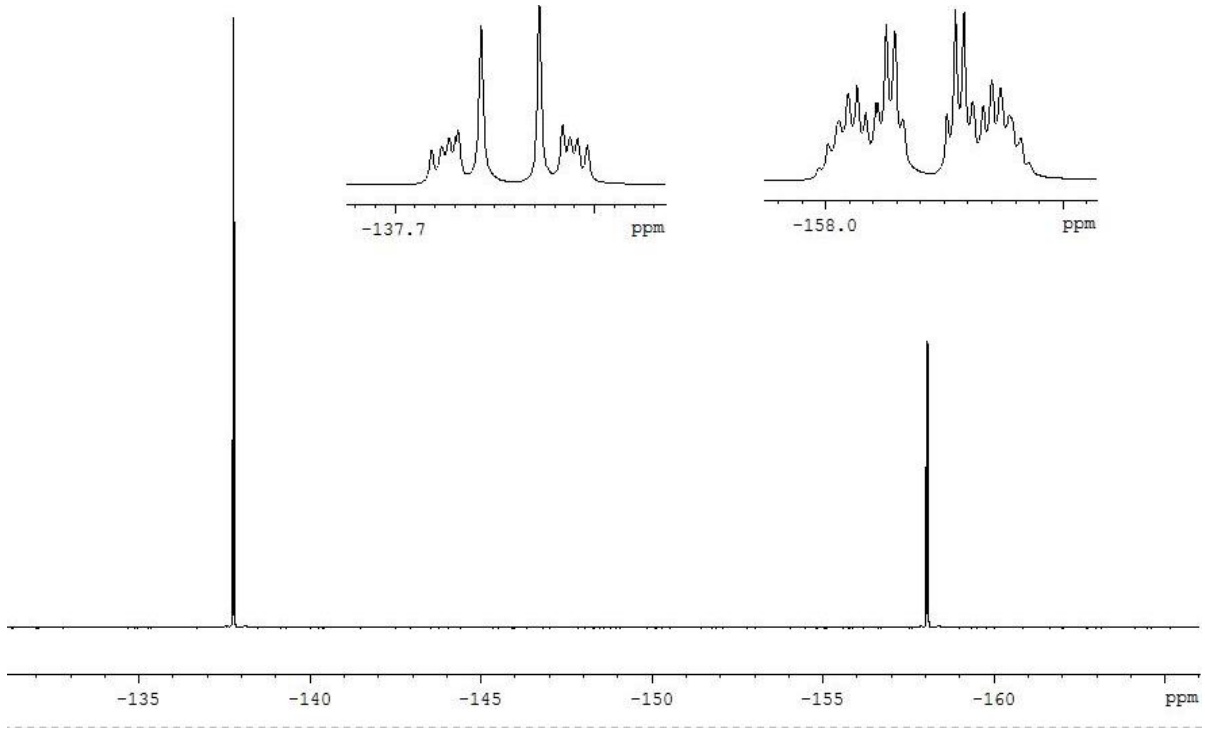


**Figure 1** $^{19}$F NMR spectrum of 1,11-bis{(*p*-methoxy)tetrafluorophenyl}undeca-1,3,8,10-tetrayne **5f'** in $C_6D_6$.

The $^{19}$F NMR spectrum (Figure 1) displays only two signals with the same integral (-137.76 and -158.04 ppm). They belong to the four fluorine atoms on the benzene ring, two in *ortho*- and two in *meta*-positions, which are chemically equivalent pairs. At the same time, this clearly demonstrates the substitution of the *para*-fluorine atom. The exceptional splitting patterns of the fluorine signals indicate the coupling to the protons of the methoxy groups at the *para*-position on each benzene ring as well as the coupling to the other fluorine atoms, and will not be discussed further here (See Chap. 5.2 for the complete characterisation).

# Chapter Two

# Generation of Organo Transition Metal Compounds

# 2. Chapter Two: Generation of Organo Transition Metal Compounds

## 2.1 Introduction

### 2.1.1 Transition Metal-Acetylene $\pi$-Complexes

Transition metal-acetylene $\pi$-complexes have been known for a long time.[24] Such complexes are generally seen as intermediates in the cyclo-oligomerisation and polymerisation of acetylenes. In fact, there are many reported mononuclear acetylene complexes of transition metals such as vanadium, tungsten, rhenium, manganese, iridium, nickel and platinum.[25-30] Ward also reported mononuclear complexes of rhodium and bis-acetylenes.[31]

There are two extreme bonding models for acetylenes coordinated to metal centres (Figure 2).[29]

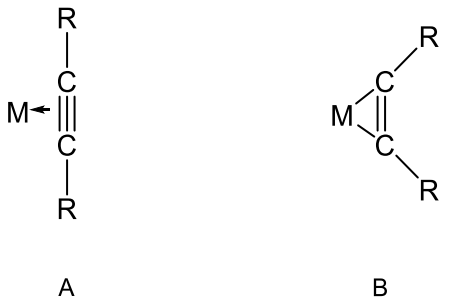


**Figure 2** Two types of binding in a $\pi$-complex.[29]

One is, in general called a "$\pi$-complex", in which the acetylene acts as monodentate ligand. The C≡C stretching frequencies are 130 to 200 $cm^{-1}$ lower than in free acetylenes. The stabilisation of $\pi$-bonded acetylenes is promoted by electron releasing ligands.

The formation of such hydrogen bonds would be impossible if the geometry of the bound acetylene would change much as is the case in structure type B. In this structure type, the coordination of the substituted acetylene to the metal centre is so strong that the triple bond is significantly weakened and gains substantial double bond character, with a stretching frequency lowered by about 500 $cm^{-1}$. In this case, two $\sigma$-bonds to the metal are formed and the acetylenes are seen as bidentate chelating ligands (Type B, Figure 2). They are stabilised by electron withdrawing groups on the alkyne, which promote back-bonding from the metal centre into the antibonding $\pi$*-orbital of the alkyne.[32]

In Figure 3, showing a general MO diagram of an alkyne, the antibonding $\pi^*$-orbital is pictured.[33]

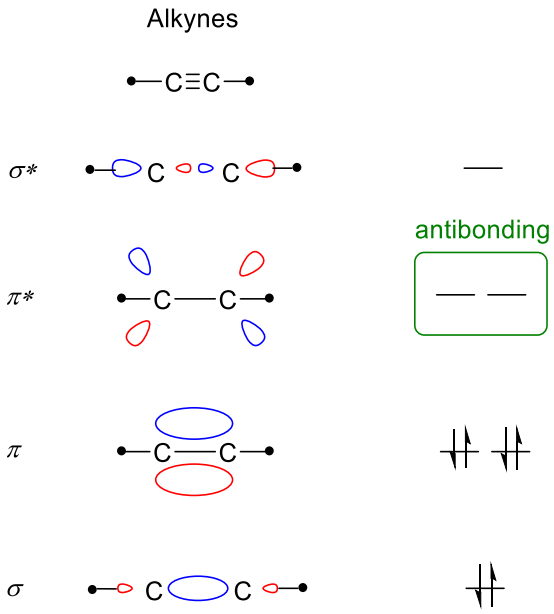


**Figure 3** General MO diagram of an alkyne, showing the antibonding ***π****-orbital. [33]

There are also terminally bound metal acetylides. It is supposed that such hydrido acetylides are also formed as intermediates during the polymerisation of terminal acetylenes promoted by nickel(0) catalysts (Scheme 18).[27]

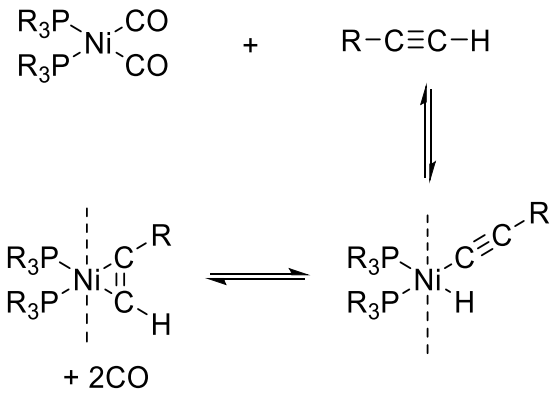


**Scheme 18** Terminal acetylide complexes, formed during the polymerisation of acetylenes.[27]

Vollhardt and co-workers have reported a large number of cobalt-catalysed [2+2+2]-cyclisations leading to efficient total synthesis of different natural products and compounds that are of theoretical interest.[34] Cobalt catalysts also can be used efficiently for the selective formation of multiple carbon-carbon bonds in only one chemical step.[35]

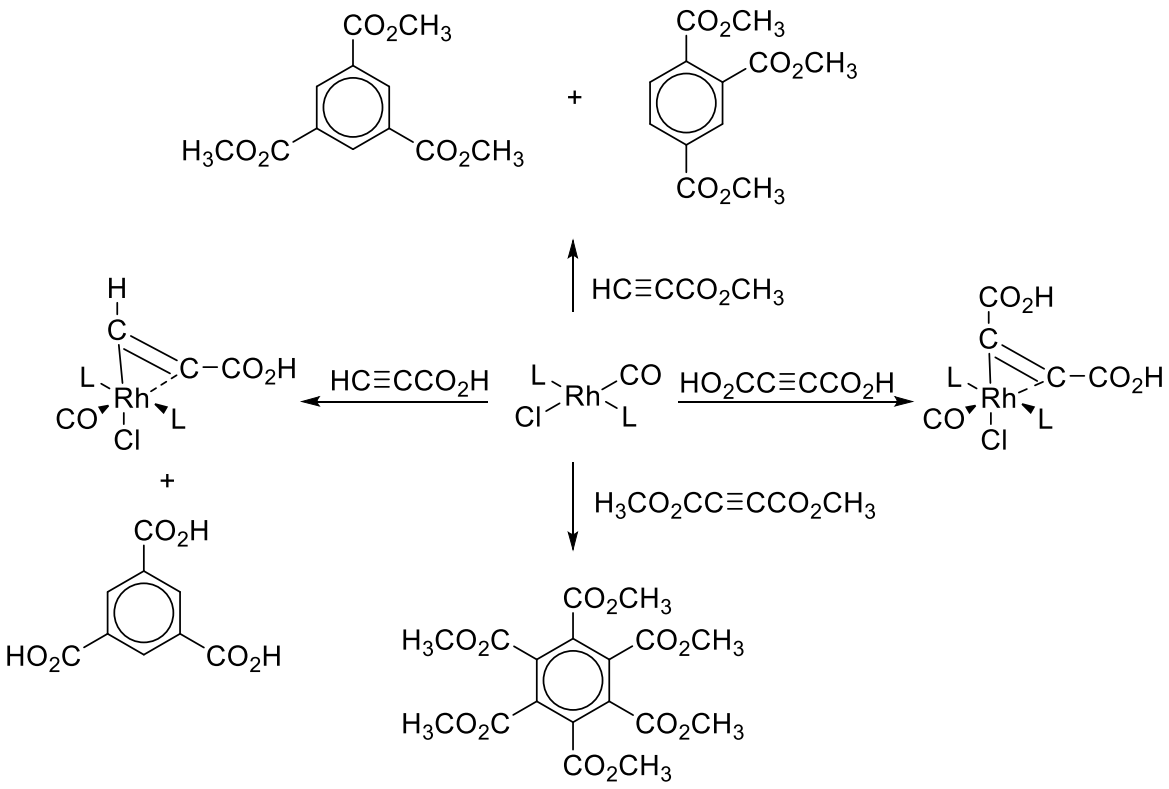


**Scheme 19** Trimerisation of acetylenedicarboxylate promoted by rhodium.[36]

During their work on $\pi$-complexes, Collman *et al.* found that reactions of rhodium complexes with acetylenedicarboxylate did not form any complexes, but resulted in the trimerisation of the acetylene (Scheme 19). The same happened with ethyl propiolate with the rhodium compound remaining at the end of the catalytic reaction.[36]

As propionic acid yielded both the 1:1 complex and the trimerisation product, Collman *et al.* presumed that the formed complexes must be intermediates in the trimerisation reaction. For the mechanism of the trimerisation, Collman *et al.* suggested a seven membered ring including the metal centre as an intermediate (Scheme 20).[36]

The catalytic cyclotrimerisation of alkynes in a [2+2+2] manner has been examined intensively and there are many transition metals known that can be employed in a catalyst system promoting the trimerisations.[37-40] During their studies of organic synthesis *via* cobalt metallacycles, Wakatsuki *et al.* proposed that cobaltacyclopentadienes can lead to pyridines,

1,2-dithiopyridones, as well as *N*-methylthiopyrones, when reacting with nitriles, carbon disulphide and methyl isothiocyanate, respectively.[39]

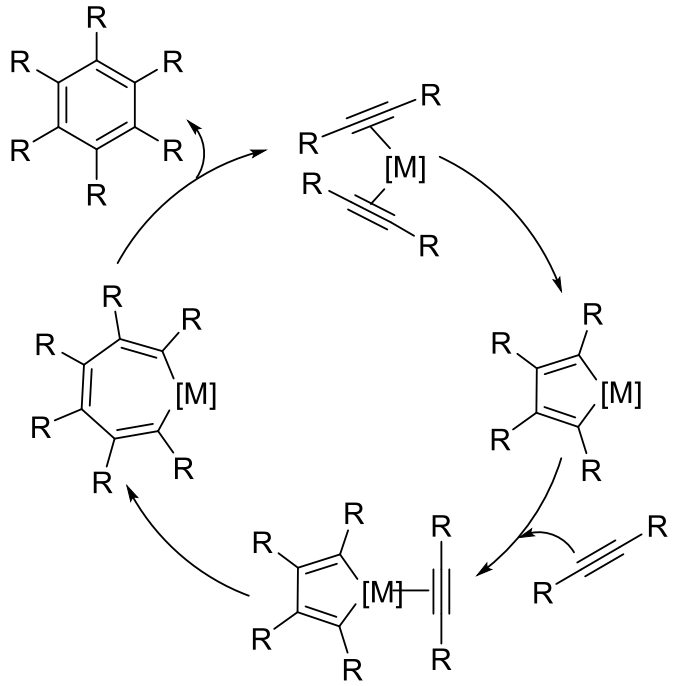


**Scheme 20** Mechanism of the [2+2+2]-cyclotrimerisation.[36]

They further reported that cobaltacyclopentadienes are good starting materials for the formation of 5- or 6-membered organic ring compounds with a variety of different substituents.[40]

The research of Gandon and co-workers was also focussed on the trimerisation of different acetylenes.[41] They succeeded in generating di- or tetra-substituted benzene derivatives, using temporarily silylated ethers in combination with up to three different, unsymmetrical alkynes. The formation promoted by a Diels-Alder mechanism was excluded as it was not possible to react maleic anhydride with the system.

The cyclotrimerisation could be inhibited when the reaction took place under a 60 psi pressure of CO. The blocking of a free coordination site with CO stopped the system from further reaction. Ward was able to trimerise alkynes based on his metallacyclopentadienes only under forcing conditions, due to a low activity of the rhodacycle catalyst.[31]

Gandon and co-workers also assumed that, with a second mole of acetylene, a metallacyclopentadiene derivative is formed according to a mechanism previously reported by Blomquist and Maitlis in 1962 (Scheme 21).[42]

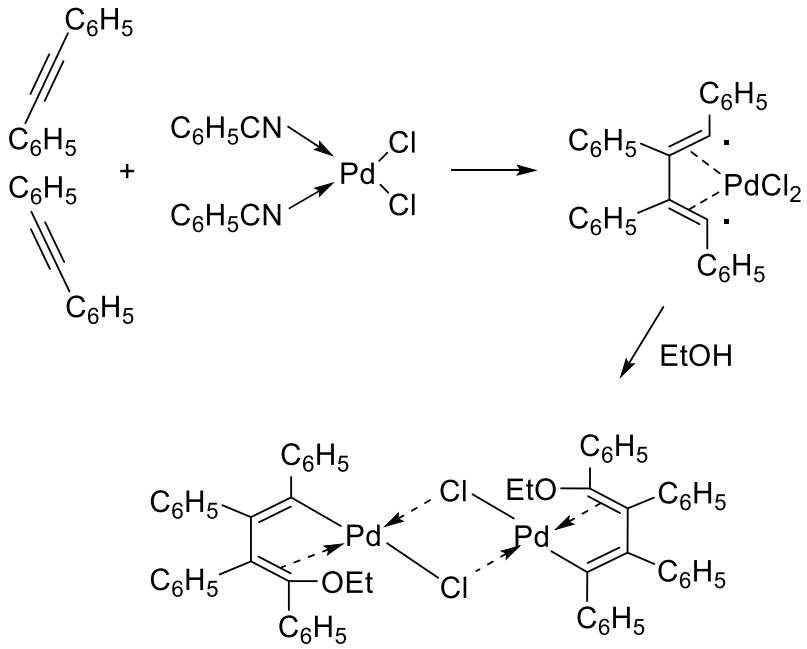


**Scheme 21** Mechanism suggested by Maitlis and Blomquist.[42]

### 2.1.2 Transition Metal $\pi$-Complexes with 1,3-Butadiynes

Besides the before introduced transition metal acetylene $\pi$-complexes, it is also worth mentioning the formation of $\pi$-complexes between transition metals and 1,3-butadiynes.[43] They have been known for several decades and aside from numerous examples of polynuclear systems,[44] there exist also mono- and dinuclear examples.[45]

Marder *et al.* have shown that $Rh(PMe_3)_3(Cl)((1,2\text{-}\eta^2)\text{-}p\text{-}F_3C\text{-}C_6H_4\text{-}C{\equiv}C\text{-}C{\equiv}C\text{-}C_6H_4\text{-}p\text{-}CF_3)$ can be formed *in situ*. From this simple monometallic $\pi$-complex a bi-metallic species can be formed, which is bound in a $\mu$-$(1,2\text{-}\eta^2)$:$(3,4\text{-}\eta^2)$-manner.[46] Werner and co-workers reported the synthesis of square planar Rh complexes of the type *trans*-$XRh(P^iPr_3)_2(\eta^2\text{-}R\text{-}C{\equiv}\text{-}CR')$, which have an alkyne bound in a $\eta^2$-manner, as well as a halide and two tri-*iso*-propyl phosphines as ligands (Scheme 22). In this class of complexes, the C≡C-bond lies perpendicular to the coordination plane, which is square planar and has 16 electrons.[47-52] They also reported the reaction of $[Ir(Cl)(COE)_2]_2$ with TMS-C≡C-C≡C-TMS in the presence of $P^iPr_3$ resulting in $[Ir(Cl)(\eta^2\text{-TMS-}C{\equiv}C\text{-}C{\equiv}C\text{-TMS})(P^iPr)_2]$. In addition, they mentioned that the compound converted thermally and photochemically to the vinylidene iridium(I) complex.

Hill and co-workers converted $[Ru(CO)_2(PPh_3)_3]$ to $Ru(\eta^2\text{-Ph-}C{\equiv}C\text{-}C{\equiv}C\text{-Ph})(CO)_2(PPh_3)_2$, which was further converted to $[Ru(Ph\text{-}C{\equiv}C\text{-}C{=}CH\text{-Ph})(CO)_2(PPh_3)_2]X$, ($X = BF_4^-, SbF_6^-, ClO_4^-$), when the complex was protonated with acid (Scheme 22).[53]

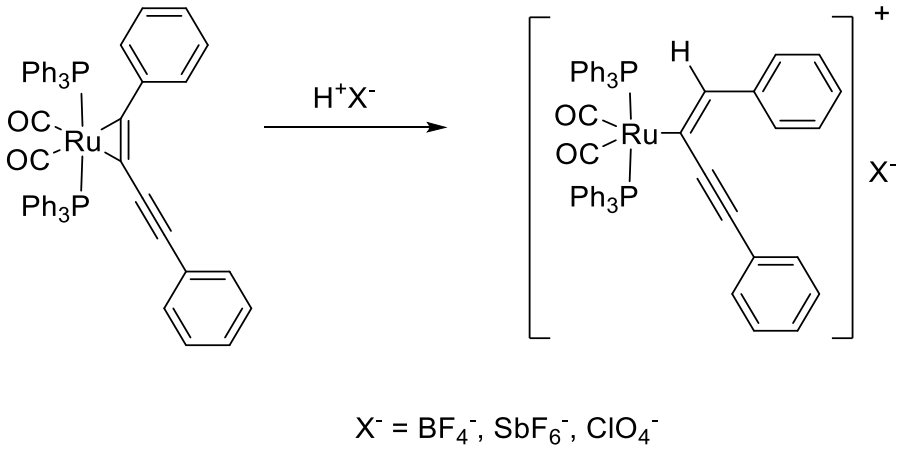


**Scheme 22** Protonation of $Ru(\eta^2\text{-Ph-}C{\equiv}C\text{-}C{\equiv}C\text{-Ph})(CO)_2(PPh_3)_2$.[53]

Complexes prepared *via* reaction of diphenylbutadiyne with $WCl_6$, which was reduced with $C_2Cl_4$, and $MoCl_5$ giving $[WCl_4(\eta^2\text{-Ph-}C{\equiv}C\text{-}C{\equiv}C\text{-Ph})]_2$ and $[MoCl_4(\eta^2\text{-Ph-}C{\equiv}C\text{-}C{\equiv}C\text{-Ph})]_2$, were reported by Dehnicke *et al.*[54,55] Furthermore, treatment with $PPh_4Cl$ in DCM in the

presence of $CCl_4$ yielded $PPh_4[WCl_5(\eta^2\text{-Ph-C}\equiv\text{C-C}\equiv\text{C-Ph})]CCl_4$. If this complex was brominated in the *trans*-positions of the free alkyne bond, $PPh_4[WCl_5(\eta^2\text{-Ph-C}\equiv\text{C-C(Br)=C(Br)-Ph})]CCl_4$ could be generated. Comparable results were obtained from the reductive reaction with Ph-C≡C-C≡C-TMS.[54,55]

Casey and co-workers reported the synthesis of $[Pt(\eta^2\text{-TMS-C}\equiv\text{C-C}\equiv\text{C-TMS})(PAr_3)_2]$ (Ar = *p*-$CH_3$-$C_6H_4$-) and also $[Pt(\eta^2\text{-Me-C}\equiv\text{C-C}\equiv\text{C-Me})(PAr_3)_2]$,[56] using the same synthetic route as Bruce *et al.* who synthesised the analogous compound $[Pt(\eta^2\text{-TMS-C}\equiv\text{C-C}\equiv\text{C-TMS})(PPh_3)_2]$ by the reaction of TMS-C≡C-C≡C-TMS with $[Pt(\eta^2\text{-}C_2H_4)(PPh_3)_2]$.[57] However, Casey and co-workers also studied the protonation of their platinum diyne complexes, using $HBF_4$ and $CF_3CO_2H$. Treatment with these acids resulted in $\sigma$-2-butadienyl complexes *via* thermally unstable $\pi$-propargyl intermediates (Scheme 23).[56]

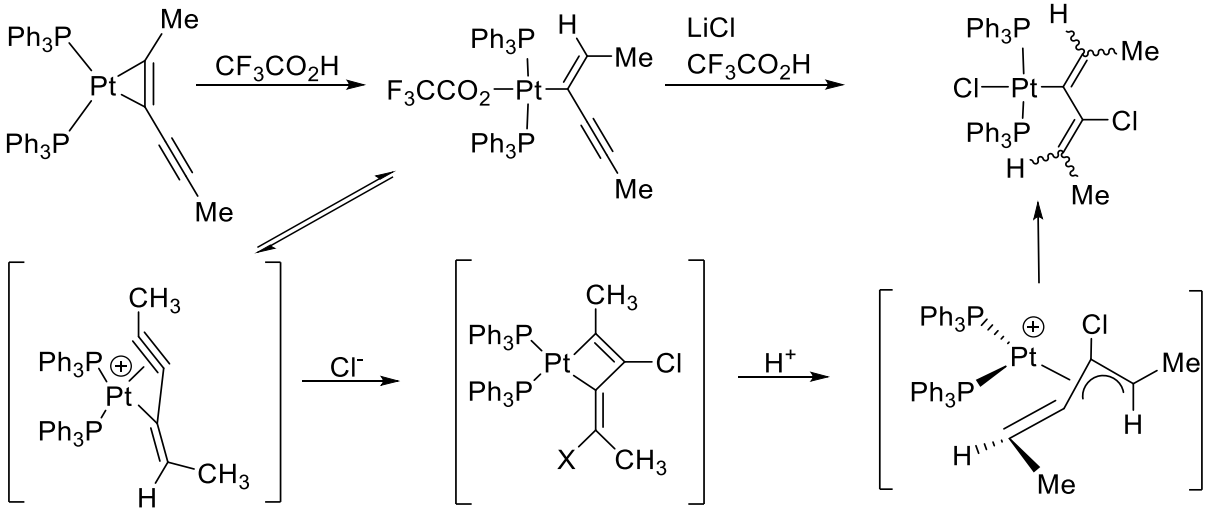


**Scheme 23** Synthesis of a Pt $\sigma$-2-butadienyl complex *via* a thermally unstable $\pi$-propargyl intermediate.[53]

Another contribution was made by Yamazaki and co-workers during their synthetic work on heteronuclear triangular cluster compounds.[58] The reaction of $[Pt(PPh_3)_4]$ with 1,4-diphenyl-butadiyne resulted in the complex $[Pt(\eta^2\text{-Ph-C}\equiv\text{C-C}\equiv\text{C-Ph})(PPh_3)_2]$. It was identified *via* X-ray crystallography, showing that the compound is nearly planar and that the bond length of the coordinated alkyne bond is stretched from 1.197(9) Å in the free diyne to 1.305(11) Å, which confirms the formation of a cyclopropenyl ring.[59]

Furthermore, they also synthesised the analogous compound $[Pt(\eta^2\text{-Ph-C}\equiv\text{C-C}\equiv\text{C-Ph})(dppe)]$. The compound was obtained with a yield of 38%. During the reaction, which takes place in refluxing toluene, the homocoupling of two acetylide ligands appears at the Pt centre, which is promoted by $[Ru_3(CO)_9(PPh_3)_3]$ (Scheme 24).[60] Very close to this is the generation of $[Pd(\eta^2\text{-Ph-C}\equiv\text{C-C}\equiv\text{C-Ph})(dppn)]$ by reacting $[PdCl_2(dppn)]$ (dppn = $Ph_2PC_6H_{10}PPh_2$, $C_6H_{10}$ =

1,8-naphthalenediyl) with two equivalents of phenylacetylene. The reaction works with $NEt_3$ used as base in a mixture of ethanol and DCM.[61]

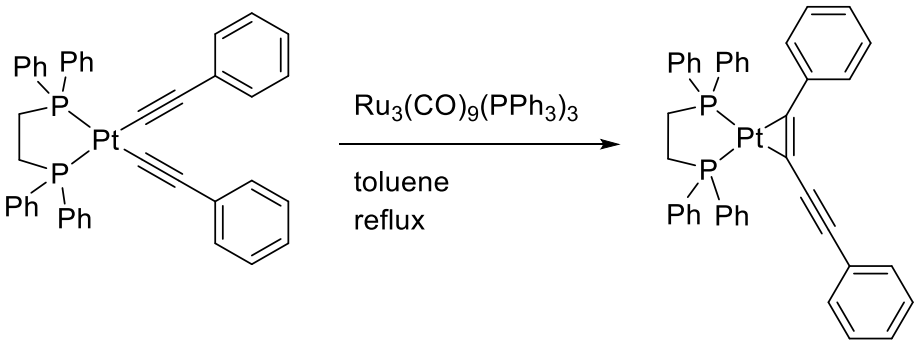


**Scheme 24** Formation of a Pt-diyne $\pi$-complex by homocoupling of two acetylide ligands.[60]

Another compound which was obtained, when a Pt-bis(acetylide) was converted into a $\pi$-coordinated diyne, is [Pt($\eta^2$-Ph-C≡C-C≡C-Ph)(dppf)].[62] The reaction was promoted by use of an excess of an electrophilic gold phosphine complex $[Au(PPh_3)]^+$.

A quite uncommon reaction of [Ni($PPh_3$)$_2$($\eta^2$-Ph-C≡C-C≡C-Ph)] with '$MCp_2$' (M = Ti, Zr), generating bicyclic compounds (Scheme 25) was found by Rosenthal *et al.*, which they referred to as a fusion of Ti and Zr metallacyclopentadienes with a nickelacyclopropene.[63]

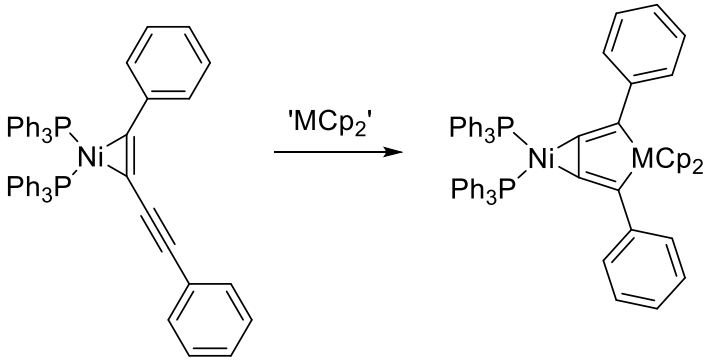


**Scheme 25** Formation of a fused bicyclic compound from [Ni($PPh_3$)$_2$($\eta^2$-Ph-C≡C-C≡C-Ph)].[63]

A very interesting contribution was made by Bruce and co-workers, who designed novel transition metal complexes *via* the coordination of transition metal complexes consisting of diphosphino butadiynes to a $Pt(PPh_3)_2$ precursor.[64] Therefor, $Ph_2P$-C≡C-C≡C-$PPh_2$ was reacted with $[Mo(CO)_5(NCMe)]$, $[W(CO)_5(THF)]$ and $[Fe_2(CO)_9]$ to obtain the corresponding transition metal complexes of the diynes.

The reaction of these with [Pt($C_2H_4$)($PPh_3$)$_2$] gave the $\eta^2$-complex *via* the displacement of the coordinated ethylene (Figure 4).

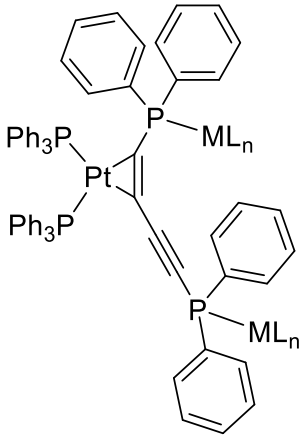


**Figure 4** Pt($PPh_3$)$_2$ complex of a diphosphino butadiyne.[64]

Ward also reported the formation of $\pi$-complexes between [Rh($PMe_3$)$_4$Me] and 1,3-butadiynes with abstraction of one $PMe_3$ ligand. In this case, the Me group occupies an axial position which generates an unsymmetrical environment for the three $PMe_3$ groups (Scheme 26).[46]

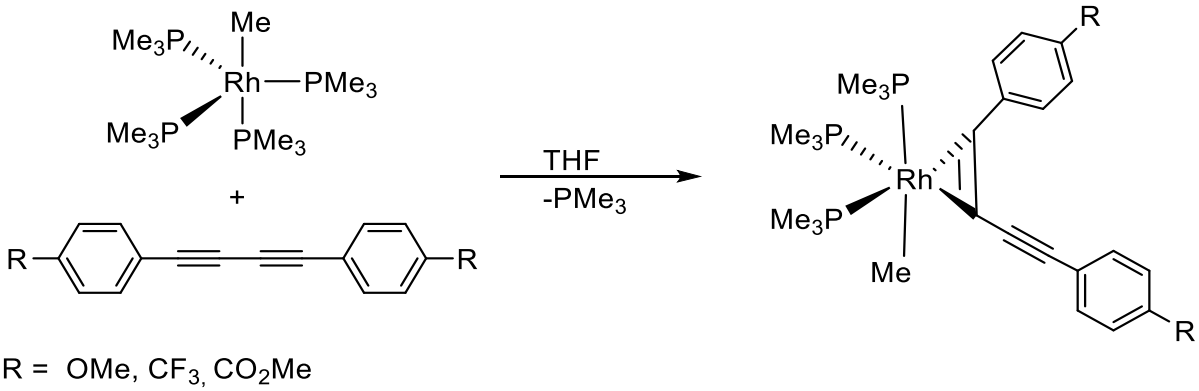


**Scheme 26** Formation of a $\pi$-complex *via* reductive coupling of a 1,3-butadiyne. [46]

Based on these results, Ward was also able to obtain this kind of $\pi$-complexes starting from [Rh($PMe_3$)$_4$]Cl.[46] It is worth mentioning, that this reaction results in a 1:1 mixture of two regioisomers (Figure 5).

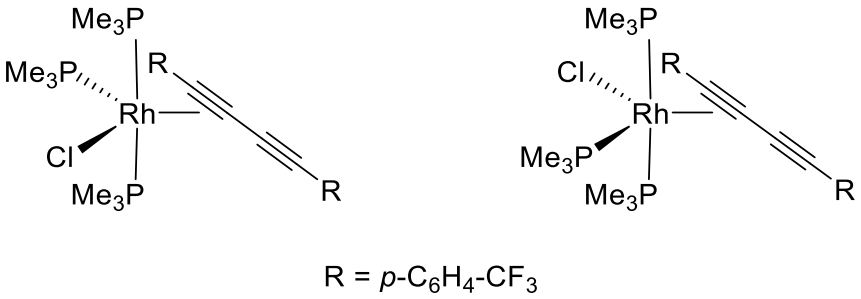


**Figure 5** Two isomeric RhCl complexes with the diyne lying in the P-Rh-Cl equatorial plane.[46]

However, the reaction did not stop at the monometallic $\pi$-complexes, but ended up giving a bimetallic $\pi$-complex with a yield of 50%. In contrast to what was observed in solution, the crystalline product showed a $\mu$-(1,2-$\eta^2$):(3,4-$\eta^2$) binding of one equivalent of *p*-$CF_3$-Ph-C≡C-C≡C-Ph-*p*-$CF_3$ to two [Rh($PMe_3$)$_3$Cl] metal centres (Figure 6).

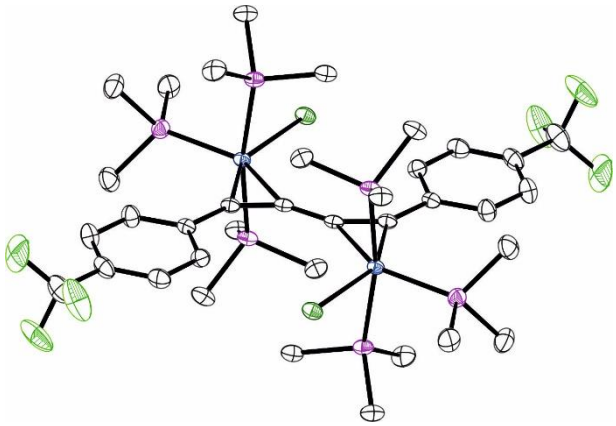

**Figure 6** Molecular structure of the bimetallic $\pi$-complex containing two Rh-centres (CCDC number: 287859).[46]

A complex which can be used to propose the structures of [Rh($Me_3$)$_3$Me($\eta^2$-(R-C≡C-C≡C-R)] (R = -$C_6H_4$-4-OMe, -$C_6H_4$-4-$CF_3$, -$C_6H_4$-4-$CO_2$Me), is the iron complex [Fe(CO)$_2$($PEt_3$)$_2$($\eta^2$-TMS-C≡C-C≡C-TMS)].

The corresponding X-ray crystal structure shows that the complex consists of a 5-coordinate, distorted trigonal bipyramid around the Fe centre.[65]

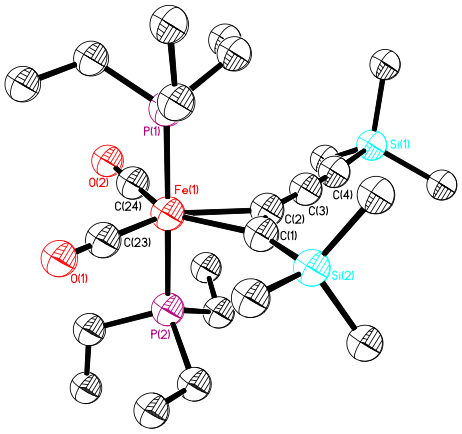


**Figure 7** Molecular structure of $[Fe(CO)_2(PEt_3)_2(\eta^2\text{-TMS-C}\equiv\text{C-C}\equiv\text{C-TMS})]$. Hydrogen atoms are omitted for clarity and thermal ellipsoids are shown at 50% probability ( CCDC number: 1251357).[65]

The bent diyne is located in the $Fe(CO)_2$ equatorial plane, whereas the two phosphine ligands occupy the axial positions (Figure 7). The alkyne substituents bent away from the Fe centre with an angle of about 140-150° speaks for a strong back bonding from the Fe-centre to the acetylenic part of the complex. Furthermore, in the IR-spectrum stretches appear, which speak for a C≡C bond (2109 $cm^{-1}$) and a C=C bond (1750 $cm^{-1}$).

### 2.1.3 Investigations on Rhodacyclopentadienes

As mentioned above, Collman *et al.* presumed that, with a second mole of acetylene, a metallacyclopentadiene derivative is formed according to the mechanism suggested by

Blomquist and Maitlis in 1962.[42] It was also mentioned that some of these metallacycles could be isolated at this stage. Reductive coupling of two equivalents of alkyne accompanied by an oxidation of the metal centre gives these intermediates. In 1995, Nishihara *et al.* coupled various diphenylbutadiynes with [$CoCp(PPh_3)_2$] which yielded three different regioisomers (Scheme 27) of diethynylcobaltacyclopentadienes and insoluble polymeric material.[66] Besides the unsymmetrical 3,5-dialkynyl metallacyclopentadiene (**B**), the 3,4-isomer (**C**) was formed as the major product, whereas the symmetrical 2,5-dialkynyl (**A**) metallacyclopentadiene was only formed when the reaction was done under elevated temperatures.

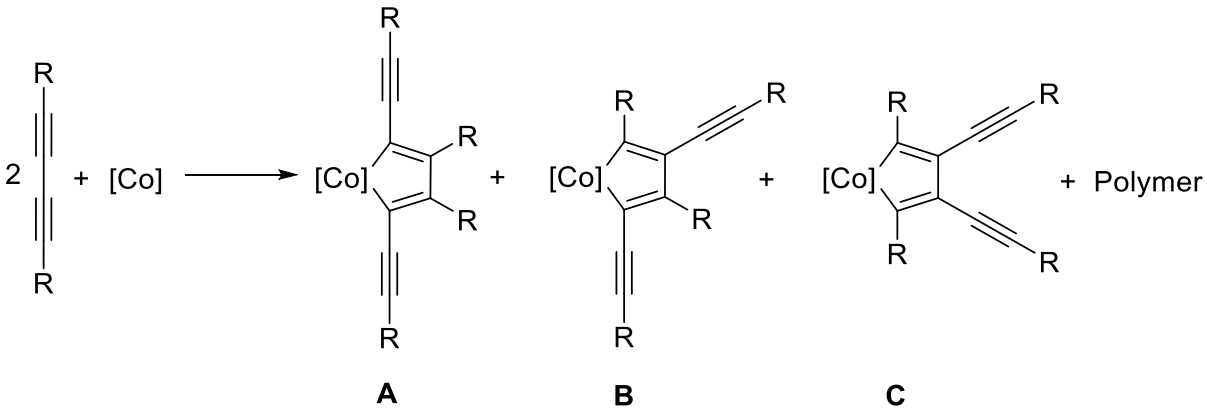


**Scheme 27** Formation of three regioisomers (**A**, **B**, **C**) by reductive coupling of butadiynes; [Co] = [$CpCo(PPh_3)$].[66]

Besides this, the group recognised that the use of the bulkier bis(TMS)-butadiyne yielded the 2,4-dialkynyl metallacyclopentadiene, whereas the less bulky 2,4-hexadiyne promoted the formation of the 2,5-dialkynyl metallacyclopentadiene.[66]

The rules proposed by Wakatsuki *et al.*, who also studied the formation of cobaltacyclopentadienes with various alkynes,[67] fit well to the results of Nishihara *et al.*[66] and are also supported well by the discoveries made by Collman *et al.*[36] They suggest that during the formation of the metallacycle, steric factors play a more important role than electronic factors.[67]

In comparison to previous studies, which usually gave rather low yields of the 2,5-isomer, Marder and co-workers discovered a high yield, one pot and totally regiospecific synthesis starting from [$RhMe(PMe_3)_4$]. First, the methyl group of the rhodium precursor was substituted by the terminal acetylides C≡C-R (R = $SiMe_3$, *p*-$C_6H_4$–$NMe_2$, C≡C–*p*-$C_6H_4$–$NPh_2$, *p*-$C_6H_4$-C≡C-*p*-$C_6H_4$-$Nhex_2$)[67,68] to give a variety of rhodium(I) compounds (Scheme 28).[68]

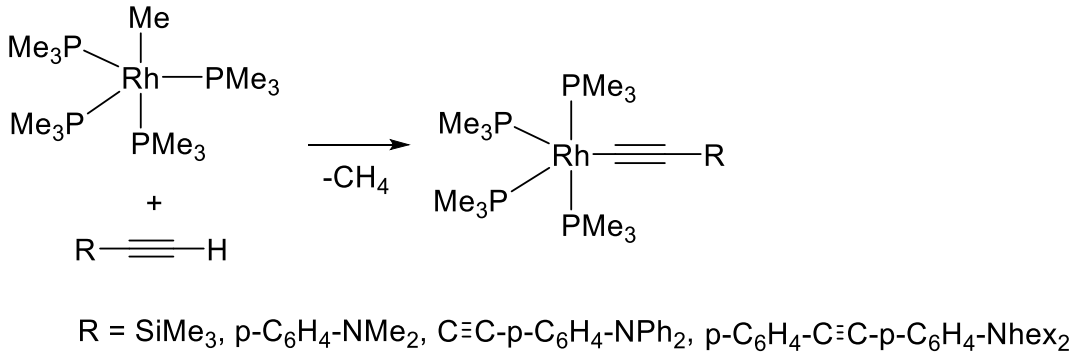


R = $SiMe_3$, p-$C_6H_4$-$NMe_2$, C≡C-p-$C_6H_4$-$NPh_2$, p-$C_6H_4$-C≡C-p-$C_6H_4$-$Nhex_2$

**Scheme 28** Formation of different Rh-precursor complexes *via* substitution with various terminal alkynes.[68]

To obtain the different 2,5-bis(*p*-R´-phenylethynyl)complexes, two equivalents of 1,4-bis(*p*-R´-phenyl)-1,3-butadiynes were reductively coupled (Scheme 29).[68]

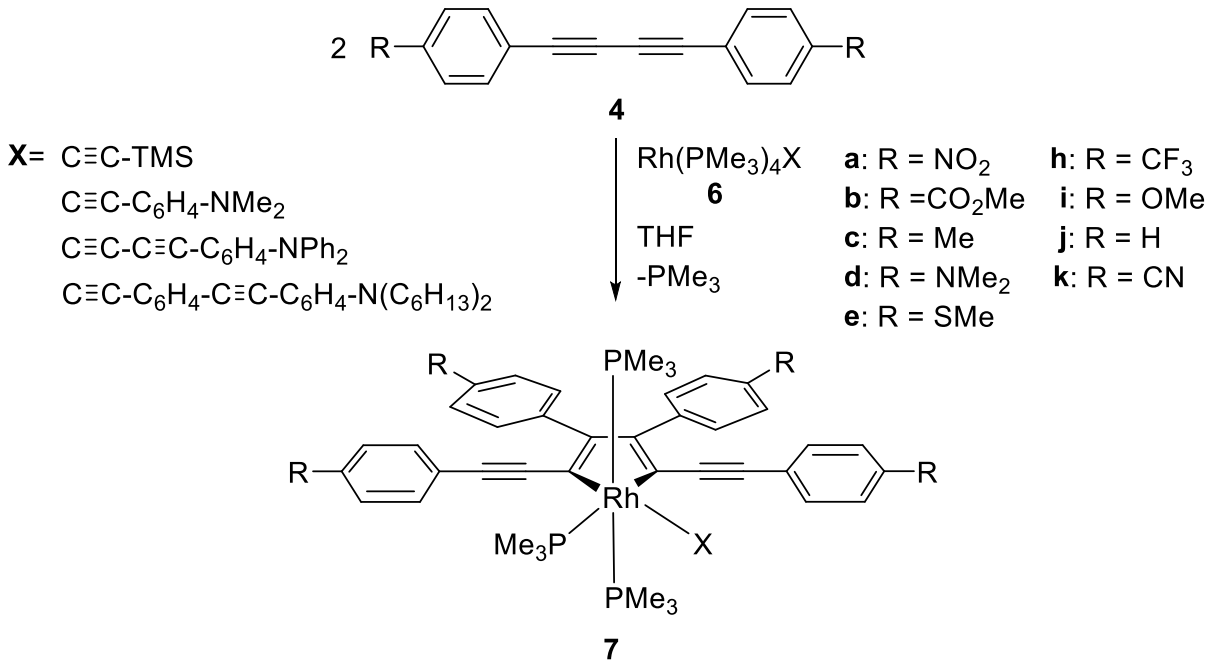


**Scheme 29** Regiospecific formation of 2,5-bis(arylethynyl)rhodacyclopentadienes **7a-j**.[68]

The *p*-R'-phenyl-1,3-butadiynes substituted with donor groups reacted slower than the diynes having an electron acceptor substituent. Marder *et al.* mentioned that this effect might be caused by decreased $\pi$-back bonding from the electron-rich Rh(I) centre in the precursor bis(diyne) complexes when donor-substituted diynes were used.[67,68]

Investigations of the photophysical properties showed that exchanging the TMS group by 4-$Me_2NC_6H_4$ on the acetylide ligand has very little influence on the shift in the absorption and

emission maxima. A reason for that might be due to CH---HC interactions between phenyl ring **V** and the phenyl ring **VI**. These interactions cause a rotation of the s-bound phenylacetylide group out of the metallacycle plane (Figure 8).

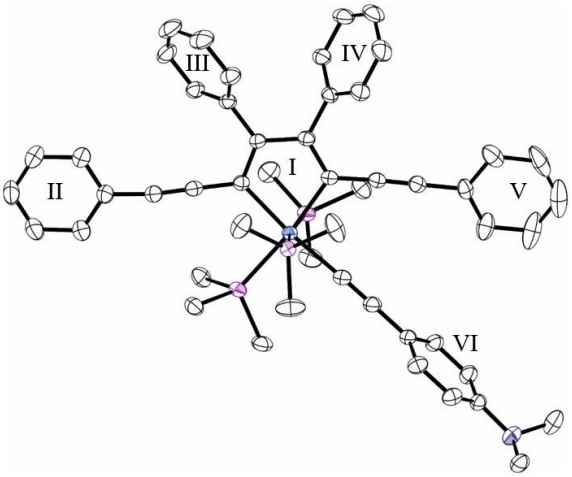


**Figure 8** Molecular structure of rhodacyclopentadiene **7j** with the acetylide ligand 4-$Me_2NC_6H_4$-C≡C (CCDC number: 171634).[68]

In addition, the introduction of further alkynyl-groups (Scheme 30) to elongate the conjugation system had very little influence on the absorption and emission spectra of the rhodacyclopentadienes. A molecular modelling study showed that the two alkynyl-groups, which were expected to result in co-planarity of the aryl rings, prevent the desired co-planarity due to steric hindrance, which came from the *p*-phenylene ortho-hydrogen atoms of the -C≡C-C≡C-(*p*-$C_6H_4$-$NPh_2$)-ligand and the aryl ring on the metallacyclopentadiene.[68]
In addition, compounds with longer conjugated chains at the *para*-positions of the aryl-rings were generated, to investigate the liquid crystal behaviour of the rhodacyclopentadienes. (Scheme 30, **9a-c**). Unfortunately, no liquid crystal behaviour was observed. Furthermore, the influence of the longer conjugation on the photophysical behaviour was examined.[66] Changing the substituents at the *para*-positions of the phenyl rings to longer conjugated chains, caused a bathochromic shift in the absorption and emission spectra and the values of the extinction coefficients were also clearly increased.

The emission lifetimes are, with a nanosecond time scale, comparable to those obtained from the former rhodacyclopentadienes (**7a-k**), which suggest a comparable excited state behaviour. Unfortunately, measuring the quantum yields results in very low values of 0.01-0.03, caused by effective non-radiative decay, which might result from additional vibrational modes.

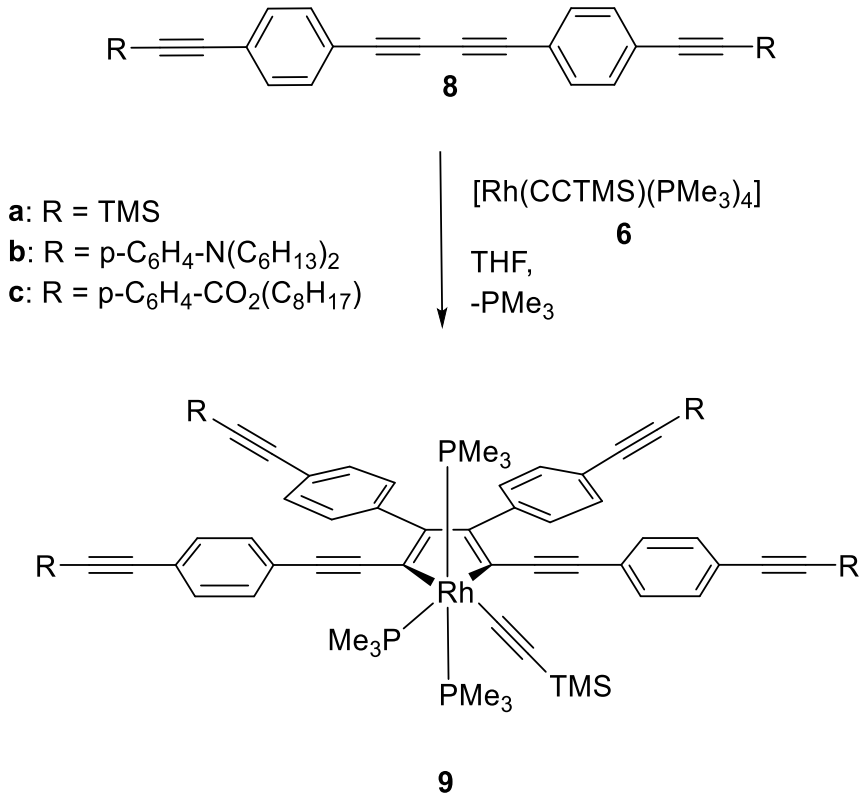


**Scheme 30** Synthesis of 2,5-bis(arylethynyl)rhodacyclopentadienes **9a-c** bearing conjugated groups at the *para*-position of the phenyl rings.[68]

Reductive coupling of the 1,4-bis(*p*-R´-phenyl)-1,3-butadiynes (R = $CO_2Me$, $CF_3$, Me, SMe, OMe, H) also occurred starting from the compound [$RhMe(PMe_3)_4$] (**6-Me**), yielding the corresponding methyl rhodacyclopentadienes (**10b-j**, Figure 9).[68]

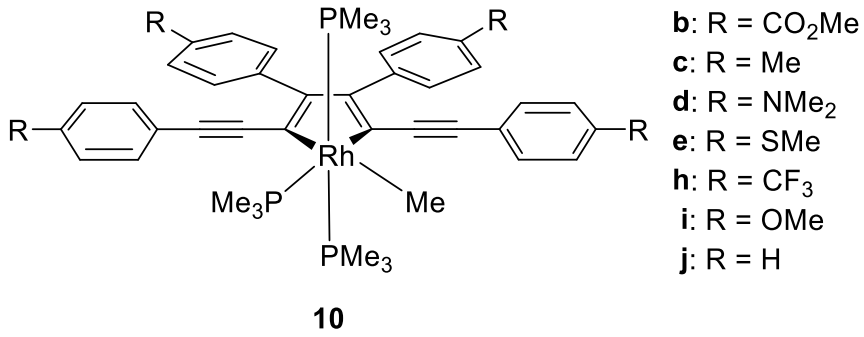


**Figure 9** Structures of compounds **10b-j**.[66]

Chloro derivatives of the rhodacyclopentadienes were observed when the Me-rhodacyclopentadiene was treated with HCl (**11**, Figure 10).[68]

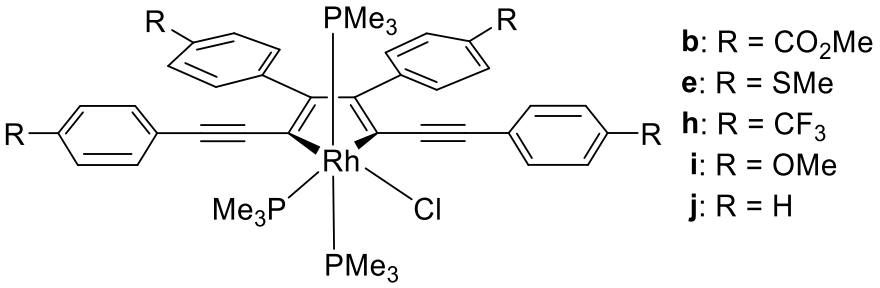


**11**

**Figure 10** Structure of compounds **11b-j**.[68]

If the TMS groups are removed at the peripheral $C_6H_4$-C≡C-TMS positions of **9a** with the use of TBAF in THF, the -C≡C-TMS ligand bound to the rhodium centre stays intact, which leads to compound **12** (Figure 11).

This demonstrates the chemical stability of the rhodacyclopentadienes. Furthermore, **7a-k** (X = -C≡C-TMS and -C≡C-*p*-$C_6H_4$-$NMe_2$) are extraordinarily robust and insensitive to air and moisture in the solid state. Compounds **7a, b** and **k** (X = -C≡C-TMS and -C≡C-*p*-$C_6H_4$-$NMe_2$), bearing acceptor substituents, are even stable to air and moisture in THF or toluene solution for months.

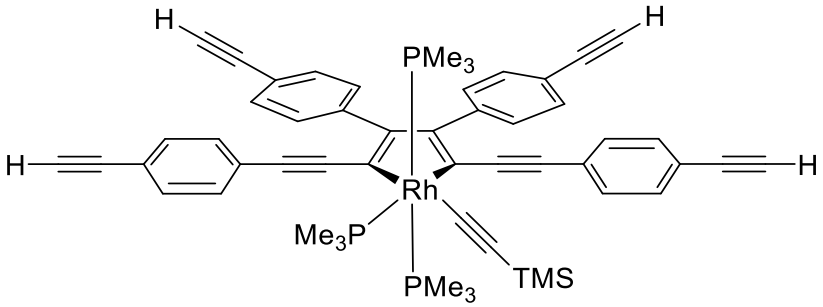


**12**

**Figure 11** Structure of **12**, after deprotection of peripheral TMS-groups.[68]

Compounds **7a-k** (X = -C≡C-C≡C-(*p*-$C_6H_4$-$NPh_2$) and -C≡C-$C_6H_4$-C≡C-$C_6H_4$-$N(C_8H_{13})_2$), **9a-c** and **12**, which are substituted with longer conjugated groups are, for some reason, sensitive to air and moisture, whereas **7k** ( X = -C≡C-$C_6H_4$-C≡C-$C_6H_4$-$N(C_8H_{13})_2$) and **12** seem to be photochemically unstable.[69] Following the work of Marder *et al.*, Hill and co-workers also reported a regioselective synthesis of the ruthenacyclopentadiene [Ru{$\kappa^2$-(Ph-C≡C)=C-Ph-C-Ph=(C≡CPh)}$(CO)_2(PPh_3)_2$].[70]

During the reaction only the formation of the 2,5-alkynyl isomer took place. The reaction works with $[Ru(CO)_2(PPh_3)_3]$ and an excess of diphenylbutadiyne. Optical properties of the compound generated were not investigated (Figure 12).[70]

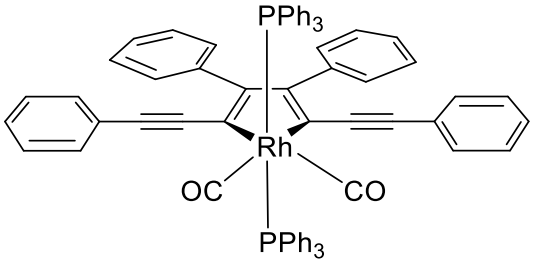


**Figure 12** Structure of $[Ru\{\kappa^2\text{-}(Ph\text{-}C\equiv C)=C\text{-}Ph\text{-}C\text{-}Ph=(C\equiv C\text{-}Ph)\}(CO)_2(PPh_3)_2]$.[70]

Marder *et al.* also succeeded in the synthesis of more rigid conjugated 2,5-bis(*p*-R-arylethynyl)rhodacyclopentadienes by the reaction of the $[Rh(C\equiv C\text{-}TMS)(PMe_3)_4]$ or $[Rh(\kappa^2\text{-}S,S`\text{-}S_2CNEt_2)(PMe_3)_2]$ precursors with 1,12-diaryldodeca-1,3,9,11-tetraynes (Scheme 31).[71,72]

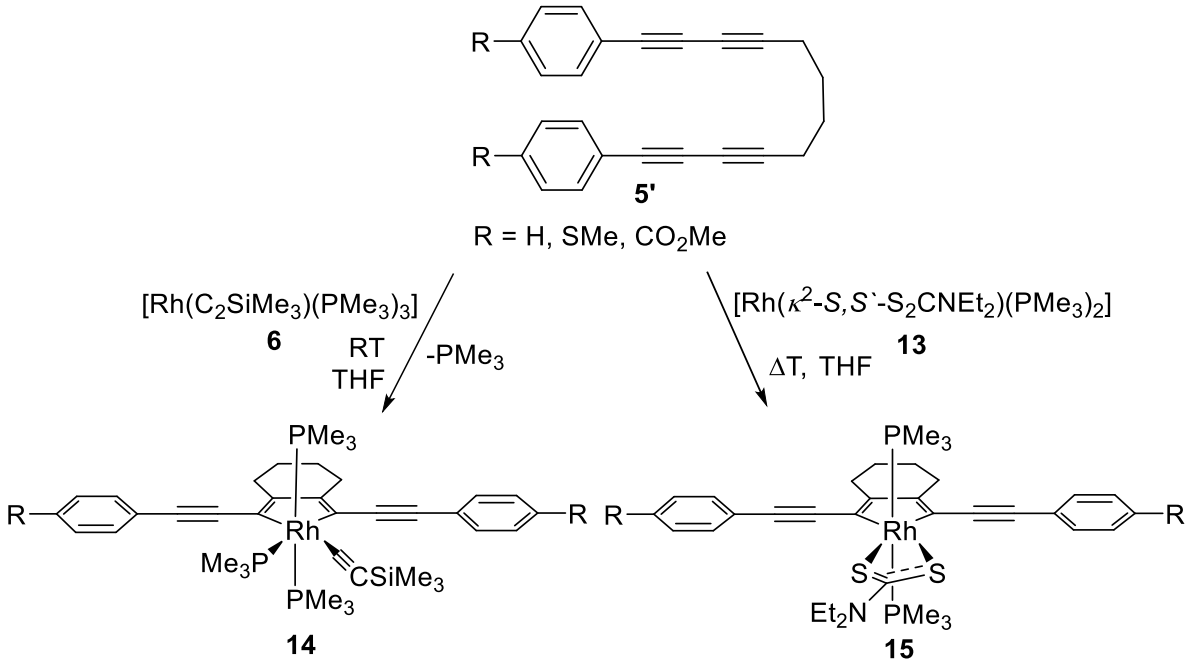


**Scheme 31** Formation of compounds **14** and **15** *via* reductive coupling of a bis-diyne.[71,72]

These systems were generated to suppress the additional vibrational motion, which was caused by the aryl groups at the 3,4-positions of the metallacyclopentadiene moiety. This allowed the quantum yield of the rhodacyclopentadienes to increase significantly. The strong electron donating ligand $S,S´\text{-}S_2CNEt_2$ was introduced to carry out further investigations on the photophysical behaviour, clarifying the role of the metal centre upon excitation.

DFT calculations showed that, due to the energetic levels of the ligand-based highest occupied molecular orbital (HOMO) and lowest unoccupied molecular orbital (LUMO) and the metal-centred orbitals, which are well separated from each other (~ 1 eV), the rhodium only seems to play a minor role in the excitation processes. Thus, the conjugated organic ligand $\pi$-system seems to win control over the excited state photophysical behaviour (Figure 13). [72]

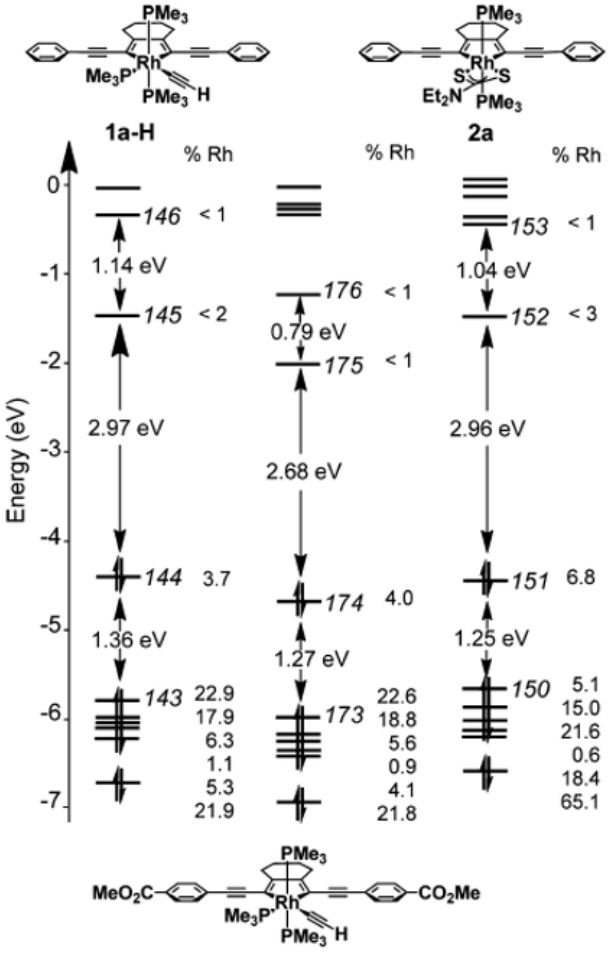


**Figure 13** Calculated orbital energies for different rhodacyclopentadienes. Reprinted from reference [72] with friendly permission of the American Chemical Society.[72]

In conclusion, the lowest excited states $S_1$ and $T_1$ are dominated by a ligand-based HOMO-LUMO transition. In combination with the cumulenic distortion of the $T_1$ state an "organic-like" photophysical behaviour is observed.[72]

Besides the photophysical aspects, changing the ligand from a monodentate one to the bidentate ligand *S,S´*-$S_2CNEt_2$ should provide a way of getting a better idea of the mechanism of the formation of the rhodacyclopentadienes. The results concerning the reaction-behaviour of Rh-complexes containing this ligand will be discussed in detail in Chapter 2.2.

As part of investigations on systems with strongly electron donating, bidentate ligands at the metal centre, acetylacetonate was introduced. Surprisingly, reactions with this ligand led not only to the expected symmetrical rhodacyclopentadienes, but also to a second product, which turned out to be a dibenzorhodacyclopentadiene (Scheme 32).[73]

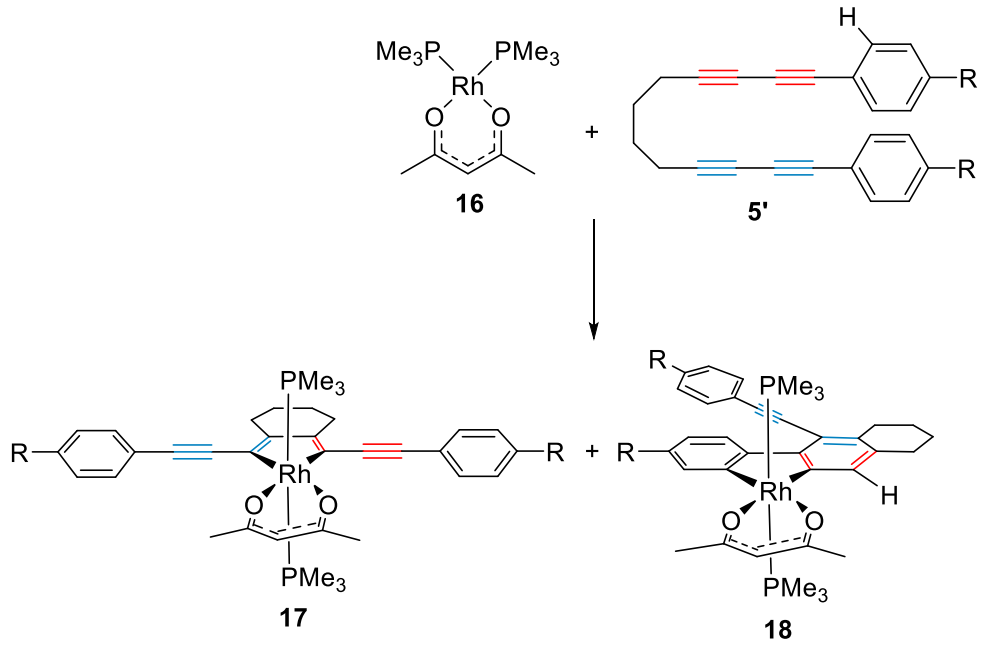


**Scheme 32** Synthesis of compound **17** *via* reductive coupling of **5'** and generation of compound **18**.

Complex **18** is apparently generated by an ortho C-H-activation in combination with a [4+2]-cycloaddition of the acetylene moieties (Scheme 33).[73]

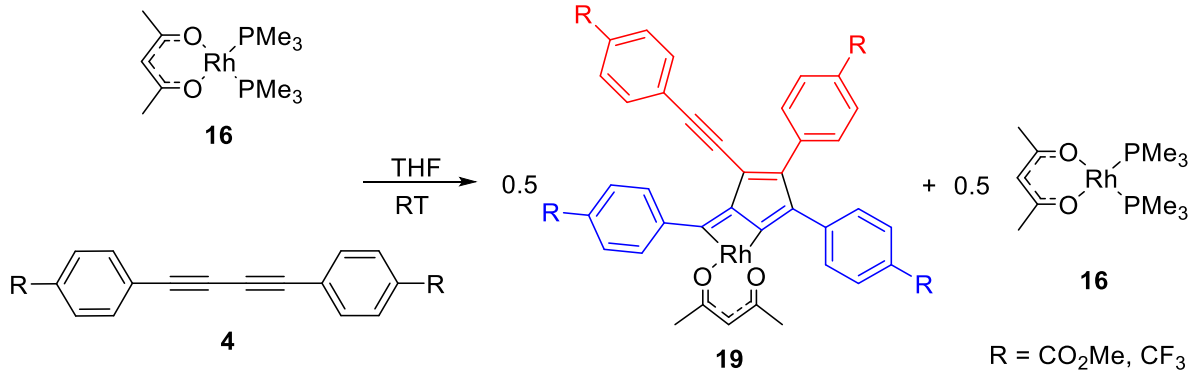


**Scheme 33** Synthesis of compound **19**.[73]

Additional studies showed that the reductive coupling of two equivalents of diarylbutadiyne at the metal centre bearing the acetylacetonate ligand (**16**), leads to another type of unsymmetrical complex **19**, namely that arising from a novel [3+2] cycloaddition. Further investigations to clarify the mechanisms of these reactions are in progress.[73]

### 2.1.4 General Routes to Dibenzometallacyclopentadienes

Various synthetic routes are known for preparing dibenzometallacyclopentadienes, also known as metal-biphenyl complexes, containing Co, Ni, Pd, Pt, Ir and Rh.[74-82] Throughout this chapter, they will be called metal-biphenyl complexes.

The main synthetic route for the formation of metal-biphenyl complexes is the direct insertion of a nucleophilic metal centre into the four-membered ring of biphenylene, which is favourable as the ring is very strained. The C-C bond is cleaved through an oxidative addition to a low valent metal centre (Scheme 34).[74,75,77,79-81]

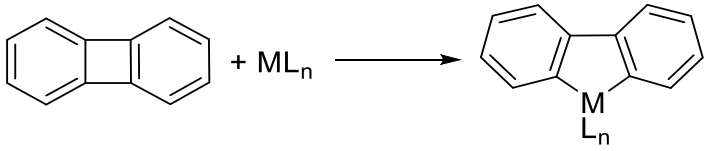


**Scheme 34** Building of metal-biphenyl complex *via* direct insertion.[76]

Jones and co-workers reported the reaction of [RhH(Ph)(Cp*)($PMe_3$)] with 1.5 equivalents of biphenylene in cyclohexane-$d_{12}$ at 85 °C yielding [RhH(1-bph)(Cp*)($PMe_3$)] as the main product (Figure 14).[81]

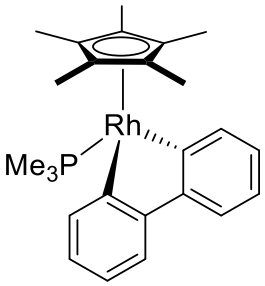


**Figure 14** Structure of [RhH(1-bph)(Cp*)($PMe_3$)].[81]

Additionally, [Ph(2,2'-bph)(Cp*)($PMe_3$)] could only be obtained in small amounts. However, when the main product was heated to higher temperature it was completely converted to the desired [Rh(2,2'-bph)(Cp*)($PMe_3$)].

They further reported the synthesis of the bimetallic complex [$(Cp^*)_2M_2$(bph)] obtained from [MCp*($\eta$-$C_2H_4)_2$] and biphenylene (M = Co, Rh).[81] During the reaction, the first [Cp*M] unit was inserted into one of the C-C-biphenylene bonds, whereas the second one binds *via* $\eta^5$-coordination to the newly generated metallacycle.

Heating the Rh analogue to 120 °C under a CO atmosphere led to a mixture of two monomeric species, the first one being [Cp*Rh(bph)(CO)] and the second one being [Cp*Rh$(CO)_2$] (Scheme 35).

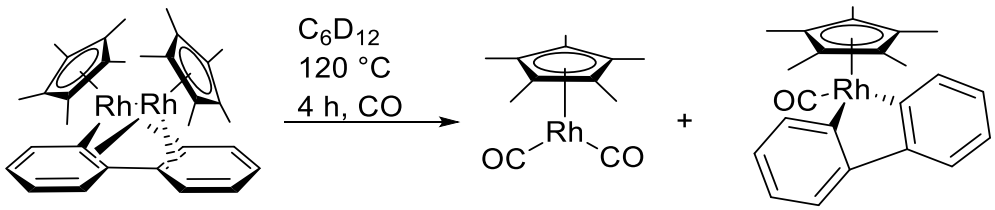


**Scheme 35** Synthesis of a Rh 2,2'-bph complex from a bimetallic starting material.[81]

Photolysis of the biphenylene and [RhCp*($\eta$-$C_2H_4$)$_2$] yielded the product within three days, whereas the reaction starting from the above mentioned side-product [Cp*Rh(CO)$_2$] under thermal condition was unsuccessful.

The analogous reaction with the Co derivative leads to the same products, but the insertion product was reported to be unstable. They obtained a 2:1 mixture of [Cp*Co(CO)$_2$] and fluorenone when the Co analogue was heated under a CO atmosphere, but no biphenyl complex could be observed (Scheme 36). The structures of both the Co and the Rh starting materials were determined *via* X-ray crystallography.

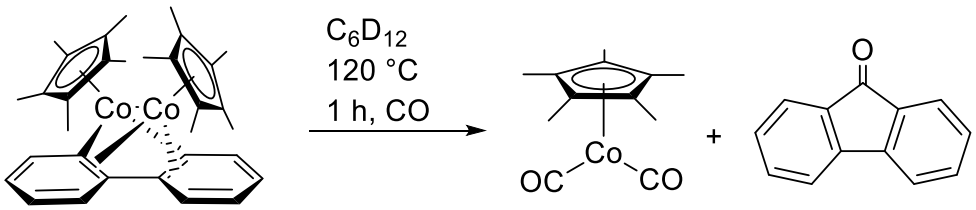


**Scheme 36** Formation of fluorenone from bimetallic bph Co complex.[81]

The authors also reported that the bimetallic Rh and Co species do not react with hydrogen even at elevated temperatures or under $H_2$-pressure.[81]

Crabtree *et al.* reported the synthesis of a dimeric chloride-bridged 2,2'-bph Ir complex arising from [Ir(COD)Cl]$_2$ and biphenylene. It reacted with $PPh_3$ yielding the 16-electron Ir(III) biphenylene adduct, [IrCl(2,2'-bph)($PPh_3$)$_2$]. However, when the reaction was repeated with the smaller and more electron donating phosphine $PMe_3$, the 18-electron compound [IrCl(2,2'-bph)($PMe_3$)$_3$] was obtained.[79,80]

The Ir(2,2')bph metallacycle was stable to various reagents to cleave the ring (CO, Ph-C≡C-Ph, $PR_3$, $NaBH_4$) except $NOBF_4$. After additional treatment with $NaBPh_4$ the unusual cationic Ir(IV)BF insertion product was obtained (Scheme 37).[79,80]

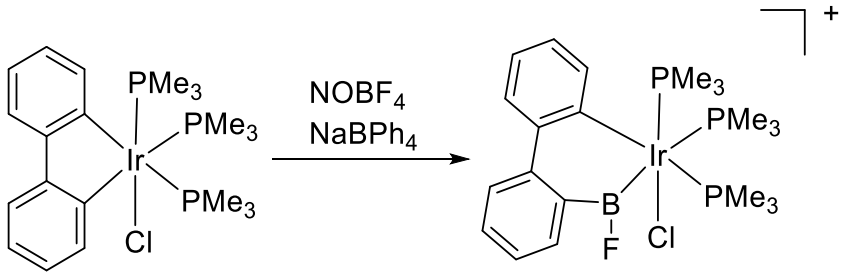


**Scheme 37** Reaction pathway to cationic Ir(IV)BF insertion product.[79,80]

More successful insertions took place between group 8 transition metals and biphenylene. The reaction of $[M_3(CO)_{12}]$ (M = Fe, Ru, Os) with biphenylene leads to major products of the type $[M_2(CO)_5(\mu\text{-}CO)(\mu\text{-}\eta^2\text{-}\eta^4\text{-}C_6H_4)_2]$ (M = Fe, Ru) and $[Os_2(CO)_6(\mu\text{-}\eta^2\text{-}\eta^4\text{-}C_6H_4)_2]$ (Scheme 38).[83]

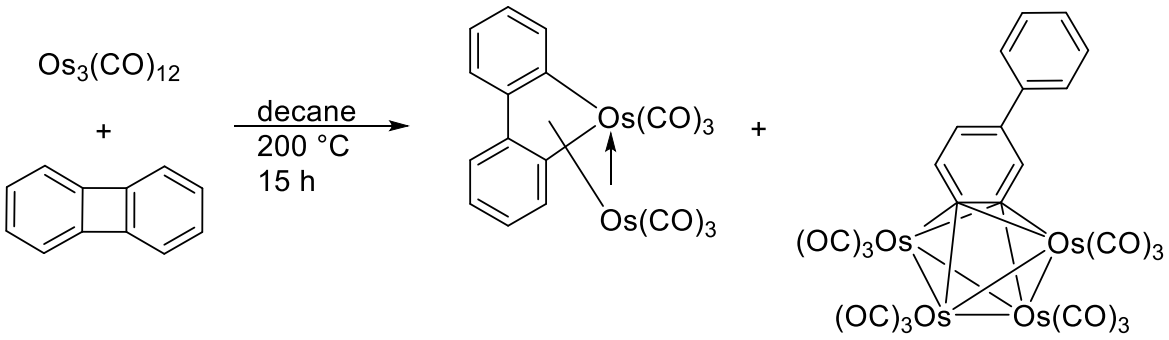


**Scheme 38** Insertion product of biphenylene and $[Os_3(CO)_{12}]$.[83]

Characterisation *via* X-ray crystallography was done for the Ru and Os analogues. Compared to Os, which is much less reactive, the reactions for Fe and Ru were complete within a few hours.

The reaction with the Co analogue was not complete after 15 hours even though it was heated to 200 °C under nitrogen in a sealed flask. This result fits well with stronger M-M and M-CO bonds in third row transition metal complexes in comparison to the transition metals of the first and second row.[83]

The synthesis of transition metal biphenyl complexes is also possible *via* transmetallation. A rather seldom used possibility reported by Rausch and co-workers in 1973, is the use of dilithiobiphenyls or biphenyl Grignard reagents. The reaction takes place between 2,2'-dilithiobiphenyl, prepared from 2,2'-dibromophenyl, and a metal dihalide. The metallacycle product results from the elimination of the lithium halide (Scheme 39).[84]

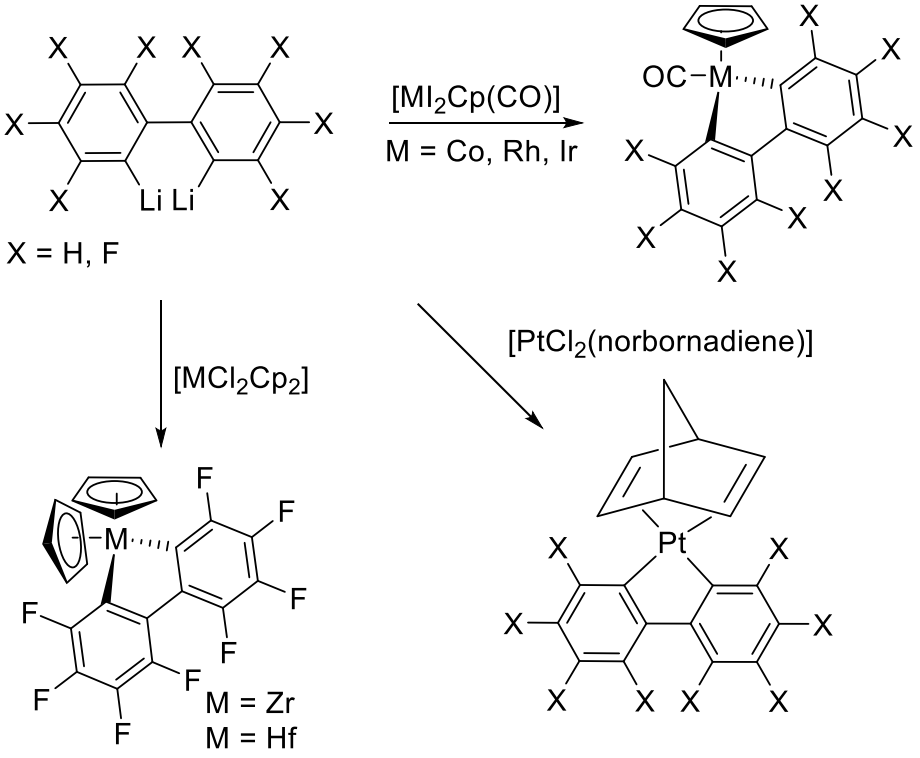


**Scheme 39** Synthesis of transition metal 2,2'-bph complexes with 2,2'-dilithiobiphenyl.[84]

The first Zr and Hf complexes were generated that way, as well as complexes with Co, Rh, Ir, Pt (Scheme 39).[84] Another possibility was reported by King and Hilton, who were able to generate the 2,2'-biphenyl complexes of Pd, Pt as well as the mono-, di- and tetra-anionic Zr complexes $[ZrCp(2,2'\text{-bph})_2]^-$ (a), $[ZrCp(2,2'\text{-bph})_3]^{2-}$ (b), $[ZrCp(2,2'\text{-bph})_4]^{4-}$(c), starting from $[ZrCl_2Cp_2]$ and 2,2'-dilithiobiphenyl (Figure 15).[85]

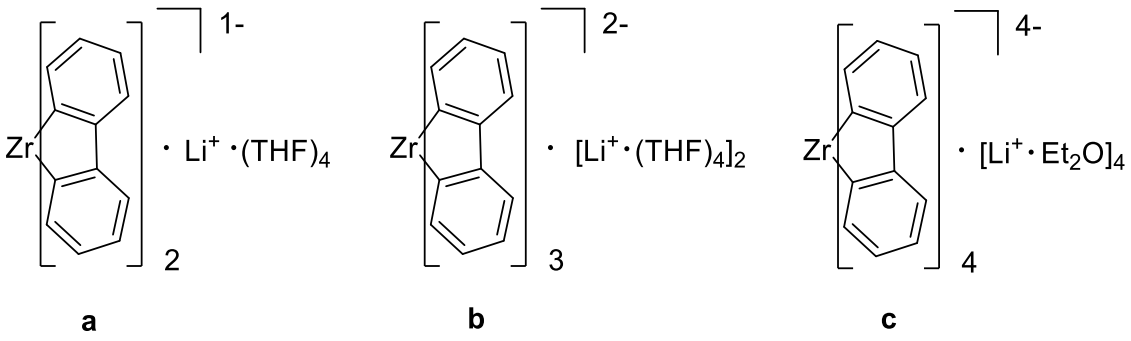


**Figure 15** Mono-, di- and tetraanionic Zr complexes.[85]

This route also appeared in the work of Romeo *et al.* as well as Rillema *et al.*, who synthesised Pt(2,2'-bph) complexes leading to two different results. Romeo *et al.* obtained the planar bridged species of $Pt_2(SEt_2)_2$,[86] whereas Rillema *et al.* obtained mononuclear [Pt(2,2'-bph)($CO_2$)] (Scheme 40).[87]

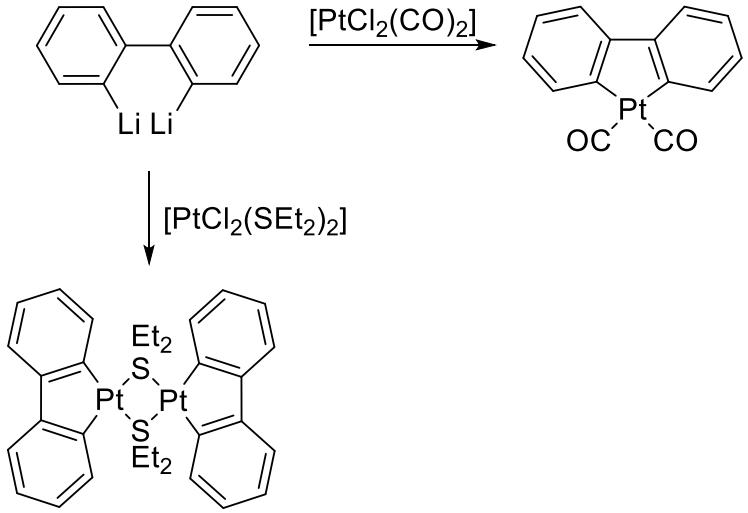


**Scheme 40** Examples of Pt(2,2'-bph) complexes formed from Pt chloride salts and 2,2'-dilithiobiphenyl.[87]

Romeo *et al.* noted further that the bridged complex (Scheme 40) can also be obtained *via* CH-activation from the dinuclear Pt(II) complex [$Pt_2(\mu$-$SEt_2)_2(Hbph)_4$], also generating biphenyl. To obtain the 2,2'-biphenyl complexes of Pd and Pt by direct insertion into the C-C bond, the strongly electron donating ligand $PEt_3$ is useful. If the weaker electron donor $PPh_3$ was used, the Pd and Pt complexes were unreactive to C-C bond cleavage. Other analogues can be synthesised by the combination of 2,2'-dilithiobiphenyl and [$PtCl_2(PPh_3)_2$].[86]

There also exist titanium analogues reported by Massey and Cohen in the 1960s, who synthesised [$TiCp_2$(perfluorobiphenyl)] from the 2,2'-octafluorobiphenyl dilithium salt.[88] Following that, the non-fluorinated analogue was reported by Rausch and Klemann.[89] The synthesis of a Ni(2,2'-bph) complex was carried out by Buchalski and co-workers.[90]

Besides syntheses involving a transmetallation process, there are other routes to generate transition metal biphenyl complexes. Jones *et al.* synthesised Pt(2,2'-biphenyl) complexes from a direct conversion of $CF_3$-substituted biphenyls (Scheme 41).[91]

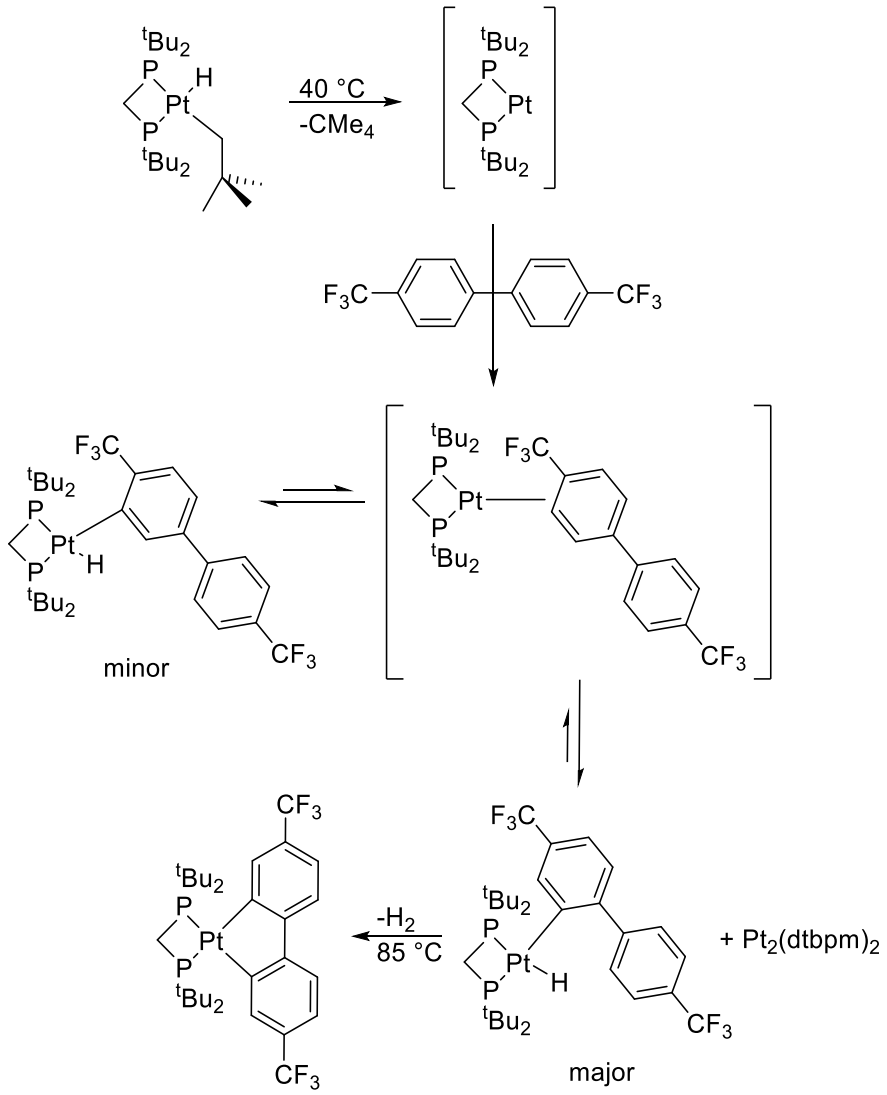


**Scheme 41** Pt(2,2'-biphenyl) complexes from a direct conversion of $CF_3$-substituted biphenyls.[91]

Wakatsuki and co-workers reported that the reaction of four equivalents of sodium fluorenone ketyl with $[Ir(Cp^*)Cl(\mu\text{-}Cl)]_2$ in THF gives the decarbonylated product [Ir(Cp*)(CO)(2,2'-bph)] in 70% yield, accompanied by free fluorenone (Figure 16).

The reaction includes a reduction of the Ir(III) complex to "IrCp", which is followed by an insertion into one of the C-C(O) bonds of fluorenone, and then a migratory elimination of CO.[78]

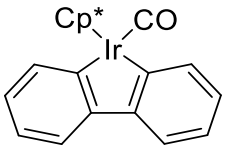


**Figure 16** Structure of [Ir(Cp*)(CO)(2,2'-bph)] *via* decarbonylation of sodium fluorenone ketyl.[78]

### 2.1.5 [EC4] Main Group Derivatives

Many studies have been carried out on main group heterocyclopentadienes, including siloles, phospholes and thiophenes (Figure 17). As they have a similar structural and photophysical properties to the rhodacyclopentadienes, a short overview over their synthesis and investigations of their photophysical properties will be given.

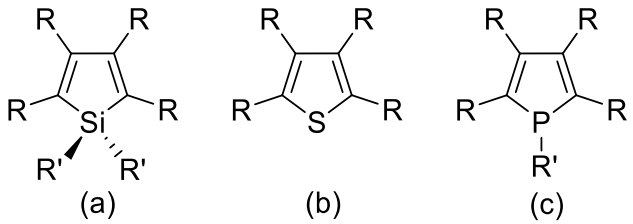


**Figure 17** Examples of different main group pentadienes analogues.

Due to the electron delocalisation in siloles ($\sigma^*$-$\pi^*$ conjugation), which causes the LUMO energy to be extremely low making them electron poor, they show unique electronic properties. For example, 2,5-di(2-pyridyl)silole served as an electronic transporting layer in organic electroluminescent devices.[92] The synthesis of siloles offers many possibilities. A major contribution was made by Tamao and co-workers who treated bis(phenylethynyl)silane with an excess of lithium dihydronaphthylide to obtain a 2,5-dilithiosilole.[93]

This very useful bis(anion), formed *via* an intramolecular reductive cyclisation (Figure 18), serves as a starting material for various derivatives.

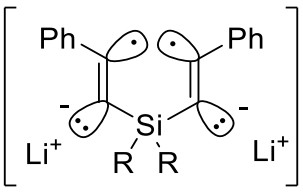


**Figure 18** Bis(anion radical) species, stabilised by two phenyl groups.[93]

Another possibility is the direct reaction starting from dimethyl-bis(phenylethynyl)silane. Following the procedure in Scheme 42, Pagenkopf *et al.* synthesised different luminescent 2,5-bis(phenylethynyl)-3,4-biphenyl-siloles in moderate yields (Scheme 42).[94]

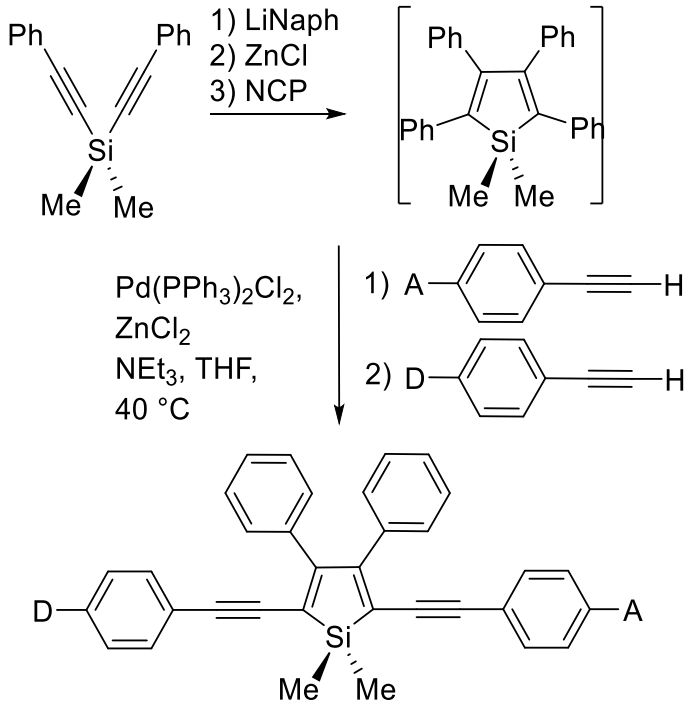


**Scheme 42** Synthetic route to donor-acceptor $\pi$-substituted siloles.[94]

The obtained compounds exhibited properties, which show a close relation to the donor-acceptor bis(phenylethynyl)benzenes prepared and investigated previously by Marder *et al*.[22,95,96] They show absorption as well as emission in the visible region. The absorption and emission maxima of the different compounds depended on the different donor- and acceptor substituents of the chromophore. In addition, the compounds showed a bathochromic shift in absorption and emission, increasing with the polarity of the solvent, which indicates the charge-transfer character of the molecule.

Bis(phenylethynyl)thiophenes (BPETs) also have been synthesised, and for that catalytic, cross-coupling using terminal alkynes[97-101] or alkynyl Grignard[102] reagents in combination with dihalothiophenes *via* Sonogashira or Kumada-Tamao reaction conditions turned out to be the methods of choice (Scheme 43).

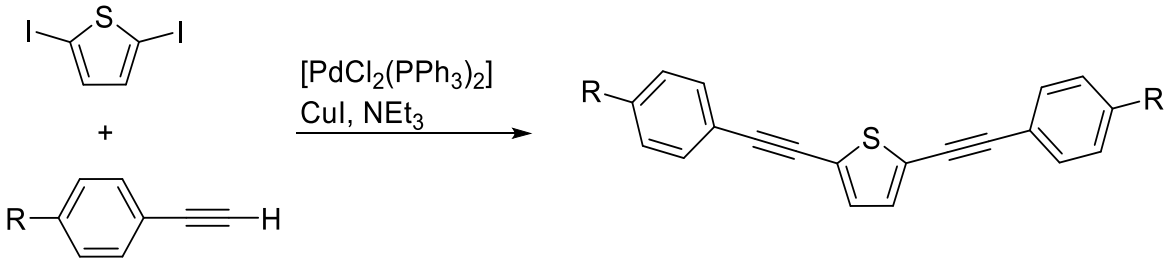


**Scheme 43** Pd/Cu-catalysed synthesis of bis(phenylethynyl)thiophenes.[101]

Pd-catalysed cross-coupling reactions were also used to generate BPETs in good yields starting from triorganoindium compounds in combination with 2,5-dibromothiophene.[103] Successful formation of symmetrical and even unsymmetrical BPETs has been achieved through a one-pot synthesis using benzyl sulfone derivatives and 2-formyl-5-phenylethynylthiophene (Figure 19).[104]

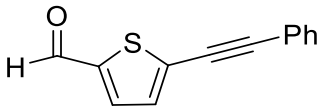


**Figure 19** Structure of 2-formyl-5-phenylethynylthiophene.[104]

The reported thiophene derivatives also show interesting luminescence as well as non-linear optical properties.[97-101], [105-108] As the alkyne residue is slightly bent due to the nature of the thiophene moiety, those systems also show interesting liquid crystal phase behaviour.[109-112]

To investigate the photophysical properties of 2,5-bis(arylethynyl)thiophenes, Marder *et al.* performed some UV/Vis and fluorescence measurements. They recorded the absorption maxima for the $\pi \rightarrow \pi^*$ transitions between 350 and 387 nm. Emission maxima appear between 382 and 435 nm depending on which substituent R was attached to the benzene rings. Photoluminescence measurements resulted in quantum yields of $\phi = 0.19 – 0.33$, and lifetimes of $\tau = 0.21 – 0.40$ ns, which indicates fluorescence.[101]

With the focus on the non-linear optical properties and on the optical power limiting of 2,5-bis(arylethynyl)thiophenes, Eliasson and Norman *et al.* theoretically and experimentally investigated their one- and two-photon excitations.[113]

Materials based on these thiophenes can find application in all optical signal processing, including fast switching from high transparency for normal light or low laser power to non-transparency at high laser power. A strong interest in this research field is the use of non-linear absorption for eye-protection or various types of sensors in optical equipment of laser beams which operate at wavelengths in the visible region.[113]

Although for phospholes a similar photophysical behaviour would be expected, only a few investigations have been reported. The first synthesis of phospholes, coupled with arylethynyls in the alpha positions, was reported by Mathey and co-workers in 1996.[114]

The phospholes were prepared *via* Sonogashira coupling, starting from the alpha-iodophospholes and terminal acetylenes or *via* $S_N2$ reactions of alpha-lithiophospholes with alkynylsulfones (Scheme 44).

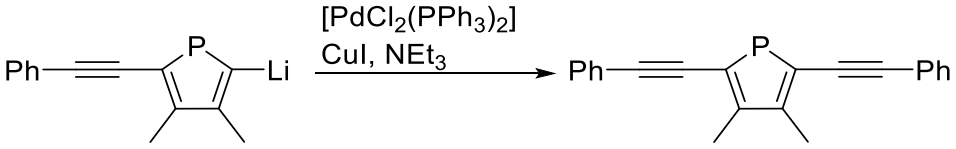


**Scheme 44** Synthesis of phospholes *via* 5-lithio-2-phenylethynylphospholes.[114]

In 2009, Matano and co-workers undertook further studies on the synthesis of phospholes. They were generated *via* a ring closure reaction with titanium and $PhPCl_2$ to give trimethylsilyl-capped 2-ethynyl-5-phenylphosphole or 2,5-diethynylphospholes followed by treatment with TBAF in THF, and further modification *via* Sonogashira reaction to couple the desired aryl halides yielding the 2-phenyl-5-(arylethynyl)- and the 2,5-bis(arylethynyl)phospholes. An oxidation in the last step generated the P-oxide products (Figure 20).[115]

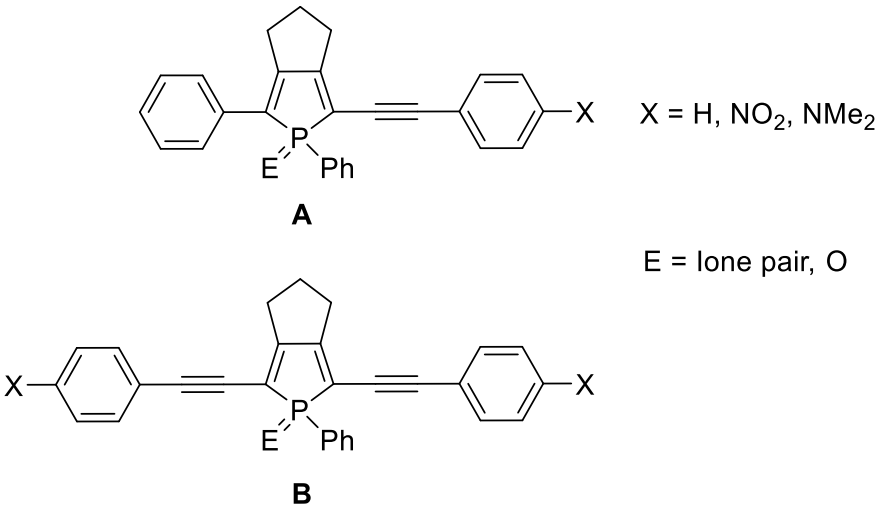


**Figure 20** 2-phenyl-5-(arylethynyl)phospholes **A** and 2,5-bis(arylethynyl)phospholes **B** and their corresponding P-oxides.[115]

Investigations on the photophysical properties of the phospholes showed that the $\pi \rightarrow \pi^*$ absorption appears between 385 and 411 nm for compound **A** and between 398 and 441 nm for compound **B**. The compounds were shown to be fluorescent with quantum yields of $\phi$ = 0.07 – 0.13 ($\lambda_{em}$ = 462-515 nm) for **A** and comparable quantum yields for **B** with $\phi$ = 0.09 – 0.13 ($\lambda_{em}$ = 449 – 518 nm). Charge transfer from the donor group R = $NMe_2$ to the phosphole moiety in the excited state was indicated by a large Stokes shift.[115]

.

## 2.2 Results and Discussion

### 2.2.1 Motivation and Aims

The promising results concerning the regioselective formation of rhodacyclopentadienes, reported by Marder *et al.* (Chap. 2.1.3), provided the motivation for the synthesis and characterisation of new luminescent rhodacyclopentadienes. Therefore, the focus was put on [Rh($\kappa^2$-*S*,*S*`-$S_2CNEt_2$)($PMe_3$)$_2$] as a precursor complex containing dithiocarbamate as a bidentate ligand, which is a good $\pi$- and $\sigma$-donor. To obtain rhodacyclopentadienes, a variety of 1,11-undecatetraynes were reductively coupled to the Rh(I)-centre. This did not only lead to the desired target complexes, but also to an isomeric compound, namely a dibenzorhodacyclopentadiene.

For further studies, a new precursor complex [Rh($\kappa^2$-*S*,*S*`-$S_2CNEt_2$)($PPh_3$)$_2$] was prepared, having the $PMe_3$ ligand replaced by $PPh_3$, which is a weaker $\sigma$-donor than $PMe_3$, and thus should dissociate more easily. As can be seen in the following, the exchange of the phosphine ligand changes the reaction behaviour of the starting complex significantly and gives rise to a new reaction pathway, forming not only the rhodacyclopentadienes, but also strongly luminescent organic dimers and trimers. The exchange of the phosphine ligand and the bidentate ligand on the already formed rhodacyclopentadienes was also investigated, yielding an alternative route to obtain some of the rhodacyclopentadienes or dibenzorhodacyclopentadienes more easily. Finally, the reactions of simple diaryl-1,3-butadiynes with a rhodium precursor were carried out, to obtain deeper insight into the mechanism of the formation of the rhodacyclopentadienes. Those diyne systems, in combination with the precursor complex [Rh($\kappa^2$-*S*,*S*`-$S_2CNEt_2$)($PMe_3$)$_2$], made it possible to isolate intermediate species in the process for rhodacycle formation, namely *trans* $\pi$-complexes. In the third part of this work, photophysical studies on all newly synthesised luminescent compounds are presented.

### 2.2.1 Synthesis of Rh(I)-Complexes

*Bis-trimethylphosphine-$\kappa^2$-S,S`-dithiocarbamate-rhodium(I)*[72]

[Rh($\kappa^2$-*S*,*S*`-$S_2CNEt_2$)($PMe_3$)$_2$] **13** was synthesised in a stepwise reaction starting from $RhCl_3 \cdot 3H_2O$ (Scheme 45). In the first step, the precursor complex $[Rh(COE)_2Cl]_2$ was formed by treating $RhCl_3 \cdot 3H_2O$ with cyclooctene (COE), following a literature procedure.[116] To synthesise $[Rh(PMe_3)_4]Cl$ **6-Cl**, the precursor complex $[Rh(COE)_2Cl]_2$ was suspended in dry and degassed THF and heated to 35 °C. Subsequently, 10 equivalents of $PMe_3$ were added dropwise to the solution (Scheme 45). When adding $PMe_3$, the product precipitated as an orange solid. To isolate the product, the reaction mixture was filtered, and the solid was washed several times with dry diethyl ether and finally dried *in vacuo*.[117]

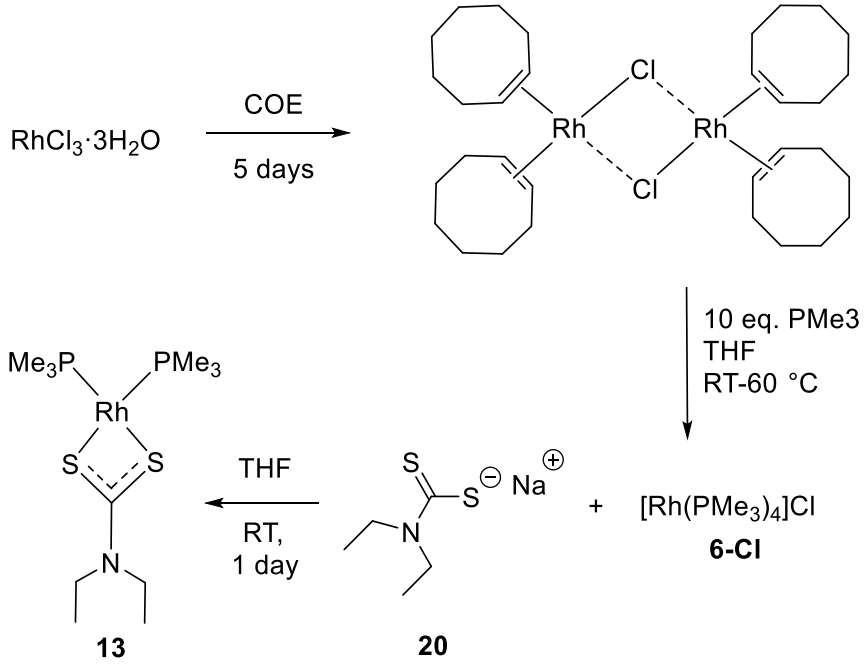


**Scheme 45** Stepwise synthesis of [Rh($\kappa^2$-*S*,*S*`-$S_2CNEt_2$)($PMe_3$)$_2$] **13**.

Sodium dithiocarbamate was synthesised following a modified literature procedure using carbon disulphide and diethylamine.[118] Nevertheless, it has to be noted that the compound used for this work was synthesised in distilled water instead of ethanol. After sodium hydroxide was dissolved in water, the basic solution was cooled to 0 °C and diethylamine was added. Afterwards, carbon disulphide was added dropwise to the solution, resulting in a yellow solution. The product precipitated subsequently as a colourless, crystalline solid. The mixture was allowed to warm to room temperature with stirring for another 2 hours. After the reaction was finished, the sodium dithiocarbamate was collected by filtration, washed with ethyl acetate and hexane and air dried. The product was obtained as a colourless, crystalline solid. In the final step, compounds **6-Cl** and **20** were dissolved in THF and the reaction mixture was stirred

overnight at ambient temperature. After starting the reaction, sodium chloride precipitated immediately, which was separated by filtration over celite from the solution when the reaction was finished. The remaining deep orange solution was evaporated *in vacuo* to give the product as a yellow powder.

*Crystal structure of [Rh($\kappa^2$-S,S`-$S_2CNEt_2$)($PMe_3$)$_2$] (**13**)*

Single crystals of compound **13** were grown in a small glass vial by slow diffusion of a hexane layer into a THF solution at -30 °C. Analysis *via* X-ray diffraction showed monoclinic crystals with the space group: $P2_1/c$ (Figure 21).

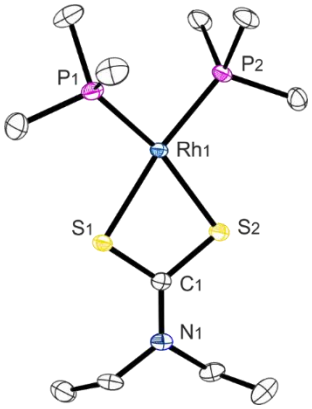


**Figure 21** Molecular structure of [Rh($\kappa^2$-*S*,*S*`-$S_2CNEt_2$)($PMe_3$)$_2$] **13**. The second independent molecule in the asymmetric unit, hydrogen atoms and solvent molecules are omitted for clarity and thermal ellipsoids are shown at 50 % probability.

Due to the small bite angle (S1-Rh1-S2, 73.89(2)°) of the dithiocarbamate ligand, and the steric hindrance of the $PMe_3$ groups, compound **13** has a distorted square planar geometry. This is shown by the angles between P1-Rh1-P2, P1-Rh1-S1, P2-Rh1-S2 with values of 95.53(2), 94.07(2) and 96.55(2)°, respectively, all being over 90°. The S1-C1-S2 angle within the dithiocarbamate molecule has a value of 112.54(12)°.

This is in stark contrast to a comparable Rh(I)-complex already mentioned in Chap. 2.1.3, namely [($PMe_3$)$_2$Rh(acac)] **16**. In comparison to the small 4-membered ring formed, when dithiocarbamate is bound to the Rh-centre, acetylacetonate forms a 6-membered ring. The O1-Rh1-O2 angle of 88.02(5)° is significantly wider than the S1-Rh1-S2 angle of compound **13**, leading to a less distorted geometry and a significantly lower strain within the molecule.

The P1-Rh1 (2.2123(6) Å) and P2-Rh1 (2.2185(6) Å) bond lengths in compound **13** are similar to each other, but not identical. The P1-Rh1-S2 and P2-Rh1-S1 angles deviate from an ideal

angle of 180°, with values of 167.61(3) and 170.38(2)°, respectively. By comparison, the P1-Rh1 and P2-Rh1 bond lengths in compound **16**, with values of 2.1953(5) and 2.1950(4) Å, are similar and slightly shorter than those in compound **13**. The P1-Rh1-O1 and P2-Rh1-O2 angles are 175.28(3) and 173.53(3)°, respectively. The deviation from an ideal angle of 180° is significantly smaller than in **13**. The S1-Rh1 and S2-Rh1 bond lengths are similar, with values of 2.3812(6) and 2.3904(6) Å, respectively. In **16**, the O1-R1 and O2-Rh1 bond lengths are significantly shorter, being 2.0850(11) and 2.0867(10) Å. Table 5 lists important bond lengths and angles for compound **13**.

**Table 5** Overview over the important bond lengths and angles. $^{31}P\{^{1}H\}$ NMR shifts, Rh-P coupling constants and isolated yields of compounds **13** and **22**.

| | **Bond lengths (Å) and angles (°)** | |
|---|---|---|
| **Bond** | **13** | **22** |
| P1-Rh1 | 2.2257(8) | 2.2123(6) |
| P2-Rh1 | 2.2473(8) | 2.2185(6) |
| S1-Rh1 | 2.3542(8) | 2.3812(6) |
| S2-Rh1 | 2.3922(8) | 2.3904(6) |
| S1-C1 | 1.718(3) | 1.722(2) |
| S2-C1 | 1.715(3) | 1.727(2) |
| C1-N1 | 1.322(4) | 1.322(3) |
| P1-Rh1-P2 | 97.33(3) | 95.53(2) |
| P1-Rh1-S1 | 93.97(3) | 94.07(2) |
| P2-Rh1-S2 | 94.85(3) | 96.55(2) |
| S1-Rh1-S2 | 73.84(3) | 73.89(2) |
| S1-C1-S2 | 112.29(16) | 112.54(12) |
| P1-Rh1-S2 | 167.05(3) | 167.61(3) |
| P2-Rh1-S1 | 168.69(3) | 170.38(2) |
| **$^{31}P\{^{1}H\}$ NMR shift [ppm]** | -5 | 49 |
| **Coupling constant [Hz]** | 170 | 178 |
| **Isolated yield [%]** | 72 | 83 |

*Bis-triphenylphosphine-$\kappa^2$-S,S`-dithiocarbamate-rhodium(I) (**22**)* [119]

The corresponding Rh(I)-precursor with $PPh_3$ instead of $PMe_3$ as ligands, [Rh($\kappa^2$-*S*,*S*`-$S_2CNEt_2$)($PPh_3$)$_2$] **22**, was synthesised by the reaction of one equivalent of [($PPh_3$)$_3$RhCl] (**21**, Wilkinson's catalyst) with a slight excess of sodium dithiocarbamate, following the procedure for compound **13**. During the synthesis of Wilkinson's catalyst,[120] a certain amount of the dimeric species [Rh($PPh_3$)$_2$($\mu$-Cl)]$_2$ was obtained, but this did not hinder the following reaction as the desired dithiocarbamate complex **22** has only two phosphine ligands. To obtain complex **22**, both starting materials were dissolved in THF, and stirred overnight at ambient temperature, in an argon filled glovebox (Scheme 46). A small excess of sodium dithiocarbamate was used, because the $^{31}P\{^1H\}$ NMR spectrum showed a small amount of **21** remaining, when the reaction was performed with a 1:1 stoichiometry.

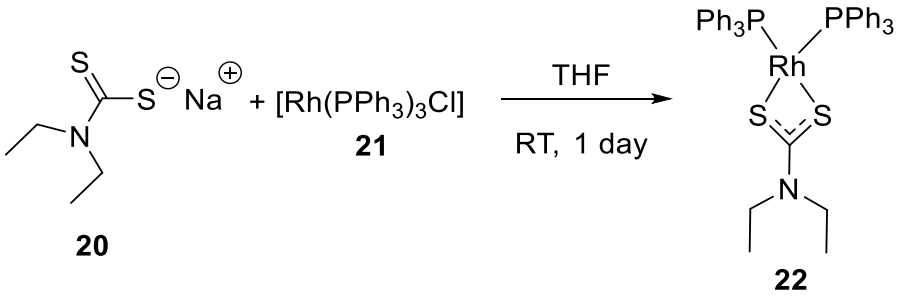


**Scheme 46** Synthesis of [Rh($\kappa^2$-*S*,*S*`-$S_2CNEt_2$)($PPh_3$)$_2$] **22**.

Addition of the sodium dithiocarbamate solution to **21**, dissolved in THF, led to a colour change of the reaction from dark red to a lighter red and sodium chloride precipitated subsequently. After the reaction was finished, the mixture was filtered through celite to remove the sodium chloride and the solvent was removed *in vacuo*. The crude product was recrystallised from THF / hexane at -30 °C to separate it from remaining phosphine and sodium dithiocarbamate. Deep orange crystals were obtained within minutes.

*Crystal structure of [Rh($\kappa^2$-S,S`-$S_2CNEt_2$)($PPh_3$)$_2$] **22***

Single crystals of **22** were grown in a small glass vial by slow diffusion of a hexane layer into a THF solution at -30 °C. Analysis *via* X-ray diffraction showed them to be monoclinic crystals with the space group being *P2$_1$/c* (Figure 22).

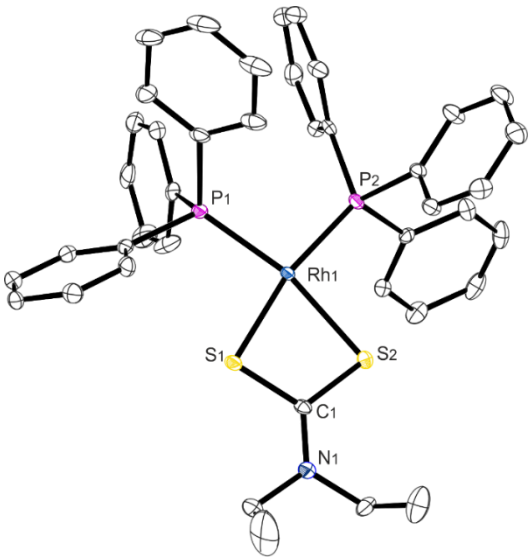


**Figure 22** Molecular structure of [Rh($\kappa^2$-*S*,*S*`-$S_2CNEt_2$)($PPh_3$)$_2$] **22**. Hydrogen atoms and solvent molecules are omitted for clarity and thermal ellipsoids are shown at 50 % probability.

As already mentioned for compound **13**, compound **22** also has a distorted square planar geometry, due to the small S1-Rh1-S2 bite angle with a value of 73.84(3)°. This is accompanied by the P1-Rh1-P2, P1-Rh1-S1 and P2-Rh1-S2 angles being 97.33(3), 93.97(3) and 94.85(3)°, respectively, all being over 90°. The S1-C1-S2 angle within the dithiocarbamate molecule has a value of 112.29(16) °. The P1-Rh1 (2.2257(8) Å) and P2-Rh1 (2.2473(8) Å) bond lengths are slightly different. As mentioned for **13**, this might be due to the P1-Rh1-S2 and P2-Rh1-S1 angles, which have different values of 167.05(3) and 168.69(3)°, respectively. Therefore, the *trans*-influences of the phosphines to S1 and S2 differ from each other, which causes a difference in the bond length. Also, the S1-Rh1 (2.3542(8) Å) and S2-Rh1 (2.3922(8) Å) bond lengths differ slightly. The S1-C1 and S2-C1 bond lengths are 1.722(2) and 1.727(2) Å, respectively.

The Rh-P bond lengths in **22** are slightly longer than those in compound **13**. This shows that the binding strength of $PPh_3$ to the Rh-centre is, as expected, weaker, probably due to its weaker $\sigma$-donor strength and larger size. The phosphine atom in $PPh_3$ is bound to an $sp^2$-hybridised carbon atom, which is more electronegative than the $sp^3$-hybridised carbon atom in $PMe_3$, as it has a higher percentage of S orbital-character. Table 5 shows all important bond lengths and

angles for compound **13** and **22**. Comparing the shifts and the coupling constants $J_{Rh-P}$ in the $^{31}P\{^{1}H\}$ NMR spectrum of compounds **13** and **22** with those of the analogous compounds having acac as the bidentate ligand, shows that the coupling constant $J_{Rh-P}$ of the acac-complex having $PMe_3$ as ligands is 186 Hz with a chemical shift of 7.41 ppm.[121] The coupling constant $J_{Rh-P}$ of the acac-complex having $P(tolyl)_3$ as ligands, which is comparable to $PPh_3$, is 195 Hz with a chemical shift of 54.9 ppm.[122] This means, that the compounds containing acac are in general shifted to lower field by 12 ppm and the Rh-P coupling constants are larger by about 15 Hz, with respect to compounds **13** and **22**. The low field shift of the acac compounds may be a result of the influence of the oxygen atoms in the acac ligand, which are more electronegative than the sulphur atoms of the dithiocarbamate ligand. It is not trivial to explain why the coupling constants of the Rh-acac complexes are, in general, larger than those of the Rh-dithiocarbamate complexes. The bidentate ligands clearly have an influence on the Rh-P coupling constant, which may be the result of electronic as well as structural factors, given by the very small bite angle of the dithiocarbamate ligand compared to acac.

### 2.2.2 Reactions of Undecatetraynes with [Rh($\kappa^2$-*S*,*S*`-$S_2CNEt_2$)($PMe_3$)$_2$]

To follow the reaction progress, test reactions on a scale of about 20 mg were set up in $C_6D_6$ or THF-$d_8$ and monitored by NMR spectroscopy over two weeks, with daily measurements, before they were performed on a larger scale. Reactions that were heated to higher temperatures were also monitored *via in situ* NMR. In contrast to those at ambient temperature, they were set up in a Young's NMR tube and heated between every measurement. The solutions underwent an immediate colour change from orange to brown or deep red. An exception is the reaction with compound **5a**. The reaction colour changed from orange to deep blue immediately, due to the strong electron withdrawing substituent (R = $NO_2$). The acceptor strength of $NO_2$ at the *para*-position of the aryl-ring of the 1,11-undecatetrayne causes a significant bathochromic shift of the absorption and emission of the rhodacyclopentadiene product, which will be discussed in detail in Chap. 3.2.

*Reactions at ambient temperature*

The reaction of different undecatetraynes with [Rh($\kappa^2$-*S*,*S*`-$S_2CNEt_2$)($PMe_3$)$_2$] at ambient temperature shows the selective formation of the expected rhodacyclopentadiene in a "normal" [2+2] cycloaddition reaction (Scheme 47).

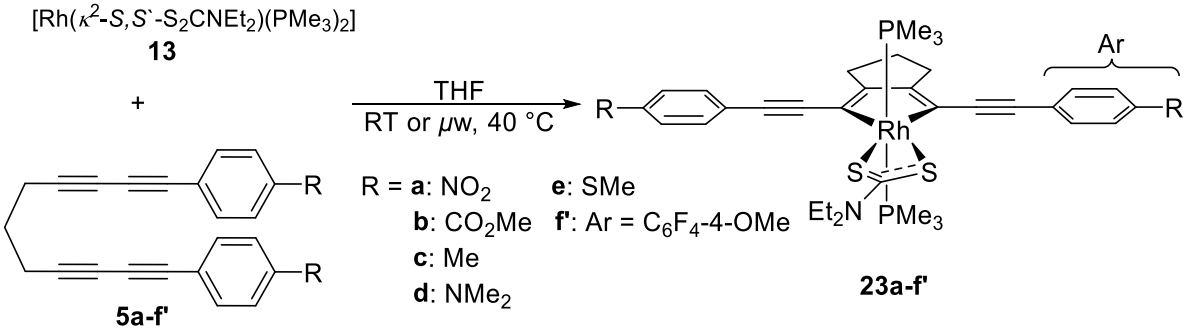


**Scheme 47** Generation of the rhodacyclopentadienes **23 a-f'** with a 5-membered ring in the backbone.

This, in fact, is structurally related to well established intermediates in metal-mediated alkyne cyclotrimerisation reactions.[38,123-126]

In general, substrates which are substituted with an electron withdrawing group react faster than substrates which are substituted with electron donating groups. The former ones pull electron density out of the system, and make the triple bonds less electron rich, favouring the $\pi$-backbonding and the oxidative addition to the Rh centre involved in the [2+2+M] cycloaddition

reaction. As reactions with undecatetraynes which are substituted with SMe and $NMe_2$ took about 2-3 weeks to show complete conversion to the product, test reactions in the microwave reactor at 40 °C for 15-24 hours were carried out, which also resulted in the formation of one main product and a significant enhancement of the reaction rate (24-48 hours). Reactions, which were carried out in the microwave were prepared in an argon-filled glovebox, using crimp-sealed vessels.

Figure 23 (spectrum of **23b**) shows an example of typical *in situ* $^{31}P\{^1H\}$ NMR spectra of the reaction after 1 day (top) and 10 days (bottom).

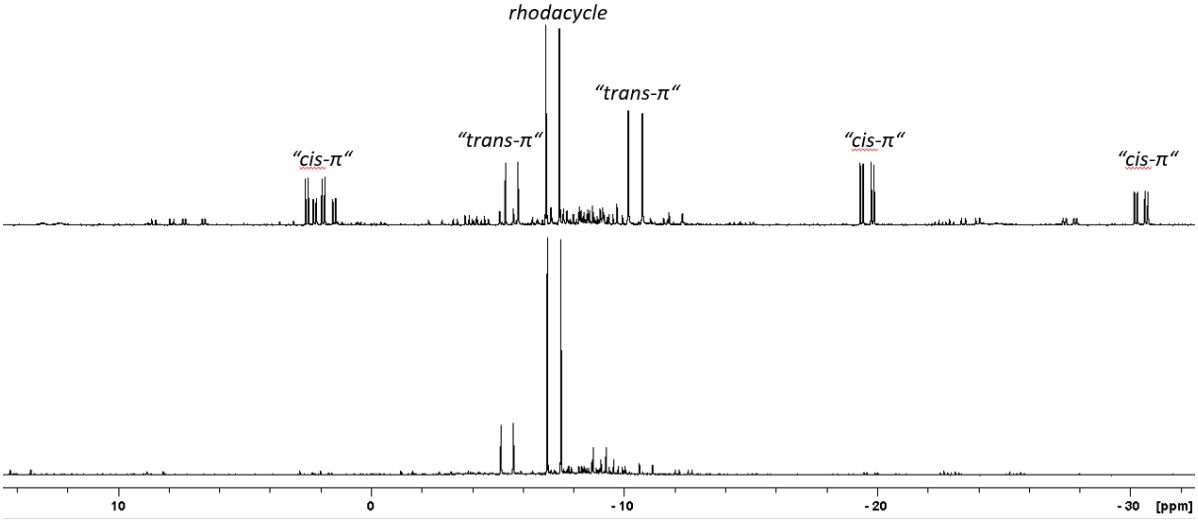


**Figure 23** Typical $^{31}P\{^1H\}$ NMR spectrum of reductive coupling of **5b** to **13** at RT after one day (top) and after 10 days (bottom) in $C_6D_6$ at 202 MHz.

In the upper spectrum, at least seven sets of signals can be observed in significant amounts. Three sets appear between -5 and -11 ppm, being doublets with a Rh-P coupling constant of about 100 Hz, which is typical for a coupling of phosphine to Rh(III) when it is *trans* to another phosphine. The middle one (at ca. -7 ppm) is the signal of the rhodacyclopentadiene **23b**. Four other sets can be observed as doublets of doublets, appearing between 4 and 0 ppm as well as -19 and 31 ppm. Doublets of doublets indicate a *cis*-disposition of the phosphines. The special pattern of the signals results from the coupling of the phosphines to each other, with a value of about 25 Hz. They are now in different chemical environments, showing coupling to the Rh-centre with two different coupling constants, one being of about 80 Hz, and the other being of about 130 Hz. The coupling constant strongly depends on the *trans*-influence of the substituent in the position *trans* to the phosphine. The more electropositive a substituent, the stronger is its *trans*-influence. The consequence is a weakening of the Rh-P bond, which causes a longer bond length and a larger coupling constant.

According to the suggested mechanism of the formation of rhodacyclopentadienes (Chap. 2.1.1), the lower NMR spectrum may show the existence of different *trans*- and *cis*-π complex intermediates, as shown in Chap 2.1.2 and, by comparison with the NMR spectrum after one week, the formation of some of the intended rhodacyclopentadiene already has occurred. Figure 26 shows the possible structures of *tans* and *cis*-*π* complexes, which may occur during the reaction to rhodacyclopentadiene **23b**. Probably coordination of the Rh-centre to the triple bonds next to the phenyl ring might also occur (Figure 24, bottom), but this seems rather unlikely, due to steric hindrance.

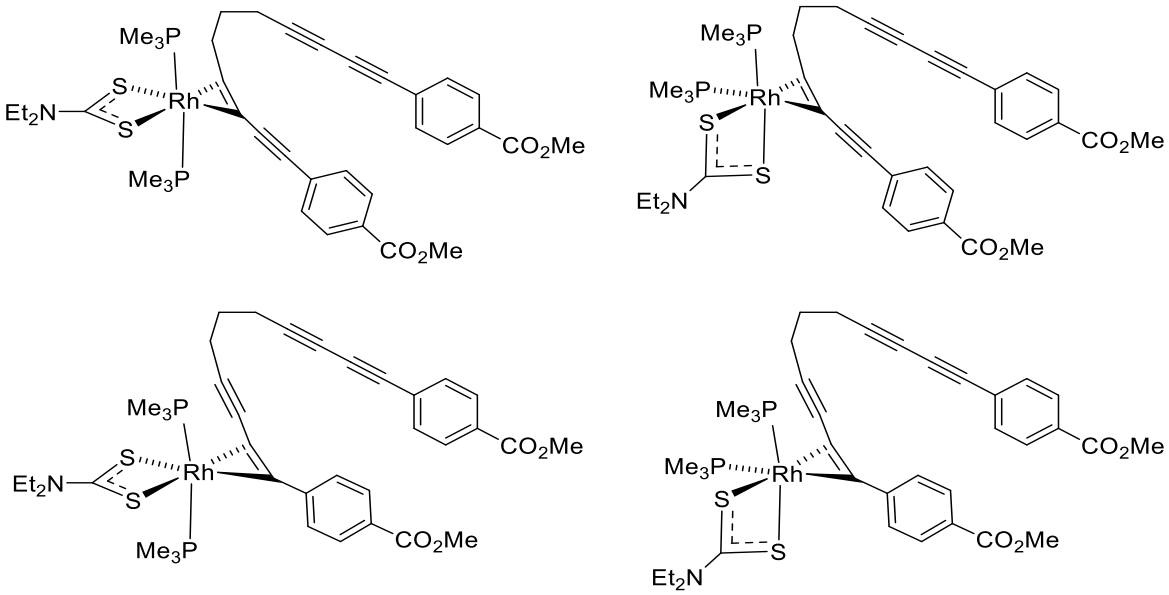


**Figure 24** Possible structures of *trans*- and *cis*-*π* complexes

The proposed structures for the *trans* *π*-complexes have the organic ligand lying in the equatorial plane, together with the dithiocarbamate ligand. As the coupling constants between rhodium and the phosphines are about 100 Hz, which is typical for a Rh(III)-species, it is likely that the organic ligand is strongly $\eta^2$-bound, tending to form a cyclopropene-like metallacycle indicative of significant *π*-backbonding. This would indicate a distorted octahedral structure, having the phosphine ligands in the axial positions and the dithiocarbamate ligand in the equatorial position for the *trans* case. For the *cis* case, one phosphine ligand would lie in the axial position, whereas the second one would occupy an equatorial position and the dithiocarbamate would occupy one axial as well as one equatorial position.

These results are consistent with earlier work of our group on the reaction of [Rh($\kappa^2$-*O*,*O*`-acac)($PMe_3$)$_2$] with different butadiynes, done by Thibault.[127]

Thus, during the reaction of [Rh($\kappa^2$-*O,O`*-acac)($PMe_3$)$_2$] with 2.5 equivalents of 4-bis(4-trifluoromethylphenyl)buta-1,3-diyne at -90 °C, three sets of doublets of doublets were observed at 20.55 ($^1J_{Rh\text{-}P}$ = 138, $^2J_{P\text{-}P}$ = 37 Hz), -7.76 ($^1J_{Rh\text{-}P}$ = 135, $^2J_{P\text{-}P}$ = 34 Hz), and -15.90 ($^1J_{Rh\text{-}P}$ = 126, $^2J_{P\text{-}P}$ = 40 Hz). At -50 °C, another set of doublets of doublets appears at 21.09 ppm ($^1J_{Rh\text{-}P}$ = 141, $^2J_{P\text{-}P}$ 40 Hz), as two sets of signals were overlapped at the lower temperature (Figure 25).

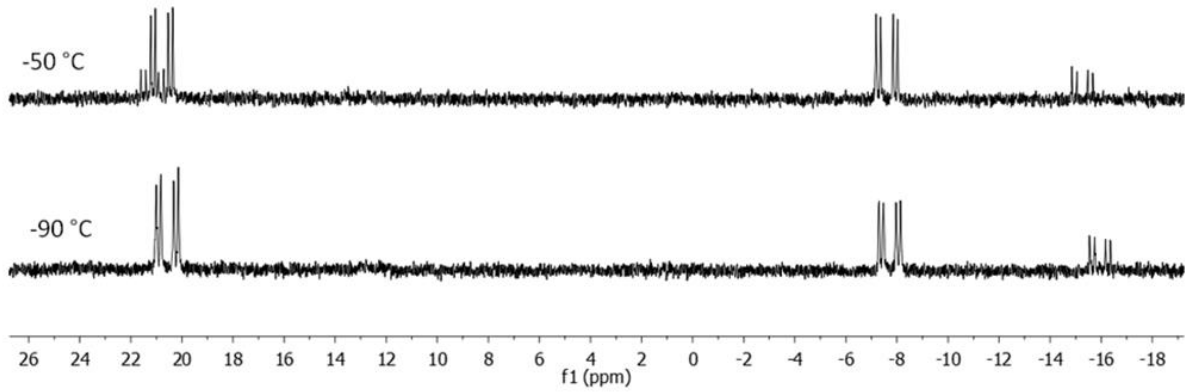


**Figure 25** $^{31}P\{^1H\}$ NMR spectra of [Rh($\kappa^2$-*O,O`*-acac)($PMe_3$)$_2$] and 2.5 eq. of 4-bis(4-trifluoromethylphenyl)buta-1,3-diyne at -50 and -90 °C in THF-$d_8$.[127]

In contrast to the proposed structures of *cis* $\pi$ complexes in Figure 24, Thibault described the $\pi$-bound butadiynes as simple Rh(I) $\pi$-complexes rather than as Rh(III)-metallacyclopropenes.

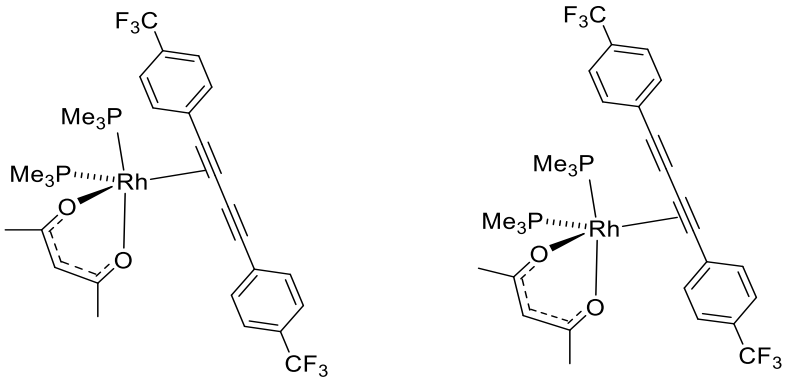


**Figure 26** Possible structures of two rotameric $\pi$-complexes proposed by Marie-Hélène Thibault.

The bonding description leads to a formally trigonal bipyramidal structure, which is pictured in Figure 26 as opposed to the pseudo-octahedral structure shown in Figure 24. The formation and properties of such $\pi$-complexes will be discussed in Chap. 2.2.4 in detail.

The lower *in situ* $^{31}P\{^1H\}$ NMR spectrum in Figure 25 shows predominantly one main doublet, indicating that the desired rhodacyclopentadiene **23b** has been formed as the major product. After no more changes in the *in situ* NMR spectra were observed, the solvent was removed *in vacuo* and the crude product was washed with hot hexane or pentane to remove residual

phosphine, phosphine oxide or any by-products formed during the reaction. The almost pure product was then washed with hexane, pentane or methanol.

High purity was attained by recrystallisation of the compound, by dissolving it in THF and layering it with hexane or pentane depending on the individual solubility of the compound. The compound was crystallised either *via* diffusion at RT to -30 °C or by slow evaporation of the solvents. Another approach was recrystallisation of the compound from hot ethanol.

Additionally, some of the compounds were pre-separated *via* flash column chromatography or standard column chromatography, using a gradient of THF and hexane, gradually increasing the polarity of the solvent. As some of the compounds (e.g. R = $CO_2Me$, SMe, $NO_2$) stick to the silica normally used, it was replaced with alumina, which was deactivated with distilled water.

The $^{31}P\{^1H\}$ NMR spectrum of the isolated rhodacyclopentadiene **23b** (Figure 27) shows the coupling constant $J_{Rh\text{-}P}$ to be 107 Hz. The signal appears at -7.22 ppm.

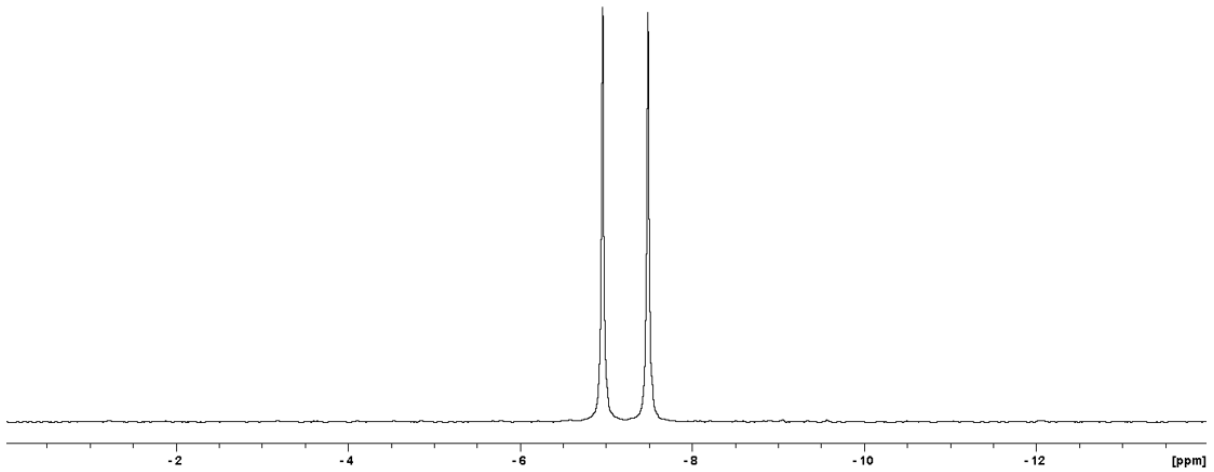


**Figure 27** $^{31}P\{^1H\}$ NMR spectrum of rhodacyclopentadiene **23b** in $C_6D_6$ at 202 MHz.

As for the Rh-starting complexes **13** and **22**, the $J_{Rh\text{-}P}$ coupling constant of the analogous compound with acac is 6 Hz larger, being 113 Hz, with a chemical shift of -3 ppm. The $^{31}P\{^1H\}$ NMR shifts and coupling constants of compounds **23a-f'** are shown in Table 7.

The formation of the rhodacyclopentadienes **23** was also confirmed by $^1H$ NMR spectroscopy. Figure 28 shows a typical example (**23b**) of such an NMR spectrum. The aromatic region shows two doublets at ca. 8.01 and 7.5 ppm with an H-H coupling constant of 9 Hz and integrals of four protons, each. They can be assigned to the eight aromatic protons of the two phenyl-rings (four in each) of the organic moiety bound to the Rh-centre. The alkyl region shows a quartet at 3.48 ppm and a triplet at 0.96 ppm with a coupling constant for each of 7 Hz and integrals of

four and six protons, respectively, assigned to the two ethyl-groups bound to the nitrogen atom of the dithiocarbamate group.

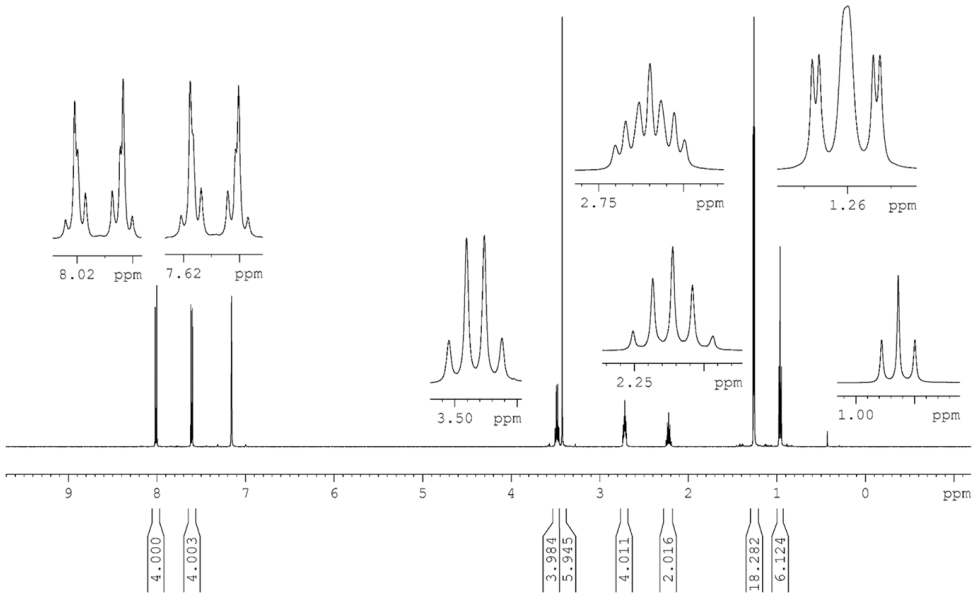


**Figure 28** $^{1}$H NMR spectrum of the reaction of compound **23b** in $C_6D_6$ at 500 MHz.

A singlet at 3.42 ppm is assigned to the two *para*-$CO_2$Me-groups, with an integral of six. An apparent septet at 2.72 ppm and an apparent quintet at 2.22 ppm, with a coupling constant of 7 Hz for each signal and integrals of four and two, respectively, result from the organic backbone. A doublet of triplets at 1.26 ppm with a virtual coupling constant of 3 Hz results from the two $PMe_3$ groups, with an integral of 18.

*Molecular structures of the symmetrical rhodacyclopentadienes **23***

Single crystals of compounds **23a-c** and **f'** were grown in a small glass vial by slow diffusion of a hexane layer into a THF solution at -30 °C. In the case of compound **23e**, the diffusion took place at ambient temperature. Single crystals of compound **23d** were grown by slow evaporation of $C_6D_6$ at ambient temperature. Analysis of compounds **23** *via* X-ray diffraction showed the crystals to be monoclinic, except for compound **23e**, which is triclinic, with the space groups being *Pn* (**23a**), *P2₁/c* (**23b**), *P2₁/n* (**23c** and **f'**), C2/*c* (**23d**) and *P*-1 (**23e**).

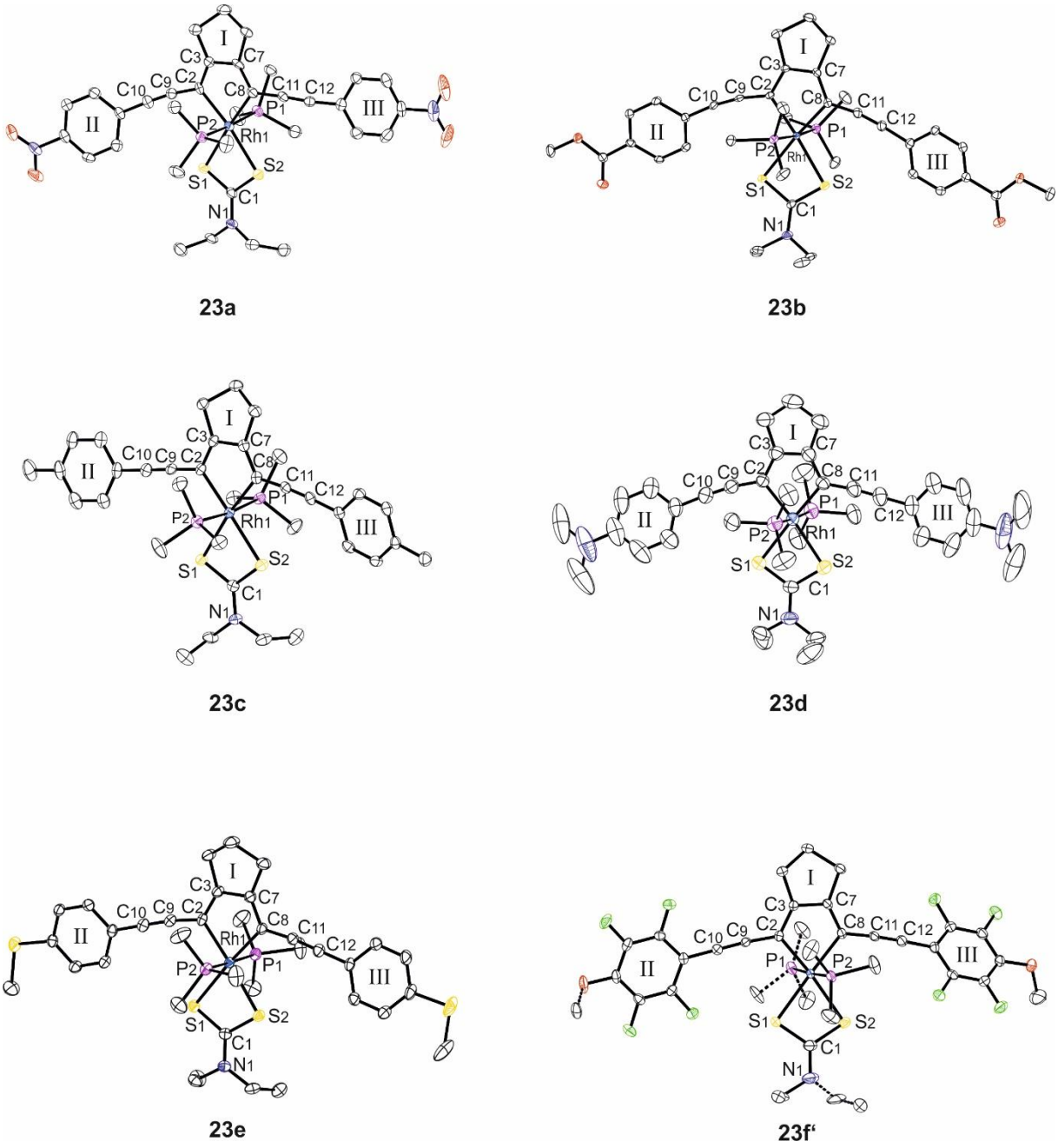


**Figure 29** Molecular structures of compounds **23a-f'**. Hydrogen atoms and solvent molecules are omitted for clarity and thermal ellipsoids are shown at 50 % probability. The second independent molecules of the asymmetric units of compounds **23d** and **e** are also omitted for clarity.

Compounds **23a-f'** have a distorted octahedral geometry with the two $PMe_3$ ligands lying in the axial positions *trans* to each other. The P-Rh bond lengths are 2.2961(7) - 2.3279(7) Å. The rhodacyclopentadiene moiety with the organic backbone as well as the dithiocarbamate lie in the equatorial plane.

The geometry is distorted mainly because of the small bite angle of the dithiocarbamate (S1-Rh1-S2, 72.03(3) - 73.89(2)°). This is promoted by the C2-Rh1-S1, C8-Rh1-S2 angles with values of 101.42(6) - 106.26(8)° and 101.48(9) - 105.67(6)°, respectively, being over 90°, compared to the C2-Rh1-C8 angle of 80.22(9) - 80.7(2)°. The Rh1-S1 and R1-S2 distances are 2.4245(6) - 2.4699(8) and 2.4361(6) - 2.4680(12) Å, respectively. The S1-C1-S2 bond angles all have values of ca. 114.0°. The S1-C1 and S2-C1 bond lengths are 1.711(3) and 1.7276(18) Å, which is comparable to the corresponding bond lengths in [Rh($\kappa^2$-*S,S*`-$S_2CNEt_2$)($PMe_3$)$_2$] **13**. The Rh-C bond lengths of 2.013(7)-2.074(5) Å are in the typical range for Rh-C bonds.

*Comparison of different C-C bonds within compounds **23a-f'***

The bond lengths of C9-C10 (1.201(3) – 1.216(4) Å) and C11-C12 (1.200(5) – 1.210(5) Å) correspond to typical C-C triple bond lengths with sp-hybridisation for both carbon atoms. In addition, the C2-C3 and C7-C8 bond lengths of 1.350(5) – 1.636(5) Å and 1.352(4) – 1.364(3) Å, are typical of $sp^2$-hybridised C-C double bonds. Due to the $sp^2$-hybridisation and the corresponding higher s-character of both carbon atoms, the bond length of C3-C7 (1.435(2) – 1.442(5) Å) is shorter than expected for a typical C-C single bond between two $sp^3$-hybridised carbon atoms. The same applies for the bond lengths of C2-C9 and C8-C11 with values of 1.402(5) – 1.418(5) and 1.393(7) – 1.409(3) Å, as the involved carbon atoms are sp- and $sp^2$-hybridised. Table 6 shows the hybridisations, bond lengths and bond types of compounds **23a-f'**.

**Table 6** Hybridisation, bond lengths and bond type of selected bonds in compounds **23a-f'**.

| | | Bond lengths (Å) | | | | | | |
|---|---|---|---|---|---|---|---|---|
| **Hybridisation** | **Bond** | **23a** | **23b** | **23c** | **23d** | **23e** | **23f '** | **Bond type** |
| sp-sp | C9-C10 | 1.208(7) | 1.209(5) | 1.216(4) | 1.211(5) | 1.209(3) | 1.201(3) | C≡C |
| sp-sp | C11-C12 | 1.207(7) | 1.210(5) | 1.202(4) | 1.200(5) | 1.208(3) | 1.201(3) | C≡C |
| $sp^2$-$sp^2$ | C2-C3 | 1.358(6) | 1.363(5) | 1.357(4) | 1.350(5) | 1.360(2) | 1.361(3) | C=C |
| $sp^2$-$sp^2$ | C7-C8 | 1.361(8) | 1.371(5) | 1.352(4) | 1.375(5) | 1.361(3) | 1.364(3) | C=C |
| $sp^2$-$sp^2$ | C3-C7 | 1.436(7) | 1.442(5) | 1.436(4) | 1.442(5) | 1.435(2) | 1.437(3) | C-C |
| sp-$sp^2$ | C2-C9 | 1.421(7) | 1.402(5) | 1.406(4) | 1.418(5) | 1.407(2) | 1.405(3) | C-C |
| sp-$sp^2$ | C8-C11 | 1.393(7) | 1.399(5) | 1.402(4) | 1.407(5) | 1.401(2) | 1.409(3) | C-C |
| | Rh1-C2 | 2.074(5) | 2.058(3) | 2.068(3) | 2.073(3) | 2.0509(17) | 2.048(2) | |
| | Rh1-C8 | 2.013(7) | 2.042(3) | 2.057(3) | 2.074(3) | 2.0572(18) | 2.067(2) | |
| | S1-C1 | 1.716(5) | 1.709(4) | 1.717(3) | 1.722(4) | 1.7188(19) | 1.711(3) | |
| | S2-C1 | 1.712(5) | 1.725(4) | 1.722(3) | 1.718(4) | 1.7276(18) | 1.727(3) | |
| | Rh1-S1 | 2.4491(17) | 2.4435(9) | 2.4699(8) | 2.4445(12) | 2.4472(6) | 2.4245(6) | |
| | Rh1-S2 | 2.4522(15) | 2.4441(10) | 2.4372(8) | 2.4680(12) | 2.4361(6) | 2.4454(7) | |
| | Rh1-P1 | 2.3109(15) | 2.3144(11) | 2.3159(8) | 2.3166(15) | 2.3139(6) | 2.2961(7) | |
| | Rh1-P2 | 2.3206(15) | 2.3104(10) | 2.3100(8) | 2.3155(15) | 2.3017(6) | 2.3279(7) | |

**Table 7** Important angles, $^{31}P\{^{1}H\}$ NMR shifts, isolated yield and space groups of single crystals of compounds **23a-f'.**

| | | **23a** | **23b** | **23c** | **23d** | **23e** | **23f '** |
|---|---|---|---|---|---|---|---|
| **Angles (°)** | S1-Rh1-S2 | 73.89(2) | 72.19(3) | 72.03(3) | 72.05(5) | 72.438(18) | 72.61(82) |
| | C2-Rh1-S1 | 102.51(14) | 104.44(9) | 106.26(8) | 102.41(10) | 103.94(5) | 101.42(6) |
| | C8-Rh1-S2 | 104.95(15) | 102.92(9) | 101.48(9) | 105.17(10) | 103.17(5) | 105.67(6) |
| | C2-Rh1-C8 | 80.7(2) | 80.44(14) | 80.22(12) | 80.38(13) | 80.45(7) | 80.22(9) |
| | S1-C1-S2 | 114.4(3) | 114.0(2) | 114.08(17) | 114.26(19) | 113.69(10) | 114.02(15) |
| **Interplanar angle (°)** | I & II | 3.10(17) | 21.91(11) | 7.01(8) | 10.26(12) | 9.21(6) | 6.21(7) |
| | I & III | 4.01(18) | 15.59(11) | 6.25(9) | 1.23(13) | 7.99(7) | 41.07(7) |
| **$^{31}P\{^{1}H\}$ NMR shift (ppm)** | | -7.34 | -7.22 | -6.97 | -6.08 | -7.05 | -7.37 |
| **Coupling constant ($J_{Rh-P}$)/Hz** | | 106 | 107 | 108 | 110 | 108 | 105 |
| **Isolated yield (%)** | | 8 % | 0.3 % | 6 % | 6 % | 3 % | 5 % |
| **Space group (single crystal)** | | *Pn* | *P2₁/c* | *P2₁/n* | C2/*c* | *P*-1 | *P2₁/n* |
| **Crystal system** | | monoclinic | monoclinic | monoclinic | monoclinic | triclinic | monoclinic |

*Reactions at elevated temperatures*

The reaction behaviour changes significantly if the different undecatetraynes **5** are reacted with [Rh($\kappa^2$-*S*,*S*`-$S_2CNEt_2$)($PMe_3$)$_2$] **13** at elevated temperatures (60-110 °C, Scheme 48).

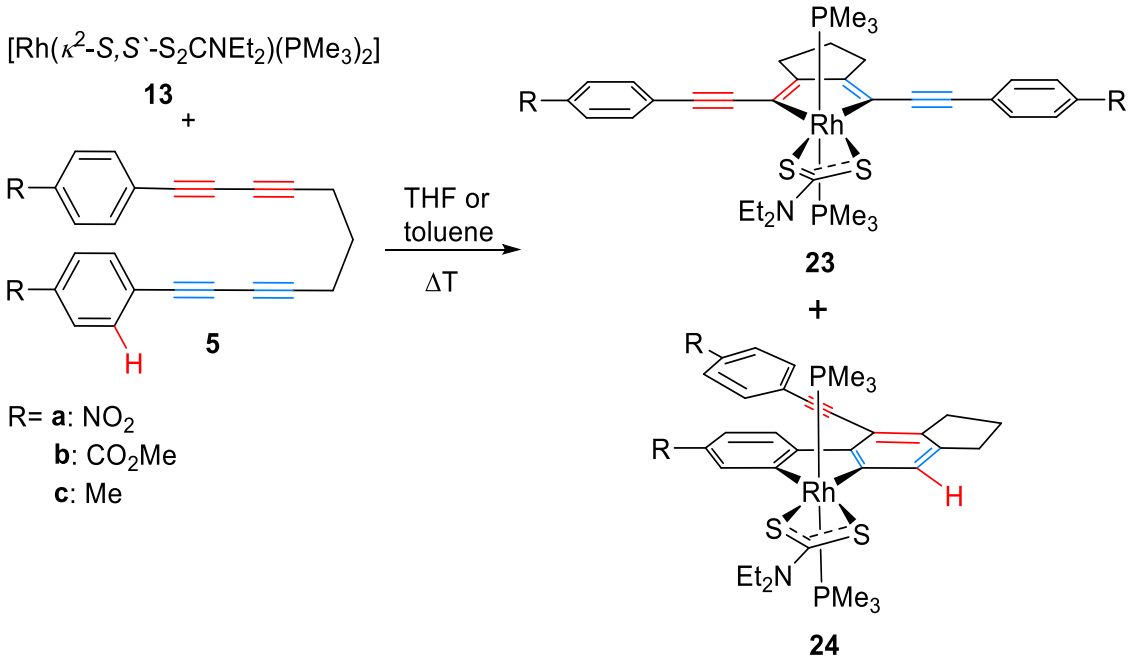


**Scheme 48** Reaction of different undecatetraynes **5** with [Rh($\kappa^2$-*S*,*S*`-$S_2CNEt_2$)($PMe_3$)$_2$] **13** at elevated temperatures.

When the reaction is heated, rhodacyclopentadiene **23** is no longer formed exclusively, but additionally, an isomeric complex, being the dibenzorhodacyclopentadiene **24**, is also formed. This complex may be formed *via* a [4+2] cycloaddition reaction between three triple bonds of the tetrayne, which forms the new benzene ring of the biphenyl moiety. Subsequently, a C-H activation and a $\beta$-H shift occur, which connects one of the two existing phenyl rings of the tetrayne directly to the Rh-centre. As already mentioned in Chap. 2.1.4, various routes to obtain organometallic biphenyl complexes have been reported. Nevertheless, with the route described here, biphenyl complexes are easily accessible in a simple one-pot synthesis.

The highest conversion to dibenzorhodacyclopentadienes **24** is obtained from the reaction of undecatetrayne **5b** (R = $CO_2Me$) with [Rh($\kappa^2$-*S*,*S*`-$S_2CNEt_2$)($PMe_3$)$_2$] **13**. This dibenzorhodacyclopentadiene is formed in a 2:1 ratio to the isomeric rhodacyclopentadiene **23b**. Reactions with other undecatetraynes only give the dibenzorhodacyclopentadienes **24** in a ratio of 1:2 or even lower.

This is in stark contrast to earlier results of our group, wherein reactions with the same undecatetraynes **5** and [Rh($\kappa^2$-*O*,*O*`-acac)($PMe_3$)$_2$] at room temperature gave the corresponding

dibenzorhodacyclopentadiene as the main product in a 20:1 ratio at ambient temperature, and in a 25:1 ratio at elevated temperatures.[121]

Figure 30 shows the *in situ* $^{31}P\{^{1}H\}$ NMR spectrum of the reaction of undecatetraynes **5b** with [Rh($\kappa^2$-*S*,*S*`-$S_2CNEt_2$)($PMe_3$)$_2$] **13** at 60 °C in comparison to the $^{31}P\{^{1}H\}$ NMR spectrum of rhodacyclopentadiene **23b** (bottom).

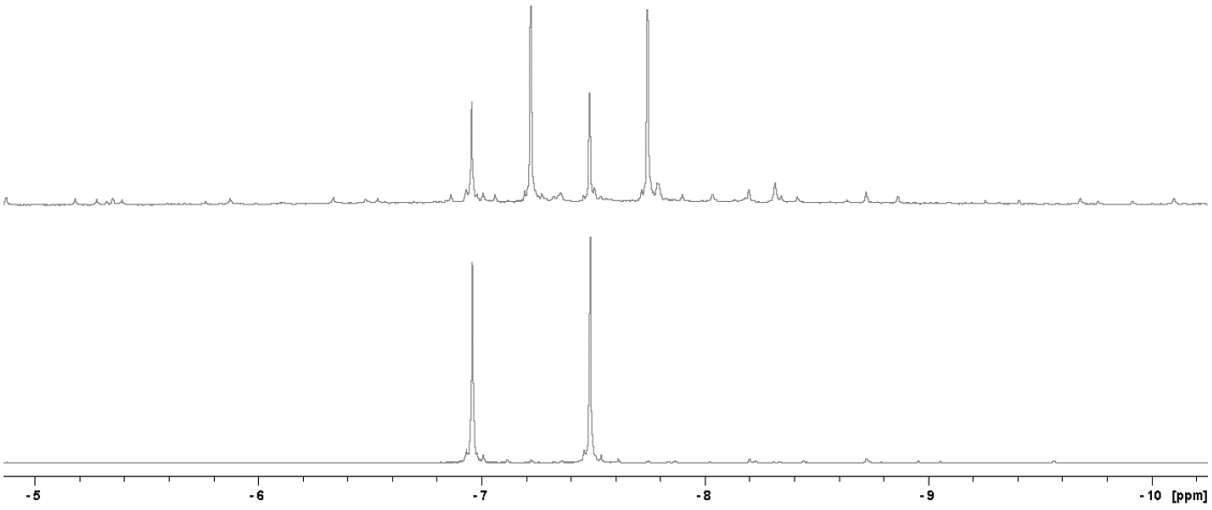


**Figure 30** *In situ* $^{31}P\{^{1}H\}$ NMR spectra of rhodacyclopentadiene **23b** (bottom) *vs.* reaction of undecatetrayne **5b** with [Rh($\kappa^2$-*S*,*S*`-$S_2CNEt_2$)($PMe_3$)$_2$] **13** at elevated temperatures (top) in THF at 202 MHz.

In the upper NMR spectrum, a mixture of rhodacyclopentadiene **23b** and the new Rh(III)-species **24b** is shown. The two compounds are formed in a 1:2 ratio. The reaction occurs with complete conversion, and only trace by-products can be observed. Although the organic moiety of the dibenzorhodacyclopentadiene molecule is unsymmetrical, the axial *trans* phosphines give rise to a doublet in the $^{31}P\{^{1}H\}$ NMR spectrum, due to the equatorial mirror plane.

The $^{1}H$ NMR-spectrum (Figure 31) of compound **24b** is typical and confirms that the new formed organic moiety is an unsymmetrical one. While the $^{1}H$ NMR spectrum of the "normal" rhodacyclopentadiene **23b** showed only two signals in the aromatic region, the aromatic protons of compound **24b** split into four, rather complex signals and two singlets. The first signal appears as a doublet at 9.55 ppm with a coupling constant of 8 Hz and an integral of one, followed by a singlet at 8.65 ppm and a multiplet at 8.41 ppm, with integrals of one for each as well. Two doublets of multiplets appear at 8.04 ppm and 7.57 ppm with an approximate coupling constant of 9 Hz and an integral of two each, and there is a singlet at 7.69 ppm, with an integral of one. The latter two doublets of multiplets are somewhat similar to the signals found in the $^{1}H$ NMR spectrum of rhodacyclopentadiene **23b** (Figure 28), and are thus assigned to the ethynylarene substituent not bound to Rh.

The alkyl region shows two singlets at 3.60 and 3.49 ppm, which belong to the two inequivalent methyl groups of the $CO_2Me$-subtituents at the *para*-position of the phenyl rings, having integrals of three each. In between, a multiplet at 3.54 ppm appears, having an integral of four, which is assigned to the ethyl-$CH_2$ groups of the dithiocarbamate. The next signals are two triplets at 3.24 and 2.94 ppm, with a coupling constant of 7 Hz, belonging to the backbone of the organic ligand, having integrals of two, each. A quintet appearing at 1.99 ppm, with a coupling constant of 7 Hz and an integral of four, is also assigned to that backbone. Another triplet at 1.03 ppm with a coupling constant of 7 Hz is assigned to the two $CH_3$-groups of the ethyl moieties of the dithiocarbamate, having an integral of six. The multiplet at 0.75 ppm belongs to the methyl groups of the two $PMe_3$ ligands, as observed in the $^1$H NMR spectrum of rhodacyclopentadiene **23b**, with an integral of 18.

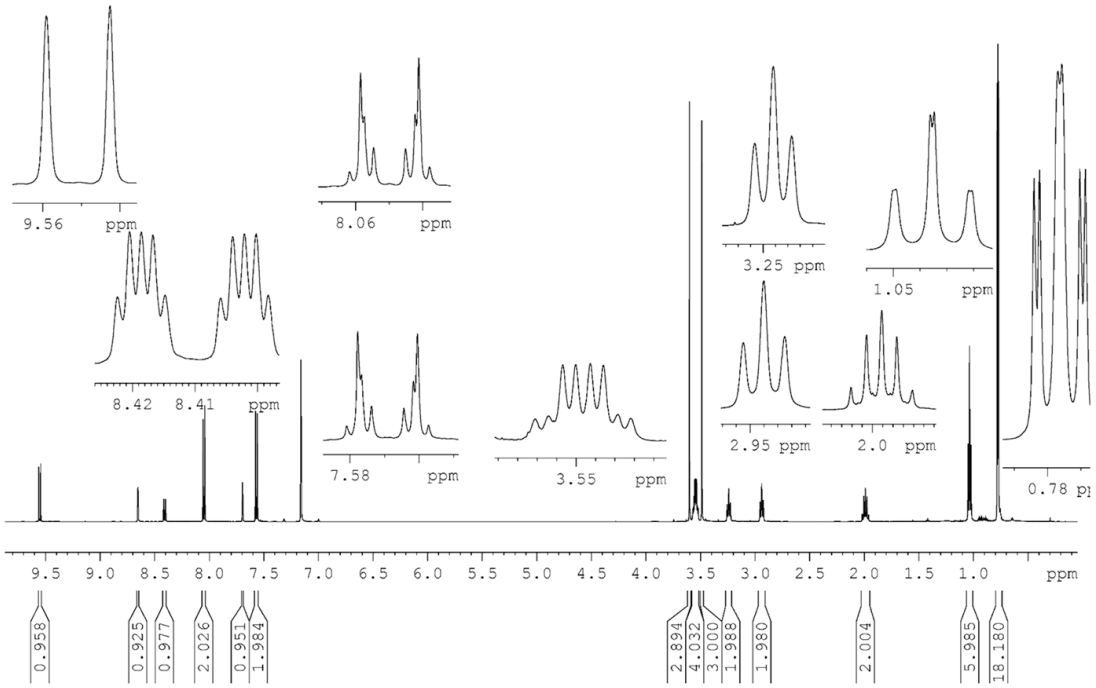


**Figure 31** $^1$H NMR spectrum of **24b** in $C_6D_6$ at 500 MHz.

The formation of the dibenzorhodacyclopentadienes **24** is also confirmed by the crystal structures shown later in this chapter.

As the C-H activation is a key step in the formation of the biphenyl complex, test reactions with undecatetrayne **5f'** were carried out to examine the effect of removing the *ortho*-aryl hydrogen atoms. As compound **5f'** has no hydrogen in a position *ortho* to the alkyne, the C-H activation should be suppressed or a C-F activation should take place, which would be visible in the $^{19}$F NMR spectrum.

The reaction did not lead to a C-F activation product, but to another surprising result. In addition to the "normal" rhodacyclopentadiene **23f'** (Figure 32), a bimetallic species was observed, which seems to be related to an intermediate during the formation of several [3+2] cycloaddition products which were observed by other members of our group when using diaryl butadiynes and [Rh($\kappa^2$-*O,O`*-acac)($PMe_3$)$_2$] (See also Chap 2.1.3). As a C-H activation is no longer possible, the intermediate species was trapped and detected in the NMR spectra. When the reaction was carried out at ambient temperature, it was possible to isolate the bimetallic complex as the main species present in the reaction mixture. Higher temperatures give the "normal" rhodacyclopentadiene **23f'** (Figure 29) as the main product.

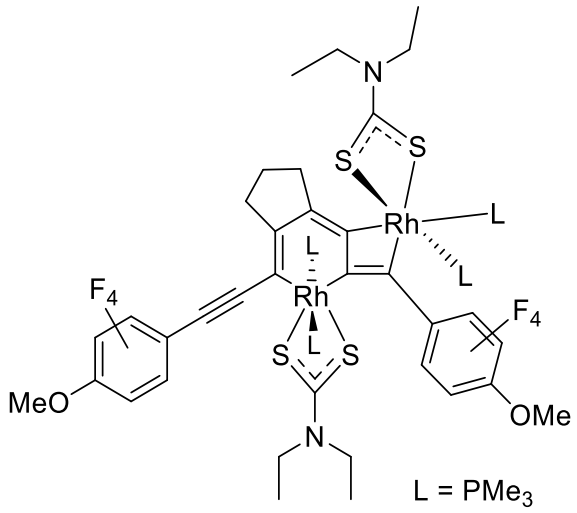


**Figure 32** Schematic structure of compound **24f'-bi**.

Figure 33 shows the structure of the bimetallic complex **24f'-bi**, which was confirmed by X-ray diffraction of a single crystal obtained by Sarah McKnight.[23]

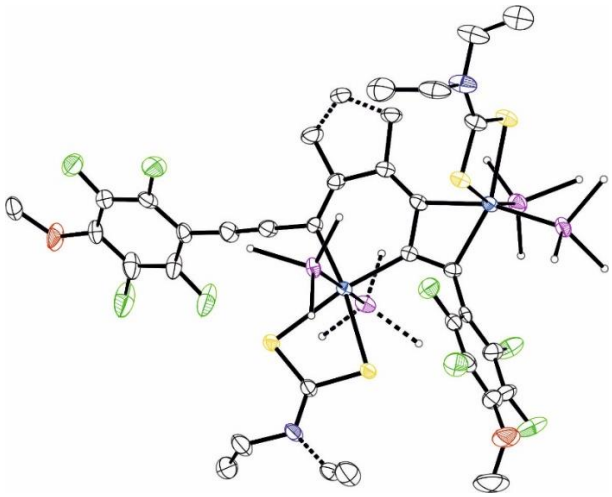

**Figure 33** Molecular structure of compound **24f'-bi**.[23]

It resulted in monoclinic crystals with the space group $P2_1/c$. The system has a distorted octahedral geometry with respect to both Rh-centres. It can be observed that two Rh-centres are bound to one undecatetrayne. One of the Rh-centres forms a six-membered ring with the undecatetrayne, having the two phosphine ligands in positions *trans* to each other. The other centre forms a strained, four-membered ring with the undecatetrayne, wherein the two phosphine ligands are *cis* to each other, with one phosphine ligand lying in the equatorial plane of the molecule. This interesting system, consisting of four different phosphine environments, results in a $^{31}P\{^1H\}$ NMR spectrum of higher order. The spectrum and the corresponding simulation are shown in Figure 34.

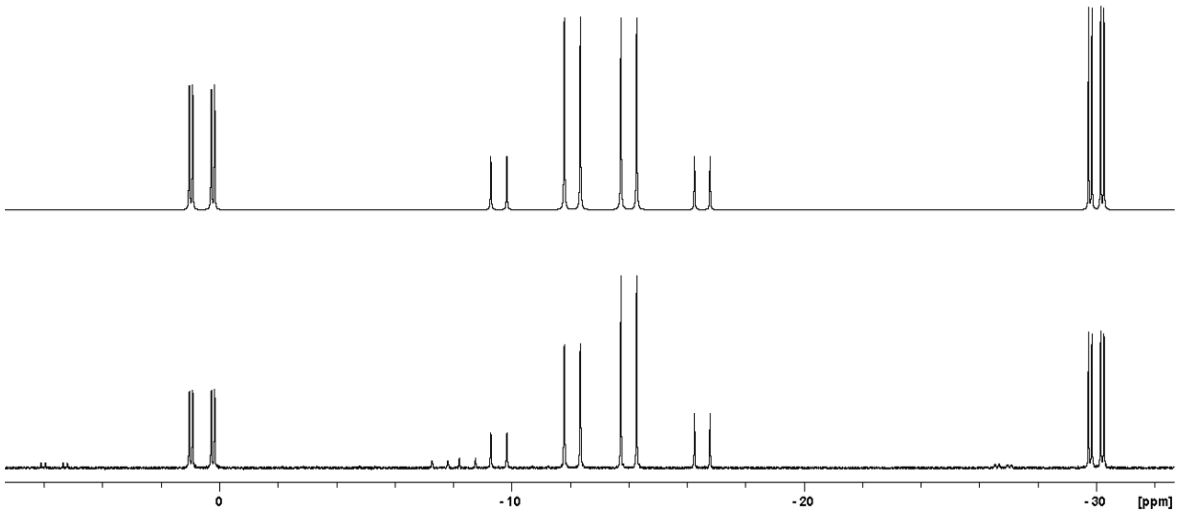


**Figure 34** 202 MHz $^{31}P\{^1H\}$ NMR (bottom) and simulated spectrum (top) of compound **24f'-bi** in $C_6D_6$.

The major signals of this NMR spectrum belong to a second-order ABX-system, in which the multiplet in the middle of the spectrum (-9 to -17 ppm) shows a roof-effect, which occurs when the following formula is valid: $\Delta\nu/J < 10$.

The above-mentioned formula is valid for this system, as the chemical shift difference ($\Delta\nu$) is ca. 800 Hz and the $^2J_{P\text{-}P}$ coupling constant is 508 Hz. The four "doublets" belong to a pair of mutually *trans* phosphines, which, due to the asymmetry of the rest of the molecule, no longer have the exact same chemical environment, although their chemical shifts are still fairly close to one another. The coupling constants $J_{Rh\text{-}P}$ of both phosphines are 112 and 108 Hz, as they are diastereotopic. This confirms that, at least this Rh-centre has an oxidation state of three. At ca. 0 and ca. -30 ppm, two doublets of doublets appear indicating, that the phosphine ligands on this Rh-centre are *cis* to each other. The smaller coupling constant of -23 Hz is the P-P coupling. The larger coupling constants of 84 and 153 Hz are the Rh-P couplings. As the two phosphines have two different ligands *trans* to them, they experience a different *trans*-influence, which

causes the significant difference in the chemical shifts and Rh-P coupling constants. Additionally, a small amount of a second set of signals can be seen in the spectrum. At ca. 6 ppm, a set of doublets of doublets appears with $J_{P\text{-}P}$ coupling constants of 28 Hz and $J_{Rh\text{-}P}$ = 153 Hz, and a second one appears at -27 ppm with $J_{P\text{-}P}$ coupling constants of 28 Hz and $J_{Rh\text{-}P}$ = 85 Hz; their integrals are roughly 1:1. Between -7 and -10 ppm, two doublets with $J_{Rh\text{-}P}$ coupling constants of 109 Hz for each, can be seen and additionally, at -4.76 and -10.97 two further doublets with very low intensity appear, having the same coupling constants. This may be an isomeric structure of the bimetallic complex **24f'-bi**, as it shows a similar pattern of the signals, with comparable coupling constants. The $J_{P\text{-}P}$ coupling constant for the other doublets is ca. 500 Hz, as in compound **24f'-bi**. The chemical shift difference (Δν) is also ca. 800 Hz. Therefore, it may also be a second-order ABX-system, as well showing a roof-effect. Figure 35 shows the solid-state $^{31}P\{^{1}H\}$ NMR spectrum of compound **24f'-bi**, confirming the $^{31}P\{^{1}H\}$ NMR spectrum in solution, showing the same pattern. The smaller *cis* P-P couplings are too small to be resolved.

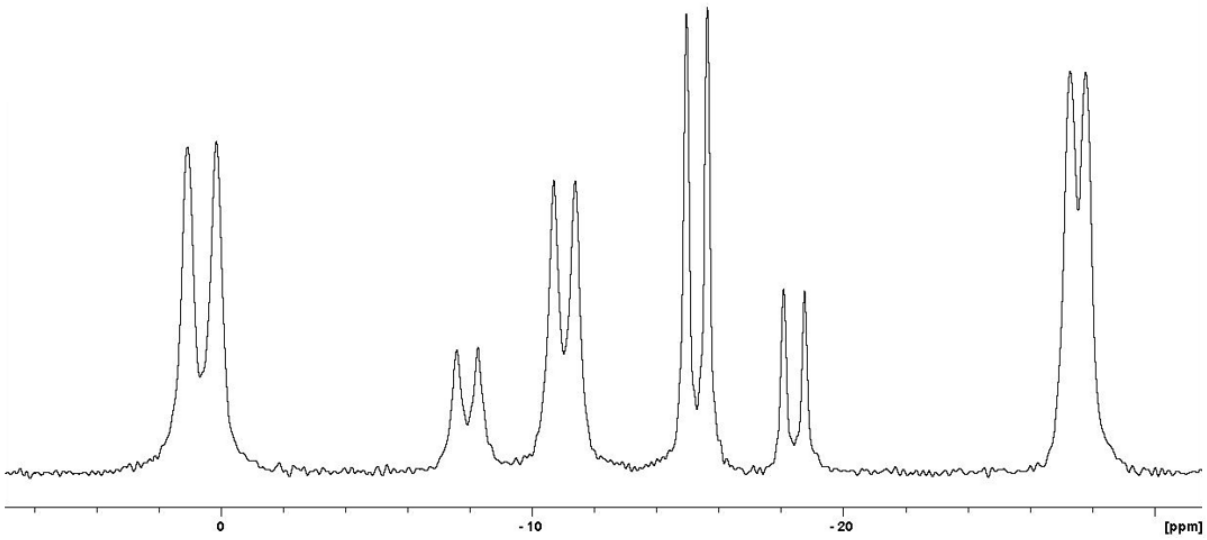


**Figure 35** Solid state $^{31}P$-CP NMR spectrum of compound **24f'-bi**. 14 kHz rotation, $^{1}H$-90°-pulse : 2.5 $\mu$s.

The signals for the *cis* phosphines appear at ca. 0 and -27 ppm, having the same Rh-P coupling constants as in the $^{31}P\{^{1}H\}$ NMR spectrum in solution. The signals for the *trans* phosphines show the roof-effect in the solid-state as well as in solution, confirming that the signals do not appear due to dynamic effects, but that the system is a higher order ABX-system.

Although the dibenzorhodacyclopentadiene may result from a metal-trapped benzyne intermediate resulting from a hexadehydro Diels-Alder (HDDA) reaction (Scheme 50), it is also possible to propose a mechanism for the formation of the dibenzorhodacyclopentadiene based on the bimetallic intermediate (Scheme 49). In the first step, there is a double switch between

the Rh-C bonds. This increases the size of the six-membered heterocyclic ring at one Rh-centre to a seven membered ring, whereas the second Rh-moiety ends up bonding to a C-C double (or triple bond), losing one $PMe_3$ ligand.

In the next step, the CH-activation takes place by an oxidative addition process. Now, the second Rh-moiety is again bound to the whole organic system. In the third step, an alkene (or alkyne) insertion could take place.

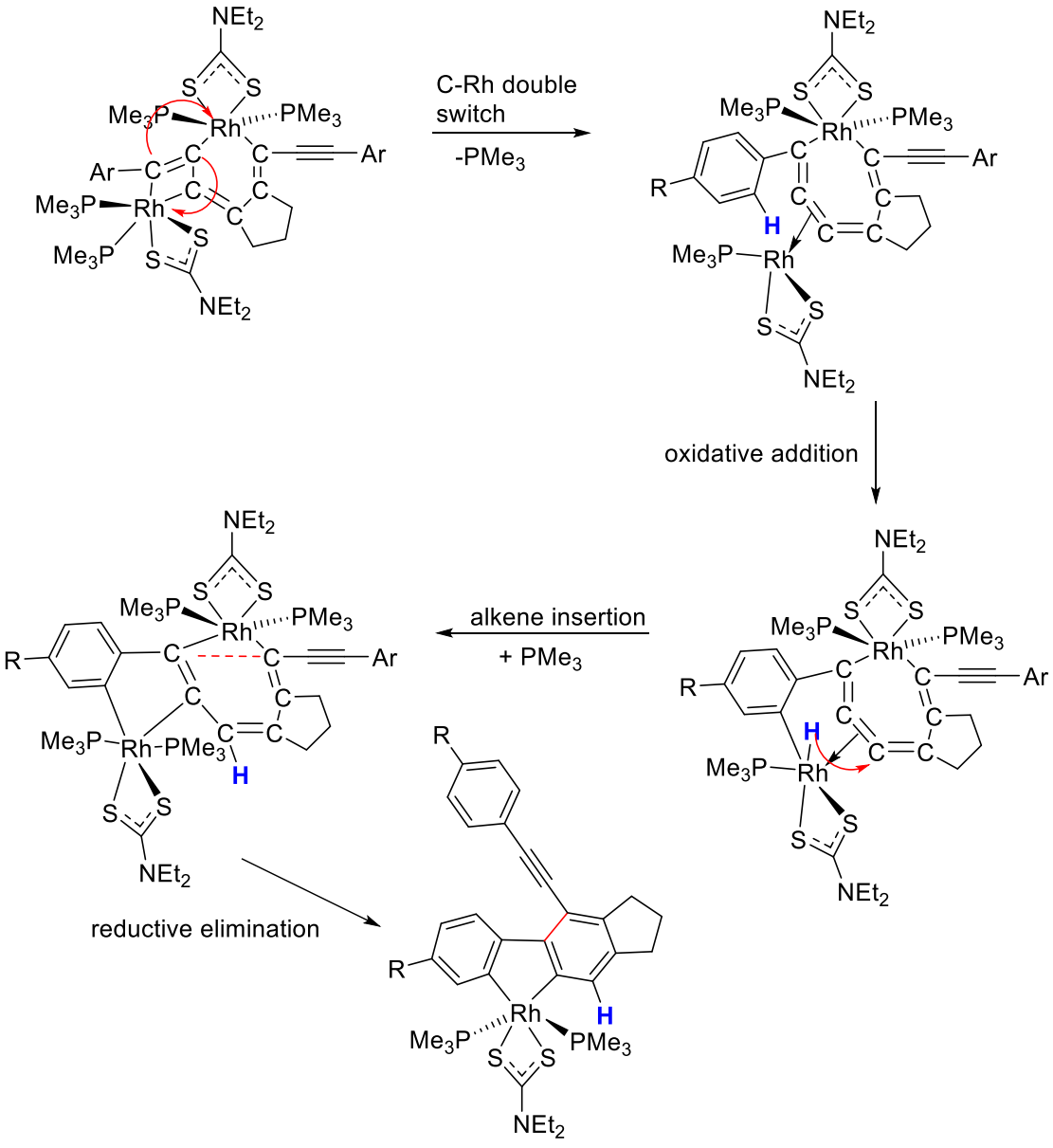


**Scheme 49** A possible mechanism for the formation of dibenzorhodacyclopentadienes **24**.

The hydrogen is shifted to a carbon of the seven-membered, metallacyclic ring. In the last step, reductive elimination takes place. The Rh-C bonds of the first Rh-moiety are cleaved and a

benzene ring is formed, ending up in the dibenzo rhodacyclopentadiene. The second $PMe_3$ ligand again binds to the Rh-centre.

Scheme 50 shows, in comparison to that, the HDDA mechanism of the formation of the dibenzorhodacyclopentadienes **24**. In the first step, an HDDA (hexadehydro Diels-Alder) reaction may take place, between three of the four triple bonds of the tetrayne. One of the phenyl groups of the tetrayne is added oxidatively to the Rh-centre, which loses one $PMe_3$ ligand. The cumulenic intermediate formed can also be drawn as its benzyne resonance structure.

In the last step, an alkyne insertion may take place, forming the second benzene ring of the dibenzorhodacyclopentadienes **24**. This is accompanied by the re-addition of the second $PMe_3$.

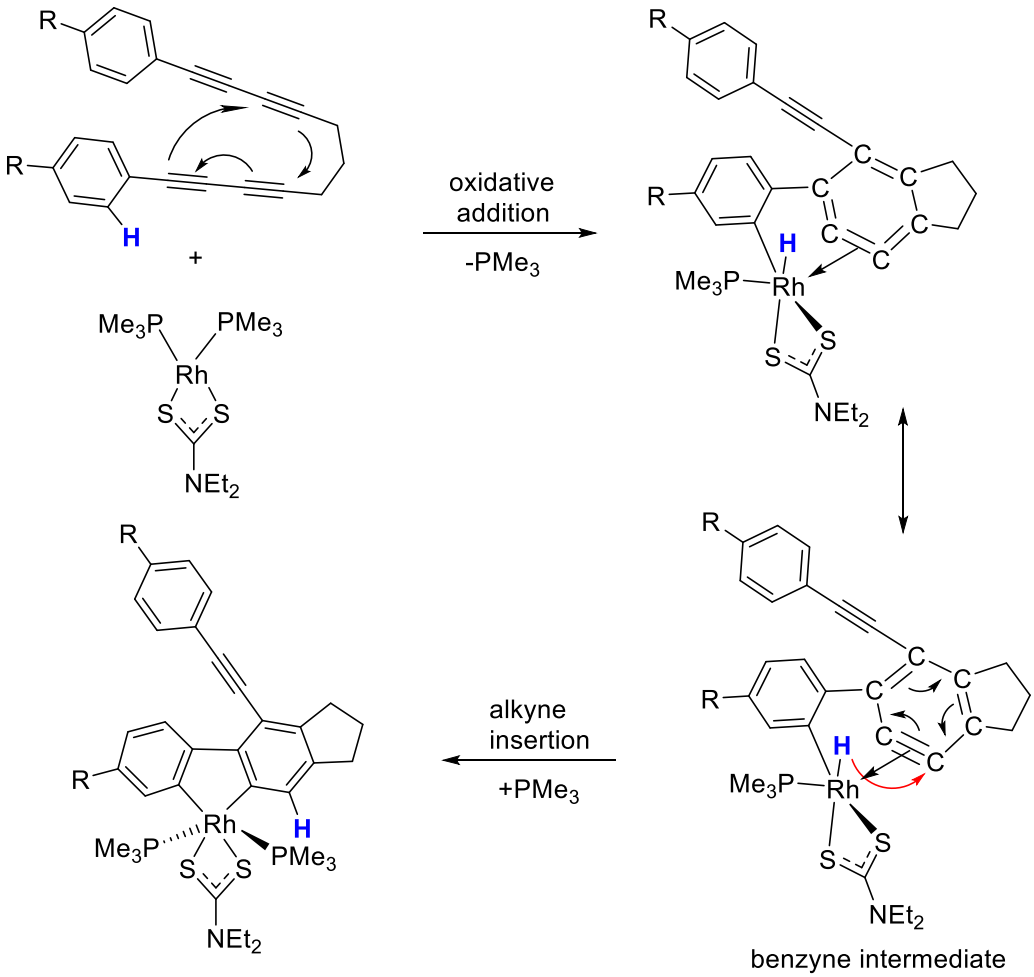


**Scheme 50** Possible HDDA mechanism of the formation the dibenzorhodacyclopentadienes **24**.

Without extensive kinetic and mechanistic studies, which are well beyond the scope of this thesis, the mono- and bimetallic pathways leading to the dibenzorhodacyclopentadienes cannot be distinguished.

*Crystal structures of dibenzorhodacyclopentadienes **24***

Single crystals of **24a** and **b** were grown in a small glass vial by slow diffusion of a hexane layer into a THF solution at RT. Analysis of compounds **24a** and **b** *via* X-ray diffraction showed both crystals to be monoclinic with the space group $P2_1/c$ (Figure 36).

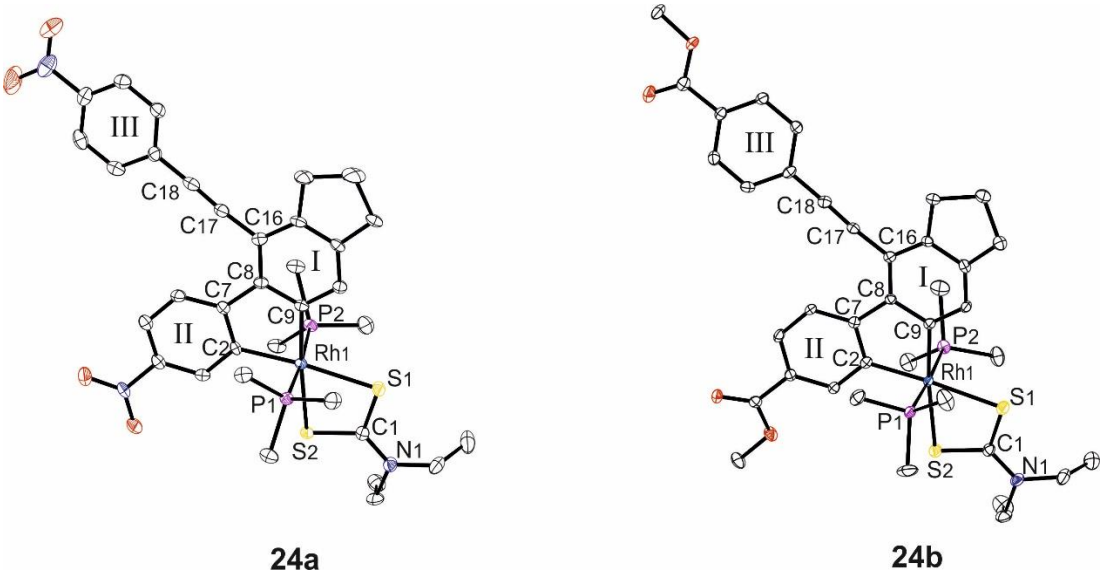


**Figure 36** Molecular structure of dibenzorhodacyclopentadiene **24a** and **24b**. Hydrogen atoms and solvent molecules are omitted for clarity and thermal ellipsoids are shown at 50% probability.

Dibenzorhodacyclopentadienes **24a** and **b** have a distorted octahedral geometry, with the two $PMe_3$ groups in axial positions *trans* to each other. The metallacyclopentadiene moiety and the dithiocarbamate ligand are both located in the equatorial plane of the octahedron. The distortion is caused by the small bite angle (S1-Rh1-S2, 71.73(2) - 71.75(4)°) of the dithiocarbamate ligand. This results in the C2-Rh1-S2 and C9-Rh1-S1 angles of 103.83(12) - 105.35(8) and 102.75(8) - 103.88(13)°, which are significantly larger than 90°. The C2-Rh1-C9 angles have values of 80.22(11) - 80.62(17)°. The P1-Rh1 and P2-Rh1 bond lengths are 2.3086(8) - 2.3091(15) and 2.3176(15) - 2.3197(8) Å, respectively, and are similar to each other. The same applies for the S1-Rh1 (2.4533(7) - 2.4564(16) Å) and S2-Rh1 (2.4545(16) - 2.4681(7) Å) bond lengths. The C2-Rh1 and C9-Rh1 bond lengths have values of 2.018(3) - 2.018(4) and 2.013(4) - 2.020(3) Å, which lie in the typical range for a Rh-C bond length (Tables 8 and 9).

*Comparison of different C-C bonds within compounds **24a** and **b***

The first part of Table 8 shows an overview of the important C-C bond lengths and types within dibenzorhodacyclopentadienes **24a** and **24b**. The C17-C18 (1.203(4) - 1.212(6) Å) bond lengths are in the typical range for sp-hybridised C-C triple bonds. The C2-C7 and C8-C9 bond lengths, with values of 1.414(6) - 1.415(4) and 1.409(6) - 1.416(4) Å are for carbons, which belong to the benzene rings of the biphenyl moiety, and are in the typical region for aromatic C-C bonds. The C7-C8 bond lengths are comparably short, with values of 1.471(6) - 1.477(4) Å, as both carbon atoms of the C-C single bond are $sp^2$-hybridised. The same applies for the C16-C17 (1.426(4) - 1.427(6) Å) bond lengths, which are also short for a C-C single bond, due to the $sp^2$- and sp-hybridisation of the two carbon atoms.

**Table 8** Important bond lengths, hybridisation and bond type of compounds **24a** and **b**.

| | | Bond length (Å) | | |
|---|---|---|---|---|
| **Hybridisation** | **Bond** | **24a** | **24b** | **Bond type** |
| sp-sp | C17-C18 | 1.212(6) | 1.203(4) | C≡C |
| sp-$sp^2$ | C17-C16 | 1.427(6) | 1.426(4) | C-C |
| $sp^2$-$sp^2$ | C7-C8 | 1.471(6) | 1.477(4) | C-C |
| $sp^2$-$sp^2$ | C2-C7 | 1.414(6) | 1.415(4) | C-$C_{arom}$ |
| $sp^2$-$sp^2$ | C8-C9 | 1.409(6) | 1.416(4) | C-$C_{arom}$ |
| | Rh1-C2 | 2.018(4) | 2.018(3) | |
| | Rh1-C9 | 2.013(4) | 2.020(3) | |
| | S1-C1 | 1.724(5) | 1.710(4) | |
| | S2-C1 | 1.715(5) | 1.712(3) | |
| | Rh1-S1 | 2.4564(16) | 2.4533(7) | |
| | Rh1-S2 | 2.4545(16) | 2.4681(7) | |
| | Rh1-P1 | 2.3091(15) | 2.3086(8) | |
| | Rh1-P2 | 2.3176(15) | 2.3197(8) | |

Table 9 also shows the interplanar angles of compounds **24a** and **b**. The angles between planes I and II are comparable with values of 7.71(15) and 7.48(8)°, showing that the biphenyl moiety is largely planar. Also, the angle between planes I and III in compound **24a** is very small with a value of 2.11(16)°. The corresponding interplanar angle in compound **24b** is larger, with a value of 20.43(9)°.

The chemical shifts in the $^{31}P\{^{1}H\}$ NMR are similar with values of -7.89 and -7.48 ppm, and the $J_{Rh-P}$ coupling constants of about 100 Hz, lie in the typical range for these compounds.

**Table 9** Important angles, $^{31}P\{^{1}H\}$-NMR shifts, yield, space group and crystal system of compounds **24a** and **b**.

| | | **24a** | **24b** |
|---|---|---|---|
| **Angles (°)** | S1-Rh1-S2 | 71.75(4) | 71.73(2) |
| | C2-Rh1-S2 | 103.83(12) | 105.35(8) |
| | C9-Rh1-S1 | 103.88(13) | 102.75(8) |
| | C2-Rh1-C9 | 80.62(17) | 80.22(11) |
| | S1-C1-S2 | 113.6(3) | 114.86(18) |
| **Interplanar angle (°)** | I & II | 7.71(15) | 7.48(8) |
| | I & III | 2.11(16) | 20.43(9) |
| **$^{31}P\{^{1}H\}$ NMR shift (ppm)** | | -7.89 | -7.48 |
| **Coupling constant $J_{Rh-P}$ [Hz]** | | 104 | 106 |
| **Isolated yield (%)** | | 0.7 | 0.7 |
| **Space group (single crystal)** | | $P2_1/c$ | $P2_1/c$ |
| **Crystal system** | | monoclinic | |

### 2.2.3 Reactions of Undecatetraynes with [Rh($\kappa^2$-*S*,*S*`-$S_2CNEt_2$)($PPh_3$)$_2$]

Exchanging the phosphine ligands in the Rh-starting complex from $PMe_3$ to $PPh_3$ changed the reaction behaviour of the system significantly. The reaction of [Rh($\kappa^2$-*S*,*S*`-$S_2CNEt_2$)($PPh_3$)$_2$] **22** with one equivalent of undecatetrayne **5b** (R = $CO_2Me$) at RT shows almost total conversion to the Rh(III)-species, which is the rhodacyclopentadiene **25b**, after one day (Figure 37). Letting the reaction mixture stand for one week, shows the re-appearance of small amount of the starting material **22**, which increases upon heating the reaction to 60-80 °C for another week (Figure 37).

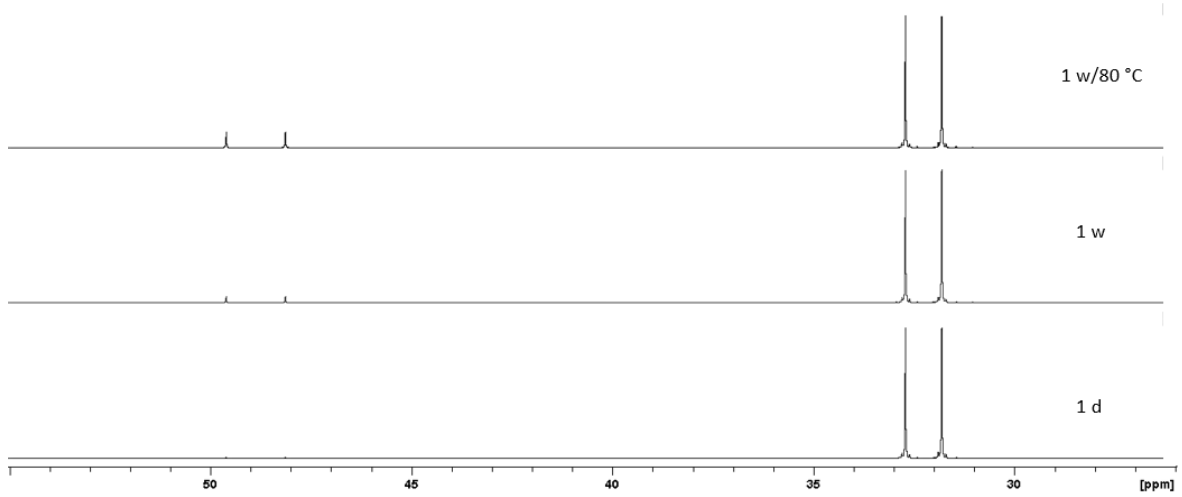


**Figure 37** *In situ* 202 MHz $^{31}P\{^1H\}$ NMR spectra of the reaction of [Rh($\kappa^2$-*S*,*S*`-$S_2CNEt_2$)($PPh_3$)$_2$] **22** and undecatetrayne **5b** after one day (bottom), one week (middle) at RT and another week at 60-80 °C (top) in $C_6D_6$ .

Following this, a 1:1 reaction between complex **22** and undecatetrayne **5d**, having $NMe_2$ as electron-donating substituent at the phenyl rings, was examined at ambient temperature (Figure 38).

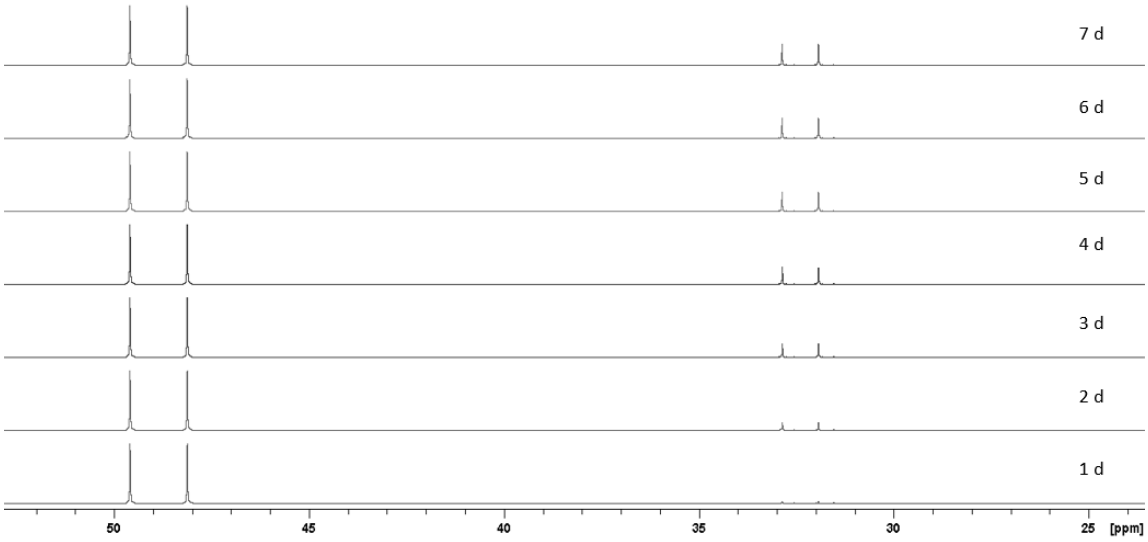


**Figure 38** *In situ* 202 MHz $^{31}P\{^1H\}$ NMR spectra at RT of the reaction of [Rh($\kappa^2$-*S*,*S*`-$S_2CNEt_2$)($PPh_3$)$_2$] **22** with undecatetrayne **5d** during one week in $C_6D_6$.

In this case, almost no Rh(III)-species was observed after one day and after five days, no significant change in the reaction took place. Heating the system pushed the reaction to the re-formation of the starting material.

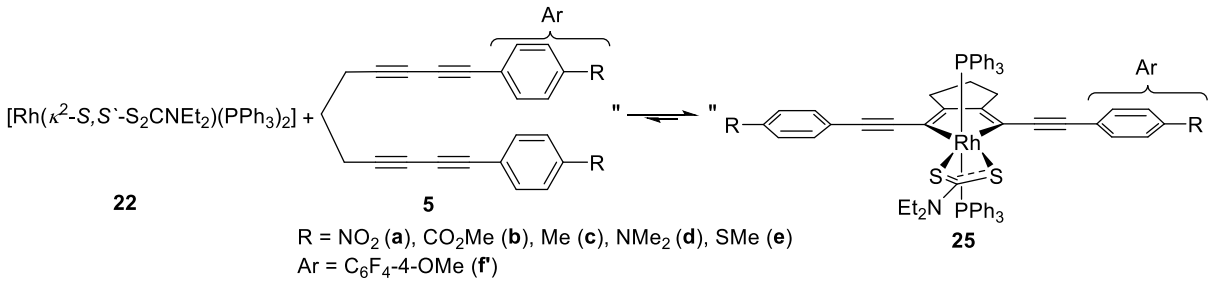


**Scheme 51** Reaction of [Rh($\kappa^2$-*S*,*S*`-$S_2CNEt_2$)($PPh_3$)$_2$] **22** with undecatetraynes **5a-f'**.

A possible equilibrium between [Rh($\kappa^2$-*S*,*S*`-$S_2CNEt_2$)($PPh_3$)$_2$] **22** and undecatetrayne **5d** and the Rh(III)-species during the reaction was considered (Scheme 51). Following this, another reaction was started, using undecatetrayne **5d** in excess (10 eq.) to push the equilibrium to the product side. Surprisingly, even less rhodacycle product than before was formed and the reaction seemed to regenerate 100 % of the starting material [Rh($\kappa^2$-*S*,*S*`-$S_2CNEt_2$)($PPh_3$)$_2$] **22** (Figure 39).

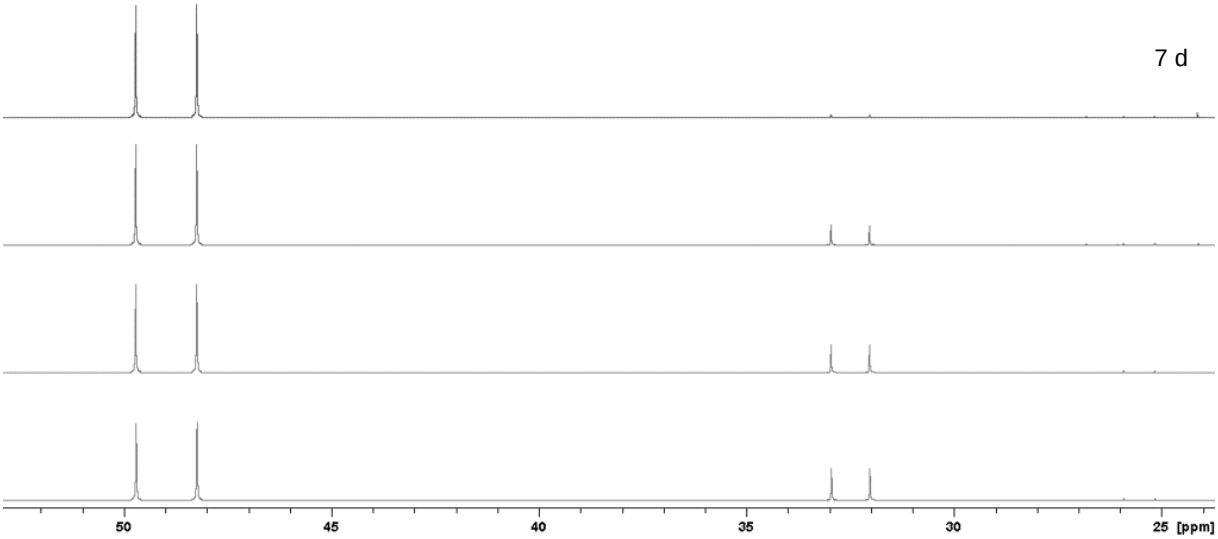


**Figure 39** *In situ* 200 MHz $^{31}P\{^1H\}$ NMR spectra at RT of the reaction of [Rh($\kappa^2$-*S*,*S*`-$S_2CNEt_2$)($PPh_3$)$_2$] **22** and an excess amount of undecatetrayne **5d** during one week in $C_6D_6$.

Figure 40 shows the $^1H$ NMR spectrum of compound **26d** after the work-up. Analysis of the $^1H$ NMR spectrum of this reaction shows the appearance of a significant number of new signals in the aromatic region. In the region of the methyl groups of the $NMe_2$ substituents, more than the two expected signals have appeared, indicating the formation of a new organic species, which

might be the result of a catalytic process. Importantly, no signals for the phosphine or dithiocarbamate ligands were observed, suggesting a purely organic compound.

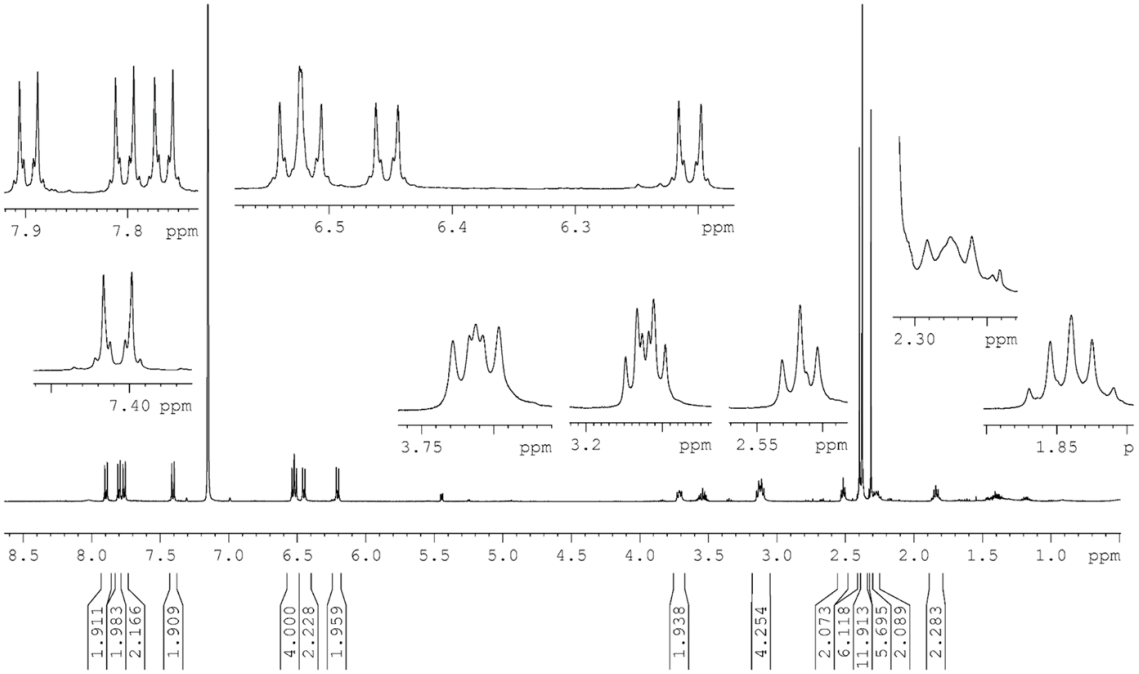


**Figure 40** $^{1}$H NMR spectrum of dimer **26d** after work-up in $CDCl_3$, with residues of $CH_2Cl_2$ and hexane.

The aromatic region shows eight doublets of multiplets at 7.90, 7.82-7.74, 7.41 6.55-6.50, 6.45 and 6.21 ppm with coupling constants of 9 Hz and an integral of two, each. In the alkyl region, a multiplet at 3.74-3.68 ppm appears with an integral of two and another one at 3.17-2.06 ppm with an integral of four protons. At 2.52 ppm a triplet appears with an integral of two protons and a coupling constant of 6 Hz, followed by four singlets at 2.40, 2.39, 2.38 and 2.32 ppm which are assigned to the methyl groups of four $NMe_2$ substituents, all having an integral of six protons. At 2.27 ppm, a multiplet appears with an integral of two protons, followed by a quintet with an integral of two protons and a coupling constant of 7 Hz. The different shifts of the methyl groups in this NMR spectrum indicate that the symmetrical organic backbone of the intermediate rhodacyclopentadiene builds one part of the catalytic product, because two signals are shifted into each other, which might result from a very similar chemical environment. The other two signals are significantly up- and downfield shifted from these two signals, which indicates, that the second part of the molecule is a second tetrayne, bound to this backbone with one triple bond, forming a 6-membered aromatic ring. The work-up of the reaction, using precipitation from THF/hexane and flash chromatography resulted in a yellow solid, showing bright turquoise emission in DCM under UV light (Figure 41), which will be discussed in Chap 3.

An example of a dimeric structure, which fits to the above shown $^{1}$H NMR spectrum, is shown in Figure 41.

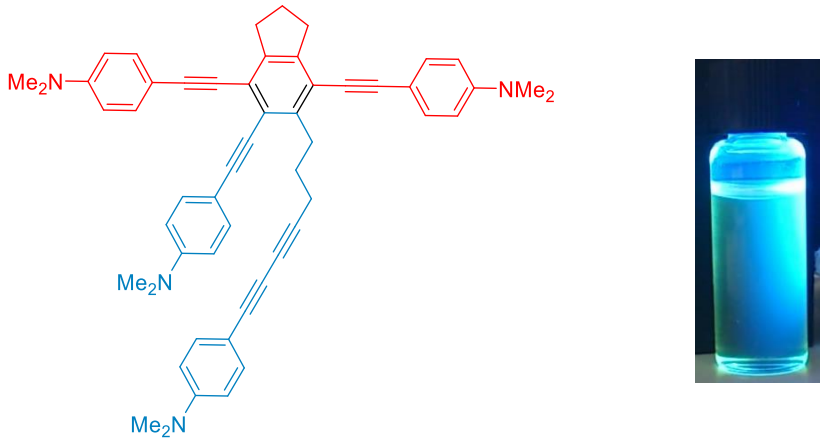


**Figure 41** Chemical structure (left) and picture (right) of product **26d** dissolved in DCM under UV-light.

The red part of the molecule shows the former organic backbone of the rhodacycle species. The blue part shows the second tetrayne, which is now bound to the former backbone, resulting in a benzene ring. This fits very well to the mechanism of the trimerisation of alkynes suggested by Collman *et al.*, shown in Chap. 2.1.1. Further reactions, using undecatetraynes **5b**, **5c** and **5f'**, also showed the formation of catalytic dimers and trimers whereas, in contrast to the reaction of [Rh($\kappa^2$-*S*,*S*`-$S_2CNEt_2$)($PPh_3$)$_2$] **22** and undecatetrayne **5d**, it was possible to isolate both the dimer and the trimer.

**Table 10** Ratio control of formation of dimers **26** (**A**) and trimers **27** (**B**), with different substrate ratios.

| | **Ratio** | |
|---|---|---|
| **Tetrayne** | **5:22** | **A:B** |
| **5b** | 10:1 | 1:3 |
| | 100:1 | 1:0.05 |
| **5c** | 10:1 | 1:0.5 |
| | 100:1 | 1:0.1 |
| **5d** | 10:1 | 1:0.2 |
| | 100:1 | 1:0.2 |
| **5f'** | 10:1 | 0.05:1 |
| | 100:1 | 1:0.8 |

The ratio of the formation of the catalytic products depends on the ratio of [Rh($\kappa^2$-*S*,*S*`-$S_2CNEt_2$)($PPh_3$)$_2$] **22** and undecatetraynes **5**. In general, a ratio of 100:1 (**5**:**22**) results in nearly total conversion to the dimeric product, whereas a ratio of 10:1 (**5**:**22**) results

in a mixture of both compounds, depending on which substituent is attached to the phenyl ring of the undecatetraynes **5**.

When using an undecatetrayne substituted with an electron-withdrawing group (**5b**, R = $CO_2Me$), it is possible to increase the formation of the trimeric species, using a 10:1 ratio of tetrayne **5** to catalyst **22**, whereas a 100:1 ratio forms predominantly the dimer. Employing undecatetrayne **5c** (R = Me), which is rather neutral, shows the effect of the different ratios to be rather small. The system can only be pushed slightly into the direction of the trimeric species with a 10:1 ratio, and forms mainly the dimeric species when used in a 100:1 ratio. A 10:1 ratio reaction using undecatetrayne **5d** was not different from a 100:1 ratio reaction. In both cases, a ca. 1:0.2 mixture of the dimer and trimer is formed, whereas it was only possible to isolate the dimer. Using the tetra-fluorinated undecatetrayne **5f'** (Ar = $C_6F_4$-4-OMe) in a 10:1 ratio reaction pushes the systems to form nearly 100 % of the trimer and using a 100:1 ratio yields a ca. 1:1 mixture of the dimer and the trimer (Table 10).

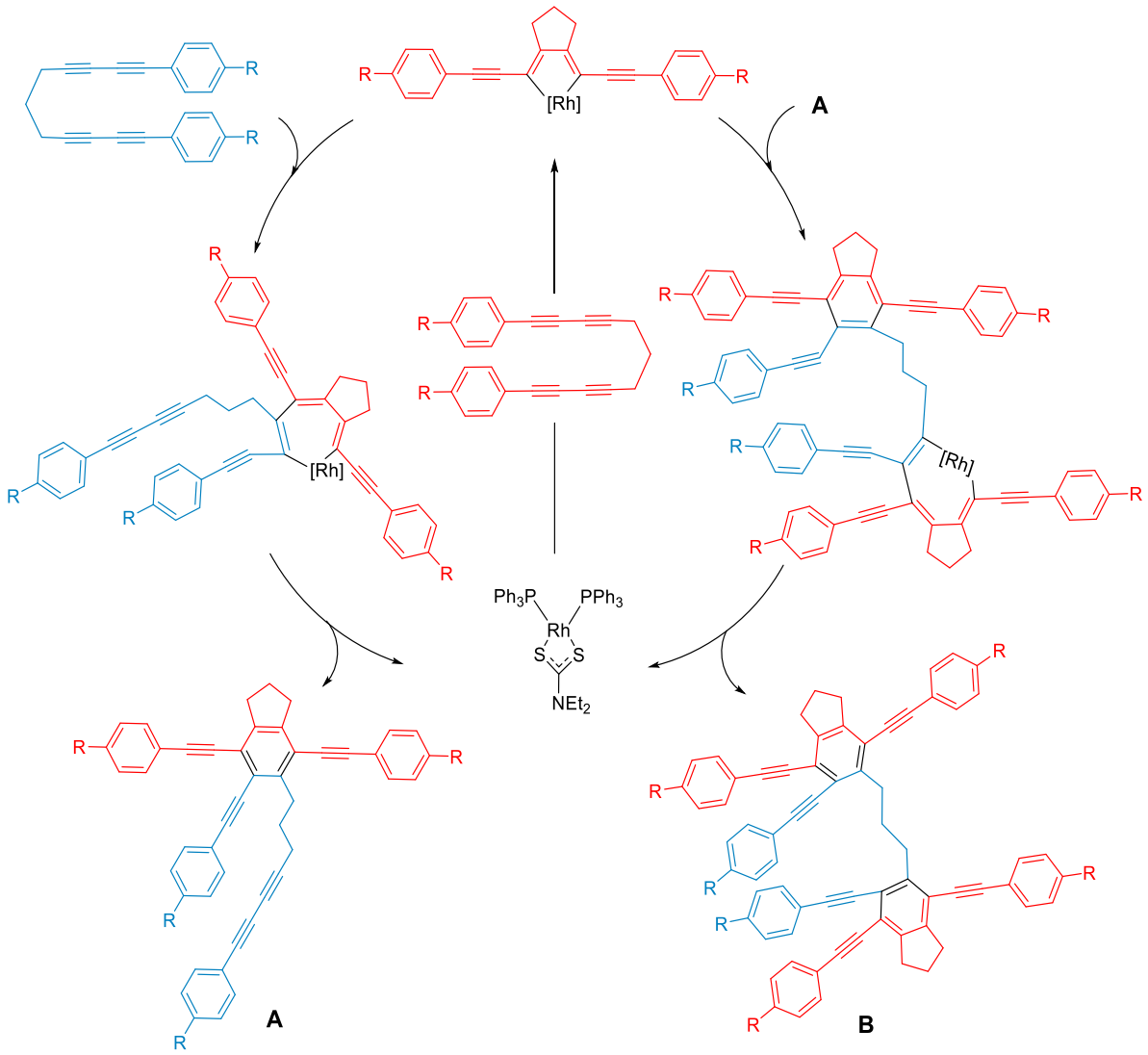


**Scheme 52** Possible pathway of the formation of dimeric (**26**/**A**) and trimeric (**27**/**B**) catalytic products.

A larger amount of catalyst **22** in the presence of less tetrayne creates the possibility of a catalytic cycloaddition reaction taking place on an already formed dimer, generating a trimer. Scheme 52 shows a possible pathway for the formation of the two catalytic products. In the route leading to **A**, a tetrayne is added oxidatively to the Rh-centre of the catalyst to form the rhodacyclopentadiene. In the next step, a second tetrayne is inserted into the rhodacyclopentadiene, and an intermediate with a seven membered ring is formed. Afterwards, a reductive elimination occurs and a benzene derivative, being the dimeric species **26**, is formed. If there is a large amount of catalyst, there will be a high concentration of the rhodacyclopentadiene present, which could react with a free triple bond of the product **A**. The reaction leads to trimer **B**. It is not clear whether the two catalytic reactions occur one after another or in one process as, besides the rhodacyclopentadiene, no intermediate complexes could be observed.

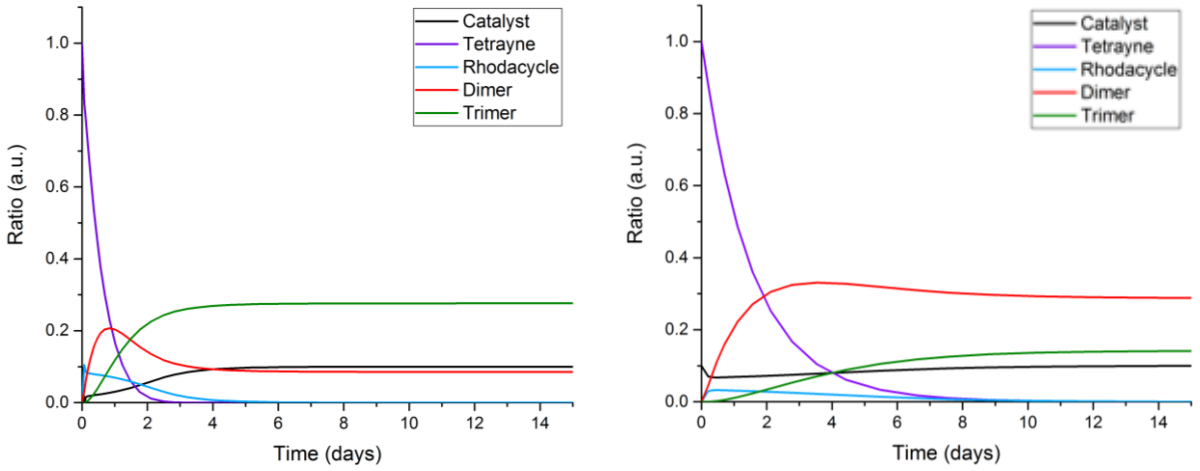


**Figure 42** Simulated kinetics of catalysis using acceptor substituted (left) and donor substituted tetraynes (right) in a 1:10 ratio. The kinetics were simulated with the java-based program Tenua.

**Table 11** Settings of relative rate constants for single steps during the simulations of 1:10 ratio reactions.

| Relative rate constant *k* | Ratio of relative rate constants per reaction step | | |
|---|---|---|---|
| | A+B→C | C+B→A+D | C+D→A+T |
| $k_{Acceptor}$ | 45 | 9 | 10 |
| $k_{Donor}$ | 5 | 10 | 3 |

A=catalyst, B=tetrayne, C=Rh-cycle, D=dimer, T=trimer.

Figure 42 shows the simulated kinetics of the catalysis using Rh-complex **22** and tetraynes **5**, using the setting shown in Table 11. In the left graph is shown the process using the acceptor-substituted tetrayne **5b** as model compound in a 1:10 ratio. It can be seen that in the beginning all of the Rh is converted into the corresponding rhodacyclopentadiene **25**, which reacts further to give the dimeric and trimeric organic products. In contrast, the graph on the right side shows

the process using the weak donor-substituted tetrayne **5c** in a 1:10 ratio, indicating that only about one third of the Rh-catalyst is converted to the corresponding rhodacyclopentadiene, yielding the dimeric organic product as the dominant one from the beginning. The acceptor-substituted tetrayne is consumed significantly faster than the donor-substituted one. The ratio of the rate of the formation and the stability of the rhodacyclopentadienes **25** as well as the consumption rate of the tetrayne **5** seem to influence the whole kinetics of the catalytic system, generally forming more trimeric species when using an acceptor-substituted tetrayne, whereas the system cannot be pushed efficiently to the trimeric species when using a donor-substituted tetrayne.

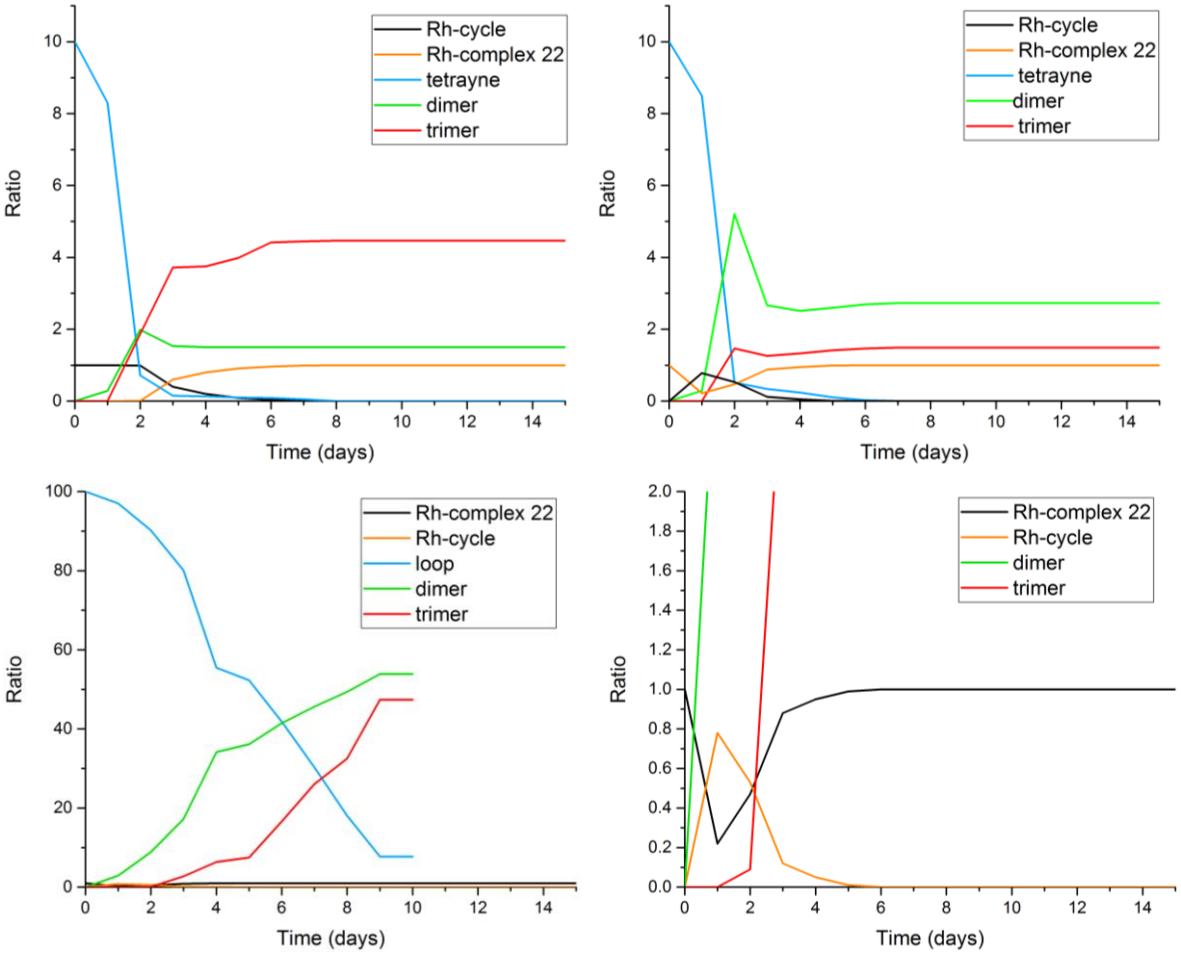


**Figure 43** Plots of NMR spectroscopic monitored kinetics of catalysis using **5b** (top left) and **5c** (top right) 10:1 and a 100:1 ratio catalysis (bottom left) with detail picture (bottom right).

In comparison, the plots of the kinetics monitored by NMR spectroscopy differ slightly from the simulations (Figure 43). In case of using tetrayne **5b**, the dimeric species increases slower than shown in the simulation, the rhodacyclopentadiene being stable for ca. 2 days (top, left). Furthermore, no difference in the consumption speed between the reaction using an acceptor and a donor in the NMR plots can be observed (top, right). In addition, the reaction using the

tetrayne **5c** shows significant differences to the simulation on the right side picture of Figure **42**. At the beginning of the reaction, significantly more rhodacyclopentadiene as in the simulation is formed, whereas the final ratios of the simulation and the monitored kinetic fit quite well.

It has to be noted that, in case of using tetrayne **5d**, which is also donor substituted (R = $NMe_2$), a comparable amount rhodacyclopentadiene to that shown in the simulation is formed (See $^{31}P\{^1H\}$ NMR spectrum, Figure 38) ending up with a slightly ratio of dimeric and trimeric species. Thus, the simulation in Figure 42 can be seen as a more general approach to the kinetic progression of a catalytic reaction using a donor-substituted tetrayne.

The plot of the NMR spectroscopic monitoring of the 100:1 catalysis using tetrayne **5b** (bottom) shows that it is consumed significantly slower than in the 1:1 case. The catalysis was only plotted until day ten, because the dimeric and trimeric species started to precipitate at that point. The detail in the bottom right picture shows that using a 100:1 ratio generates more of the rhodacyclopentadiene after one day, which decreases quickly with further progress of the reaction. It was not possible to generate a suitable kinetic simulation for a 100:1 ratio of any substrate, which therefore will not be discussed here.

All of the obtained dimers **A** (compounds **26**) and trimers **B** (compounds **27**) were characterised *via* $^1H$, $^{13}C$, $^{19}F$ NMR spectroscopy and HRMS, as well as elemental analysis. Furthermore, it was possible to obtain single crystals of the isolated dimer **26c** and trimers **27c** and **f'** and thus confirm their structures by X-ray diffraction. (Figure 44).

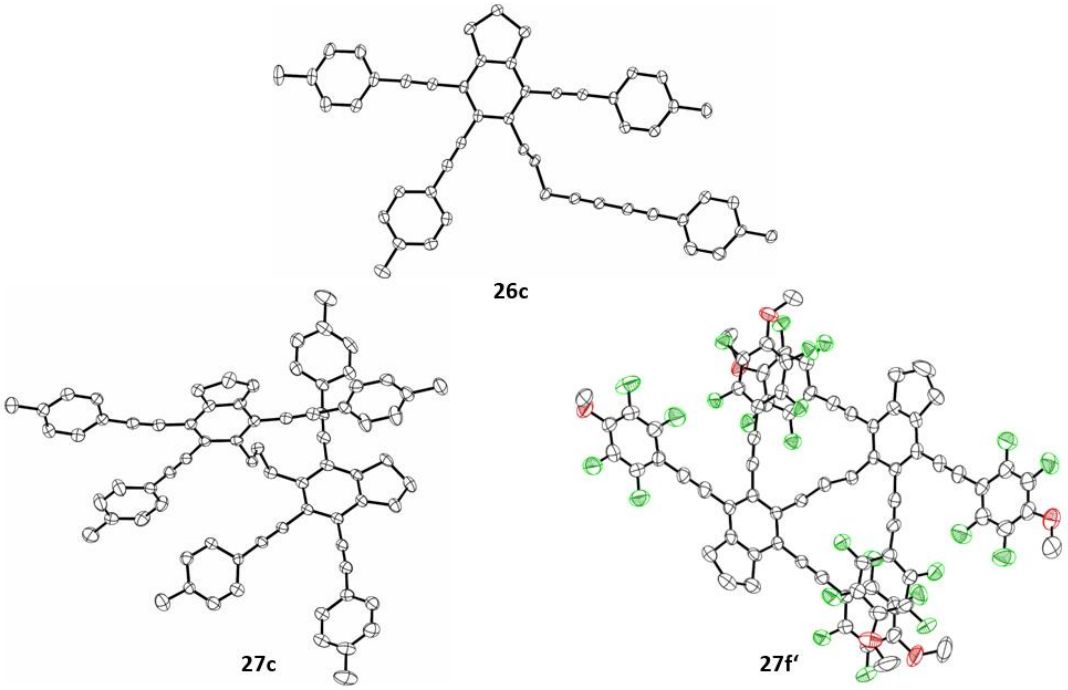


**Figure 44** Molecular structures of dimer **26c** and trimer **27c**. Hydrogen atoms and solvent molecules are omitted for clarity. Thermal ellipsoids are shown at 50 % probability. The structure of **27f'** serves as connectivity proof.

The structure of compound **27f'** only serves as connectivity proof, as the crystals cracked during the measurement to release toluene, which was captured in the crystal structure (Figure 44).
The reactions yielding compounds **25a** and **f'** were stopped at a time at which the formation of the rhodacycle had reached its maximum. The residual catalyst **22** was separated from the crude mixture *via* recrystallisation, by slow diffusion of a hexane layer into a THF solution at -30 °C, as it crystallises easily. The already formed catalysis product was removed the same way, or by precipitation. Afterwards, the crude product was washed several times with hot hexane to remove any phosphine oxide, and purification was achieved *via* recrystallisation by slow diffusion of a hexane layer into a THF solution at -30 °C.

Compounds **25a**, **b**, **d** and **f'** were characterised by $^{1}H$, $^{31}P$, $^{13}C$ and $^{19}F$ NMR spectroscopy, as well as by HRMS and elemental analysis. Their structures were also confirmed by X-ray diffraction. Compound **25c** was not obtained in analytically pure form.

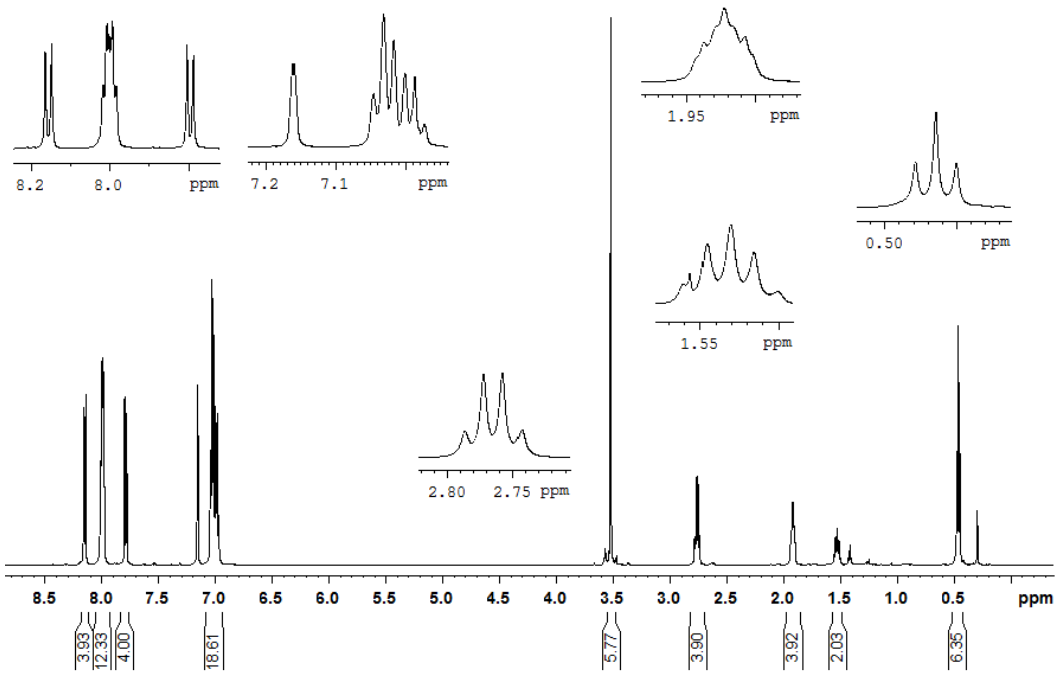


**Figure 45** $^{1}H$ NMR spectrum of compound **25b** in $C_6D_6$.

Figure 45 shows an example of a typical $^{1}H$ NMR spectrum of compounds **25**. As for compounds **23** ($PMe_3$ ligands) , the aromatic region shows two doublets at 8.15 and 7.79 ppm, with a coupling constant of 8 Hz and an integral of four, which are assigned to the aromatic protons of the two phenyl rings at the former tetrayne. The signals for the $PPh_3$ groups appear in the aromatic region as well, as multiplets from 8.04 - 7.95 ppm and 7.06 - 6.95 ppm with integrals of 12 and 18, respectively. In the alkyl region, a singlet at 3.52 ppm with an integral of six, is assigned to $CO_2Me$ substituents. A quartet appears at 2.76 ppm with a coupling

constant of 7 Hz and an integral of four, is assigned to the ethyl-$CH_2$ of the dithiocarbamate. This is followed by a multiplet from 1.95-1.88 ppm with an integral of four and a quintet at 1.53 ppm with a coupling constant of 7 Hz and an integral of two, both being assigned to the backbone of the organic moiety of the rhodacycle. A triplet appearing at 0.46 ppm, with a coupling constant of 7 Hz and an integral of six, belongs to the ethyl-$CH_3$ of the dithiocarbamate.

The $^{31}P\{^1H\}$ NMR spectrum shows a doublet, which appears at 32.58 ppm, with a coupling constant $J_{Rh\text{-}P}$ = 109 Hz, typical for a Rh(III)-species (Figure 46).

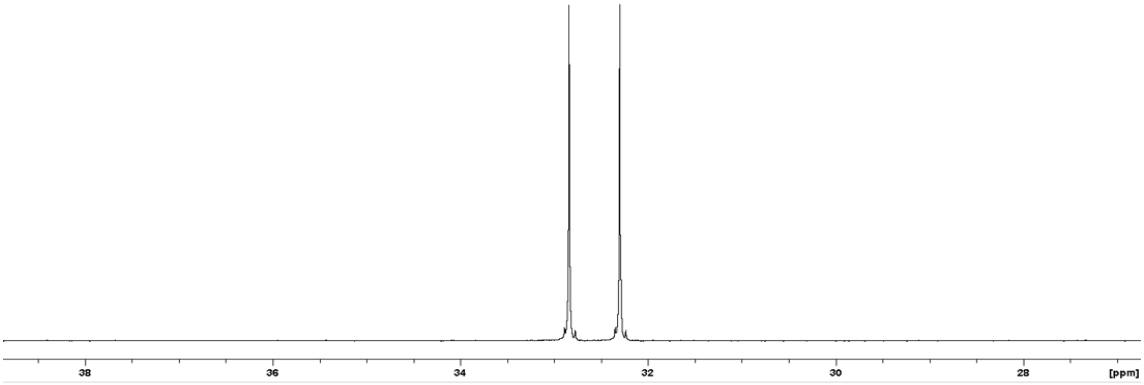


**Figure 46** $^{31}P\{^1H\}$ NMR spectrum of **25b** in $C_6D_6$ at RT.

When compared to the analogous compounds having acac as the bidentate ligand instead of dithiocarbamate, the signals of the rhodacyclopentadienes **25** are shifted by about 8 ppm to high field, as is the case for compounds **23**. In addition, the coupling constants ($J_{Rh\text{-}P}$) are also smaller by about 5 Hz than those of the corresponding rhodacyclopentadienes with acac.[122] Table 12 shows the $^{31}P\{^1H\}$ NMR shifts and Rh-P coupling constants for compounds **25a**, **b**, **e** and **f'**. The observation of compounds **25** in solution by $^{31}P\{^1H\}$ NMR spectroscopy during the catalytic reactions, and their successful isolation, indicates that they are resting states in the catalytic cycle.

The long-term stability of the obtained rhodacyclopentadienes **25** in solution was checked *via* NMR spectroscopy, using rhodacyclopentadiene **25b** as a model compound. The pure rhodacycle was diluted in deuterated benzene and heated to 90 °C for two weeks. Reformation of a modest amount of the starting complex **22** occurs, indicating a possible cycloreversion. Figure 47 shows the NMR spectrum of compound **25b** after heating for one week (bottom) and for two weeks (top). The rhodacyclopentadiene **25** is still the major species, appearing at 32.64 ppm with a $J_{Rh\text{-}P}$ coupling constant of 114 Hz. Additionally, a significant amount of the starting complex **22** appears within two weeks, at 49.37 ppm with a $J_{Rh\text{-}P}$ coupling constant of 176 Hz, accompanied by a doublet at 39.35 ppm with a $J_{Rh\text{-}P}$ coupling constant of 156 Hz, and a broad

singlet at about -5.34 ppm. Another singlet appears at 24.75 ppm after heating the system for two weeks, being phosphine oxide.

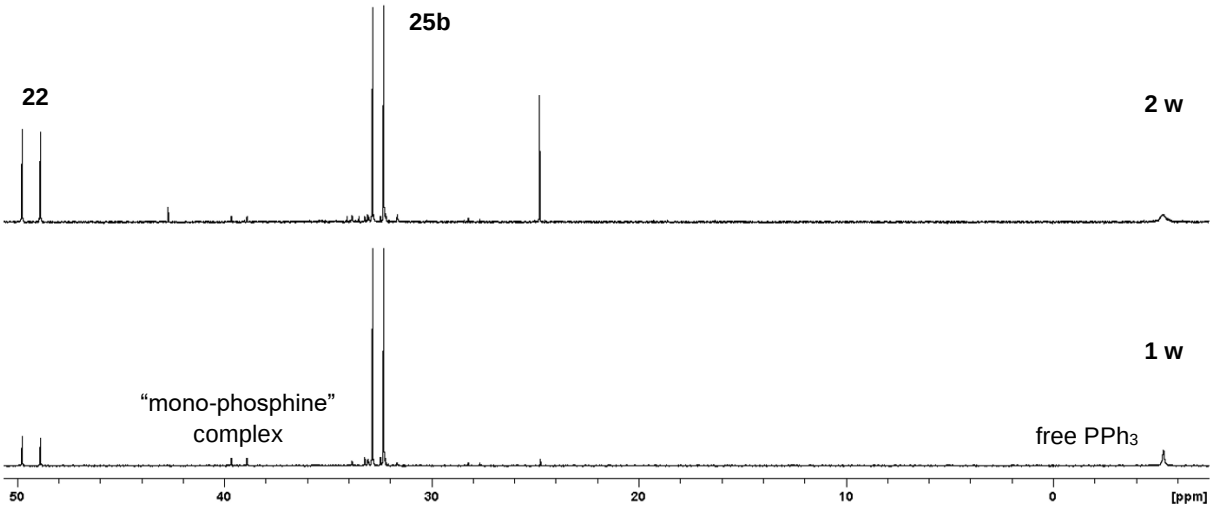


**Figure 47** $^{31}P\{^{1}H\}$ NMR spectrum of isolated rhodacyclopentadiene **25b**, heated in $C_6D_6$ for one week.

As the singlet a -5.34 ppm is assigned to free $PPh_3$, the doublet at 39.35 ppm probably can be assigned to a mono-phosphine Rh-complex, caused by dissociation of one phosphine ligand. The formation of a vacant site, free for a nucleophilic attack at the Rh-centre, in combination with cycloreversion of the cyclopentadiene ring may lead to catalytic cyclisation of the free tetrayne **5b**. The dimeric and trimeric species **26** and **27** would be formed subsequently, leading to the reappearance of the starting complex **22**. To check for any dimeric or trimeric species, a high-resolution mass spectrum was recorded (Figure 48, for the complete mass spectrum see appendix, Chap. 8.3).

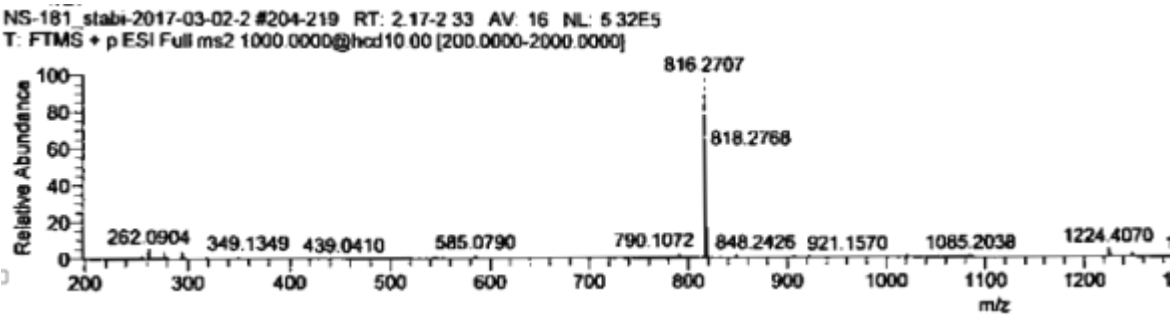


**Figure 48** Detail of mass spectrum recorded of compound **25b** heated in $C_6D_6$.

It clearly shows that the dimeric (calcd: 816.2718, obs.: 816.2707, **26b**) and traces of the trimeric (calcd. 1224.4079, obs.: 1224.4070, **27b**) benzene derivatives have been formed. This proves the cycloreversion of the organic backbone of the rhodacyclopentadiene **25b** to reform the tetrayne **5b** and the Rh(I)-complex **22**.

*Molecular structures of the rhodacyclopentadienes **25***

Single crystals of **25a**, **b**, **e** and **f'** were grown in small glass vials by slow diffusion of a hexane layer into a THF solution at -30 °C. Analysis *via* X-ray diffraction showed compounds **25a**, **b** and **f'** to be triclinic and compound **25e** to be monoclinic, with the space groups *P*-1 (**25a**, **b** and **f'**) and $P2_1/c$ (**25e**) (Figure 49).

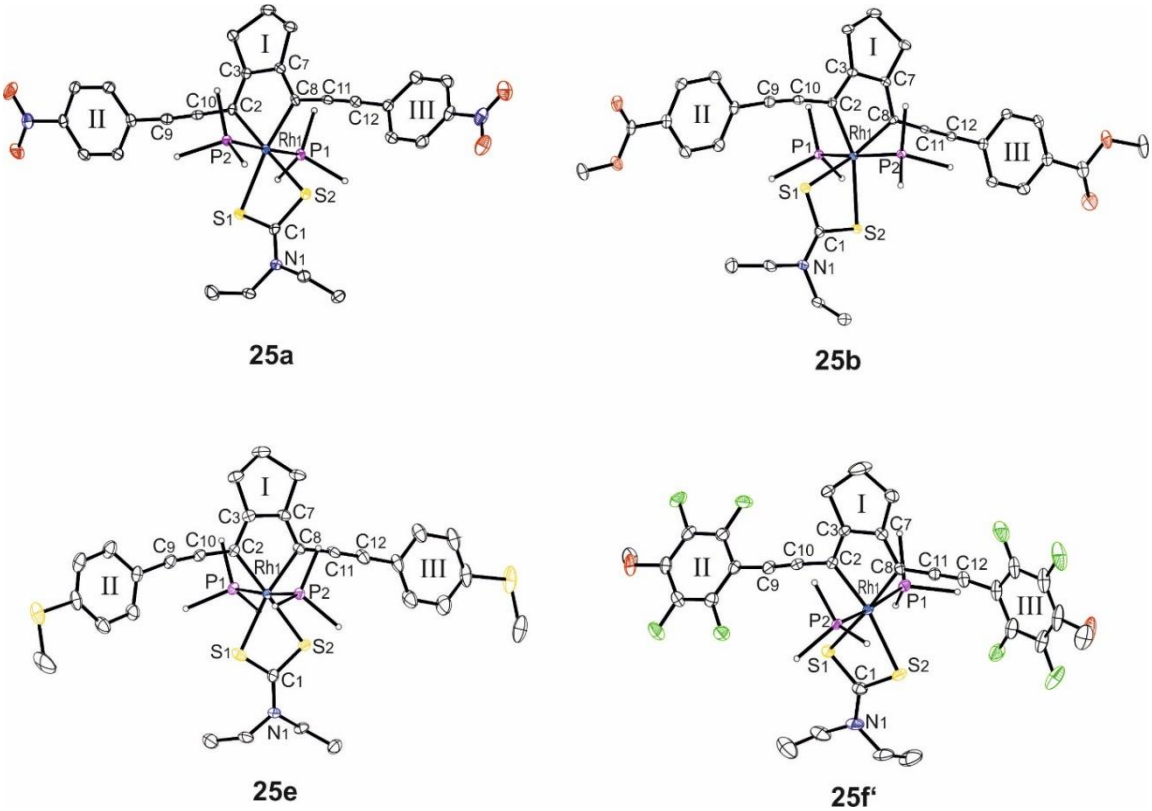


**Figure 49** Molecular structures of **25a**, **b**, **e** and **f'**. Hydrogen atoms are omitted and phenyl groups on P are represented by a simplified "atom" for clarity. Thermal ellipsoids are shown at 50% probability. The second independent molecule of the unsymmetric unit of **25a** is also omitted for clarity.

Compound **25a**, **b**, **e** and **f'** have a distorted octahedral geometry, with the two $PPh_3$ groups in axial positions *trans* to each other. The metallacyclopentadienyl moiety and the dithiocarbamate ligand are both located in the equatorial plane of the octahedron. The distortion is caused by the small bite angle (S1-Rh1-S2, 70.610(18) - 71.55(4)°) of the dithiocarbamate ligand. This results in the C2-Rh1-S1 and C8-Rh1-S2 angles with values of 91.36(5) - 118.19(5)°, which are over 90°. The C2-Rh1-C8 angles have values of 79.88(10) - 80.28(9)°. The P-Rh bond lengths are 2.3143(7) - 2.3637(7) Å, respectively, and are similar to each other. The same applies for the S1-Rh1 (2.3971(6) - 2.5504(6) Å) bond lengths. The C2-Rh1 and C8-Rh1 bond lengths have values of 2.041(3) - 2.1192(19) Å, which lie in the typical range for a Rh-C bond length (Table **12** and 13).

*Comparison of different C-C bonds within compounds **24a** and **b***

Table 12 shows an overview over the important C-C bond lengths and types within compounds **25a**, **b**, **e** and **f'**. The C9-C10 (1.199(5) - 1.210(3) Å) and C11-C12 (1.204(5) - 1.212(4) Å) bond lengths correspond to typical bond lengths of C-C triple bonds with sp-hybridisation for both carbon atoms. In addition, C2-C3 and C7-C8 have bond lengths with values of 1.350(4) - 1.366(3) Å and 1.353(3) - 1.372(3) Å, which fit to typical $sp^2$-hybridised C-C double bonds.

**Table 12** Hybridisation, bond lengths and bond type of selected bonds in compounds **25a**, **b**, **e** and **f'**.

| | | Bond lengths (Å) | | | | Bond type |
|---|---|---|---|---|---|---|
| **Hybridisation** | **Bond** | **25a** | **25b** | **25e** | **25f '** | |
| sp-sp | C9-C10 | 1.204(4) | 1.207(3) | 1.210(3) | 1.199(5) | C≡C |
| sp-sp | C11-C12 | 1.212(4) | 1.207(3) | 1.206(4) | 1.204(5) | C≡C |
| $sp^2$-$sp^2$ | C2-C3 | 1.360(3) | 1.357(3) | 1.366(3) | 1.350(4) | C=C |
| $sp^2$-$sp^2$ | C7-C8 | 1.357(4) | 1.372(3) | 1.353(3) | 1.360(5) | C=C |
| $sp^2$-$sp^2$ | C3-C7 | 1.429(4) | 1.441(3) | 1.429(4) | 1.434(5) | C-C |
| sp-$sp^2$ | C2-C9 | 1.408(4) | 1.417(3) | 1.405(3) | 1.408(5) | C-C |
| sp-$sp^2$ | C8-C11 | 1.406(4) | 1.418(3) | 1.410(3) | 1.406(5) | C-C |
| | Rh1-C2 | 2.085(2) | 2.0570(19) | 2.081(2) | 2.041(3) | |
| | Rh1-C8 | 2.069(2) | 2.1192(19) | 2.062(2) | 2.112(3) | |
| | S1-C1 | 1.715(3) | 1.707(2) | 1.707(3) | 1.710(4) | |
| | S2-C1 | 1.710(3) | 1.7291(18) | 1.702(3) | 1.720(3) | |
| | Rh1-S1 | 2.4653(12) | 2.3971(6) | 2.4623(7) | 2.3973(7) | |
| | Rh1-S2 | 2.4309(11) | 2.5504(6) | 2.4465(6) | 2.4968(8) | |
| | Rh1-P1 | 2.3321(11) | 2.3143(7) | 2.3548(6) | 2.3510(9) | |
| | Rh1-P2 | 2.3317(12) | 2.3637(7) | 2.3368(6) | 2.3492(9) | |

Due to the $sp^2$-hybridisation and the corresponding higher s-character of both carbon atoms, the C3-C7 (1.429(4) - 1.441(3) Å) bond length is shorter than expected for a typical C-C single bond between two $sp^3$-hybridised carbon atoms. The same applies for the C2-C9 and C8-C11 bond lengths with values of 1.405(3) –1.418(3) Å, as the carbon atoms involved are sp- and $sp^2$-hybridised.

Table 12 shows the interplanar angles of compounds **25a**, **b**, **e** and **f'**. The angles between planes I and II are comparable with values of 7.71(15) and 7.48(8)°, showing that the two phenyl rings are nearly coplanar. The angle between planes I and III in compound **24a** is very small with a

value of 2.11(16)°. The corresponding angle in compound **24b** is larger, with a value of 20.43(9)°.

**Table 13** Important angles, $^{31}P\{^{1}H\}$ NMR shifts, isolated yield and space groups of single crystals of **25a**, **b**, **e** and **f'**.

| | | **25a** | **25b** | **25e** | **25f '** |
|---|---|---|---|---|---|
| **Angles (°)** | S1-Rh1-S2 | 71.55(4) | 70.610(18) | 71.08(2) | 71.32(3) |
| | C2-Rh1-S1 | 110.43(7) | 91.36(5) | 109.20(7) | 95.22(8) |
| | C8-Rh1-S2 | 98.15(7) | 118.19(5) | 99.63(6) | 113.59(9) |
| | C2-Rh1-C8 | 79.88(10) | 80.04(7) | 80.28(9) | 79.88(12) |
| | S1-C1-S2 | 113.41(13) | 112.79(11) | 113.65(13) | 112.62(15) |
| **Interplanar angle (°)** | I & II | 21.50(7) | 8.74(6) | 8.24(7) | 32.44(10) |
| | I & III | 20.62(8) | 5.69(6) | 0.75(7) | 5.7(3) |
| **$^{31}P\{^{1}H\}$ NMR shift (ppm)** | | 32.18 | 32.58 | 32.70 | 32.21 |
| **Coupling constant ($J_{Rh-P}$)/Hz** | | 109 | 109 | 111 | 107 |
| **Isolated yield (%)** | | 5 | 43 | 2 | 20 |
| **Space group (single crystal)** | | *P*-1 | *P*-1 | $P2_1/c$ | *P*-1 |
| **Crystal system** | | triclinic | triclinic | monoclinic | triclinic |

### 2.2.4 Ligand Exchange Reactions

As already mentioned before, the reaction of [Rh($\kappa^2$-*S,S`*-$S_2CNEt_2$)($PMe_3$)$_2$] **13** and undecatetraynes **5** results in a mixture of compounds **23** and **24** (Scheme 53).

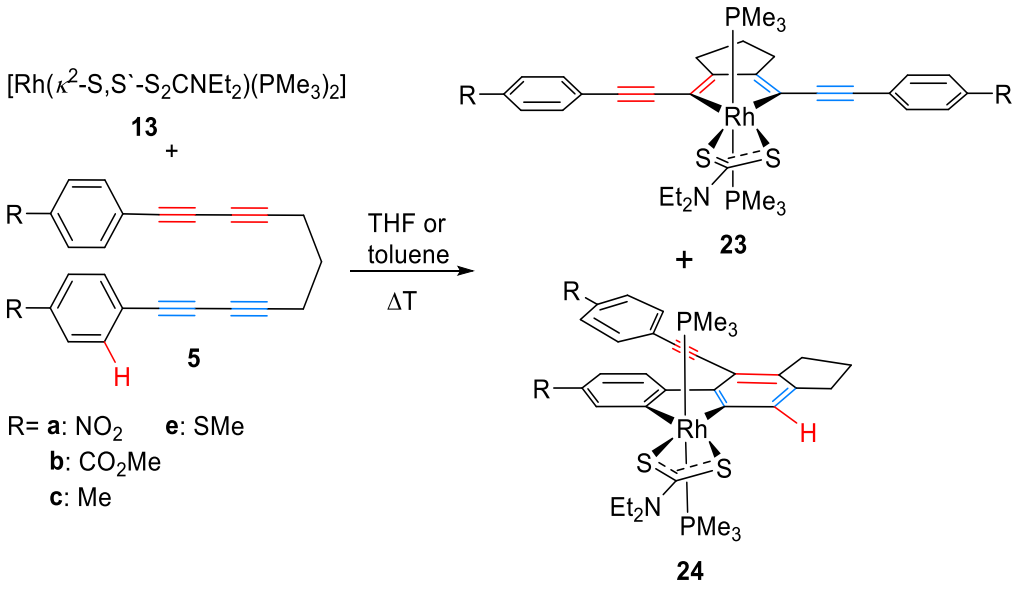


**Scheme 53** Reaction of [Rh($\kappa^2$-*S,S`*-$S_2CNEt_2$)($PMe_3$)$_2$] **13** with tetraynes **5** to give mixture of products **23** and **24**.

Therefore, attempts to obtain compound **23** *via* a different route, namely *via* ligand exchange have been made. This route removes the problem of separating the two isomers from each other.

*Exchange of phosphine ligands $PPh_3$ to $PMe_3$*

The first attempt was to exchange the phosphine ligands to obtain rhodacyclopentadienes **23** starting from compounds **25** and using an excess of $PMe_3$, (Scheme 54).

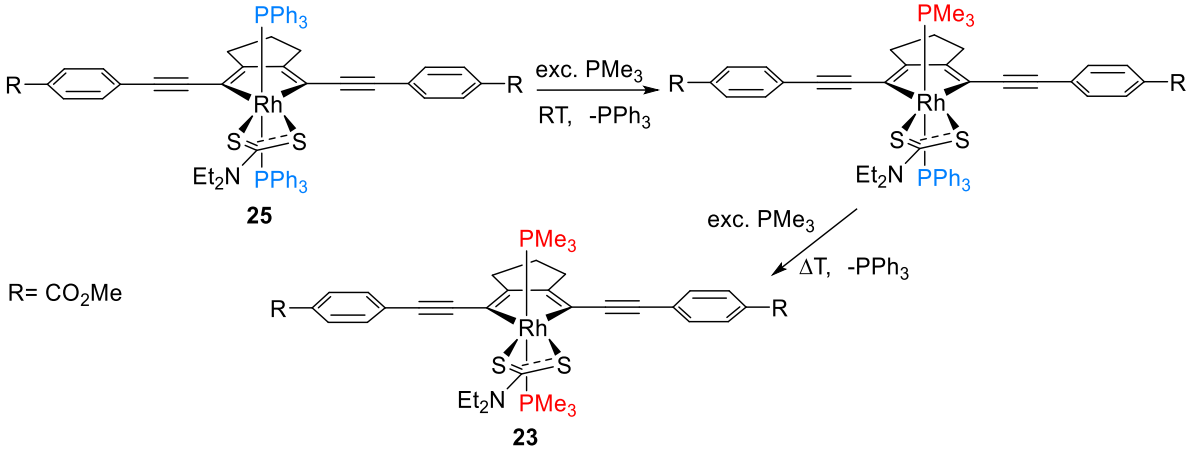


**Scheme 54** Synthesis of compound **23b** *via* stepwise exchange of $PPh_3$ by $PMe_3$.

A sample of the pure, isolated compound **25b** (R = $CO_2Me$) was diluted in THF under an argon atmosphere and charged directly with $PMe_3$ (15-20 eq.). The reaction was monitored by $^1H$ and $^{31}P\{^1H\}$ NMR spectroscopy. Following the reaction at ambient temperature showed that only one phosphine ligand is exchanged, whereas the second ligand is exchanged at higher temperatures (60 °C) (Figure 50). Obviously, the dissociation of the first phosphine ligand is easier, as the dissociation of the second one only takes place at elevated temperatures. Figure 50 shows the *in situ* $^{31}P\{^1H\}$ NMR spectra of the exchange reaction at ambient (upper one) and elevated (lower one) temperatures after four days. The spectrum at ambient temperature shows two doublets of doublets at 31 ppm and -22 ppm with a coupling constant $J_{PP}$ of 20 Hz, which indicates that there are two inequivalent *trans* phosphines bound to the rhodium centre. At ca. -5 ppm, a singlet, assigned to free $PPh_3$, appears. The upfield-shifted signal of free $PMe_3$ appears at ca. -60 ppm and is not shown in the figure.

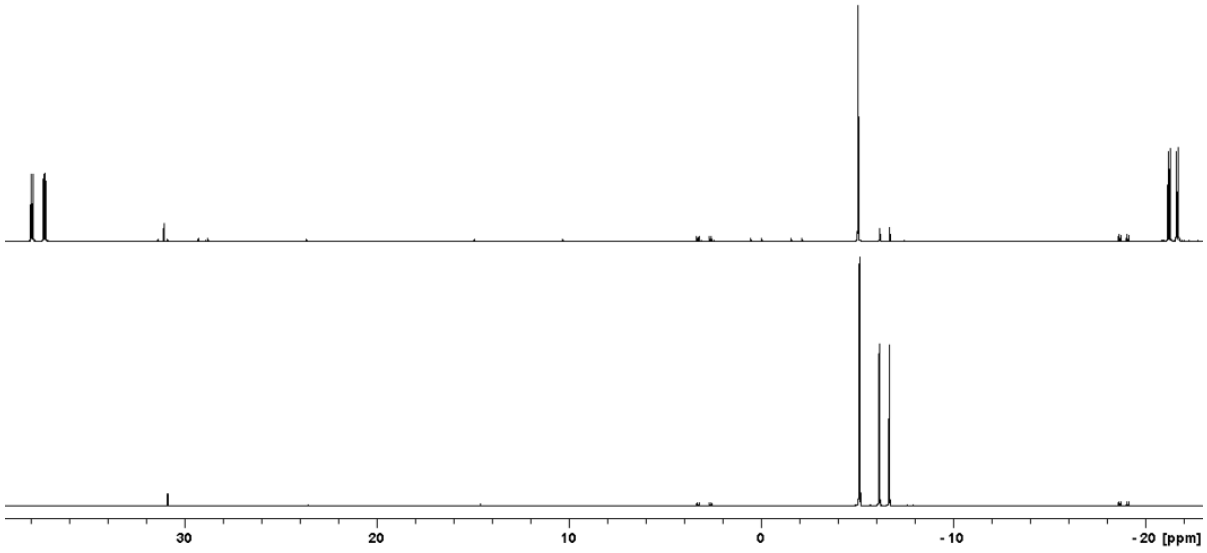


**Figure 50** *In situ* 202 MHz $^{31}P\{^1H\}$ NMR spectra of the exchange reaction of $PPh_3$ by $PMe_3$ at RT (top) and 60 °C (bottom) in THF.

The lower spectrum shows, instead of the two doublets of doublets, only one main doublet at ca. -7 ppm, which belongs to the rhodacyclopentadiene **23b**, now, bearing two $PMe_3$ ligands. To isolate the compound, it was washed with hexane several times and then recrystallised from a THF/hexane mixture at -30 °C to remove the residual $PPh_3$. The free $PMe_3$ was removed *in vacuo*.

*Exchange of bidentate ligand acac to dithiocarbamate*

A second attempt was the formation of the dibenzorhodacyclopentadiene **24** *via* exchange of the bidentate ligands (Scheme 55).

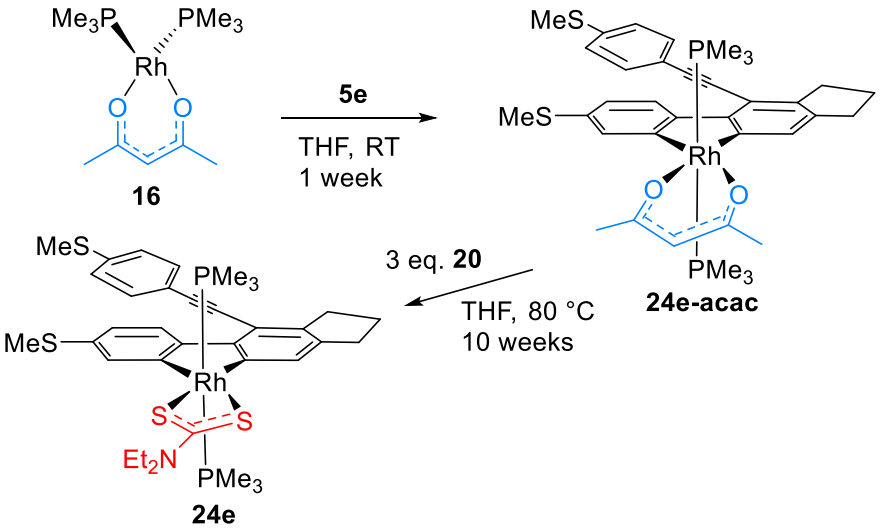


**Scheme 55** Synthesis of dibenzorhodacyclopentadiene **24e** starting from [Rh($\kappa^2$-*O*,*O*`-acac)($PMe_3$)$_2$] **16**.

The idea was to start from the dibenzorhodacyclopentadiene **24e-acac**, bearing acac as bidentate ligand, as reactions with compound [Rh($\kappa^2$-*O*,*O*`-acac)($PMe_3$)$_2$] **16** resulted in the dibenzorhodacyclopentadiene as the main product. A test reaction was carried out to obtain compound **24e** (R = SMe), as the isolation of that compound was unsuccessful up to that point. Therefore, [Rh($\kappa^2$-*O*,*O*`-acac)($PMe_3$)$_2$] **16** and undecatetrayne **5e** were dissolved in THF and stirred at ambient temperature under argon for one week. After the successful isolation of the dibenzorhodacyclopentadiene **24e-acac**, the exchange of acac by dithiocarbamate was carried out.

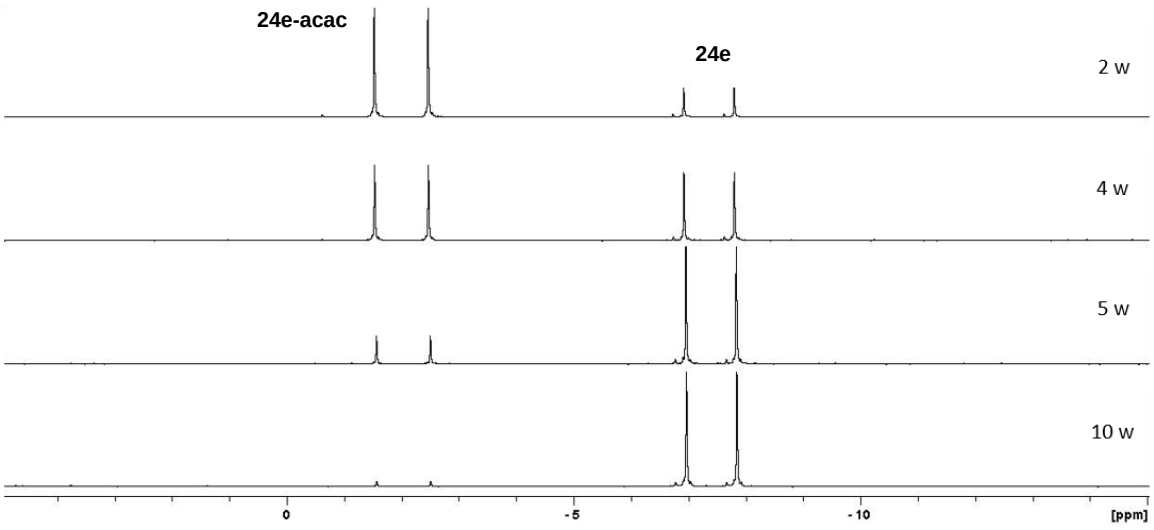


**Figure 51** *In situ* 202 MHz $^{31}P\{^1H\}$ NMR spectra in THF of dithiocarbamate exchange reaction of **24e-acac** to obtain **24e**.

The dibenzorhodacyclopentadiene **24-acac** and sodium dithiocarbamate **20** (3 eq.) were dissolved in THF and heated to 80 °C for 10 weeks, under argon. The reaction was monitored *via* $^{31}P\{^{1}H\}$ NMR spectroscopy. Figure 51 shows the *in situ* $^{31}P\{^{1}H\}$ NMR-spectra of the reaction to form compound **24e**. After two weeks, the doublet at 2.0 ppm with a $J_{Rh\text{-}P}$ coupling constant of 114 Hz, indicates that the dibenzorhodacyclopentadiene **24e-acac** is still the major species present but, at about -6.30 ppm, a doublet is growing in, with a coupling constant $J_{Rh\text{-}P}$ of 117 Hz which is assigned to the desired dibenzorhodacyclopentadiene **24e**, with traces of its corresponding rhodacyclopentadiene **23e** at -6.25 ppm.

The exchange of the acac ligand is very slow, compared to the phosphine exchange. Nevertheless, it is possible to exchange the bidentate ligand by dithiocarbamate, to obtain the corresponding dibenzorhodacyclopentadiene with 98% conversion, after heating the reaction to 80 °C for 10 weeks.

Other attempts in this group to exchange the acac ligand by dithiocarbamate were carried out, starting from a normal rhodacyclopentadiene **25f'-acac** bearing P(*p*-tolyl)$_3$ instead of PMe$_3$ (Scheme 56).[128]

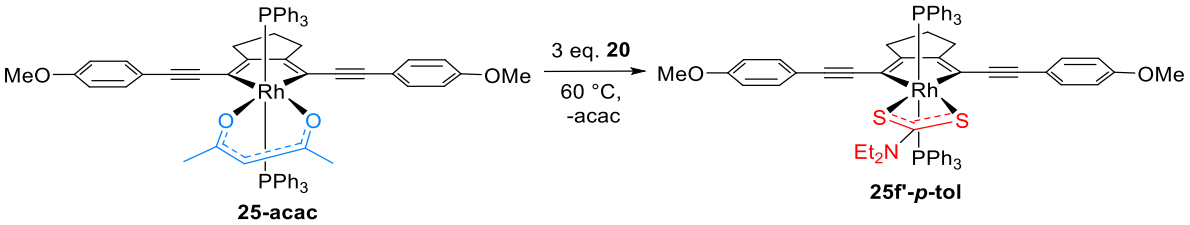


**Scheme 56** Exchange reaction of compound **25-acac** to give rhodacyclopentadiene **25f'-*p*-tol**.[128]

The exchange of the bidentate ligand in this case only took several days, with heating the system at 60 °C. Probably the exchange reaction rate is enhanced by the P(*p*-tolyl)$_3$ groups as they easily dissociate to offer a free coordination side and thus a possibility for dithiocarbamate to attack the Rh-centre. The faster reaction may be also attributed to the electronic influence of the organic backbone.

The time dependent *in situ* $^{31}P\{^{1}H\}$ NMR spectra of the reaction of compound **25f'-acac** with dithiocarbamate show that after three days 100% conversion was obtained, resulting in the corresponding rhodacyclopentadiene **25f'-*p*-tol** (Figure 52). The spectrum at the bottom, recorded directly after starting the reaction, shows one doublet at 23.60 ppm, with a coupling constant $J_{Rh\text{-}P}$ of 112 Hz, which can be assigned to the starting compound **25f'-acac**.

After heating the system to 60 °C for 16 h, another doublet appears at 30.78 ppm, which is already the main species in solution. It has a coupling constant $J_{Rh-P}$ of 107 Hz and can be assigned to the desired rhodacyclopentadiene **25f'-*p*-tol**.

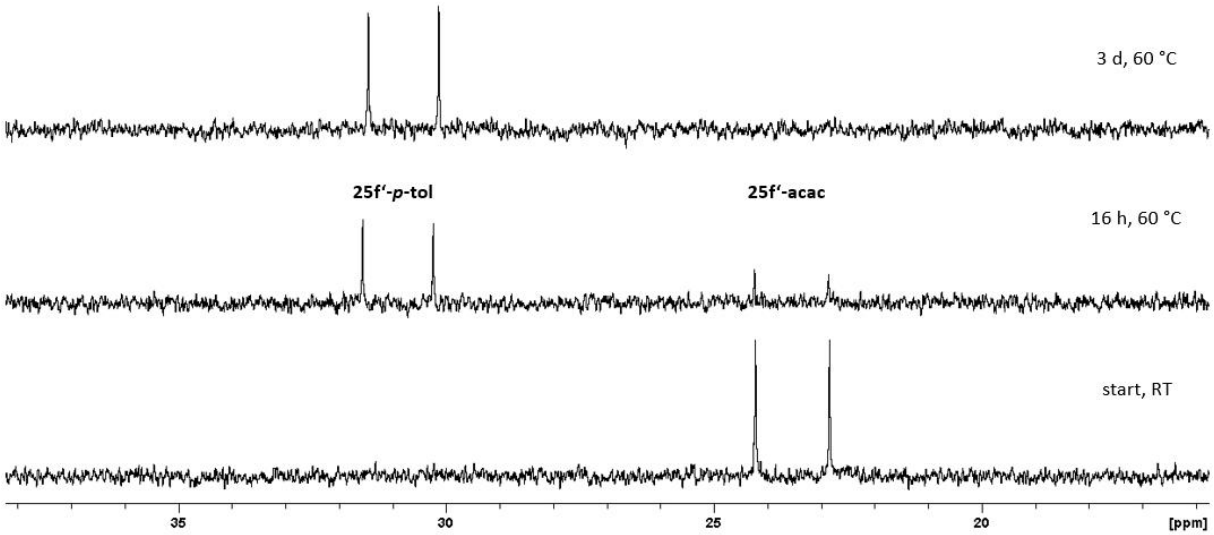


**Figure 52** *In situ* 80 MHz $^{31}P\{^{1}H\}$ NMR spectra of the reaction of compound **25f'-acac** with dithiocarbamate at RT (bottom) directly after the start, after 16 h at 60 °C (middle) and after three days at 60 °C (top) in THF.[128]

*Exchange of $PPh_3$ by N-heterocyclic carbenes (NHC)*

NHCs are strong $\sigma$-donors and $\pi$-acceptors and thus should be suitable for replacement of $PPh_3$. For a test reaction, 1,3-Di-*n*-propylimidazolium was used. Thus, compound **25b** was dissolved in $C_6D_6$ and charged with an excess (20 eq.) of $^{n}Pr$-NHC (Scheme 57). It was only possible to exchange one $PPh_3$ ligand, even when heating the reaction mixture. The exchange of the ligands was monitored *via* $^{1}H$, $^{13}C\{^{1}H\}$ and $^{31}P\{^{1}H\}$ NMR spectroscopy. Figure 53 shows the *in situ* $^{31}P\{^{1}H\}$ NMR spectrum of the ligand exchange reaction.

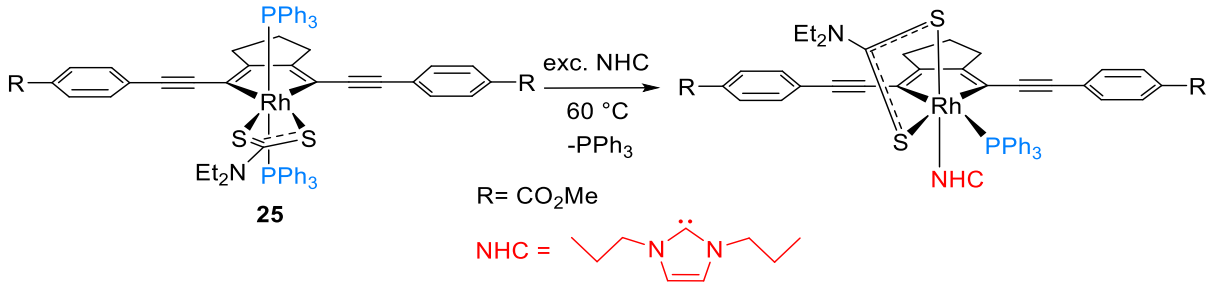


**Scheme 57** Exchange of one phosphine ligand by an NHC.

In the $^{31}P\{^{1}H\}$ NMR spectrum, two signals appear, one being a doublet at about 40 ppm, with a coupling constant of 130 Hz, which corresponds to the coupling between $PPh_3$ and the rhodium centre. The other signal, showing up at about -5.5 ppm, is assigned to free $PPh_3$ (Figure

53). These two signals indicate the exchange of only one phosphine ligand against an $^{n}Pr$-NHC ligand. The increase of the coupling constant $J_{Rh\text{-}P}$ of about 20 Hz compared rhodacyclopentadiene **25b** with two $PPh_3$ ligands bound to the rhodium centre indicates that, the binding strength between the rhodium and the second phosphine left after the exchange, is also increasing, which may be a reason why it is only possible to exchange one phosphine ligand.

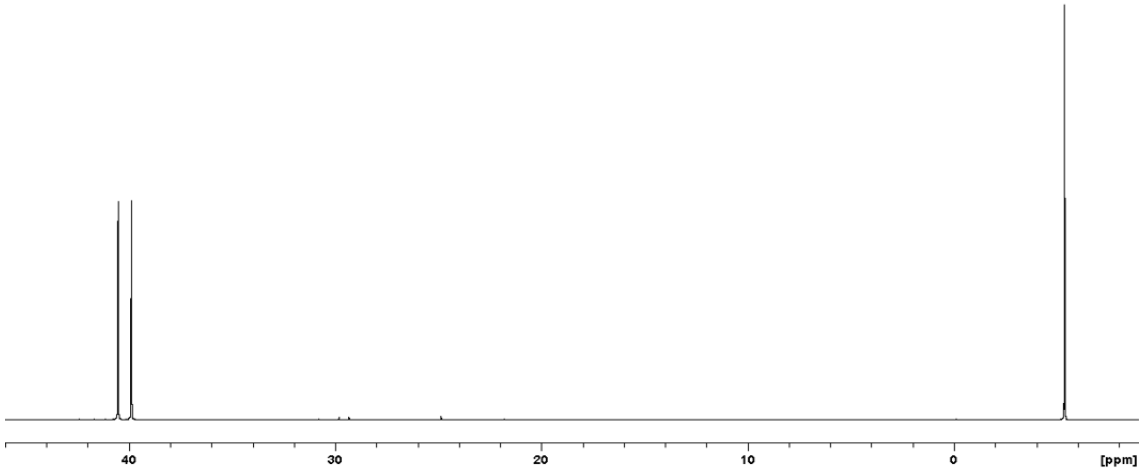


**Figure 53** *In situ* 202 MHz $^{31}P\{^{1}H\}$ NMR spectrum of the exchange of one $PPh_3$ ligand by an $^{n}Pr$-NHC ligand at 60 °C in $C_6D_6$.

The $^{13}C\{^{1}H\}$ NMR spectrum shown in Figure 54, proves that, one $^{n}Pr$-NHC is, indeed, linked to the Rh-centre because at ca. 185 ppm a typical doublet of doublets appears, which is highly downfield shifted. Its coupling constants are $J$ = 7 and 38 Hz, which fits to two of the coupling constants found by Crudden and co-workers, who exchanged a $PR_3$ ligand at various $[Rh(PR_3)_3]Cl$ catalysts by an NHC ligand.[129]

After the exchange of one phosphine ligand by an NHC in the Crudden systems, there are still two phosphines left, one *cis* and *trans* to the NHC. Therefore, Crudden and co-workers report a doublet of doublets of doublets in the $^{13}C\{^{1}H\}$ NMR spectrum at about 200 ppm, with coupling constants of $J$ = 117, 49 and 14 Hz, the first being a *trans* P-C coupling. In earlier work in our group, using the corresponding rhodacyclopentadiene **25b**, having acac as the bidentate ligand, it was also possible to exchange one $PR_3$ ligand (R = *p*-tolyl) by a *Me*-NHC, yielding a rhodacyclopentadiene with the NHC and the phosphine ligands *trans* to each other. The corresponding coupling constants of the doublet of doublets in the $^{13}C\{^{1}H\}$ NMR spectrum are $J$ = 146 and 48 Hz (Figure 54).[130] This shows, that the position of the $PR_3$-ligand with respect to the NHC has a significant influence on the Rh-C coupling constant of the complex, making it possible to predict its symmetry.

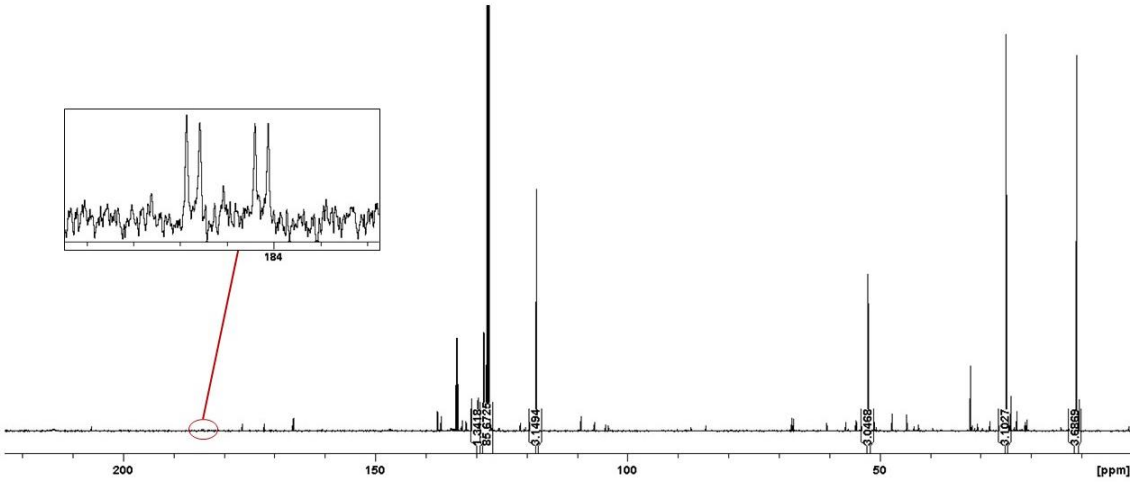


**Figure 54** $^{13}C\{^{1}H\}$ NMR spectrum of the exchange of a $PPh_3$ ligand against an NHC ligand in compound **25b** at 125 MHz in $C_6D_6$.

This was additionally supported by the crystal structures of the complexes obtained from the exchange reactions. The crystal structure obtained from the exchange reaction of the rhodacyclopentadiene with acac instead of dithiocarbamate using compound **4e** (R = SMe) shows the NHC and the $PR_3$ ligand to be *trans* to each other.[130]

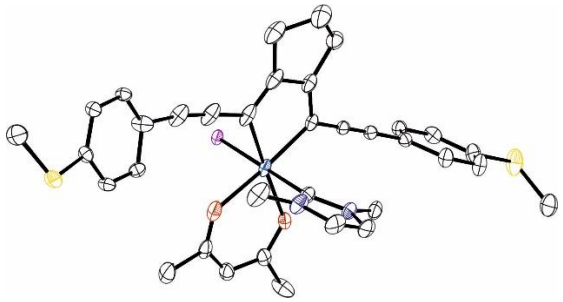

**Figure 55** Molecular structure of Rh-acac rhodacyclopentadiene bearing an *Me*-NHC. Hydrogen atoms and the phenylrings of the $PPh_3$ ligand are omitted for clarity (CCDC number : 1531335).[130]

It is therefore striking that in rhodacyclopentadiene **25b-NHC** the two ligands are *cis* to each other (Figure 56).

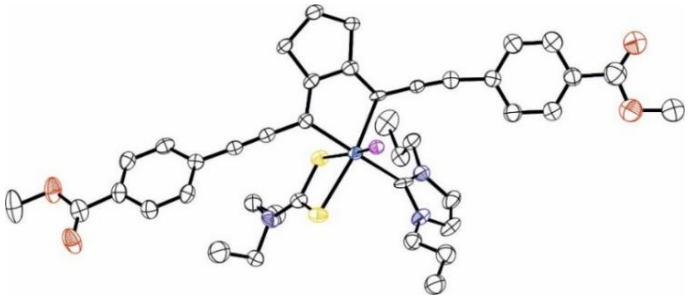

**Figure 56** Molecular structure of compound **25-NHC** to confirm the connectivity of the molecule. R = 9.81, due to strong solvent molecule disorder. Hydrogen atoms, solvent molecules and the phenyl rings of the $PPh_3$ ligand are omitted for clarity.

The steric demands of the two NHC molecules are not very different, but the *$^{n}$Pr* ligand is, in general, expected to be slightly larger than the *Me* one. Thus, the *$^{n}$Pr*-NHC should rather occupy an axial position, sitting *trans* to the $PPh_3$ ligand. Probably, the *cis*-disposition is caused by a difference in the electronic influence of the dithiocarbamate and the acac ligand, or by the small bite angle of the dithiocarbamate ligand, which causes a distortion of the molecule. The Rh-C bond length between the Rh centre and the NHC carbon of the acac-complex is slightly shorter than the corresponding bond of complex **25-NHC**, with values of 2.0889(17) and 2.144(9) Å, respectively. Additionally, the Rh-C bond lengths in the cyclopentadiene ring of complex **25-NHC** are similar with values of 2.095(8) and 2.108(7) Å and slightly longer than the corresponding bond lengths in the acac-complex (2.0602(19) and 2.0513(18) Å). We do not yet know why the *cis* disposition of the NHC and phosphine ligands occurs in complex **25-NHC**.

### 2.2.5 Reactions of 1,3-Butadiynes with [Rh($\kappa^2$-*S,S*`-$S_2CNEt_2$)($PMe_3$)$_2$]

The first test reactions to investigate further the mechanism of the reductive coupling of the 1,3-diynes **4** to [Rh($\kappa^2$-*S,S*`-$S_2CNEt_2$)($PMe_3$)$_2$] **13** were carried out with 1,4-bis(*p*-carbomethoxyphenyl)buta-1,3-diyne **4b**, 1,4-bis(*p*-tolyl)buta-1,3-diyne **4c** and 1,4-bis(*p*-N,N'-dimethylaminephenyl)buta-1,3-diyne **4d** in a 2:1 ratio in deuterated benzene at ambient temperature. The reaction carried out with compound **4b** showed an immediate colour change from orange to deep red, indicating that the reaction has started. In contrast, the reactions with diynes **4c** and **d** showed no significant colour change, and the reaction with diyne **4d** did not show any conversion at all by NMR spectroscopy. According to earlier works of Marder *et al.* using compounds **4** (Chap. 2.1.3, compounds **7** and **9**-**12**) and Rh-complexes with monodentate ligands $PMe_3$ and either, C≡C-TMS, Me or Cl, the most likely product expected was the "normal" rhodacyclopentadiene, as shown in Scheme 58.

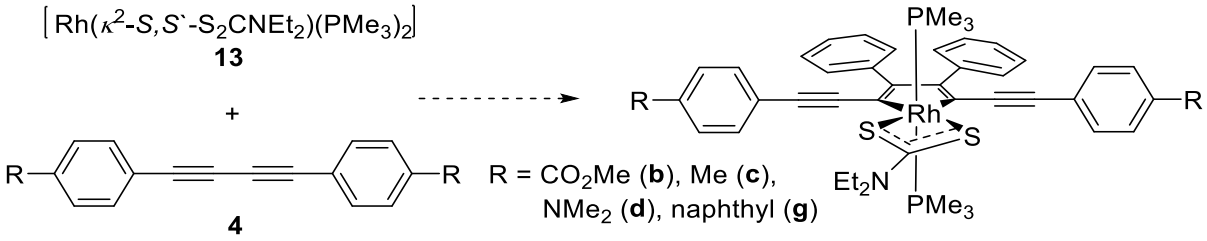


**Scheme 58** Expected formation of rhodacyclopentadienes *via* reductive coupling of 1,3-diynes **4b, c, d and g** to the Rh-complex **13**.

Another possibility might be the formation of a [3+2] cycloaddition product **19**, found during the work of Tay, Thibault and Murata, when investigating the reaction behaviour of [Rh($\kappa^2$-*O,O*`-acac)($PMe_3$)$_2$] **16** with butadiynes **4**, as shown in Scheme 58 (see also Chap. 2.1.3).[73,127,131]

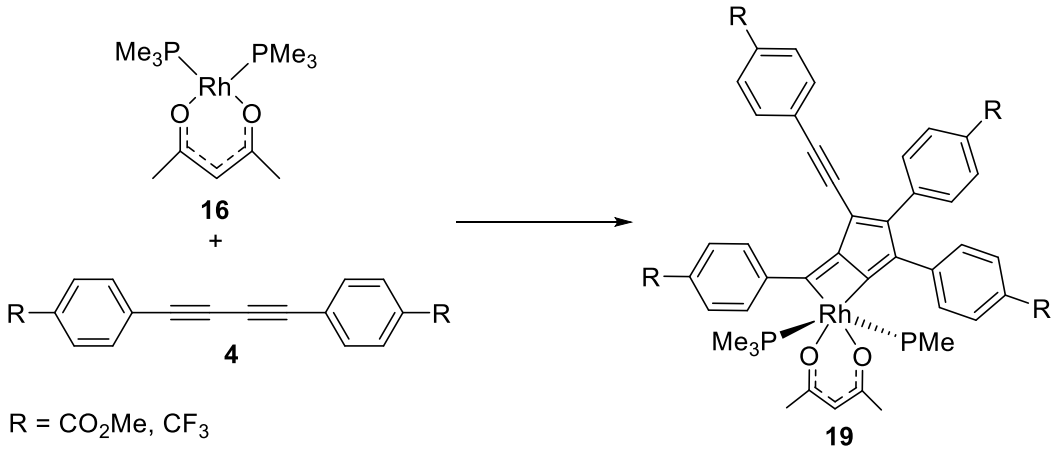


**Scheme 59** Reaction of [Rh($\kappa^2$-*O,O*`-acac)($PMe_3$)$_2$] **16** with butadiynes **4** to yield the [3+2] addition product **19**.

A typical *in situ* $^{31}P\{^{1}H\}$ NMR spectrum recorded during the reaction of complex **13** with diyne **4b** (1:2 ratio), shows one main doublet at -6 ppm with a Rh-P coupling constant of 103 Hz and three smaller doublets at -5.06 (104 Hz), -8.37 (115 Hz) and -13.34 (104 Hz) (Figure 57).

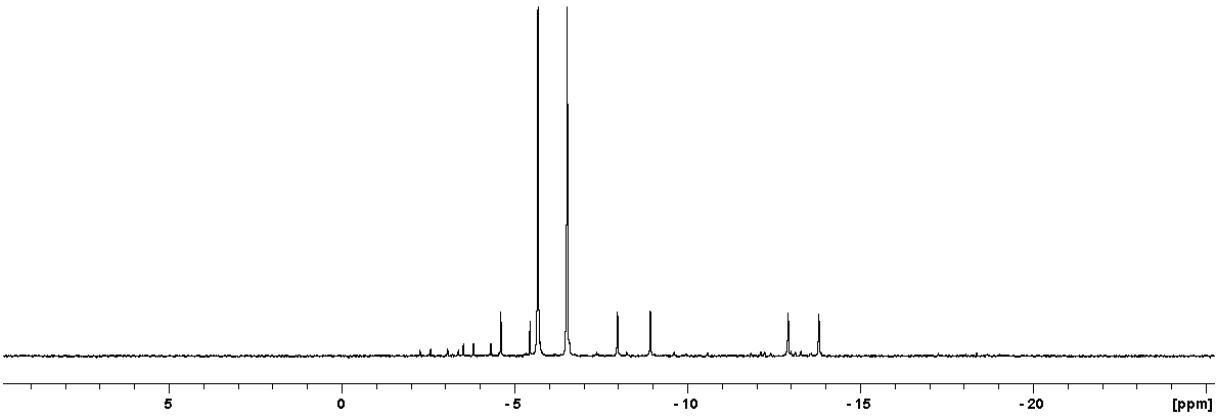


**Figure 57** *In situ* 121 MHz $^{31}P\{^{1}H\}$ NMR spectrum of the reaction of complex **13** with diyne **4b** (1:2) after one week in $C_6D_6$.

The main doublet fits well to a Rh(III)-species, as is found in rhodacyclopentadienes or in the [3+2] addition product **19**. The *in situ* $^{1}H$ NMR spectrum of this reaction (Figure 58) shows four doublets of multiplets at 7.95, 7.93, 7.70 and 7.52 ppm in the aromatic region, which can be assigned to the aromatic protons of the phenyl groups of the part of compound **4b** which is bound to the Rh(III)-centre.

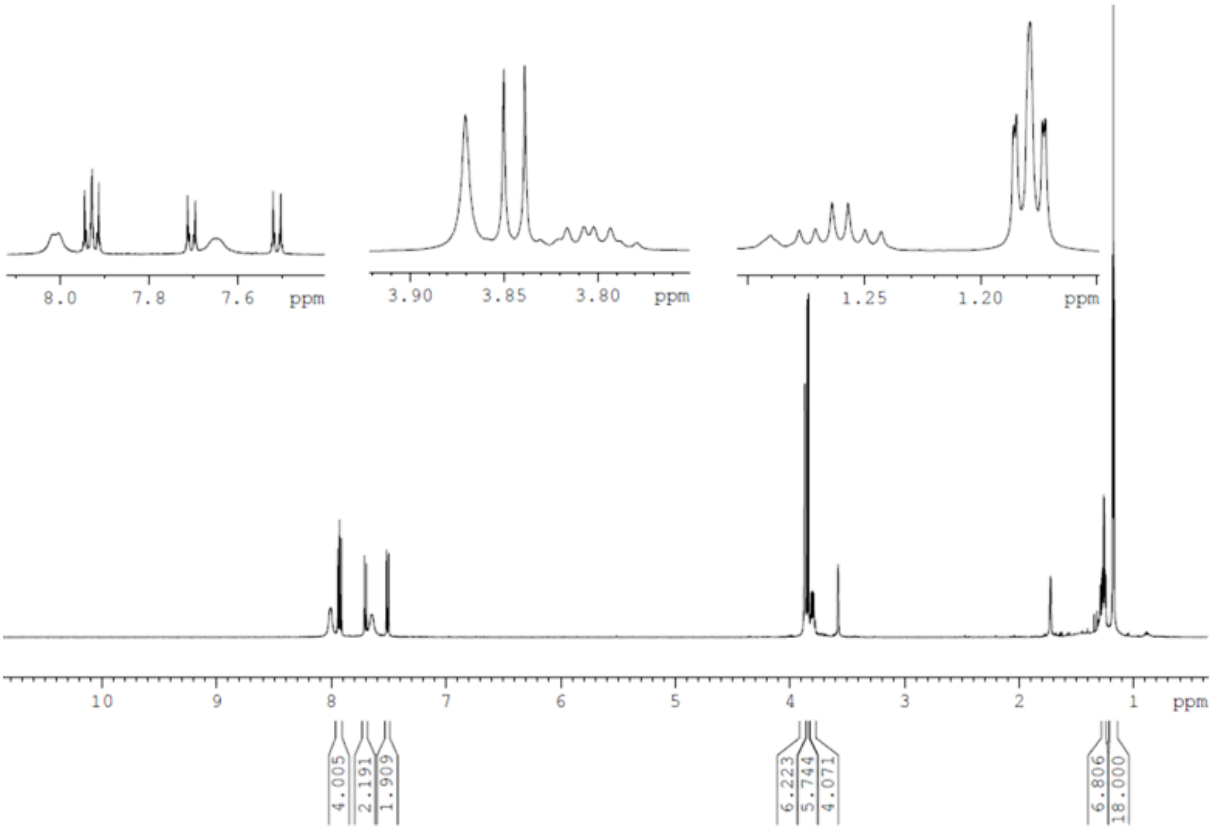


**Figure 58** *In situ* 500 MHz $^{1}H$ NMR spectrum the reaction of complex **13** with diyne **4b** (2:1) in $C_6D_6$.

Additionally, two singlets in the alkyl region appear at 3.85 and 3.84 ppm, which can be assigned to the methyl groups of the ester substituent of the bound diyne. The aromatic region also shows two broad signals at 8.01 and 7.66 ppm, which can be assigned to residual organic starting material. The same is true of the broad singlet at 3.87 ppm. The signal for the phosphine ligands is shown at 1.18 ppm. However, the signals for the dithiocarbamate ligand at 3.80 and 1.26 ppm do not show the expected quartet and triplet of the ethyl groups, but appear as a doublet of quartets and a doublet of triplets, indicating, that the two ethyl groups are not in the exact same chemical environment.

Analysing the integrals of the species formed shows clearly that the diyne to Rh-complex ratio in the product formed, is not in a 2:1, but in a 1:1 manner, as the integrals in the aromatic region should be four for each signal. This is supported by the fact that there is still unreacted diyne left over, although the reaction was carried out with a 2:1 ratio of diyne to Rh-complex. A comparison of the aromatic region of the *in situ* NMR shown in Figure 57 and that of compound **4b** shows that the broad signals can be assigned to the starting material (Figure 59).

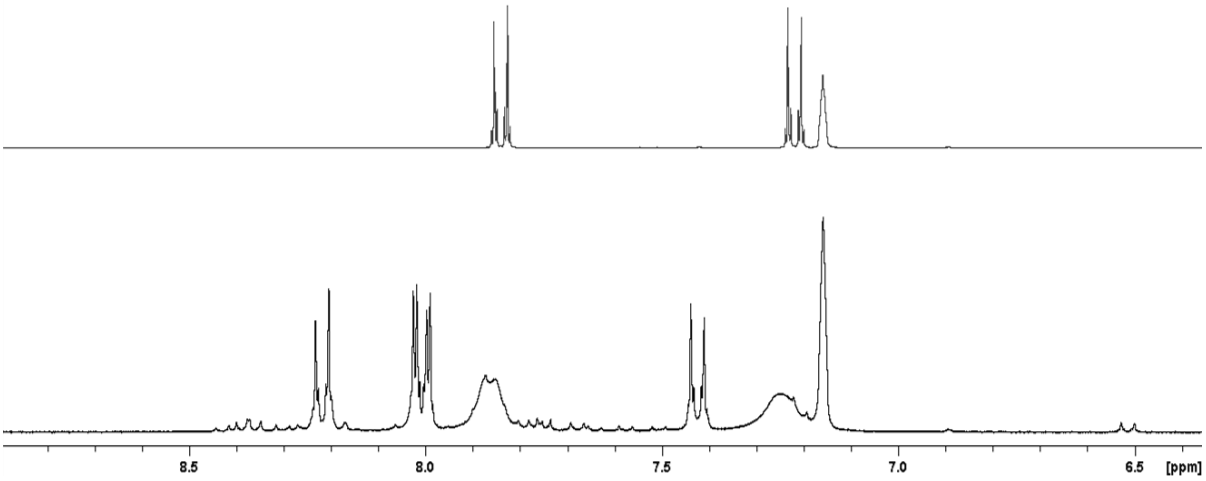


**Figure 59** Comparison of aromatic region of compound **4b** and reaction of complex **13** with **4b** in $C_6D_6$.

This result is considered with the formation of a 1:1 $\pi$-complex, as is known from the catalytic cycle of the alkyne trimerisation, reported by Collman *et al*. (Chap. 2.1.1).[36]

Also, Ward reported the formation of $\pi$-complexes during the reactions of [Rh($PMe_3$)$_4$Me] and [Rh($PMe_3$)$_4$]Cl with 1,3-butadiynes, accompanied by the dissociation of one $PMe_3$ ligand (Chap. 2.1.2).[31] Although he was not able to isolate crystals from those complexes, it was possible to obtain a crystal structure from a related complex by coordination of the tolan, MeO-$C_6H_4$-C≡C-$C_6H_4$-CN to Rh($PMe_3$)$_3$Me, resulting in Rh($PMe_3$)$_3$Me($\eta^2$-MeO-$C_6H_4$-C≡C-$C_6H_4$-CN).

The asymmetry in this compound is generated by the two different *para*-substituents (Figure 60).

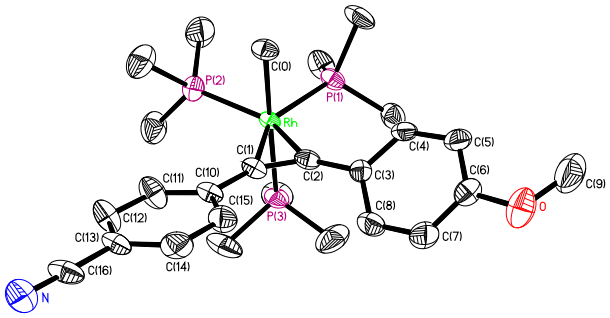


**Figure 60** Molecular structure of $Rh(PMe_3)_3Me(\eta^2\text{-}MeO\text{-}C_6H_4\text{-}C{\equiv}C\text{-}C_6H_4\text{-}CN)$ reported by Ward.[31]

Later results in this group obtained by Thibault and Murata also showed the formation of such $\pi$-complexes at low temperatures as intermediates during the [3+2] cycloaddition reaction of $[Rh(\kappa^2\text{-}O,O`\text{-acac})(PMe_3)_2]$ **16** with butadiynes **4** (R = $NO_2$, $CF_3$, $CO_2Me$, Me, OMe and SMe, Scheme 60).

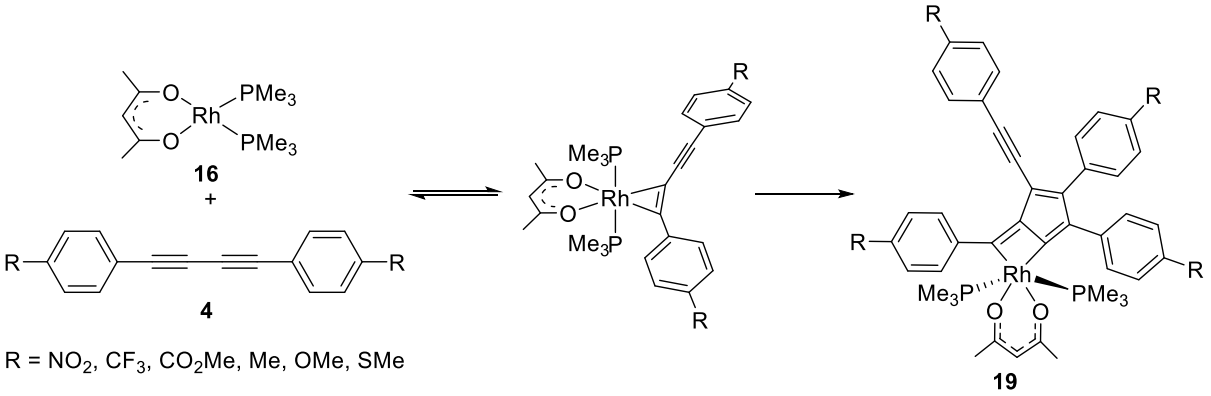


**Scheme 60** Formation of the *trans* $\pi$-complex during the [3+2] cycloaddition reaction of $[Rh(\kappa^2\text{-}O,O`\text{-acac})(PMe_3)_2]$ **16** with butadiynes **4**.

Following the reaction of $[Rh(\kappa^2\text{-}O,O`\text{-acac})(PMe_3)_2]$ **16** with butadiyne **4b** (R = $CO_2Me$) *via in situ* $^{31}P\{^1H\}$ NMR spectroscopy, showed a very broadened doublet of the starting material ($\delta$ = 7.40 ppm, $J_{Rh\text{-}P}$ = 186 Hz) at the beginning of the reaction, which indicates the existence of a dynamic equilibrium involving reversible coordination of the diyne (Figure 61).[127,131]
At -4.10 ppm a doublet with a coupling constant $J_{Rh\text{-}P}$ = 111 Hz is assigned to an intermediate $\pi$-complex species with the two $PMe_3$ ligands occupying the axial positions and the acac ligand and the diyne lying in the equatorial position, $\eta^2$-bound to the Rh-centre.

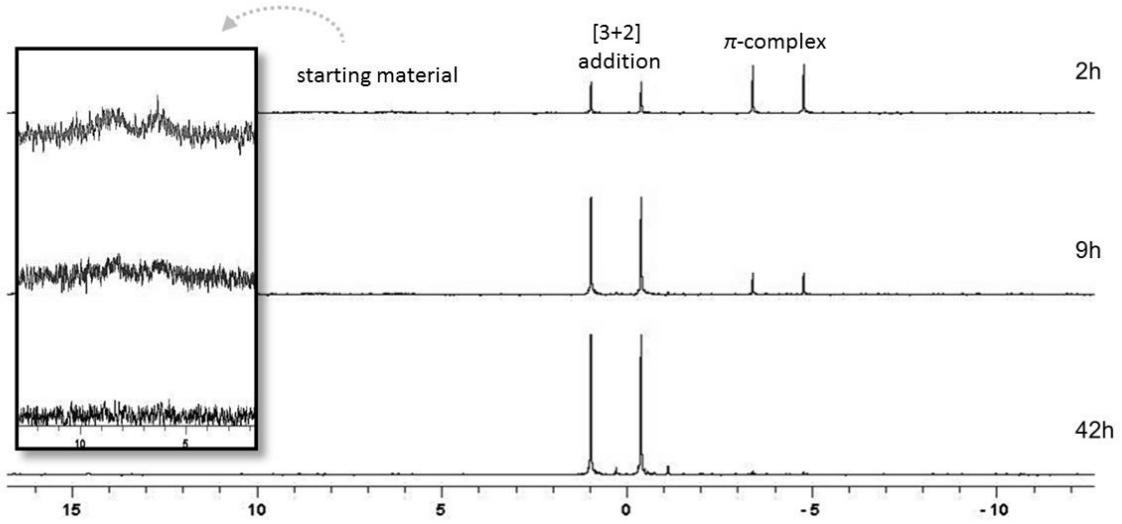


**Figure 61** *In situ* $^{31}P\{^{1}H\}$ NMR spectra of the [3+2] cycloaddition reaction of [Rh($\kappa^2$-*O*,*O*`-acac)($PMe_3$)$_2$] **16** with **4b**.[127,131]

Murata also suggests a ligand rearrangement of the *π*-complexes between *cis*- and *trans*-orientations of the phosphines as shown in Scheme 61. [131]

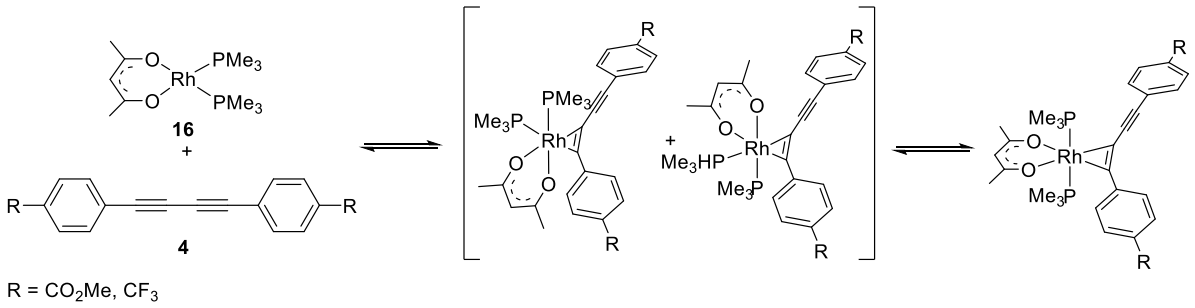


**Scheme 61** Formation of *cis* and *trans* *π*-complexes during the reaction of [Rh($\kappa^2$-*O*,*O*`-acac)($PMe_3$)$_2$] **16** with butadiynes **4.**[131]

$^{31}P\{^{1}H\}$ NMR measurements of the reaction of Rh-complex **16** with 2.5 equivalents of butadiyne **4h** (R = $CF_3$) at various temperatures prove that two different intermediate species with a *cis*-disposition of the phosphine ligands are formed at -90 °C, being stable up to 10 °C (Figure 62).

They show up as three sets of signals at 20.55 ($J_{Rh-P}$ = 138, $J_{P-P}$ = 37 Hz), -7.76 ($J_{Rh-P}$ = 135, $J_{P-P}$ = 34 Hz) and -15.90 ($J_{Rh-P}$ = 126, $J_{P-P}$ = 40 Hz) ppm, being doublets of doublets. One set of signals is overlapped with the signal at 20.32 ppm, but appears at -50 °C, at 21.09 ppm ($J_{Rh-P}$ = 141, $J_{P-P}$ 40 Hz). Around 10 °C, the signals disappear and two new doublets appear which are assigned to the *trans* π-complex (-2.23 ppm) and the [3+2] addition product (2.67 ppm). The fact that the [3+2] addition product is already formed at this temperature indicates a very low barrier for conversion of the *trans* *π*-complex, explaining why it is not possible to isolate it up

to that point. The formation of the [3+2] cycloaddition product took place in quantitative yields within 48 hours at ambient temperature.[131]

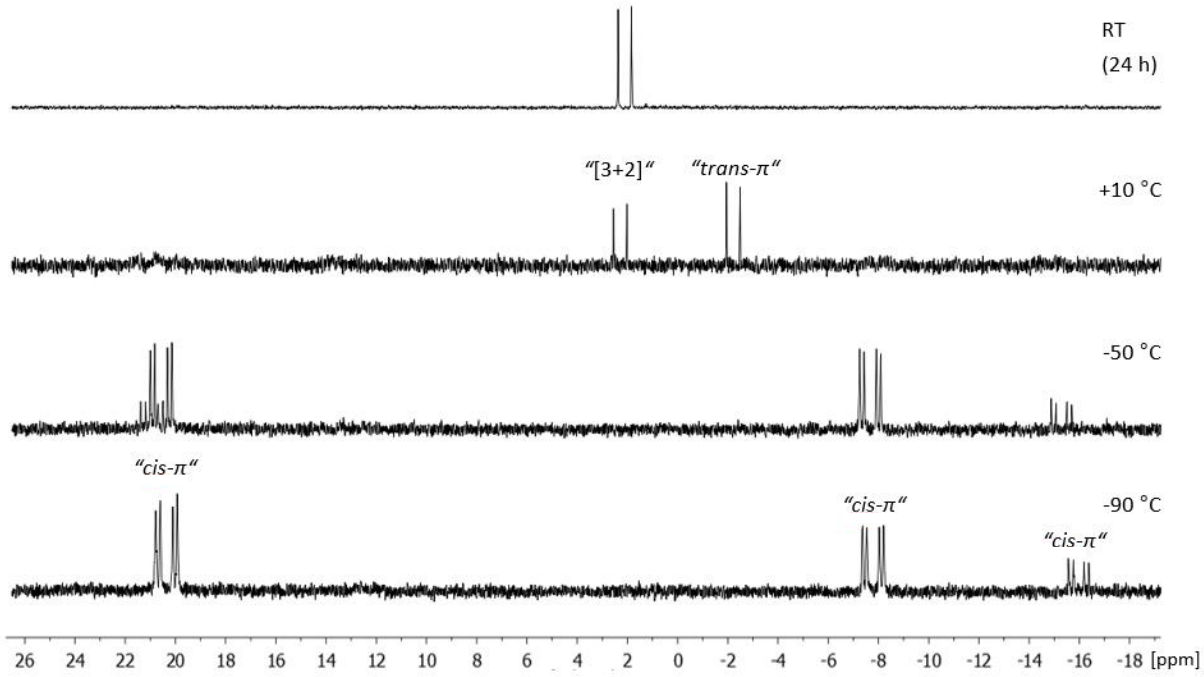


**Figure 62** 202 MHz VT-$^{31}P\{^1H\}$ NMR spectra of the reaction of Rh-complex **16** with 2.5 eq. of butadiyne **4h** (R = $CF_3$) at -90 °C (bottom), -50 °C (low middle), 10 °C (high middle) at after 24 h at RT (top). [131]

Based on these results, the structure of the *trans* $\pi$-complex formed during the reaction of [Rh($\kappa^2$-*S*,*S*`-$S_2CNEt_2$)($PMe_3$)$_2$] **13** with diynes **4** may have the same structural motifs as the corresponding *trans* $\pi$-complexes bearing acac (Figure 63).

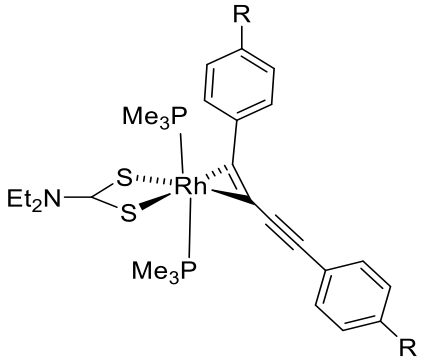


**Figure 63** Model structure of a *trans* $\pi$-complex of [Rh($\kappa^2$-*S*,*S*`-$S_2CNEt_2$)($PMe_3$)$_2$] and diyne **4**.

The ligand molecule should be $\eta^2$-bound to the Rh(III)-centre, forming a distorted octahedral complex. The two phosphine ligands occupy the axial positions, whereas the dithiocarbamate and the butadiyne occupy the equatorial positions of the complex.

Comparable *in situ* $^{31}P\{^1H\}$ NMR measurements at various temperatures show that during the reaction of [Rh($\kappa^2$-*S*,*S*`-$S_2CNEt_2$)($PMe_3$)$_2$] **13** with two equivalents of butadiyne **4b** (R =

$CO_2Me$) at -80 °C, only small signals indicating the existence of the c*is* $\pi$-complexes are visible. They appear as three sets of doublets of doublets at 14.95 ($J_{Rh-P}$ = 134, $J_{P-P}$ = 35 Hz), -0.99 ($J_{Rh-P}$ = 96, $J_{P-P}$ = 37 Hz) and -16.97 ppm ($J_{Rh-P}$ = 128, $J_{P-P}$ = 35 Hz), whereas one set of signals is missing (presumably overlapped), and does not appear at higher temperatures.

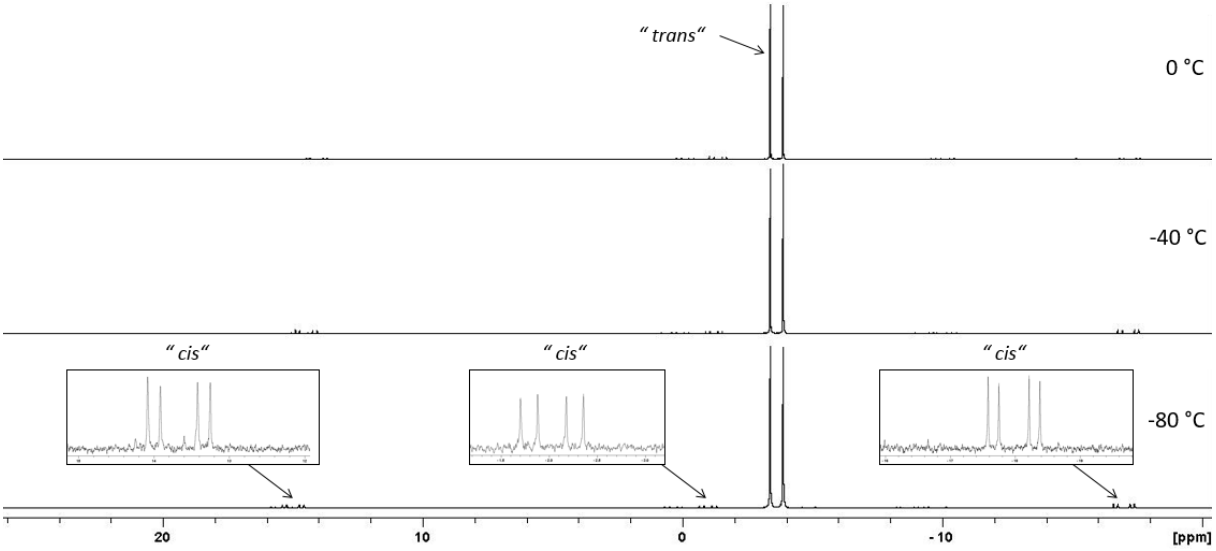


**Figure 64** 202 MHz VT-$^{31}P\{^1H\}$ NMR spectra of the reaction of [Rh($\kappa^2$-*S*,*S*`-$S_2CNEt_2$)($PMe_3$)$_2$] **13** with 2 eq. of butadiyne **4b** (R = $CO_2Me$) at -80 (bottom), -40 (middle), and 0 °C (top) in THF-$d_8$.

At -3.62 ppm the main species, which is assigned to the *trans* $\pi$-complex appears as a doublet, having a coupling constant $J_{Rh-P}$ of 103 Hz (Figure 64). It is likely that the formation of *trans* $\pi$-complex is rapid, as it is the dominant species, which supports the idea that the *cis* $\pi$-complexes is not stable. The appearance of another doublet, which would indicate the formation of the [3+2] addition product or any comparable Rh(III)-species, was not observed.

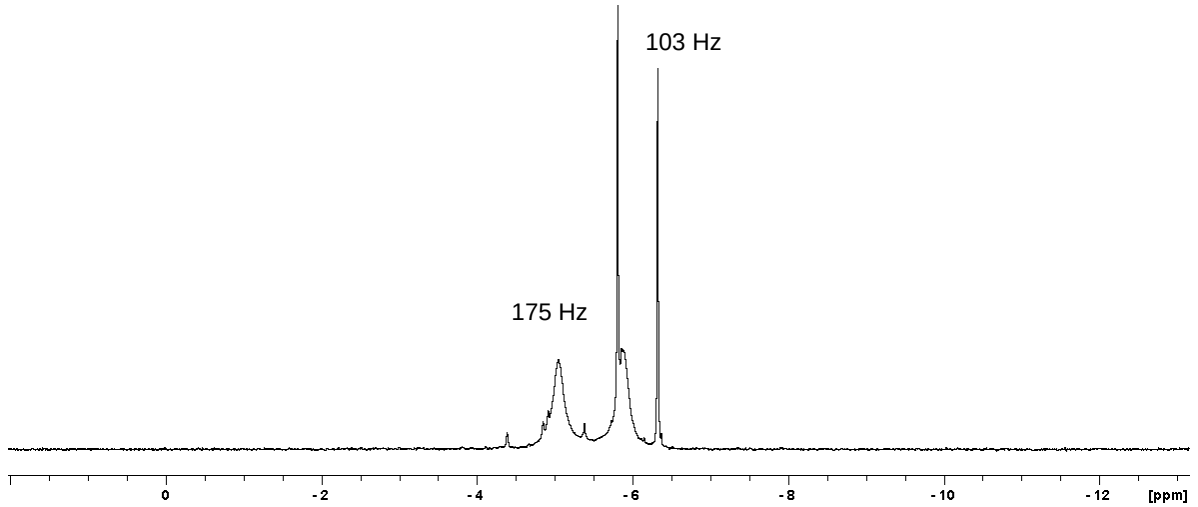


**Figure 65** *In situ* $^{31}P\{^1H\}$ NMR spectrum of the reaction of [Rh($\kappa^2$-*S*,*S*`-$S_2CNEt_2$)($PMe_3$)$_2$] **13** and butadiyne **4c** at RT at 80 MHz in THF.

Further test reactions, which were performed in a 1:1 ratio of butadiynes **4c** or **4g** and complex **13** showed the formation of the same product. However, performing the reaction with a 1:1 ratio, leaves at least 50 % of the Rh-complex unreacted (Figure 65). The reason could be, that butadiynes **4b** and **4g** are substituted with rather neutral groups or very weak donors (methyl, naphthyl), which are already known to cause slower reactions as when using acceptor-substituted compounds. A twofold excess (or more) of diyne seems to be necessary to consume the complete Rh-starting material. In addition, heating the reactions to 80 °C did not result in any significant change in the product to starting material ratio.

It has to be noted that, the *in situ* $^{1}$H NMR of the reaction of Rh-complex **13** with diyne **4b**, shown at the beginning, shows broadened peaks of the starting compound **4b** in the aromatic region. This leads to the supposition, that in this reaction there is a certain dynamic process involving the second diyne molecule and the Rh-centre (Figure 58).

To clarify the dynamic processes involving the butadiynes and the Rh-complex **13**, VT-$^{1}$H NMR spectra were recorded at ambient temperature, 0, -20, -40, -60 and -80 °C (Figure 66).

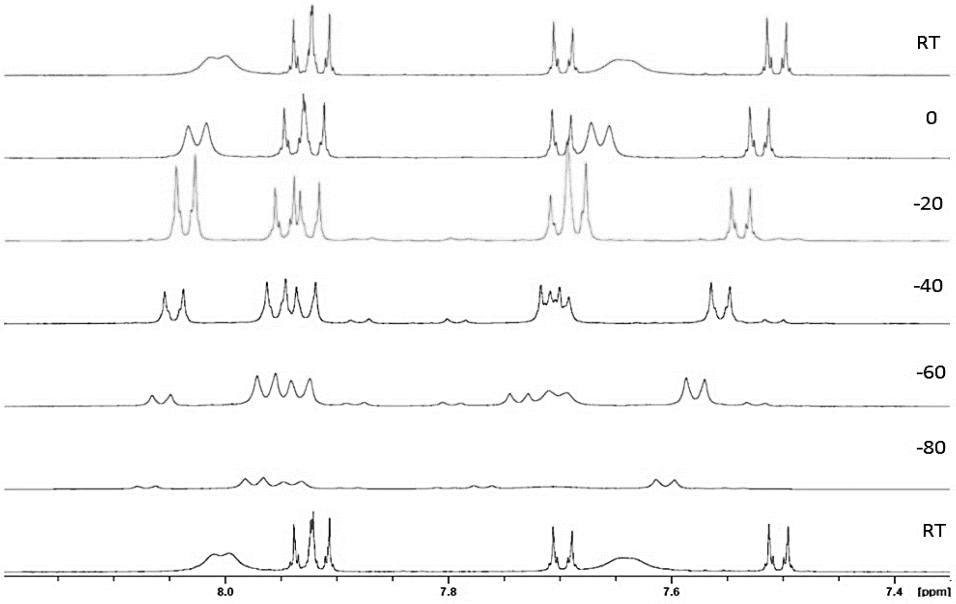


**Figure 66** VT-$^{1}$H NMR spectra of the reaction of [Rh($\kappa^2$-*S*,*S*`-$S_2CNEt_2$)($PMe_3$)$_2$] **13** with butadiyne **4b** (RT to -80 °C) in THF-$d_8$.

The low temperature $^{1}$H NMR spectra confirm, that with the decrease of temperature to -20 °C, the signals of the residual starting material are sharpening, as the dynamics between the Rh-centre and the ligand molecule are slowed down. Below -20 °C the intensity of the signals is strongly decreasing, which might be due to solubility problems at those temperatures. Letting the mixture warm to ambient temperature, results in the initial $^{1}$H NMR spectrum, which supports the existence of dynamics between the butadiyne and the Rh-complex, as heating the reaction also does not lead to the binding of the second diyne.

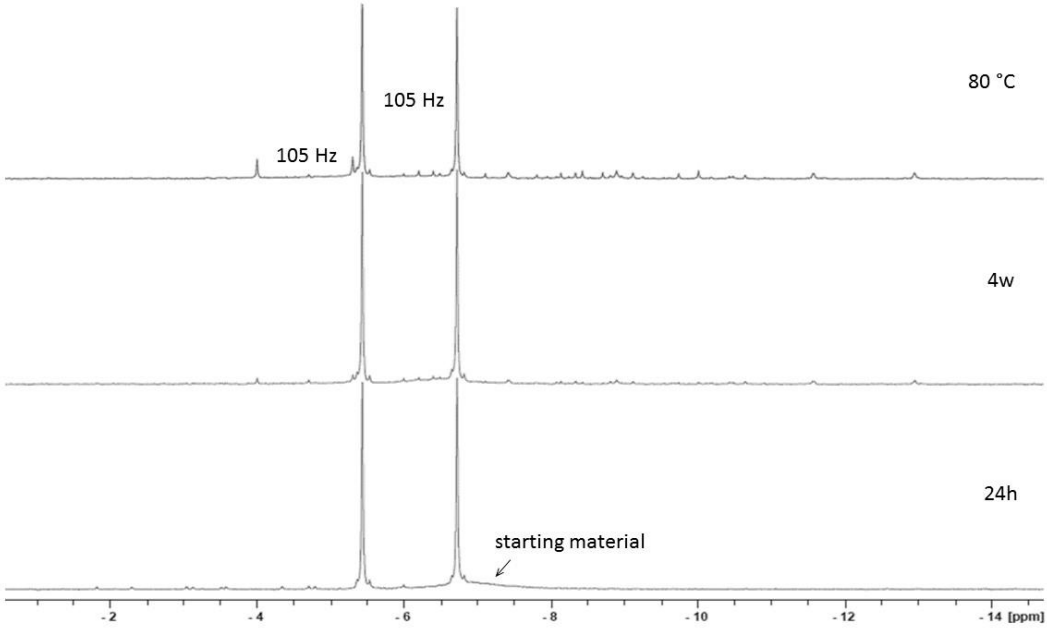


**Figure 67** *In situ* $^{31}P\{^{1}H\}$ NMR spectra of the reaction of complex **13** with butadiyne **4c** (1:2) after one day, four weeks and heating to 80 °C.

Having a look at the *in situ* $^{31}P\{^{1}H\}$ NMR spectra of the reaction of [Rh($\kappa^2$-*S*,*S*`-$S_2CNEt_2$)($PMe_3$)$_2$] **13** with butadiyne **4c** show that there is not much change during four weeks at ambient temperature. After heating the reaction to 80 °C, only one main doublet with a coupling constant $J_{RhP}$ of 105 Hz and traces of other species can be observed, where the most intense trace signal also has a coupling constant $J_{RhP}$ of 105 Hz and probably may indicate the formation of the [3+2] addition product (Figure 67).

To prove the formation of the *trans* $\pi$-complex, the solvent was removed from the reaction and the crude product was extracted with hot hexane. After removal of the solvent, the residue was dissolved in tetrahydrofuran, layered with hexane and the mixture was put into the freezer to obtain crystals at -30 °C (Figure 69). Other attempts to isolate the product at ambient temperature failed, because even if the reaction seemed to have reached completion, analysis *via* NMR spectroscopy always showed a certain amount of both starting materials, compounds **13** and **4c**, in the NMR spectrum. The same applies for reactions with butadiyne **4b** and **4g**, indicating the existence of an equilibrium between the starting materials and the $\pi$-complex.

To get a better idea of the stability of the formed $\pi$-complexes **28**, a VT-NMR study of compound **28c** was carried out in deuterated toluene, ranging from -40 to 20 °C in 10° steps. The spectra show that the complex is only stable in solution up to -20 °C, explaining, why it was difficult to obtain complexes **28** in high purity (Figure 68).

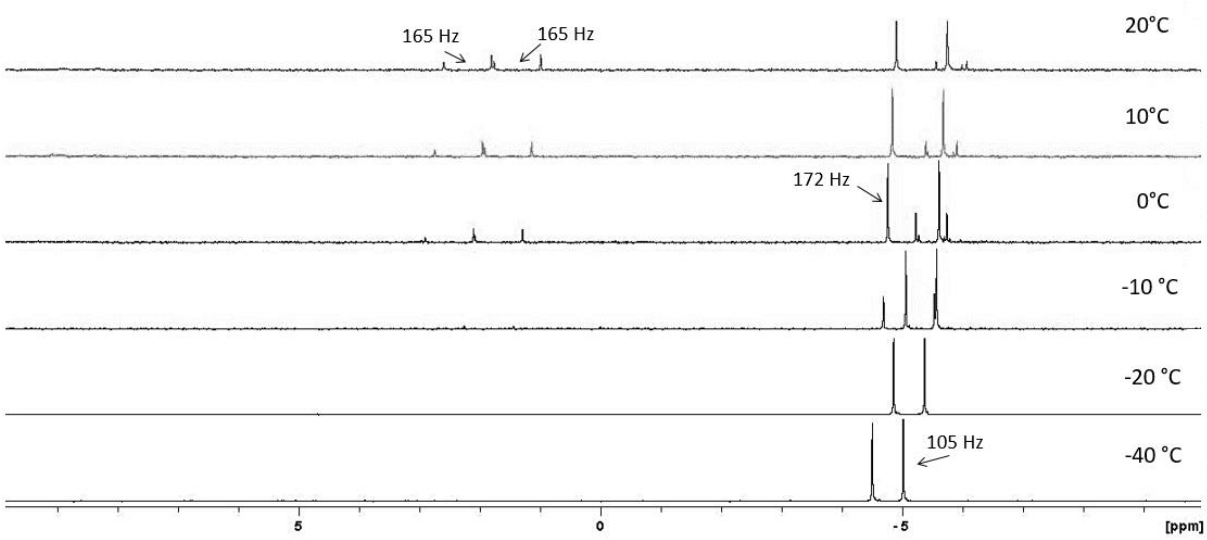


**Figure 68** $^{31}P\{^{1}H\}$ VT-NMR spectrum of compound **28c** in toluene-$d_8$, at -40 to 20 °C.

From -40 to -20 °C, only one doublet was observed at -4.76 ppm ($J_{Rh\text{-}P}$ = 105 Hz), which is the signal of the $\pi$-complex **28c**. Starting from -10 °C another doublet appears at 5 ppm ($J_{Rh\text{-}P}$ = 172 Hz), which can be assigned to the starting complex **13**, increasing in amount as the temperature is raised to 20 °C. Starting from 0 °C, two other species, which were identified, appeared ($J_{Rh\text{-}P}$ of 165 Hz, each). This could also indicate that compound **28c** decomposes at that temperature in solution. Cooling the solution to -40 °C again did not lead to the reformation of compound **28c**. Possibly, letting the solution stay at that temperature for a longer time or cooling it more slowly would lead to the reformation. Due to very small amounts of compound **28c**, it was not possible to examine this further.

An analogous reaction was also carried out with dinaphthyl-butadiyne **28g**. As it has a larger conjugated $\pi$-system than the other butadiynes discussed, it was expected to form crystals suitable for X-ray readily due to the better possibility to form $\pi$-$\pi$ interactions, which could enhance crystal-packing forces.

To obtain compound **28g**, [Rh($\kappa^2$-*S*,*S*`-$S_2CNEt_2$)($PMe_3$)$_2$] **13** and one equivalent of butadiyne **4g** (1:2) were dissolved in THF and stirred at ambient temperature overnight and the reaction mixture turned dark red immediately. As expected, the *in situ* $^{31}P\{^{1}H\}$ NMR spectrum shows one main doublet at -5.55 ppm, with a coupling constant $J_{Rh\text{-}P}$ of 104 Hz. It was not possible to isolate compound **28g** pure, as it also exists at equilibrium with the starting materials or decomposes in solution at ambient temperature, but it was possible to obtain a crystal suitable for X-ray to confirm the formation of the $\pi$-complexes **28** (Figure 69).

*Molecular structures of π-complexes **28c** and **g***

Single crystals of **28c** and **g** were grown in a small glass vial by cooling hexane solutions to -30 °C. Analysis *via* X-ray diffraction resulted in orthorhombic (**28c**) and monoclinic (**28g**) crystals with the space groups: $P2_12_12_1$ (**28c**) and *Pc* (**28g**) (Figure 69).

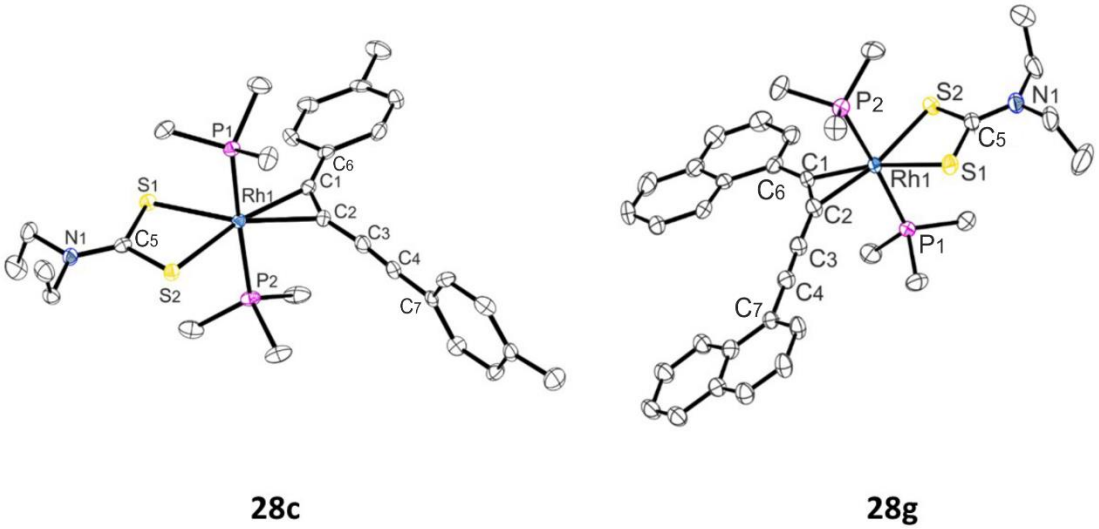


**Figure 69** Molecular structures of compounds **28c** and **28g**. Hydrogen atoms are omitted for clarity. Thermal ellipsoids are shown at 50 % probability.

Compounds **28c** and **g** (Table 14 and 15) have a distorted octahedral geometry, with the two $PMe_3$ groups in axial positions *trans* to each other. The metallacyclopropenyl moiety and the dithiocarbamate ligand are both located in the equatorial plane of the octahedron. The distortion is caused especially by the very small angle of the metallacyclopropenyl moiety (C1-Rh1-C2, 36.50(14) – 37.4(2)°) and the small bite angle (S1-Rh1-S2, 71.34(4) - 77.55(3)°) of the dithiocarbamate ligand. This results in C1-Rh1-S1 and C2-Rh1-S2 angles with values of 123.12(11) - 124.41(18) and 126.90(13) - 128.83(11)°, which are well over 90°. The C1-C2-C3 (149.8(5)-152.0(4)°) and C6-C1-C2 angles (145.4(4)-146.0(5)°) at the alkyne bound to the Rh-centre deviate significantly from an ideal 180° angle. The C2-C3-C4 (174.3(4)-177.0(5)°) and C3-C4-C7 angles (176.4(5)-177.8(4)°) around the free triple bond of the diyne differ only slightly from the ideal 180° angle. The P-Rh bond lengths are 2.3020(11) - 2.3114(14) Å, and similar to each other. The same applies for the S1-Rh1 (2.4657(9) - 2.4822(13) Å) and S2-Rh1 (2.4616(11) - 2.4711(10) Å) bond lengths. The C1-Rh1 and C2-Rh1 bond lengths have values of 2.042(5) - 2.050(4) and 2.070(4) - 2.098(4) Å, which lie in the typical range for a Rh-C bond length (Table 14 and 14). The long C1-C2 (1.300(5)-1.317(7) Å) bond distances and large deviations from linearity of the C1-C2-C3 and C6-C1-C2 angles indicate very strong π-backbonding and are consistent with a metallacyclopropenyl picture of the bonding.

**Table 14** Important bond lengths, hybridisation and bond type of compounds **28c** and **g**.

| | | Bond length (Å) | | |
|---|---|---|---|---|
| **Hybridisation** | **Bond** | **28c** | **28g** | **Bond type** |
| sp-sp | C1-C2 | 1.300(5) | 1.317(7) | C≡C |
| sp-sp | C2-C3 | 1.381(5) | 1.383(7) | C-C |
| sp-sp | C3-C4 | 1.209(5) | 1.208(7) | C≡C |
| | Rh1-C1 | 2.050(4) | 2.042(5) | |
| | Rh1-C2 | 2.098(4) | 2.070(4) | |
| | S1-C5 | 1.721(4) | 1.710(5) | |
| | S2-C5 | 1.718(4) | 1.736(5) | |
| | Rh1-S1 | 2.4657(9) | 2.4822(13) | |
| | Rh1-S2 | 2.4711(10) | 2.4616(11) | |
| | Rh1-P1 | 2.3026(11) | 2.3114(14) | |
| | Rh1-P2 | 2.3020(11) | 2.3046(13) | |

**Table 15** Important angles, $^{31}P\{^{1}H\}$-NMR shifts, yield, space group and crystal system of compounds **28c** and **g**.

| | | **28c** | **28g** |
|---|---|---|---|
| **Angles (°)** | S1-Rh1-S2 | 71.55(3) | 71.34(4) |
| | C1-Rh1-S1 | 123.12(11) | 124.41(18) |
| | C2-Rh1-S2 | 128.83(11) | 126.90(13) |
| | C1-Rh1-C2 | 36.50(14) | 37.4(2) |
| | S1-C5-S2 | 71.55(3) | 113.6(2) |
| | C1-C2-C3 | 152.0(4) | 149.8(5) |
| | C6-C1-C2 | 145.4(4) | 146.0(5) |
| | C2-C3-C4 | 174.3(4) | 177.0(5) |
| | C3-C4-C7 | 177.8(4) | 176.485) |
| **Interplanar angle (°)** | I & II | 97.72(14) | 19.8 (2) |
| **$^{31}P\{^{1}H\}$-NMR shift (ppm)** | | -5.72 | -5.55 |
| **Coupling constant $J_{Rh\text{-}P}$ / Hz** | | 105 | 104 |
| **Space group (single crystal)** | | $P2_12_12_1$ | $Pc$ |
| **Crystal system** | | orthorhombic | monoclinic |

*Efforts to bind a second butadiyne*

In contrast to the reaction of [Rh($\kappa^2$-*S*,*S*`-$S_2CNEt_2$)($PMe_3$)$_2$] **13** with two equivalents of butadiynes **4c** and **g**, where even after several weeks no significant progress of the reaction beyond the $\pi$-complex could be observed, the $^{31}P\{^1H\}$ NMR spectra of the analogous reaction with butadiyne **4b** show, besides the signal of the *trans* $\pi$-complex, the appearance of three additional signals after three days at ambient temperature.

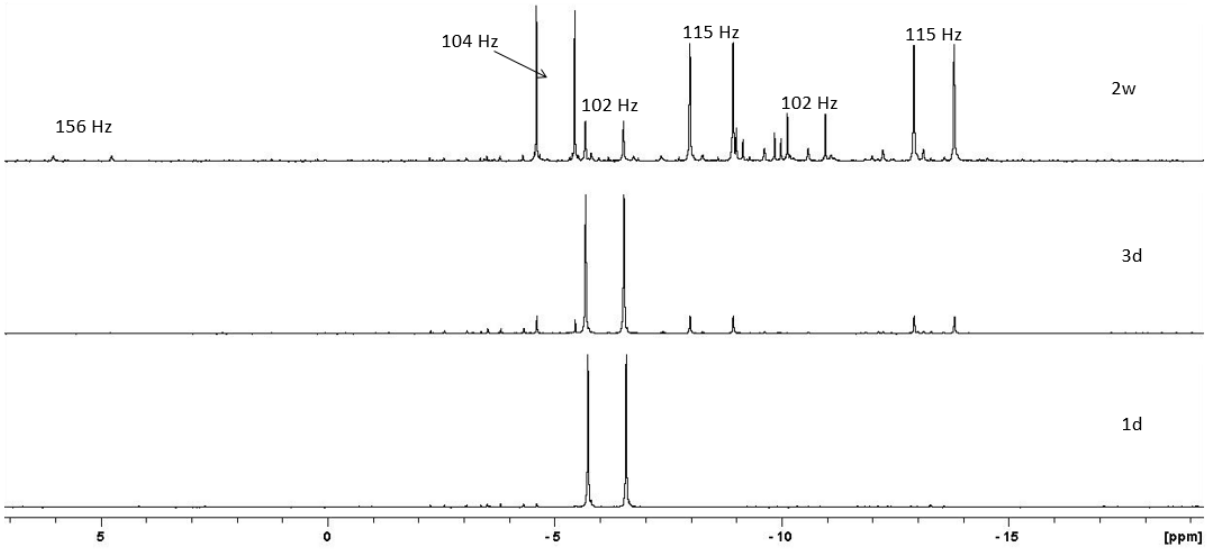


**Figure 70** *In situ* $^{31}P\{^1H\}$ NMR spectra of reaction of complex **13** with butadiyne **4b** (2:1 ratio) in $C_6D_6$, after 1 day, 3 days and 2 weeks.

The signals are doublets at -5.00 ($J_{Rh\text{-}P}$ = 104 Hz), -8.72 ($J_{Rh\text{-}P}$ = 115 Hz) and -13.52 ($J_{Rh\text{-}P}$ = 115 Hz) ppm, which can all be assigned to be Rh(III)-species. After two weeks, the three doublets have increased significantly, whereas the signal for the *trans* $\pi$-complex has decreased. Additionally, another doublet has appeared at -10.63 ppm ($J_{Rh\text{-}P}$ = 102 Hz), which can also be assigned to a Rh(III)-species. Furthermore, at 5.47 ppm, another small doublet appears, with a coupling constant $J_{Rh\text{-}P}$ of 156 Hz, which may be assigned to a Rh(I) species (Figure 70).

As the reaction using butadiynes **4b** seemed to be quite promising, test reactions using the microwave reactor were carried out, to attempt to activate the system and push it to bind a second butadiyne. Figure 70 shows the $^{31}P\{^1H\}$ NMR spectra after 10 min (bottom), 10 h (low middle), 24 h (top middle) and 72 h (top) in the microwave reactor at 80 °C. After 10 min, the $^{31}P\{^1H\}$ NMR spectrum shows comparable signals to those in the spectrum of the reaction at ambient temperatures after two weeks, indicating a significant speed-up of the reaction, when carried out under microwave conditions.

After 10 hours, the doublet at -5.00 ppm has increased significantly, whereas the other two main species at -8.72 and -13.52 ppm have decreased. After 12 more hours reaction time, the doublet

at 5.47 ppm has mainly disappeared and, after 72 hours, the doublet at -5.00 ppm has become the main species, accompanied by several small doublets.

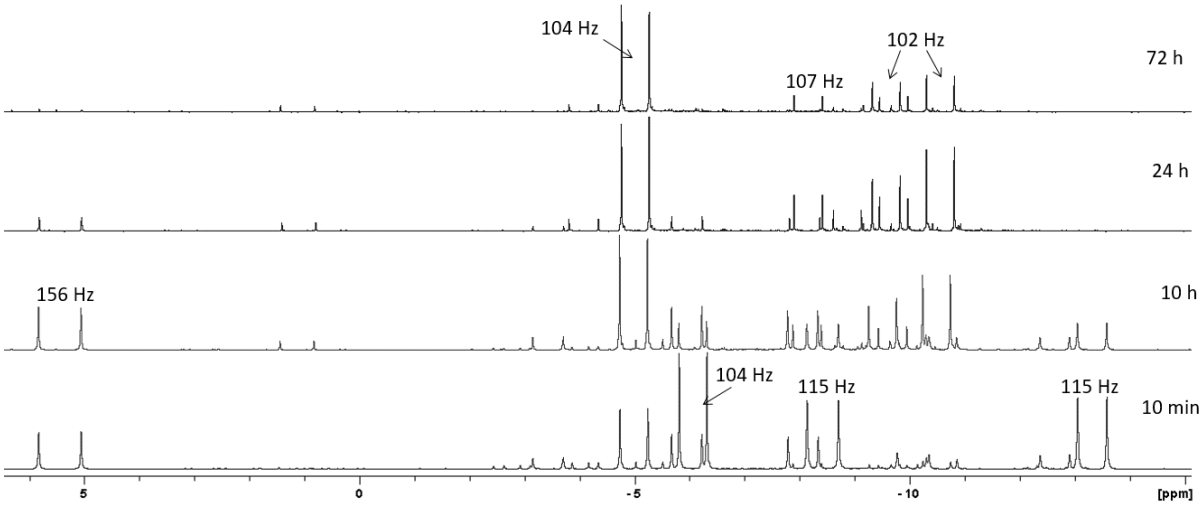


**Figure 71** 202 MHz $^{31}P\{^{1}H\}$ NMR spectra of reaction of butadiyne **4b** with [Rh($\kappa^2$-*S*,*S*`-$S_2CNEt_2$)($PMe_3$)$_2$] **13** (2:1) in $\mu$W after 10 min, 10 h, 24 h, 72 h, at 80 °C in THF.

Due to the long reaction time in the microwave reactor, the reaction was stopped at that point and an attempt was made to purify the crude product *via* flash column chromatography, using THF/hexane as eluent. Figure 72 shows the $^{31}P\{^{1}H\}$ NMR spectrum of the crude product after purification *via* flash column chromatography.

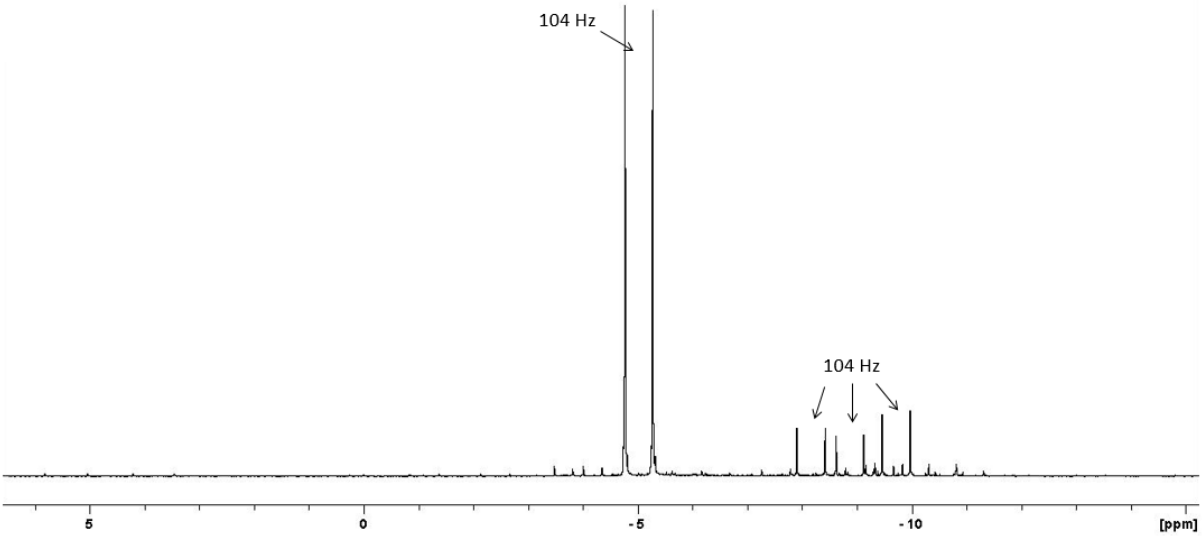


**Figure 72** $^{31}P\{^{1}H\}$ NMR of crude product after flash column chromatography of reaction of [Rh($\kappa^2$-*S*,*S*`-$S_2CNEt_2$)($PMe_3$)$_2$] **13** with two equivalents of butadiyne **4b** in $C_6D_6$ at 202 MHz.

The three small remaining doublets could not be removed completely. Further attempts to clean the product by repeated column chromatography, precipitation, washing or recrystallisation failed. However, the $^{1}H$ NMR (Figure 73) gives some information about the structure of the obtained product. The aromatic region shows eight doublets at 8.43, 8.30, 8.26, 8.19, 7.89,

7.82, 7.58 and 7.41 ppm, with a coupling constant $J_{HH}$ of 9 Hz and an integral of two protons each. The signals can be assigned to the protons of the phenyl rings at the para position of the butadiynes. As for a symmetric compound only four signals are expected, the obtained compound is likely to be an asymmetric Rh-complex, having two butadiyne molecules bound.

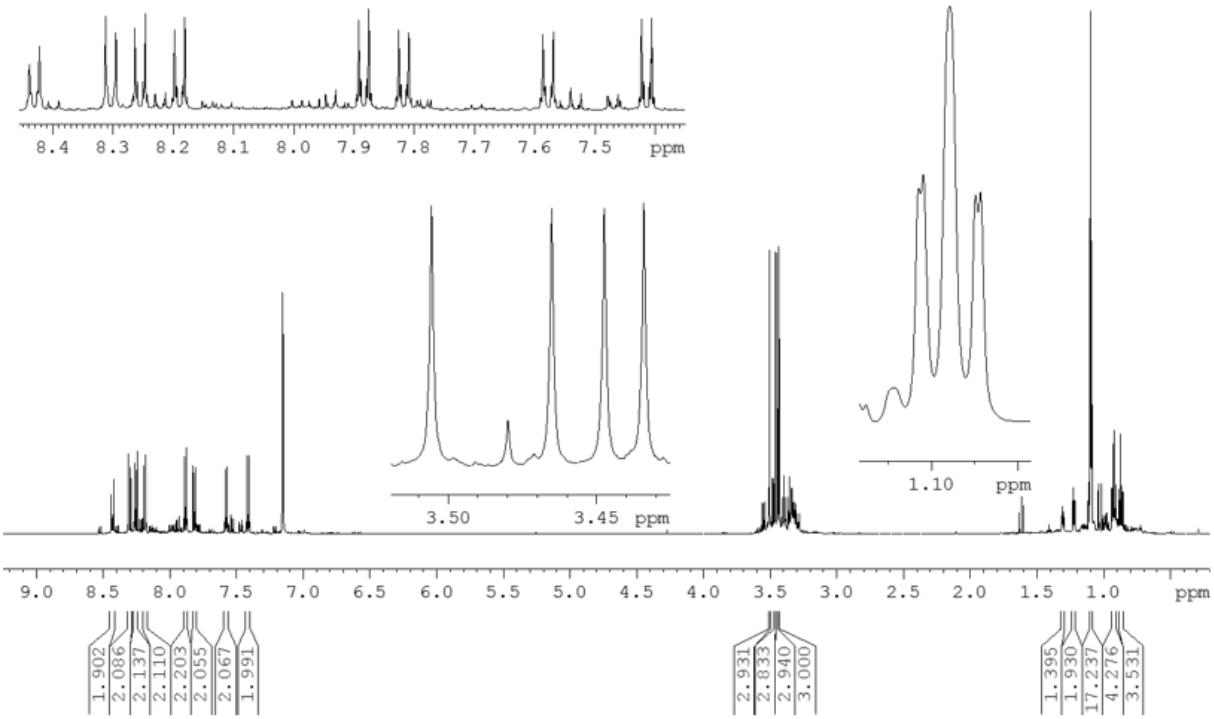


**Figure 73** $^1$H NMR spectrum of asymmetric Rh(III)-complex after work-up in $C_6D_6$ at 500 MHz.

This is supported by the four singlets for the $CO_2Me$ groups at 3.50, 3.46, 3.45 and 3.43 ppm, having an integral of three, each. Due to this, all four methyl groups of the two butadiynes have a different chemical environment. At 1.09 ppm, the signal of the $PMe_3$ groups is detected, with an integral of 18 protons. They show only one signal, as they are located in equivalent axial positions. At 0.92 and 0.87 ppm, two triplets for the methyl-groups of the dithiocarbamate ligand are detected, with a coupling constant $J_{HH}$ of 7 Hz and an integral of three each. The signals for the $CH_2$-groups of the dithiocarbamate ligand appear at 3.35-3.29 ppm, with an integral of four and are partially covered by residual by-product.

There are at least two possible structures, which can be described by this $^1$H NMR spectrum. The first possibility is the formation of an unsymmetric rhodacyclopentadiene, as was proposed by Nishihara in 1995 (Chap. 2.1.3) from the reaction of various diphenylbutadiynes with $[CoCp(PPh_3)_2]$ which yielded three different regioisomers.[66] The unsymmetric isomer would have the connectivity of **US-dithio**, shown in Figure 74.[66]

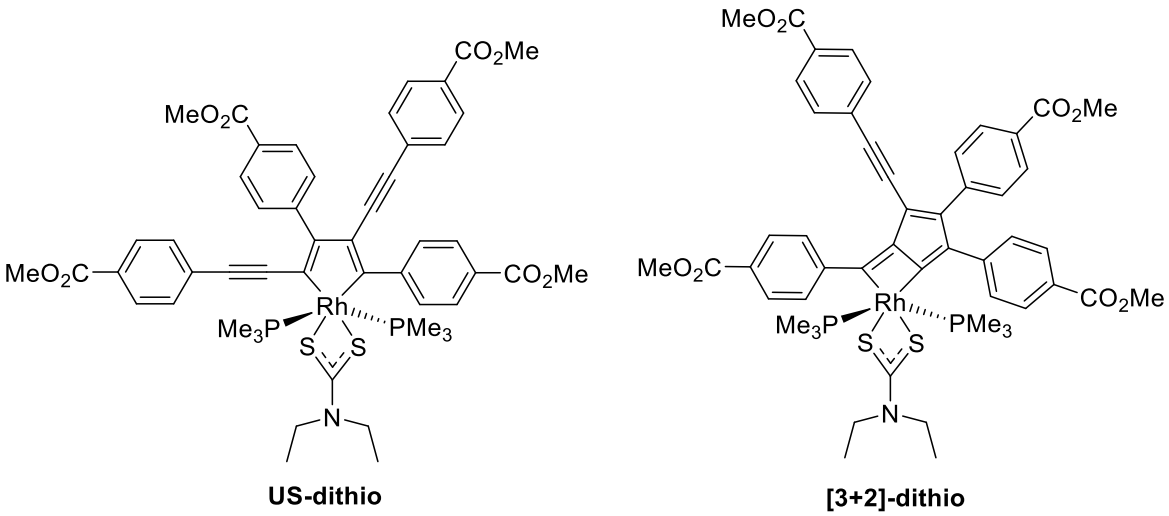


**Figure 74** Two different possibilities of rhodacycles to be formed during the reaction of [Rh($\kappa^2$-*S*,*S*`-$S_2CNEt_2$)($PMe_3$)$_2$] **13** with two equivalents of butadiyne **4b**.

The rhodium forms a metallacyclopentadiene ring, with two of the four alkyne groups of the butadiynes, having the diynes connected in a 2,4 manner, with respect to the substituents. The second possibility is the [3+2] addition compound **[3+2]-dithio**, as was also found for the analogous reaction of [Rh($\kappa^2$-*O*,*O*`-acac)($PMe_3$)$_2$] **16** with butadiyne **4b** (R = $CO_2Me$).[127,131] The rhodium forms a cyclobutenyl ring with one butadiyne, whereas the second butadiyne is bound to the first one, *via* one alkyne group, forming a fulvene-like skeleton.

As [Rh($\kappa^2$-*S*,*S*`-$S_2CNEt_2$)($PMe_3$)$_2$] **13** in general tends to have a comparable reaction behaviour to [Rh($\kappa^2$-*O*,*O*`-acac)($PMe_3$)$_2$] **16**, it is likely, that it forms the [3+2] cycloaddition product rather than the asymmetric rhodacyclopentadiene. To be sure which isomer is formed, the reaction should be repeated and the product characterised *via* 2D $^1$H NMR spectroscopy. An analysis *via* X-ray diffraction would clarify the structure of the unsymmetric compound obtained.

# Chapter Three

# Optical Properties

# 3. Chapter Three: Optical Properties

## 3.1 Introduction

### 3.1.1 Optical Properties of Organo Transition Metal Complexes

Compared to excited singlet states ($S_n$) excited triplet states ($T_n$) have different photophysical as well as photochemical properties. Among these are lower energy emission $\lambda_{em}$, longer lifetimes $\tau$, different redox potentials $E_{ox}/E_{red}$, diradical character and many more.[132]

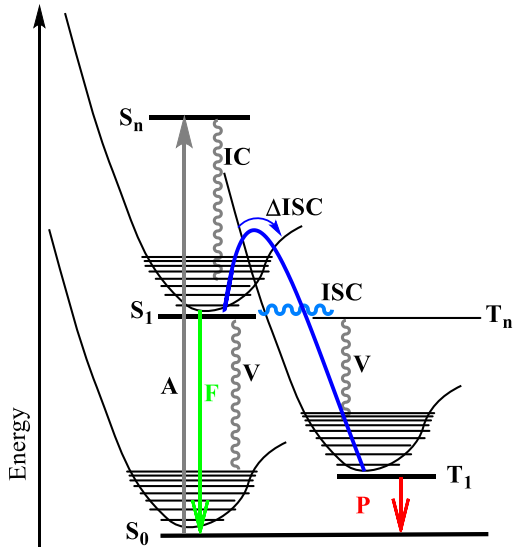


| Process | Name | Time Scale ($t = 1/k_p$)/s |
|---|---|---|
| A | Absorption | $10^{-15}$ |
| IC | Internal Conversion | $10^{-12}$-$10^{-6}$ |
| ISC | Intersystem Crossing (S→T) | $10^{-12}$-$10^{-6}$ |
| V | Vibrational Relaxation | $10^{-9}$-$10^{1}$ |
| F | Fluorescence | $10^{-9}$-$10^{-7}$ |
| P | Phosphorescence | $10^{-6}$-$10^{-3}$ |

**Figure 75** Jablonski diagram illustrating the fundamental processes and their typical transitions in organometallic complexes after photoexcitation and list of the corresponding timescale of the processes.

When electrons are excited from the $S_0$ to the $S_1$ state, they normally release their energy *via* fluorescence $S_1 \rightarrow S_0$. The intersystem-crossing (ISC) which can also occur during photoexcitation, to $T_1$, and the corresponding emission from $T_1$ to $S_0$, known as phosphorescence, are usually spin-forbidden due to a weak spin-orbit coupling (SOC). However, a strong SOC can be achieved when a heavy atom is introduced into the system. This can lead to efficient formation of excited triplet states $T_n$ and emission from them (Figure 75). The stronger the SOC caused by the heavy atom located in the molecule, the more efficient is the ISC process, as seen in halogen-substituted naphthalenes.[133]

Transition metal complexes of the 2nd and 3rd row often show strong phosphorescence as they have a strong heavy atom effect. For example, diimine complexes of ruthenium and rhenium as well as the C-N cyclometallated complexes of iridium are able to form highly emissive triplet excited states. Looking at mononuclear metal complexes, a very fast conversion from singlet

into triplet excited states can be obtained. For that reasons, these systems have gained special attention for triplet state formation in photocatalysis and as phosphorescent materials.[134-152]

Balzani *et al.* investigated, amongst others, the model compound $[Ru(bpy)_3]^{2+}$. They showed that, by using heavy metals, which have a very high intrinsic SOC, in combination with different kinds of ligands it is quite easy to influence the energies of the excited states.[153,154]

The resulting very fast ISC enables the quenching of the fluorescence from the $S_1$ states and achieves highly efficient radiative decay from the $T_1$ state *via* phosphorescence.

Kozheynikov and co-workers generated a series of oligothienylpyridine cyclometallated complexes of platinum and iridium and investigated their photophysical properties. They found the complexes to be fluorescent as well as phosphorescent.[155] They mentioned the metal character being sufficiently involved in the photophysical process to promote phosphorescence, but it was not able anymore to cause the ultrafast depletion of the singlet state which, for complexes with a discrete arylpyridine ligand, is usually the case.

Dipyrromethane complexes with Rh as the central metal were found to show a comparable behaviour, as reported by Kirsch-De Mesmaeker and co-workers. The complexes showed fluorescence due to a domination of the organic ligand at room temperature, whereas at 77 K phosphorescence turned out to be predominant.[156]

The suppression of $S_1 \rightarrow T_1$ ISC can also occur if the distance between the metal centre and the ligand chromophore is too long, which lowers the MLCT character, and at the same time, the influence of the metal in the excited states. This phenomenon was found for fused aromatic systems such as anthracene or pentacene, which are connected to the metal *via* an alkynyl or a keto group.[155,156] With a fluorescence quantum yield of $\Phi_f$ = 0.97 $[\{C_6H_3(CH_3)_2\}NCPt(PEt_3)_2]_2$-5,12-diethynyltetracene serves as an extraordinary example.

### 3.1.2 Optical Properties of Rhodacyclopentadienes

Marder *et al.* investigated the optical properties of a series of 2,5-bis(*p*-R-arylethynyl)-3,4-bis(aryl)rhodacyclopenta-2,4-dienes, and emission lifetimes of $\pi$ = 0.45-1.21 ns were observed. This fact led to the conclusion that, in case of the 2,5-bis(*p*-R-arylethynyl)-3,4-bis(aryl)-rhodacyclopenta-2,4-dienes, fluorescence is taking place from the $S_1$ state.[69]

The rhodacyclopentadienes bearing a –C≡C–$SiMe_3$ ligand in the equatorial plane show intense bands in the UV/Vis absorption spectra, having their maxima at $\lambda_{abs}$ = 453-517 nm with extinction coefficients of $\varepsilon$ = 21.000-35.000 $Lmol^{-1}cm^{-1}$. All complexes emit in the visible region ($\lambda_{em}$ = 496-590 nm) and experience only small Stokes shifts (ca. 1870-2390 $cm^{-1}$). Besides their strong emission, the rhodacyclopentadienes also show moderate photoluminescence quantum yields of $\phi_{PL}$ = 0.01-0.18, compound **7a** (x = CC-TMS) showing the highest quantum yield. This is rather unusual, as in organic molecules, quenching of the luminescence is often caused by the $n \rightarrow \pi^*$ transition of the nitro group. The R substituents of the aryl rings at the *para*-position induce a bathochromic shift in the absorption and emission maxima, with electron-withdrawing substituents showing a stronger effect than electron-donating ones, influencing the energy gap between the ground state $S_0$ and the emissive excited state.[69]

Furthermore, the synthesised compounds **7b, 7e** and **7j** (X = CC-TMS) show singlet oxygen sensitisation quantum yields between 0.45 - 0.61. These values indicate comparable quantum yields for the ISC in the rhodacyclopentadienes. ISC between the $S_1$ and the $T_1$ state of compounds **7a–j** (x = CC-TMS) takes place, unusually slowly (10 ns), leading to emission from the $S_1$ states.[69] After the introduction of longer conjugated substituents at the *para*-position of the phenyl rings, (**9a-c**) a bathochromic shift appears in both absorption and emission, accompanied by an increase of the values of the extinction coefficients. The short emission lifetimes, which lie in the nanosecond timescale, point out that the excited state behaviour is comparable to that of compounds **7a-j**.[69] Nevertheless, the rather low quantum yields of 0.01-0.03 show that effective non-radiative decay takes place, which is caused by additional vibrational modes.

The introduction of a series of ligands with different conjugation lengths and different $\sigma/\pi$-donor strengths should clarify the influence of the $\sigma$-donor ligand lying in the plane of the metallacyclopentadiene as well the influence of the rhodium centre on the photophysical properties of the excited states. A more intense effect could be obtained when the acetylides ligand was replaced by the strongly $\sigma$-donating methyl ligand in **10b-e** and **10h-j**.[69]

This exchange was expected to increase the electron density at the metal centre and cause an increase of the MLCT character of the emitting excited state, yielding higher ISC rates. However, only a small bathochromic shift of about 35 $cm^{-1}$ of the emission- and absorption maxima of compounds **10b**, **10d**, **10i**, and **10j** was observed, accompanied by a decrease of the fluorescence quantum yield to below 0.02.[69]

Previous studies on cyclometallated $d_6$-rhodium compounds rather concentrate on homoleptic and heteroleptic bipyridine and phenylpyridine complexes, being the type $[Rh(bpy)_{3-n}\text{-}(ppy)_n]^{(3-n)+}$ (n = 0-3) and their derivatives. Luminescence at room temperature was only observed for a small number of those compounds. Because of this, the main part of the rhodium complexes were measured in a glass matrix at 77 K or in their crystalline form, showing, that they exhibit only weak phosphorescence with emission lifetimes of $\tau$ = 3 – 500 $\mu$s. This is because the contribution of the $^3$MLCT($d$-$\pi^*$) or $^3$MC($d$-$d^*$) to the excited state is very small, whereas the major contribution comes from the $^3$IL($\pi$–$\pi^*$) charge transfer. This causes a very slow ISC from $S_1 \rightarrow T_1$, being orders of magnitude slower in comparison to the ISC of other heavy transition metal complexes of Ru, Ir or Pt.[69] However, the SOC of the Rh-centre is large enough to lead to some intersystem crossing from the $S_1$ to the $T_1$ state. Due to their excited state and photophysical behaviour the 2,5-bis(arylethynyl)rhodacyclopentadienes can be compared to organo maingroup cyclopentadienes, such as the siloles, thiophenes and phospholes mentioned above. These main group analogues of the rhodacyclopentadienes, amongst others investigated by Pagenkopf and Marder *et al.*[97,101,106,107,113] usually show fluorescence in the visible region of the electromagnetic spectrum. It seems that the general excited state processes hardly depend on the substituents on the aryl rings at the *para*-positions or at the rhodium centre.

A comparison to the main group analogues of the rhodacyclopentadienes shows that their absorption and emission spectra look quite similar. However, the thiophene compounds experience a hypsochromic shift ($\lambda_{abs}$ = 345-387 nm, $\lambda_{em}$ = 382-435 nm) and the extinction coefficients ($\varepsilon$ = 33000-52000) as well as the fluorescence quantum yields ($\phi_f$ = 0.19-0.33) achieve higher values. A reason for the hypsochromic shift of the $S_0 – S_1$ state might be the nature of the structure of the 2,5-bis(arylethynyl)thiophenes, which is bent, changing the bind angles and thus influencing the orbital energies of the core-structure.

Besides this, the larger rhodium atom causes a change of the bond angles of the $MC_4$ building block and changes the energies of the carbon $\pi$-system. With a fluorescence quantum yield of about 0.60, and with emission lifetimes of 210-400 ps the thiophene is able to obtain faster ISC ($\xi$ = 100 $cm^{-1}$) on a timescale of $10^{-9}$-$10^{-8}$ s in comparison to that of rhodium, which shows an

ISC of about one order of magnitude slower (**7-12**). The ISC in other octahedral organometallic complexes is usually several orders of magnitude faster than that of the rhodacyclopentadienes.[150,154,157-160] It seems that the ISC, which would lead to an efficient formation of the triplet state, is largely suppressed.

Besides the 2,5-bis(arylethynyl)rhodacyclopentadienes mentioned above, Marder *et al.* further investigated the optical properties of comparable systems, which are more rigid due to the reductive coupling of various 1,12-(*p*-R-phenyl)dodeca-1,3,11,12-tetraynes. These compounds also show unexpectedly strong fluorescence from their $S_1$ states instead of phosphorescence. The short emission lifetimes of $\tau_f$ = 1-3 ns in degassed toluene solution at room temperature and the overlap of the excitation and emission spectra support this impression.[72]

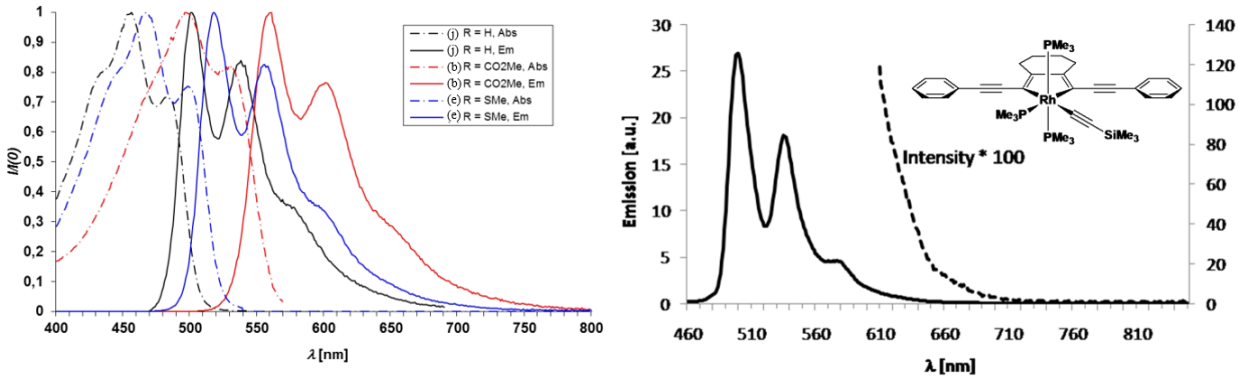


**Figure 76** Absorption and emission spectra with excitation at the respective absorption maximum of **14b, e, j** (left). Emission spectrum of **14j** at 77 K in an *iso*-pentane/$Et_2O$/EtOH glass matrix ($\lambda_{ex}$ = 450 nm) (right). Reprinted from reference [72] with friendly permission of the American Chemical Society. [72]

They show very high fluorescence quantum yields $\Phi_f$ (up to 0.69) and as $^1O_2$ formation takes place in an $O_2$ saturated solution ($\Phi_\Delta$), it is also shown that ISC takes place, but on a nanosecond timescale, yielding very little to no non-radiative decay from the $S_1$ state. Emission with no further bathochromic shift appears between 400 and 1000 nm, recorded at 77 K in a glass matrix (Figure 76).

As this behaviour is rather unusual for 2nd and 3rd row transition metal complexes, Marder *et al.* also investigated the influence of the transition metal centre of the metallacyclopentadiene ring. The central rhodium was substituted by iridium to form an analogous compound from [IrCl($PEt_3$)$_3$] with 1,12-bis(*p*-carbomethoxyphenyl)dodeca-1,3,9,11-tetrayne.[72]

In contrast to the rhodium containing compounds, those containing iridium are well known for their triplet emission and have also been intensively examined, due to their use in OLED applications.[161-164]

The electromagnetic spectrum of the 2,5-bis[*p*-$CO_2Me(C_6H_4)$-C≡C]-iridacyclopenta-2,4-diene **20** (Figure 77) shows a rather poorly resolved low energy absorption band in the visible region with a maximum at $\lambda_{abs}$ = 515 nm ($\varepsilon$ = 21000 $cm^{-1}$). The emission band is broad with a maximum at $\lambda_{em}$ = 595 nm.

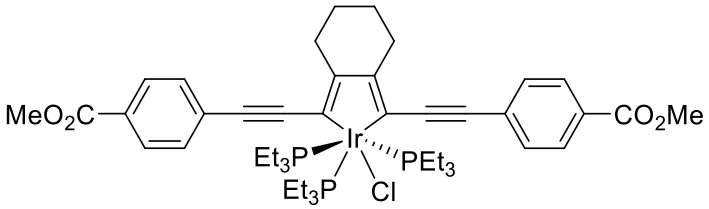


**20**

**Figure 77** Structure of 2,5-bis[*p*-$CO_2Me(C_6H_4)$-C≡C]-iridacyclopenta-2,4-diene **20**.[72]

If the toluene solution is degassed, the model compound **20** displays fluorescence ($\phi_f$ = 0.08). Previously examined iridium compounds do not typically show a comparable behaviour. The short luminescence lifetime of $\phi_f$ = 0.9(59%)/1.9(41%) ns and the observed overlap of the absorption and emission bands also suggest fluorescence.[72]

The behaviour of the compound is comparable to that of the 2,5-bis(*p*-R-arylethynyl)rhodacyclopenta-2,4-dienes **14a-c** and **15a-c**. This again indicates a very slow ISC process on a nanosecond time scale ($k_{ISC} = 10^8$ $s^{-1}$). A recorded emission spectrum at 77 K in a glass matrix also showed no phosphorescence taking place between 500 and 1000 nm. Unfortunately, the compound is not stable in solution under oxygen. All of the results obtained, and the intrinsic spin-orbit coupling constant of iridium, which is three times higher than that of Rh ($\xi$ = 3909 $cm^{-1}$ *vs.* 1200 $cm^{-1}$), indicate that the metal centre incorporated into the metallacycle has either very little or no influence on the photophysical properties of the system.[72]

Marder *et al.* suggest that this is the first organometallic system having iridium as the central metal atom for which only fluorescence instead of phosphorescence is observable, even under the above-mentioned conditions. They also reported that the ISC process must occur under thermal activation at room temperature as the emission lifetime of **14j** at 77 K is $\tau_f$ = 3.2 ns which is nearly consistent with the pure radiative lifetime of the first excited singlet state ($\tau_0 = \tau_f / \phi_f$ = 3.6 ns).[72]

Due to its photoluminescence properties 2,5-bis(phenylethynyl)-rhodacyclopenta-2,4-diene **14j** served as a model compound for picosecond time-resolved IR studies aiming to clarify the excited state behaviour of this type of conjugated, rod-like metallacyclopentadiene.[71]

The formation of the $T_1$-state turned out to be very slow, as it takes place on a nanosecond time scale. This formation is usually on a femto- or picosecond time scale for octahedral organometallic complexes. Figure 78 shows the ps-time resolved IR of compound **14j**, which indicates the formation of the different states from 11-3000 ps. Within 11 ps, the $S_1$ state at 2008 $cm^{-1}$ reaches its maximum, accompanied by a depletion of the $S_0$ state at 2128 $cm^{-1}$. Subsequently, relaxation of the $S_1$ state back to the $S_0$ state takes place, accompanied by the formation of a new species at 1941 $cm^{-1}$, which is assigned to formation of the $T_1$ state.[71]

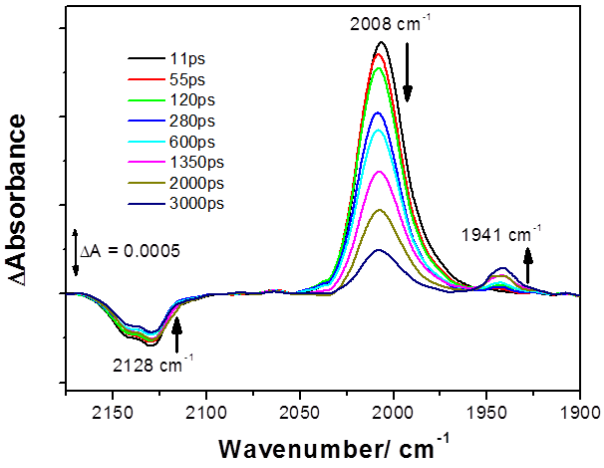


**Figure 78** Ps-time resolved IR-spectrum of compound **14j**. Reprinted from reference [71] with friendly permission of Wiley and Sons.[71]

### 3.1.3 Optical Properties of Dibenzometallacyclopentadienes

Dibenzometallacyclopentadienes or biphenyl complexes are of current interest, due to their phosphorescence and long emitting lifetimes, indicative of accessible triplet states, which are required for the use in OLEDs and further luminescent applications. Several investigations had been made, for example, on Pt and Pd 2,2'-biphenyl complexes.[87,165-168] The use for luminescent applications requires the efficient formation of triplet states. Extensive studies by Rillema and co-workers on Pt(2,2'-biphenyl) complexes, containing mono- as well as bidentate ligands (e.g. pyridine, CO, [87,167] dppm[166,169] and the bridging ligand $SEt_2$[166]) showed HOMO-LUMO $d\pi \rightarrow \pi^*_{(bph)}$ transitions between 300 and 400 nm, and intra-ligand $\pi \rightarrow \pi^*$ transition at higher energies. In solution, strong emission takes place, which may come from excited intra-ligand triplet states ($^3$IL) and may be dominated by the ligand. The vibrational fine structure in the photoluminescence spectra also supports that conclusion.

The recorded spectra showed lower energy bands between 490 and 620 nm, which did not change significantly for the different compounds. At 77 K, only a small change in the profile was observed. For the monometallic species, triplet lifetimes between 3-14 µs and quantum yields of ca. 0.16 were observed. For the bimetallic complexes, the quantum yields were about 0.08.

The complex [Pt(2,2'-bph)$(CO)_2$] turned out to be a weak emitter in solution, with emission at 562 and 594 nm. The triplet lifetimes lay between 2 and 3 µs in dichloromethane and a 4:1 mixture of ethanol and methanol. The complex had strong tendencies to self-association, which led to various emitting species, due to the formation of dimers and higher aggregates in solution. In the solid state, the stacked complex emitted at 726 nm, and a lifetime shortened to 0.84 µs could be observed.[170]

Another species which was reported by Zhen *et al.* in 1999, is the hetero-bimetallic complex [Fe($\eta^5$-$C_5H_4PPh_2$)$_2$Pt(bph)].[171] After the [Fe($\eta^5$-$C_5H_4PPh_2$)$_2$] complex is coupled to the platinum centre, the d$\pi_{(Fe)}\rightarrow\pi^*_{(Cp)}$ MLCT transition shows a blue shift from 442 to 425 nm. Furthermore, a d$\pi_{(Pt)}\rightarrow\pi^*_{(bph)}$ MLCT caused by the introduced platinum centre, can be observed at 337 nm, with a lifetime of 6.7 $\mu$s (at 77 K). Using a nanosecond laser, the group was not able to record the lifetime at room temperature, as it was too short. They concluded the triplet emission to be quenched by the ferrocenyl moiety, *via* an electron transfer mechanism.

## 3.2 Results and Discussion

### 3.2.1 Optical Properties

*Optical properties of rhodacyclopentadienes **23** and **25***

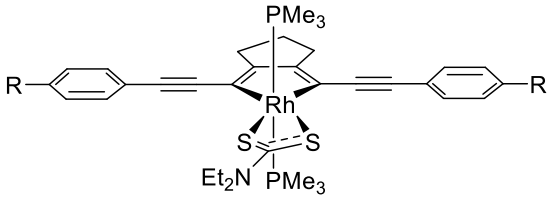


**23**

The rhodacyclopentadienes **23a-f'** show intense absorption bands in the visible region with $\lambda_{max}$ ranging from 478-594 nm, depending on the *para*-substituents of the phenyl rings (Figure 79), and large extinction coefficients $\varepsilon$ of 14000-33000 $Lmol^{-1}cm^{-1}$ (Table 16). Interestingly, electron donating substituents, Me, $NMe_2$ and SMe hardly influence the absorption maxima, whereas the extinction coefficients $\varepsilon$ show significant differences, that of **23d** ($NMe_2$) being less than half of that of **23e** (SMe) and significantly smaller than that of **23c** (Me). Electron accepting substituents lead to a strong bathochromic shift, which correlates with their Hammett constant. Compound **23a**, bearing the very strong acceptor substituent $NO_2$, shows the strongest bathochromic shift, followed by that of compound **23b** ($CO_2Me$), which has its maximum at the same wavelength as compound **23d**. With the absorption maximum at 478 nm, compound **23f'** shows the smallest bathochromic shift. Interestingly, the vibrational bands of this compound, bearing two tetra-fluorinated phenyl rings, change completely. Possibly, the fluorine atoms at the phenyl ring cause a difference in the vibronic coupling. The extinction coefficients of the acceptor-substituted compounds show comparable values of about 30000 $Lmol^{-1}cm^{-1}$.

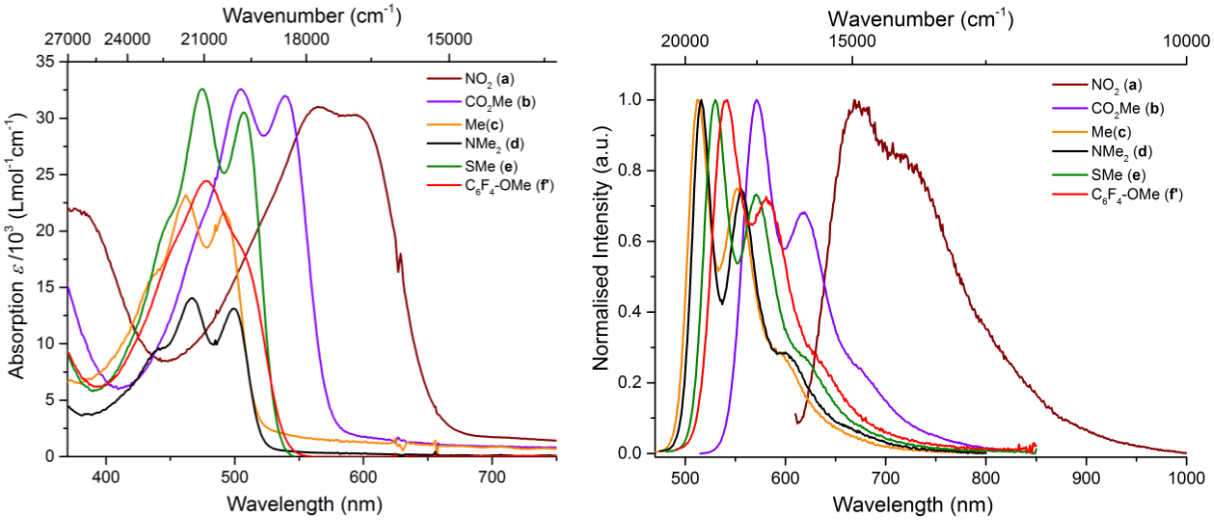


**Figure 79** Absorption (left) and emission spectra (right) of compounds **23a** ($NO_2$), **b** ($CO_2Me$), **c** (Me), **d** ($NMe_2$), **e** (SMe) and **f'** ($C_6F_4$-4-OMe) in toluene at RT.

Compounds **23** emit in the UV/visible region with emission maxima $\lambda_{em}$ ranging from 512-671 nm. They show unusual fluorescence, indicated by the large overlap of the absorption and emission bands and the very short lifetimes, the longest being 1.41 ns (Figure 79). The Stokes shifts of compounds **23a-f'** are small with values of 660-1200 $cm^{-1}$, the smallest shifts being those of compounds **23c** and **d** (Table 16). The emission bands show the same trend in the bathochromic shift as observed in the absorption spectra. In general, both, donor and acceptor substituents at the *para* positions of the phenyl rings cause a bathochromic shift, that of the acceptors being larger than that of the donors.[101] This behaviour is consistent with previous reports on analogous rhodacyclopentadienes bearing acac or C≡C-TMS as ligands.[71,72,121] Compound **23a** shows the strongest shift, causing its emission to appear mainly in the near infrared region (NIR).

**Table 16** Absorption, extinction coefficient, emission, Stokes shifts, quantum yields, lifetimes and rate constants of compounds **23a-f'** and **25a**, **b**, **e** and **f'**.

| | R / Ar | $\lambda_{max}$ (abs) [nm] | $\varepsilon$ [$Lmol^{-1}cm^{-1}$] | $\lambda_{max}$ (em) [nm] | Stokes shift [$cm^{-1}$] | $\phi_{PL}$ | $\tau_f$ [ns] | $\tau_0$ [ns] | $k_f$ [$10^8$ $s^{-1}$] | $k_{nr}$ [$10^8$ $s^{-1}$] | $\tau_0$ [ns][a] | $k_f$ [$10^8$ $s^{-1}$][a] |
|---|---|---|---|---|---|---|---|---|---|---|---|---|
| **23a** | $NO_2$ | 566, 594 | 31 000 | 671 | 1900 | 0.07 | 0.38 | 5.42 | 1.85 | 24.58 | 5.11 | 1.95 |
| **23b** | $CO_2Me$ | 504, 540 | 33 000 | 570 | 980 | 0.48 | 1.41[b] | 2.93 | 3.34 | 3.17 | 3.02 | 3.31 |
| **23c** | Me | 462, 491 | 23 000 | 512 | 840 | 0.02 | n.a. | n.a. | n.a. | n.a. | 2.85 | 3.51 |
| **23d** | $NMe_2$ | 466, 499 | 14 000 | 516 | 660 | 0.01 | n.a. | n.a. | n.a. | n.a. | 4.42 | 2.26 |
| **23e** | SMe | 475, 507 | 33 000 | 529 | 860 | 0.11 | 0.53[b] | 4.81 | 2.10 | 38.92 | 2.04 | 4.93 |
| **23f'** | $C_6F_4$-4-OMe | 478 | 25 000 | 540 | 1200 | 0.28 | 1.28 | 4.57 | 2.18 | 11.75 | 2.60 | 3.84 |
| **25a** | $NO_2$ | 583, 619 | 31 000 | 686 | 1600 | 0.04 | n.a. | n.a. | n.a. | n.a. | 3.94 | 2.54 |
| **25b** | $CO_2Me$ | 520, 559 | 30 000 | 586 | 820 | <0.01 | n.a. | n.a. | n.a. | n.a. | 2.62 | 3.82 |
| **25e** | SMe | 489, 526 | 29 000 | 508 | 760 | <0.01 | n.a. | n.a. | n.a. | n.a. | 1.50 | 6.68 |
| **25f'** | $C_6F_4$-4-OMe | 495 | 23 000 | 527 | 1200 | <0.01 | n.a. | n.a. | n.a. | n.a. | 2.56 | 3.91 |

a) Calculated values based on the Strickler-Berg relationship[172] b) The lifetime was determined *via* tail fit.

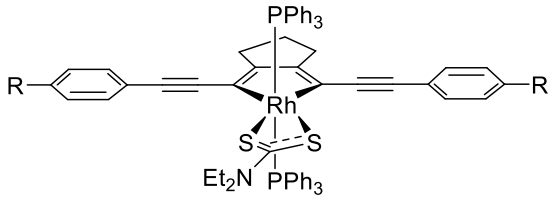


**25**

The absorption spectra of the corresponding compounds **25a**, **b**, **e** and **f'**, bearing triphenylphosphine instead of trimethylphosphine ligands, show a similar behaviour. They exhibit intense absorption bands in the visible region with $\lambda_{max}$ ranging from 495-619 nm, depending on the *para*-substituents of the phenyl rings (Figure 80), and large extinction coefficients ε of 23000-31000 $Lmol^{-1}cm^{-1}$. The absorption maxima seem to be bathochromically shifted by ca. 20 nm compared to those of compounds **23**. This indicates that the exchange of the phosphine ligand causes a decrease of the energy gap between the first excited ($S_1$) and ground state ($S_0$) in the rhodacyclopentadienes **25**. The substituents on the phenyl rings of the $\pi$-system of rhodacyclopentadienes have the same effect on the absorption spectra as found for compounds **23**. Accordingly, the largest shift is observed for compound **25a** (R = $NO_2$), followed by compound **25b** ($CO_2Me$), and compounds **25e** (SMe) and **f'** (Ar = $C_6F_4$-4-OMe) absorb at higher energies. The latter compound shows different vibrational bands in its absorption, supporting the idea of a difference in the vibronic coupling caused by the C-F bonds.

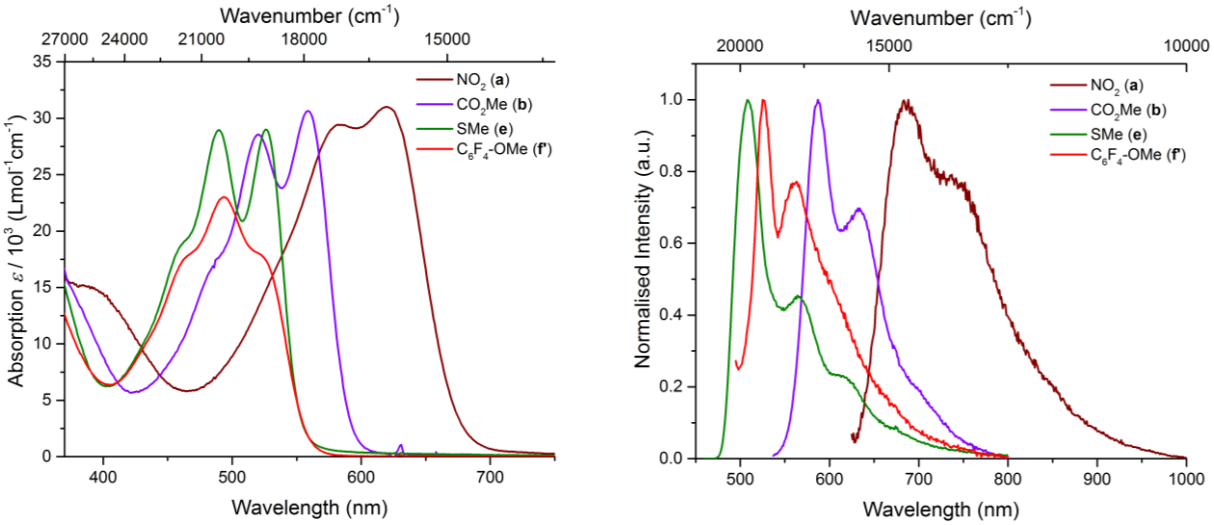


**Figure 80** Absorption (left) and emission spectra (right) of compounds **25a** ($NO_2$), **b** ($CO_2Me$), **e** (SMe) and **f'** ($C_6F_4$-OMe) in toluene at RT.

The emission of compounds **25a**, **b**, **e** and **f'** occurs in the visible region with $\lambda_{max}$ ranging from 508-686 nm, showing the same trend in the bathochromic shift as in the absorption spectra (Figure 80). The energetically lower vibrational band of the emission of compound **25e** is significantly weaker in its intensity than the corresponding vibrational bands of the other compounds.

The Stokes shifts of 760-1600 $cm^{-1}$ lie in the same region as those of compounds **23** (Table 16). Fluorescence is indicated by the large overlap of the absorption and emission bands and the very short lifetimes.

The strongest fluorescence is exhibited by compound **23b**, with a quantum yield of 48% and a typical lifetime $\tau_f$ of 1.41 ns. [71,72,121] With quantum yields of 11 and 28%, compounds **23e** and **f'** show moderate fluorescence, that of compounds **23a**, **c** and **d** being weak with only 1-7% quantum yield. The corresponding fluorescence lifetimes of compounds **23c** and **d** are extremely short and therefore were not measurable. The emission of compounds **25** is too weak to give a reasonable quantum yield and, accordingly, it was not possible to determine the corresponding lifetimes. Obviously, the exchange of trimethylphosphine by triphenylphosphine lowers the quantum yields of the rhodacyclopentadienes **25** extremely, presumably due to alternative vibrational relaxation modes.

Usually, the fluorescence lifetime is directly measured *via* time-correlated single photon counting (TCSPC, Chap. 3.2.1), and using the following equation, the natural lifetime $\tau_0$ can be obtained:

$$\tau_0 = \frac{\tau_f}{\phi_f} \qquad \text{Equation 1}$$

In general, the natural fluorescence lifetime can be seen as the upper border of the fluorescence lifetime in the absence of all non-radiative processes, giving an idea on the efficiency of the emission of a luminescent compound.

If the fluorescence lifetime is not detectable, the natural lifetime can alternatively be calculated from the reciprocal value of its corresponding radiative rate $k_r$, which can be calculated *via* the Strickler-Berg equation:[172]

$$k_r = \frac{1}{\tau_0} = 2.880 \cdot 10^{-9} \cdot n^2 \cdot \langle \tilde{\nu}_F^{-3} \rangle_{A\nu}^{-1} \cdot \frac{g_1}{g_0} \cdot \int \varepsilon(\tilde{\nu}) d \ln \tilde{\nu} \qquad \text{Equation 2}$$

It relates the transition probabilities of absorption and emission of light, whereas $n$ is the refractive index of the solvent, $\varepsilon$ is the extinction coefficient depending on the wavenumber $\tilde{\nu}$ (absorption spectrum) and $g_1$ and $g_0$ are the multiplicities of the excited (upper) and the ground (lower) state, respectively.

The integration takes place over the whole region of the $S_0 \rightarrow S_1$ absorption or $S_1 \rightarrow S_0$ emission band. The term $\langle \tilde{\nu}_F^{-3} \rangle$ originates from the stationary emission spectrum:

$$\langle \tilde{\nu}_F^{-3} \rangle_{Av}^{-1} = \frac{\int I(\tilde{\nu}) d\tilde{\nu}}{\int \tilde{\nu}^{-3} I(\tilde{\nu}) d\tilde{\nu}} \qquad \text{Equation 3}$$

*I(ṽ)* being the spectral photon density depending on the wavenumber *ṽ*.

As radiative and non-radiative decay of an excited singlet state are competitive processes, a comparison of $\tau_f$ and $\tau_0$ as well as $k_r$ and $k_{nr}$ can clarify whether or not a compound is an efficient emitter. It can be determined whether the low quantum yields are caused by a fast non-radiative decay or if another relaxation mechanism (e.g. ISC) is responsible. When the quantum yield $\phi_f$ and $k_r$ are known, $k_{nr}$ can be calculated from the following equation:

$$k_{nr} = k_r \cdot \frac{1 - \phi_f}{\phi_f} \qquad \text{Equation 4}$$

The rate constant of the inter system crossing process $k_{ISC}$ can give information on how fast and efficient ISC is occurring compared to radiative or non-radiative relaxation processes from the excited singlet state.

For compound **23b**, the calculated natural lifetime $\tau_0$ of 2.93 ns obtained from the quantum yield and the fluorescence lifetime at RT agrees well with the value of 3.02 ns, obtained *via* the Strickler-Berg equation, confirming its applicability for these systems. The same applies for the natural lifetime of compound **23a**, which is 5.42 ns when obtained from the measured values of the fluorescence lifetime and the quantum yield, and 5.11 ns when calculated *via* the Strickler-Berg equation. In contrast, the natural lifetimes of compounds **23e** (4.81 ns) and **f'** (4.57 ns) obtained from the measured fluorescence lifetime and quantum yield are twice the value obtained from the Strickler-Berg approach (2.04 and 2.60 ns, respectively). As the different terms in the Strickler-Berg equation consist of the integrals of the emission and the extinction coefficient, they may be inaccurate and thus would lead to errors in the calculated values. The $k_r$ values corresponding to the natural lifetimes are given in Table 16, together with the calculated data for compounds **23c** and **d**.

Compared to rhodacyclopentadienes **23**, the quantum yields for compounds **25** are extremely small (0.1-4%), rhodacyclopentadiene **25e** not showing any detectable fluorescence at all. Thus, the natural lifetimes of these compounds were only accessible by calculation *via* the Strickler-Berg equation.

The calculated natural lifetimes in combination with the low quantum yields of these systems indicate that strongly competing processes take place during the relaxation of the excited state, such as vibrational relaxation and intersystem crossing (ISC) to the excited triplet states. We have found that the ISC rate constant of other rhodacyclopentadienes is of the same order of magnitude ($10^8 s^{-1}$) as radiative relaxation from the $S_1$ state.[71,72] As already mentioned in Chap. 3.1.2, usually the ISC of octahedral complexes bearing a transition metal centre is several orders of magnitude faster than found for the rhodacyclopentadienes.

A method to investigate ISC after excitation of the rhodacyclopentadienes **23** and **25**, was to see whether they generate singlet oxygen ($^1O_2$), as the $T_1$ state can sensitise $^1O_2$, which can be detected by its emission at ca. 1270 nm. To quantify the formation of singlet oxygen, the quantum yield of its emission $\Phi_\Delta$ has to be determined. For model compounds **23b** and **25b**, the quantum yield of $^1O_2$ was measured relative to that of a standard, following a method reported by Resch-Genger.[173] The singlet oxygen sensitising was carried out in acetonitrile, which was saturated by bubbling with $O_2$ for ten minutes.

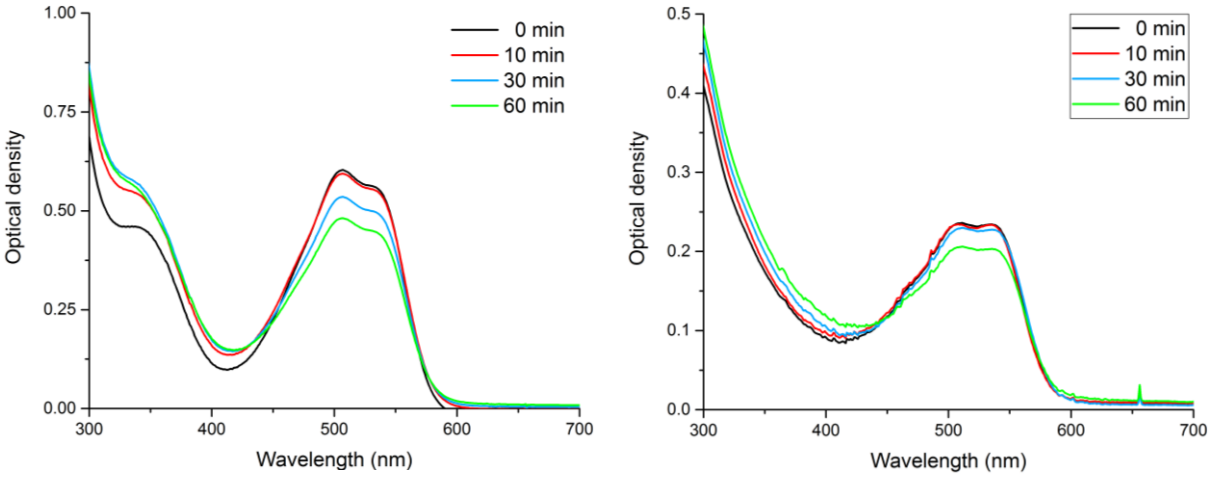


**Figure 81** UV/Vis spectra of compounds **23b** (left) and **25b** (right) after preparation of the solution and after 10, 30 and 60 min of bubbling $O_2$.

Bubbling $O_2$ for more than ten minutes caused the intensity of the absorption to decrease, which indicates that the compounds are only stable for a limited time in an oxygen-saturated solution. As a standard, perinaphthenone was chosen, as it is known to have a quantum yield for singlet oxygen emission close to unity (0.99 +/- 0.05 in 1,4-dioxane).[174] The relative determination of the singlet oxygen quantum yields resulted in 27% (**23b**) and 37% (**25b**) (Figure 82). Earlier reports from our group showed that the sum of the fluorescence quantum yields of rhodacyclopentadiene **14j** and that for singlet oxygen formation is 100% ($\Phi_f + \Phi_\Delta \approx 1$; vide supra), meaning that the only relaxation pathways of the singlet excited state of that compound are fluorescence and ISC.[71]

In contrast, rhodacyclopentadienes **23** and **25** obviously experience an additional relaxation pathway, being non-radiative decay (vibration, rotation), which is more significant for **25**.

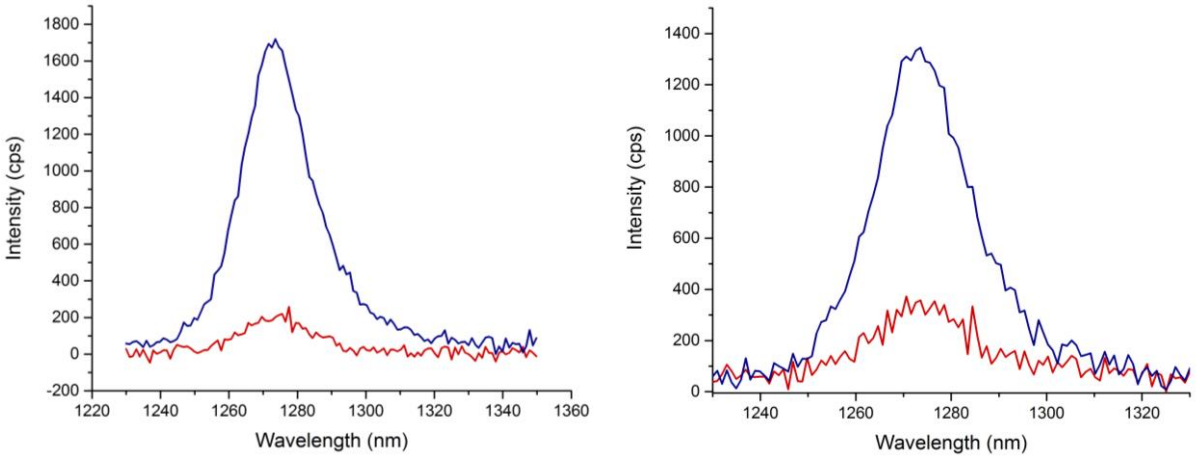


**Figure 82** Emission spectrum of singlet oxygen of perinaphthenone (blue) *vs.* emission of singlet oxygen of rhodacyclopentadiene **23b** excited at 344 nm (red, left) and **25b** excited at 348 nm (red, right).

Lifetime measurements at low temperatures using rhodacyclopentadiene **14j** (Chap. 3.1.2 and Figure 83), confirmed the existence of only two deactivation paths.[72] At 77 K, a $\tau_f$ value of 3.2 ns was obtained, which is only slightly shorter than the calculated natural lifetime of the first singlet excited state ($\tau_0$ = 3.6 ns).[72]

It was concluded that the ISC process occurs *via* thermal activation at ambient temperature and thus should be inhibited at low temperatures. This was confirmed by fluorescence lifetime measurements from 315 K to 183 K in 5 K steps, resulting in the plot shown in Figure 83.

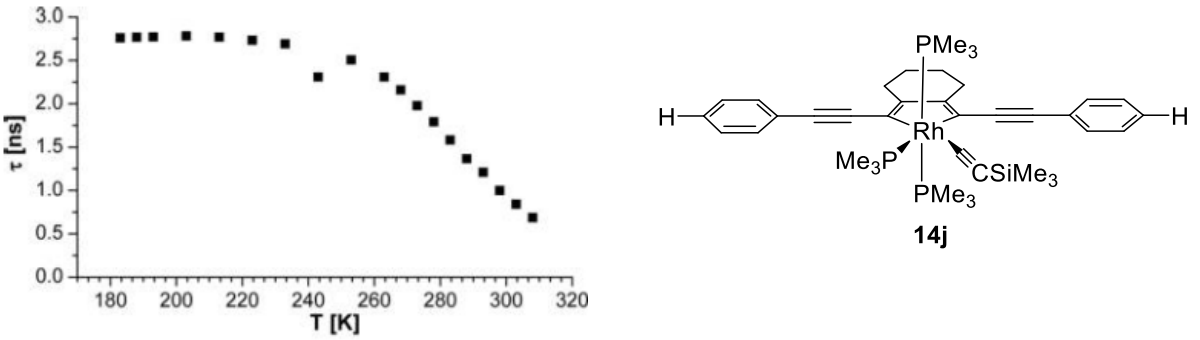


**Figure 83** Plot of **14j**, showing lifetimes at different low temperatures (315-185 K). Reprinted from reference [72] with permission of the American Chemical Society. [72]

The lifetime plot in Figure 83 and equations 4-6, which are valid if radiative decay takes place from $S_1$ to $S_0$, show that as the temperature decreases to 233 K, the lifetime $\tau_f$ and the fluorescence quantum yield $\phi_f$ increase, and thus the rate constant for ISC ($k_{ISC}$) decreases.

Between 233 and 183 K, a plateau of the observed lifetime (ca 2.7 ns) is found, indicating a constant $\phi_f$ value of 0.77 in solution.[72]

$$\phi_f = \frac{k_f}{k_f + k_{ISC}} \qquad \text{Equation 5}$$

$$k_{ISC} = \frac{1-\phi_f}{\tau_f} = \frac{1}{\tau_f} - \frac{1}{\tau_0} \qquad \text{Equation 6}$$

It can be concluded that ISC is not completely inhibited at lower temperatures, but is at least reduced to 23%. In an EPA glass matrix at 77 K, the ISC was further reduced to 11%. It was expected that rhodacyclopentadienes **23** and **25** would show a comparable behaviour. To clarify the excited-state behaviour and to find a reason for the low emission intensity of the compounds, the lifetime measurements at low temperatures were repeated, using rhodacyclopentadienes **23b** **25b** (R = $CO_2Me$) as model compounds.

The left side of Figure 84 shows the plot of the fluorescence lifetimes of **23b** from 175 to 295 K in 10 K steps in toluene.

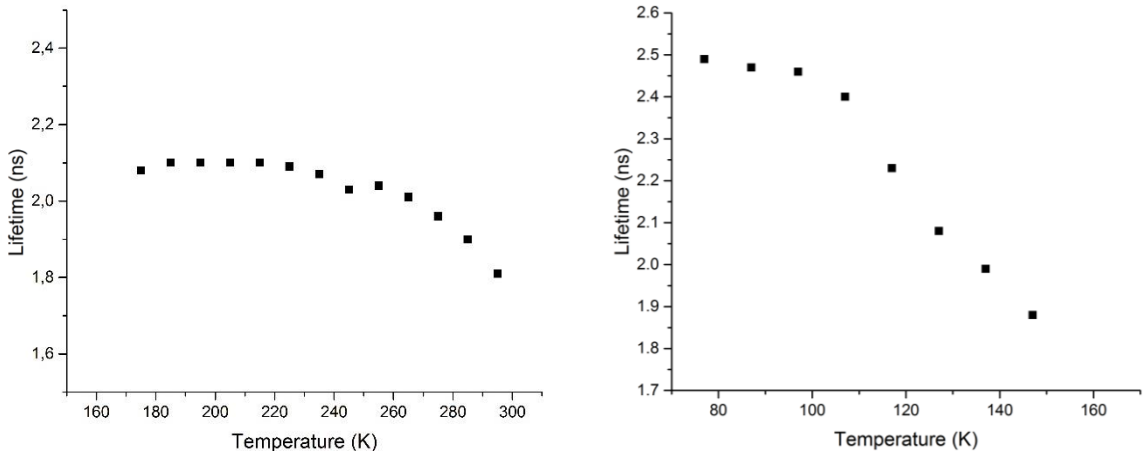


**Figure 84** Left side: Plot of **23b**, showing lifetimes at different low temperatures (295-175 K) in toluene; right side: Plot of **25b**, showing lifetimes at different low temperatures (147-77 K) in Me-THF. Note: Due to technical problems, the lifetimes were determined *via* tail fit.

From 175 to 225 K, a plateau at ca. 2.1 ns can be observed, which corresponds to ca. 72% of the natural lifetime ($\tau_0$ = 2.93 ns). The corresponding lifetime at ambient temperature was measured to be 1.41ns which, accordingly, is 48% of the natural lifetime. This indicates that non-radiative decay, which should be significantly reduced at low temperatures, is responsible for at least 24% of the relaxation from $S_1$ at ambient temperature. Furthermore, the lifetime in a Me-THF glass matrix at 77 K was measured to be 2.20 ns, still not attaining the natural lifetime. It is concluded that ISC, which was determined to be responsible for 27% of the relaxation from $S_1$, is not inhibited at low temperatures ($\Phi_f + \Phi_\Delta \approx 1$), and thus is not thermally activated.

The right side of Figure 84 shows the plot of the fluorescence lifetimes of compound **25b** from 77 to 147 K in 10 K steps in Me-THF. From 77 to 97 K, a plateau at ca. 2.49 ns can be observed, corresponding to ca. 95% of the natural lifetime ($\tau_0$ = 2.62 ns, in toluene). This indicates that non-radiative decay and ISC are both reduced at low temperatures and in contrast to compound **23b**, the ISC process of compound **25b** appears to be thermally activated. Thus, the character of the non-radiative decay seems to be significantly changed, leading to an increase of the activation energy of the ISC. The two Jablonski diagrams in Figure 85 describe the different radiative and non-radiative processes which may occur from the first excited singlet state $S_1$ after excitation of the compounds **23b** (left) and **25b** (right).

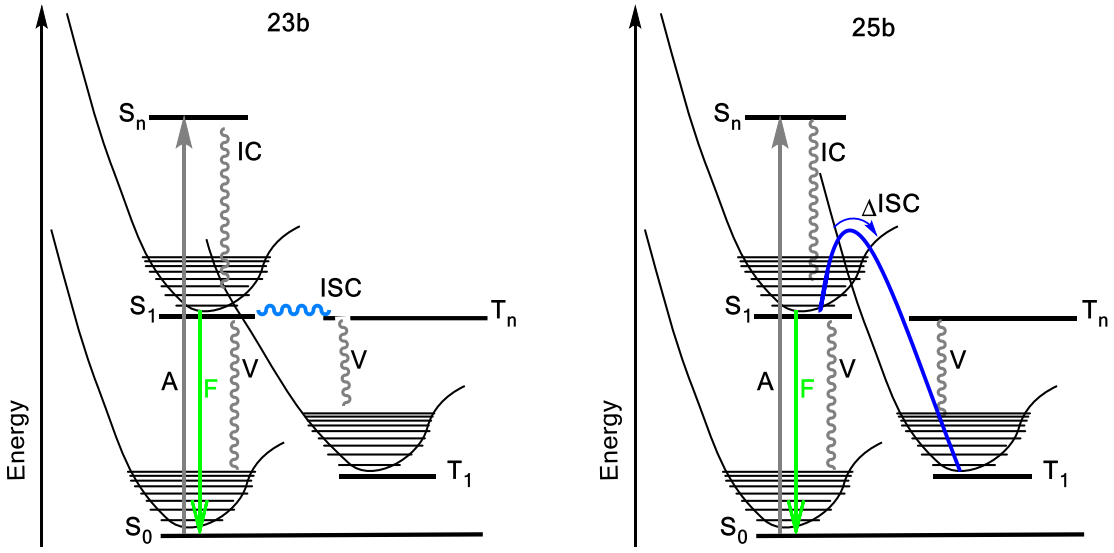


**Figure 85** Jablonski diagrams of the radiative and non-radiative processes of compounds **23b** (left) and **25b** (right).

In case of compound **23b**, the energetic barrier between the excited $S_1$ and $T_n$ state is small, which enables intersystem crossing without additional thermal energy, even at low temperatures. For compound **25b**, a change in the energetic levels of the excited $S_1$ and $T_n$, may cause an increase in the energetic barrier. Accordingly, intersystem crossing at low temperatures is suppressed and can only be observed at higher temperatures, *via* thermal activation.

*Solvatochromic effects of rhodacyclopentadienes **23a** and **25a***

Compound **23a** (R = $NO_2$) shows an intense colour change when dissolved in solvents of different polarity. The hexane solution appears pink, changing to lighter violet in toluene and to a dark violet in THF (Figure 86, top left). For compound **25a** (R = $NO_2$), all three solutions appear dark blue (top right).

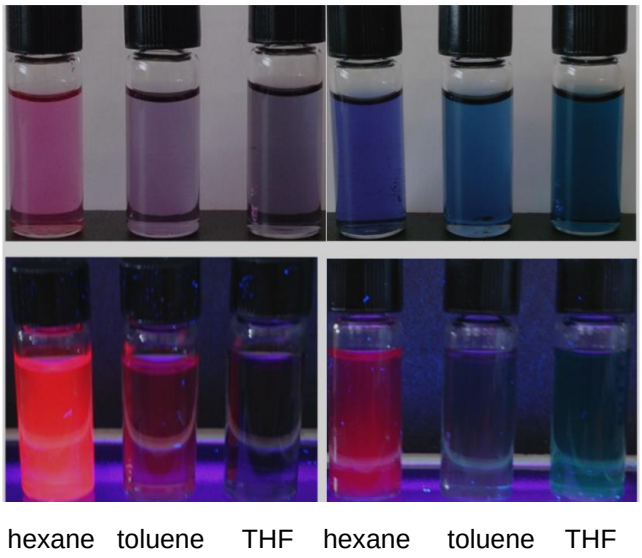


**Figure 86** Solvatochromic properties of rhodacyclopentadienes **23a** (left) and **25a** (right) under daylight (top) and UV-light (bottom) in THF, toluene and hexane.

When excited by UV-light, compound **23a** shows a bright pink emission in hexane, a weak emission in toluene and no visible emission in THF, the emission of compounds **25a** not being visible in toluene and THF and weak in hexane (Figure 86, bottom). These observations led us to carry out a detailed investigation of the solvatochromic properties of the two compounds.

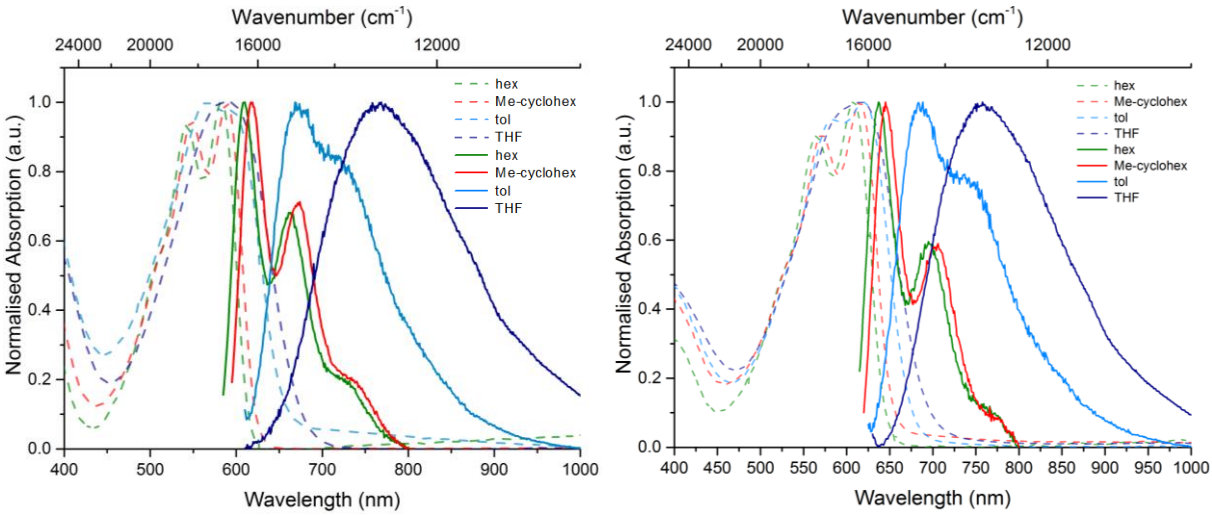


**Figure 87** Absorption (dashed) and emission (solid) of rhodacyclopentadiene **23a** (left) and **25a** (right) in hexane (green), Me-cyclohexane (red), toluene (light blue) and THF (dark blue).

Absorption and emission spectra were recorded in methylcyclohexane, hexane, toluene and THF (Figure 87). The emission shows a large bathochromic shift of the emission maximum (> 100 nm) and an increase in the Stokes shift of 2290-3100 $cm^{-1}$, indicating strong charge-transfer character in the emissive excited state (Table 17). The pink appearance observed in daylight may result from a combination of its absorption and emission.

**Table 17** Solvatochromic emission and absorption properties of compounds **23a** and **25a**.

| | $\lambda_{max}$ (abs) | $\lambda_{max}$ (em) | Stokes shift | Quantum yield |
|---|---|---|---|---|
| **23a** | [nm] | [nm] | [$cm^{-1}$] | $\Phi_f$ |
| hexane | 581 | 609 | 790 | 0.22 |
| Me-cyclohexane | 589 | 618 | 800 | 0.20 |
| toluene | 594 | 671 | 1900 | 0.07 |
| THF | 589 | 765 | 3900 | n.a. |
| **25a** | | | | |
| hexane | 608 | 637 | 750 | 0.03 |
| Me-cyclohexane | 613 | 645 | 810 | 0.04 |
| toluene | 619 | 686 | 1600 | 0.04 |
| THF | 612 | 756 | 3100 | n.a. |
| **23b** | | | | |
| hexane | 530 | 551 | 719 | 0.34 |
| Me-cyclohexane | 533 | 555 | 744 | 0.35 |
| toluene | 541 | 575 | 1093 | 0.48 |
| THF | 541 | 583 | 1332 | 0.36 |

The emission in THF is shifted to the NIR. The resolution of the vibrational modes is significantly diminished in both the absorption and the emission (Figure 87). The corresponding quantum yields of compound **23a** decrease significantly, that in hexane and methylcyclohexane being ca. 20% and 7% in toluene. In THF, the quantum yield could not be determined. Compound **25a** exhibits quantum yields of 3-4% in methylcyclohexane, hexane and toluene. In THF, accordingly, no quantum yield was determined (Table 17).

To confirm that the unusual strong solvatochromism shown by compounds **23a** and **25a** is caused by the $NO_2$ group at the phenyl rings of the $\pi$-system, the solvatochromism of compound **23b** (R = $CO_2Me$) was additionally investigated (Figure 88). The compound shows intense absorption in the visible region with maxima $\lambda_{max}$ ranging from 530-541 nm and corresponding Stokes shifts of 719-1332 $cm^{-1}$. It emits in the visible region with maxima $\lambda_{max}$ ranging from

551-583 nm, showing intense fluorescence in all solvents with values of $\phi_f$ = 34-48 % (Table 17). The bathochromic shift of the emission maxima is only 10-20 nm and thus significantly smaller than that observed for compounds **23a** and **25a**.

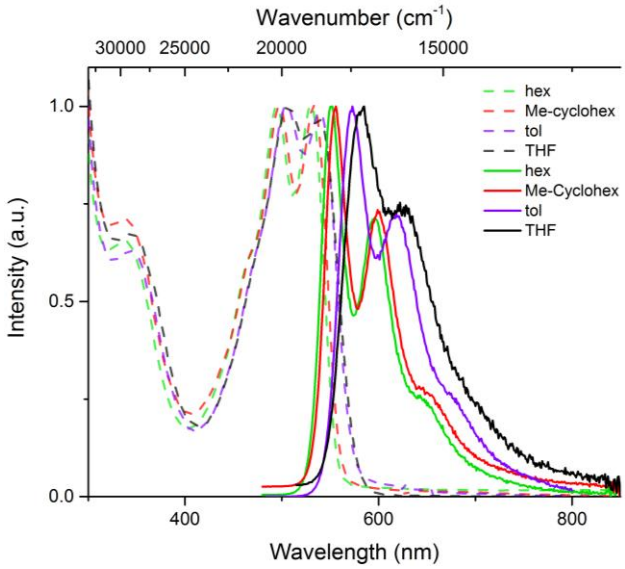


**Figure 88** Absorption (dashed) and emission (solid) of rhodacyclopentadiene **23b** in hexane (orange), Me-cyclohexane (red), toluene (violet) and THF (darkblue).

Compared to compound **23a**, the different solutions show only slight colour changes when irradiated by daylight (Figure 89, left), exhibiting weak orange emission. When excited by UV-light (Figure 89, right), the emission in methylcyclohexane and hexane appears to be light yellow, changing to a light orange in toluene and ending up in a darker orange in THF.


**Figure 89** Solvatochromic properties of rhodacyclopentadiene **23b** under daylight (left) and UV-light (right) in methylcyclohexane hexane, toluene and THF.

The comparison of the emission properties of compounds **23a** and **25a** with those of compound **23b** confirms that the unusual solvatochromism shown for the former two is an exception.

*Optical properties of compounds **24a** and **24b***

Dibenzorhodacyclopentadienes **24a** and **b** show intense absorption with maxima $\lambda_{max}$ ranging from 370-379 nm and extinction coefficients $\varepsilon$ of 19000 and 23000 $Lmol^{-1}cm^{-1}$, respectively (Table 18). Compound **24a** (R = $NO_2$), shows a bathochromic shift in comparison to compound **24b** (R = $CO_2Me$). The difference in the vibrational bands indicates a change in the vibronic coupling depending on the substituent at the phenyl ring. The same can be observed for the vibrational bands of the emission spectra.

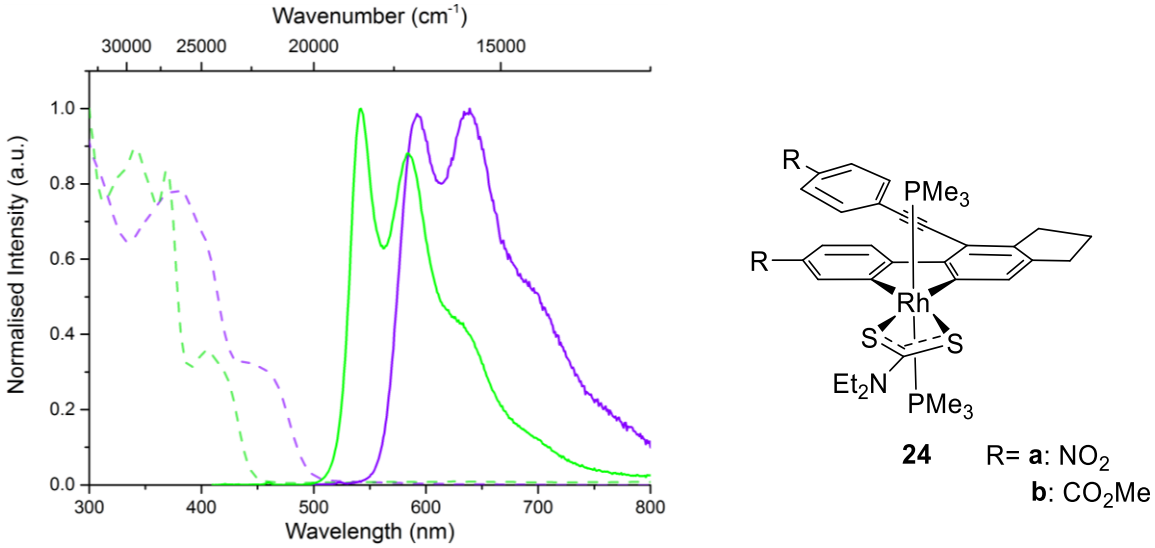


**Figure 90** Absorption and emission spectra of rhodacyclopentadienes **24a** (pink) and **b** (orange) in toluene at RT.

The emission occurs in the visible region with maxima $\lambda_{max}$ ranging from 541-592 nm and large Stokes shifts of 8500-9500 $cm^{-1}$ indicating phosphorescence (Table 18, also see Chap. 3.1.3). The quantum yields are moderate with values of 14 and 23% from long lived excited triplet states with phosphorescence lifetimes of 94 (**24a**) and 185 $\mu$s (**24b**) (Table 18).

**Table 18** Emission and absorption properties, quantum yields and lifetimes of compounds **24a** and **b**.

| | $\lambda_{max}$ (abs) [nm] | $\varepsilon$ [$mol^{-1}$ $cm^{-1}$ $dm^3$] | $\lambda_{max}$ (em) [nm] | Stokes shift [$cm^{-1}$] | $\phi_{PL}$ | $\tau_f$ [$\mu$s] |
|---|---|---|---|---|---|---|
| **24a** | 379 | 19 000 | 592 | 9500 | 0.23 | 94 |
| **24b** | 370 | 23 000 | 541 | 8500 | 0.14 | 185 |

Marder *et al.* found that the unusual emission behaviour of the rhodacyclopentadienes in comparison to the expected behaviour shown by their isomeric dibenzorhodacyclopentadienes is the energetic position of their frontier orbitals (also see Chap. 2.1.3).

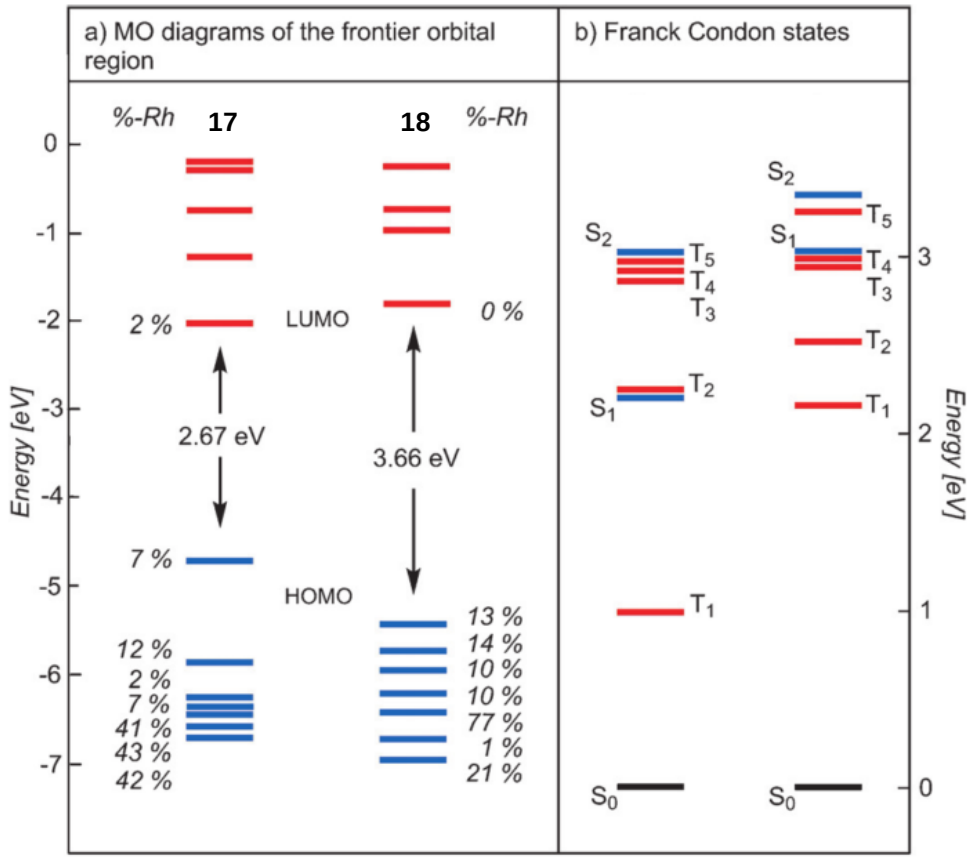


**Figure 91** a) MO diagrams of the frontier orbital region of **17** and **18**. b) Calculated vertical excitations of **17** and **18** (blue: singlet states, red: triplet states).[121]

This is pictured in the MO diagrams and the Franck Condon states of the isomeric rhodacyclopentadiene **17** and dibenzorhodacyclopentadiene **18**, both bearing acac as a bidentate ligand (Figure 91).[121]

Obviously, the rhodium only plays a minor role in the excitation process, as the ligand based HOMO and LUMO and the metal-centred orbitals are well separated from each other (~1 eV). In consequence, the conjugated organic ligand $\pi$-system dominates the excited state emissive behaviour.[72] Low-energy MLCT transitions, which could support the SOC (Spin orbit coupling), are non-existent, leading to a low triplet state density around the $S_1$-state, compared to dibenzorhodacyclopentadiene **18** (Figure 91).

*Optical properties of dimers **26** and trimers **27***

Dimers **26** show intense absorption in the UV/visible region with maxima $\lambda_{max}$ ranging from 297-332 nm and large extinction coefficients $\varepsilon$ of 55000-95000 $Lmol^{-1}cm^{-1}$ (Figure 92, Table 19). The absorption maximum of dimer **26d** appears to be slightly bathochromically shifted with respect to the other dimers. The vibrational bands of the different substituted dimers differ strongly from each other, indicating significant changes in the vibronic coupling, depending on the different substituents at the *para* position of the phenyl rings. Emission occurs in the visible region with maxima $\lambda_{max}$ ranging from 377-438 nm. The Stokes shifts are small, being 2900-5300 $cm^{-1}$, indicating fluorescence, typical of organic emitting compounds (Table 19).[175] The emission spectra of dimers **26** show, in contrast to the absorption spectra, a bathochromic shift of the dimers substituted with electron-withdrawing and -donating groups, compound **26d** showing the strongest bathochromic shift.

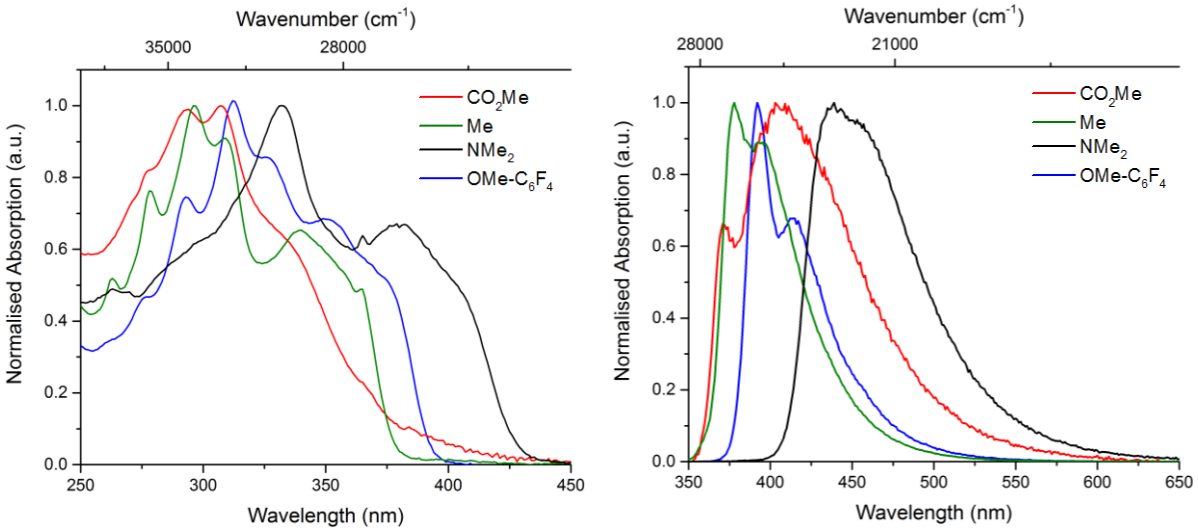


**Figure 92** Absorption (left) and emission spectra (right) of dimers **26b**, **c**, **d** and **f'** in DCM at RT.

The vibrational bands show significant differences between all four compounds. An overview of the absorption and emission properties of compounds **26** is shown in Table 19.

**Table 19** Absorption, emission, extinction coefficients, Stokes shift, quantum yield, lifetimes and radiative and non-radiative rate of compounds **26b**, **c**, **d** and **f'** and **27b**, **c** and **f'**.

| | R / Ar | $\phi_f$ | $\tau_f$ [ns] | $\tau_0$ [ns] | $k_r$ [$10^8$ $s^{-1}$] | $k_{nr}$ [$10^8$ $s^{-1}$] | $\lambda_{max}$ (abs) [nm] | ε [$mol^{-1}$ $cm^{-1}$ $dm^3$] | $\lambda_{max}$ (em) [nm] | Stokes shift [$cm^{-1}$] |
|---|---|---|---|---|---|---|---|---|---|---|
| **26b** | $CO_2Me$ | 0.78 | 0.83 | 1.06 | 9.43 | 2.66 | 307 | 77 000 | 406 | 5300 |
| **26c** | Me | 0.66 | 2.36 | 3.57 | 2.80 | 1.44 | 297 | 74 000 | 377 | 2900 |
| **26d** | $NMe_2$ | 0.27 | 1.22 | 4.52 | 2.21 | 5.98 | 332 | 95 000 | 438 | 3400 |
| **26f'** | $C_6F_4$-4-OMe | 0.09 | 1.61 | 17.89 | 0.56 | 5.66 | 311 | 55 000 | 391 | 2900 |
| **27b** | $CO_2Me$ | 0.72 | 1.57 | 2.18 | 4.59 | 1.79 | 325 | 131 000 | 392 | 1100 |
| **27c** | Me | 0.24 | 2.60 | 10.83 | 0.92 | 2.91 | 310 | 115 000 | 378 | 1900 |
| **27f'** | $C_6F_4$-4-OMe | 0.12 | 1.60 | 13.33 | 0.75 | 5.50 | 305 | 84 000 | 400 | 2500 |

Trimers **27** show intense absorption in the UV/visible region with maxima $\lambda_{max}$ ranging from 305-325 nm and large extinction coefficients $\varepsilon$ of 84000-131000 $Lmol^{-1}cm^{-1}$ (Table 19). Depending on the substituent in *para* position of the phenyl ring a small bathochromic shift appears with respect to trimer **27c** (R = Me). Compound **27b**, (R = $CO_2Me$), shows the strongest bathochromic shift, whereas the absorption of compound **27f'** (Ar = $C_6F_4$-4-OMe), is mainly overlapped with that of trimer **27c**. In contrast to the dimeric species, the vibrational bands of the absorption show only slight differences (Figure 93). Trimers **27** emit in the visible region with maxima $\lambda_{max}$ ranging from 378-400 nm and small Stokes shifts of 1100-2500 $cm^{-1}$. As found for the dimers **26**, the vibrational bands of the emission spectra differ significantly, indicating differences in the vibronic couplings, caused by the different substituents at the phenyl rings.

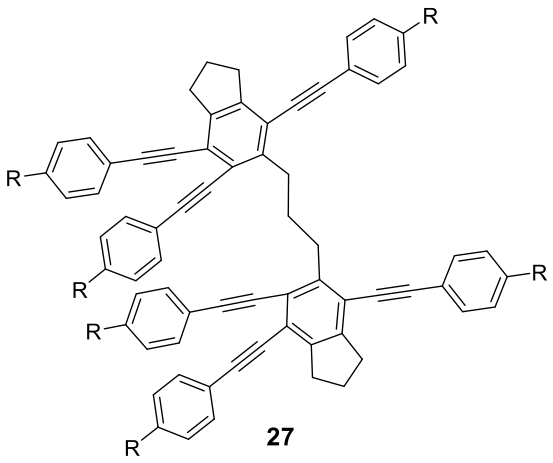


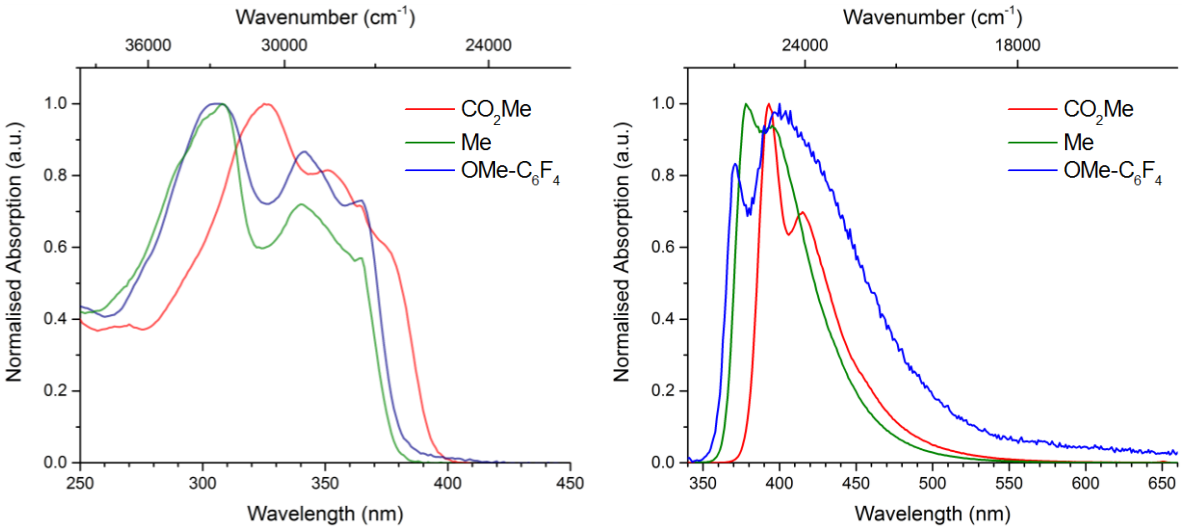


**Figure 93** Absorption (left) and emission spectra (right) of Trimers **27b**, **27c** and **27f'** in DCM at RT.

The fluorescence quantum yields of both, dimers **26** ($\phi_f$ = 9-78%) and trimers **27** ($\phi_f$ = 12-72%), are moderate to excellent, compounds **26** and **27b** (R = $CO_2Me$) showing the strongest fluorescence, whereas compounds **26** and **27f'** clearly exhibit the weakest emission (Table 19). The lifetimes are in the typical scope of fluorescent emitters, giving values of 0.83-2.36 ns for dimers **26** and 1.57-1.60 ns for trimers **27**. The shortest lifetimes are obtained for compounds **26** and **27b**, whereas compounds **26** and **27c** (R = Me) exhibit the longest lifetimes, being about as twice as long. The radiative and non-radiative rate constants lie in the same order of magnitude, the individual rates being consistent with the fluorescence quantum yield.

## 4. Summary

Based on former works of Marder *et al.* the present work aimed the synthesis and characterisation of new luminescent rhodacyclopentadienes using the complexes [Rh($\kappa^2$-*S*,*S*`-$S_2CNEt_2$)($PMe_3$)$_2$] **13** and [Rh($\kappa^2$-*S*,*S*`-$S_2CNEt_2$)($PPh_3$)$_2$] **22**, both bearing the bidentate ligand dithiocarbamate, which is a good $\pi$- and $\sigma$-donor.

The first part discusses the synthesis of the organic starting materials, namely the 1,3-butadiynes **4b-h** and the 1,3,9,11-undecatetraynes **5a-f'** and **5h**. The second part contains the synthesis and characterisation of the metal-containing starting materials [Rh($\kappa^2$-*S*,*S*`-$S_2CNEt_2$)($PMe_3$)$_2$] **13** and [Rh($\kappa^2$-*S*,*S*`-$S_2CNEt_2$)($PPh_3$)$_2$] **22**. Their reactivity towards the butadiynes **4b-d** and **g** and the undecatetraynes **5a-f'** is clarified and the resulting rhodacyclopentadienes **23a-f'** and **25a-c**, **e** and **f'**, dibenzorhodacyclopentadienes **24a-c**, organic dimers **26b-c** and **f',** trimers **27b**, **c** and **f'** as well as the *trans* $\pi$-complexes **28c** and **g** are characterised and discussed. In addition, test reactions concerning the exchange of the phosphine and bidentate ligands are discussed. The third part of the present thesis includes the characterisation and discussion of the photophysical properties of the obtained organometallic and organic products.

## Chapter One

A series of 1,3-butadiynes and 1,3,9,11-undecatetraynes was synthesised (compounds **4b-h** and **5a-f** and **5h**). In the first step, the TMS-protected benzyl alkynes (**2a-h**) were synthesised *via* Sonogashira cross-coupling reactions. This was followed by deprotection under basic conditions to obtain the terminal ethynylarenes (**3a-h**). All substances obtained were characterised *via* $^1$H, $^{13}$C and $^{19}$F NMR spectroscopy as well as GCMS and mass spectrometry. Literature known compounds were only characterised *via* $^1$H NMR spectroscopy and GCMS.

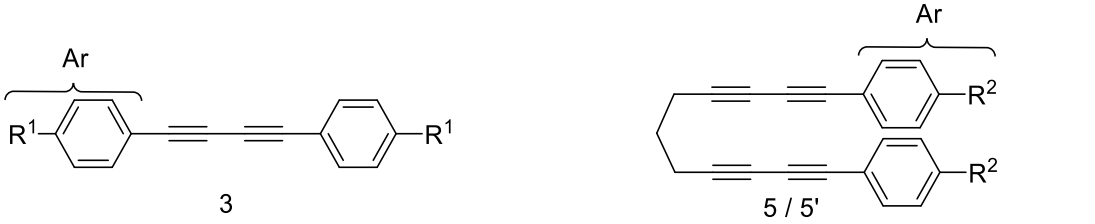


$R^1$ = $NO_2$ (**a**), $CO_2Me$ (**b**), Me (**c**), $NMe_2$ (**d**), SMe (**e**), $CF_3$ (**h**)
Ar = $C_6F_5$ (**f**), naphthyl (**g**)

$R^2$ = $NO_2$ (**a**), $CO_2Me$ (**b**), Me (**c**), $NMe_2$ (**d**), SMe (**e**), $CF_3$ (**h**)
Ar = $C_6F_4$-OMe (**f'**)

**Figure 94** Overview of the synthesised butadiynes **4b-h** and undecatetraynes **5a-f** and **5h**.

The synthesis of compounds **2f**, **3f** and **3f'** was challenging as they have a perfluorinated phenyl ring, which is likely to undergo hydro-dehalogenation in combination with Pd-catalysts. Furthermore, the amount of TMSA in the Sonogashira cross-coupling reaction had to be increased, which caused the appearance of more homocoupled TMSA in the product and made the work-up more extensive, as it had to be distilled and then separated from the homocoupled TMSA by several precipitations.

Another challenge was the isolation of compound **2f**, as it is very volatile. Furthermore, the fluorine at the phenyl ring *para* to the alkyne can easily undergo nucleophilic substitution.

For this reason the deprotection in methanol gave compound **2f'**, which turned out to be very useful during the synthesis of the perfluorinated undecatetrayne **5f'**.

In contrast to the 1,3-butadiynes, which were synthesised using the Glaser-type homocouplings, the undecatetraynes were synthesised following the procedure of Cadiot and Chodkiewicz. As the synthesis of compound **5f** was unsuccessful, due to a possible side reaction at the *para*-position of the phenyl ring with the trimethylamine used as base, the alternative product **5f'** was synthesised, bearing a methoxy group in the *para* position.

## Chapter Two

In the second part of this thesis, a variety of luminescent organometallic and organic complexes was synthesised. Therefore, the two starting complexes [Rh($\kappa^2$-*S*,*S*`-$S_2CNEt_2$)($PMe_3$)$_2$] **13** and [Rh($\kappa^2$-*S*,*S*`-$S_2CNEt_2$)($PPh_3$)$_2$] **22** were synthesised and characterised. Their structures were confirmed by X-ray diffraction (Figure 95).

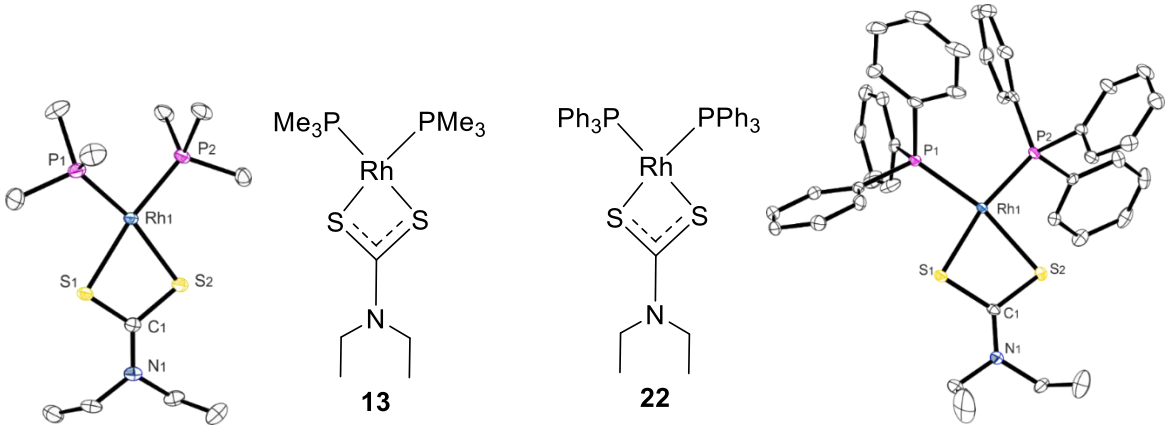


**Figure 95** Chemical and molecular structure of [Rh($\kappa^2$-*S*,*S*`-$S_2CNEt_2$)($PMe_3$)$_2$] **13** and [Rh($\kappa^2$-*S*,*S*`-$S_2CNEt_2$)($PPh_3$)$_2$] **22**.

*Reactions of [Rh($\kappa^2$-S,S`-$S_2CNEt_2$)($PMe_3$)$_2$] **13** with undecatetraynes **5***

The reaction of [Rh($\kappa^2$-*S,S`*-$S_2CNEt_2$)($PMe_3$)$_2$] **13** with a series of undecatetraynes **5** at ambient temperature yields the rhodacyclopentadienes **23** with high conversion, *via* a [2+2+M] cycloaddition reaction. Depending on the substituent at the phenyl ring of the undecatetraynes **5**, the reaction takes at least one to several weeks, whereas the reactions with donor substituted undecatetraynes **5** (R = $NMe_2$, SMe) are even slower. To speed up the reactions they were carried out in a microwave reactor at 80 °C, lowering the reaction time significantly. Full conversion of the starting materials was obtained after ca. 24 hours.

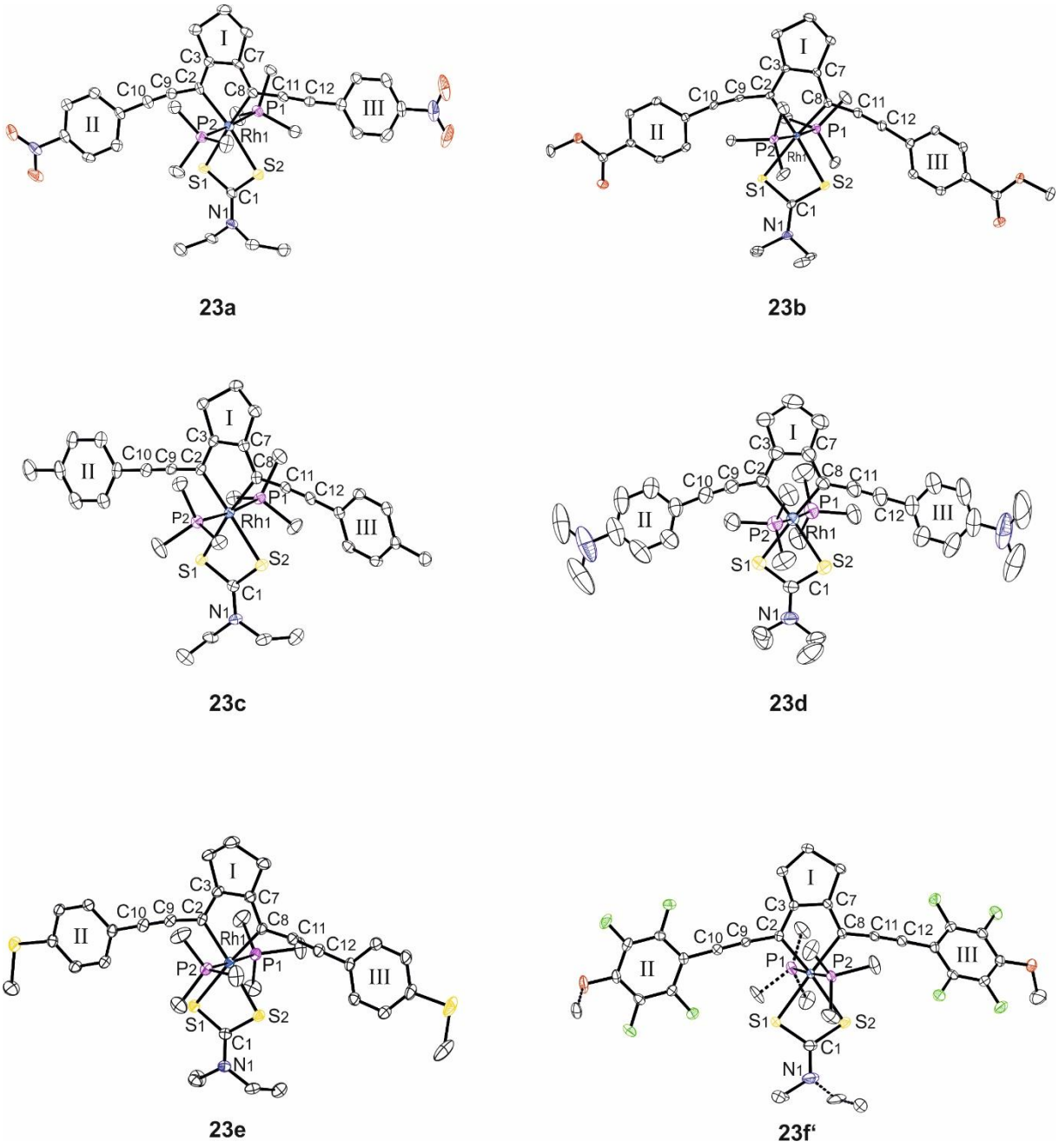


**Figure 96** Molecular structures of rhodacyclopentadienes **23a-f’**.

Rhodacyclopentadienes **23a-f'** were isolated successfully and characterised by X-ray diffraction (Figure 96). It has to be noted, that compound **23f'** was only synthesised with 100% conversion at elevated temperatures.

The system changed its reaction behaviour significantly when heated. According to what was found during investigations of the reactions of [Rh($\kappa^2$-*O,O`*-acac)($PMe_3$)$_2$] **16** with a variety of undecatetraynes **5**, a mixture of the rhodacyclopentadienes **23** and their isomeric dibenzorhodacyclopentadienes **24** was now formed. In contrast to the dibenzorhodacyclopentadienes discussed in this work, the corresponding dibenzorhodacyclopentadienes bearing acac as bidentate ligand are formed in preference to the "normal" rhodacyclopentadienes at ambient temperature

The ratio of the formation of the two isomers depends on the substituent in *para*-position. Electron-withdrawing substituents (e.g. R = $CO_2Me$) at the undecatetrayne **5** enhance the formation of the dibenzorhodacyclopentadiene, whereas electron-donating substituents (R = $NMe_2$, SMe) lead to significantly less formation of this isomer, causing the isolation of the dibenzorhodacyclopentadiene to be quite challenging. The dibenzorhodacyclopentadienes **24a**, **b** and **c** were isolated successfully and compounds **24a** and **b** were characterised *via* X-ray diffraction.

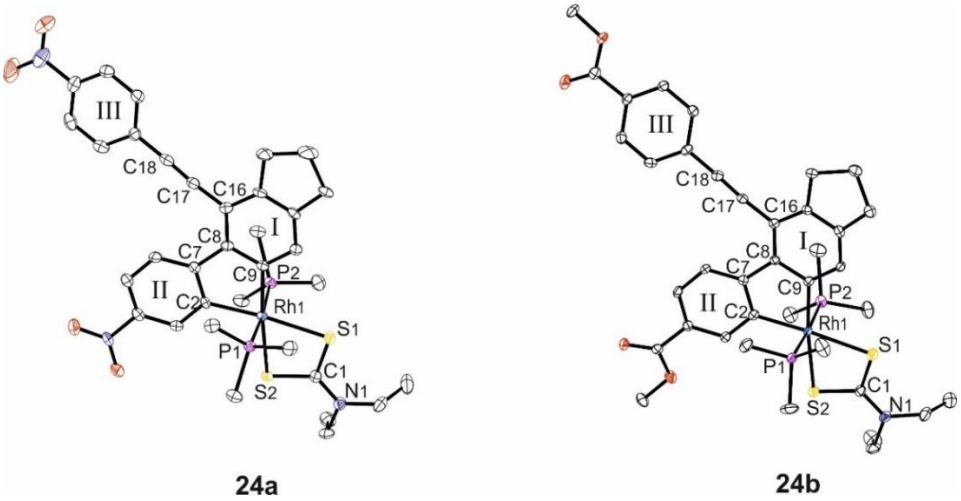


**Figure 97** Molecular structures of dibenzorhodacyclopentadienes **24a** and **b**.

The dibenzorhodacyclopentadienes **24** appear to be formed *via* a [4+2] cycloaddition reaction followed by a CH-activation and a *ß*-H shift. To prove this, test reactions with undecatetrayne **5f'** were carried out at ambient and elevated temperatures. Using the tetra fluorinated undecatetrayne **5f'** (Ar = $C_6F_4$-OMe) suppresses the formation of the

dibenzorhodacyclopentadiene, as a CH-activation is no more possible. At ambient temperature, no dibenzorhodacyclopentadiene was formed, but the rhodacyclopentadiene **23f'**, accompanied by another product, which turned out to be the bimetallic Rh-complex **24f'-bi** (Figure 98). It was successfully isolated and characterised *via* X-ray diffraction.

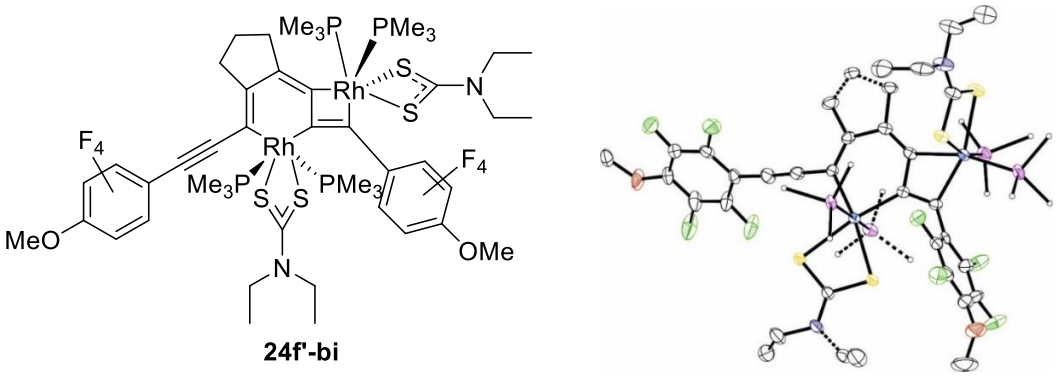


**Figure 98** Chemical and molecular structure of the bimetallic complex **24f'-bi**.

Heating the reaction did not lead to the formation of the dibenzorhodacyclopentadiene **24f'**. Instead, rhodacyclopentadiene **23f'** was formed exclusively.

*Reactions of [Rh($\kappa^2$-S,S`-$S_2CNEt_2$)($PPh_3$)$_2$] **22** with undecatetraynes **5***

The reaction behaviour changes completely if the reactions are carried out using [Rh($\kappa^2$-S,S`-$S_2CNEt_2$)($PPh_3$)$_2$] **22** and the undecatetraynes **5**. The expected rhodacyclopentadienes **25** are still formed. However, the reaction does not stop at this step, but catalysis takes place, forming a mixture of the highly luminescent dimers **26** and trimers **27** (Figure 99).

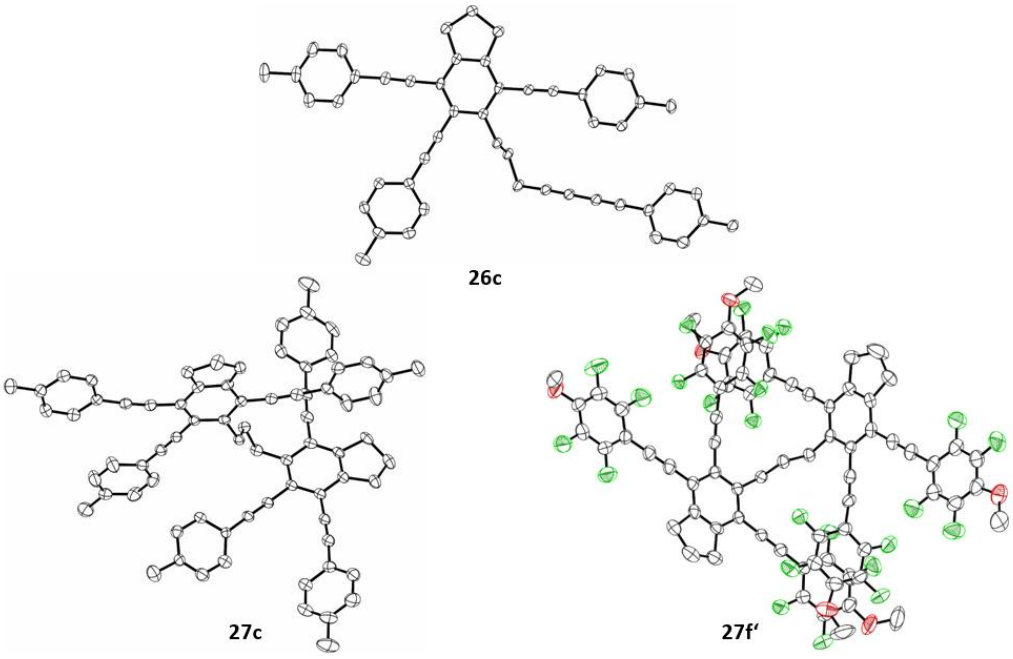


**Figure 99** Molecular structures of dimer **26c** and trimers **27c** and **f'**.

Dimers **26b-d** and **f'** as well as trimers **27b**, **c** and **f'** were successfully isolated and characterised and the structures of compounds **26c**, **27c** and **f'** were confirmed by X-ray diffraction.

The ratio of dimer to trimer within the reaction mixture depends on the ratio between [Rh($\kappa^2$-*S,S*`-$S_2CNEt_2$)($PPh_3$)$_2$] **22** and the undecatetrayne **5**. Thus, a 100:1 ratio (**5** to **22**) enhances the formation of the dimer **26**, whereas a 10:1 ratio (**5** to **22**), in comparison, gives more of the trimer **27**. The ratio of the formation of the two benzene derivatives **26** and **27** also depends on the substituents at *para* positions of the phenyl rings of the undecatetraynes **5**. Employing undecatetrayne **5b** (R = $CO_2Me$), it is possible to push the system to synthesise more of the trimeric species, using a 10:1 ratio of tetrayne **5** to catalyst **22**, whereas a 100:1 ratio forms nearly exclusively the dimer. With use of undecatetrayne **5c** (R = Me), which is rather neutral, the effect of the different ratios is rather small. The system can only be pushed slightly into the direction of the trimeric species with a 10:1 ratio, and forms mainly the dimeric species when used in a 100:1 ratio. A 10:1 ratio reaction employing undecatetrayne **5d** makes no difference to a 100:1 ratio reaction. In both cases a ca. 1:0.2 mixture of the dimer and trimer is formed, whereas it was only possible to isolate the dimer. Using the tetra-fluorinated undecatetrayne **5f'** (Ar = $C_6F_4$-OMe) in a 10:1 ratio reaction even pushes the systems to form nearly 100 % of the trimer and, using a 100:1 ratio yields a ca. 1:1 mixture of the dimer and the trimer (Table 20).

**Table 20** Ratio control of formation of dimers **26** (A) and trimers **27** (B), with different substrate ratios.

| Tetrayne | Ratio 5:22 | A:B |
|---|---|---|
| **5b** | 10:1 | 1:3 |
| | 100:1 | 1:0.05 |
| **5c** | 10:1 | 1:0.5 |
| | 100:1 | 1:0.1 |
| **5d** | 10:1 | 1:0.2 |
| | 100:1 | 1:0.2 |
| **5f'** | 10:1 | 0.05:1 |
| | 100:1 | 1:0.8 |

Additionally, it was possible to stop the reaction at the intermediate step and isolate the rhodacyclopentadienes **25a**, **b**, **e** and **f'** (Figure 100). Compound **25c** was also isolated, but it was not obtained in analytically pure form.

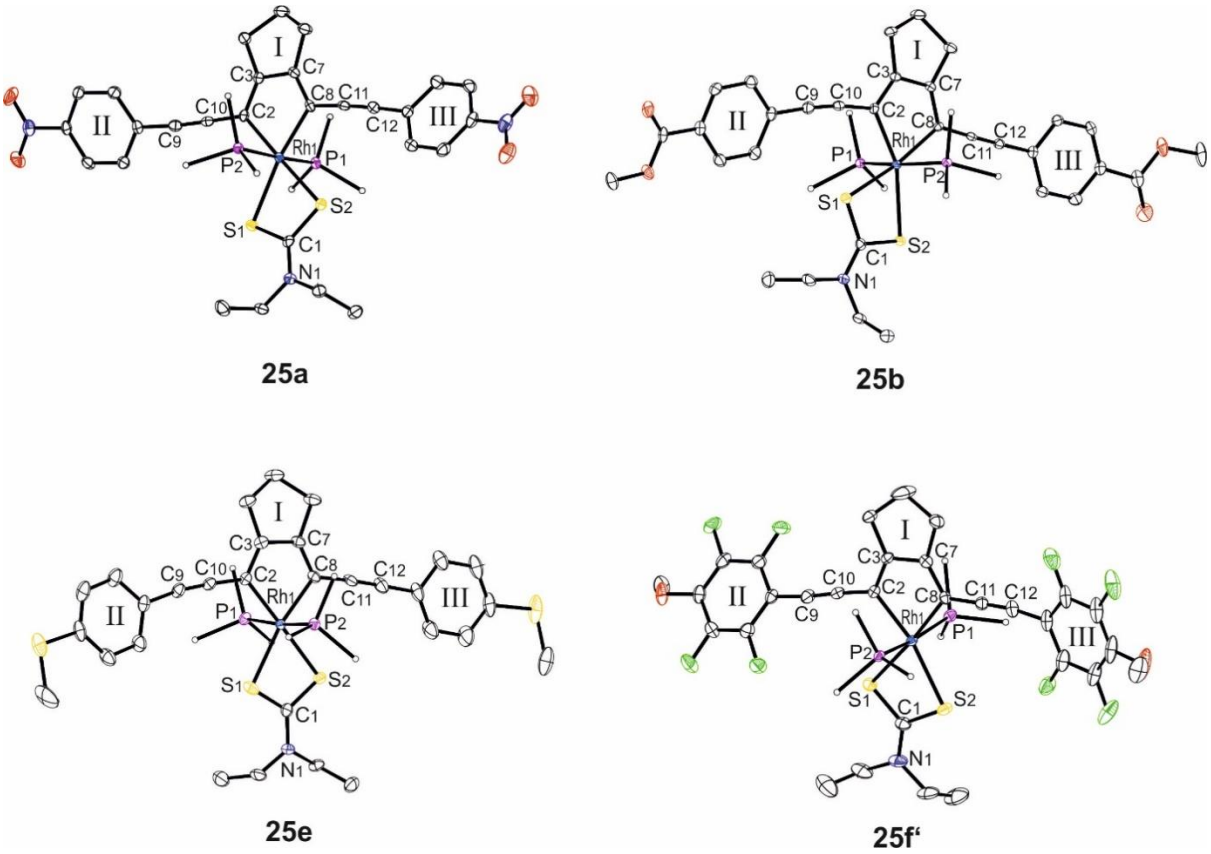


**Figure 100** Molecular structures of rhodacyclopentadienes **25a, b, e** and **f'**.

*Ligand exchange reactions*

Three different ligand exchange reactions were carried out, two of which served as alternative routes to obtain the rhodacyclopentadienes **23** and the dibenzorhodacyclopentadienes **24** independently from each other, preventing the time-consuming separation of the isomers.

Therefore, the first attempt was a test reaction, starting from rhodacyclopentadiene **25b** (R = $CO_2Me$), bearing triphenylphosphine as ligand. With an excess of trimethylphosphine it was possible to exchange one of the phosphine ligands at ambient temperature, whereas by heating the reaction mixture the second phosphine ligand was also exchanged to reach full conversion to the desired rhodacyclopentadiene **23b** (Scheme 62).

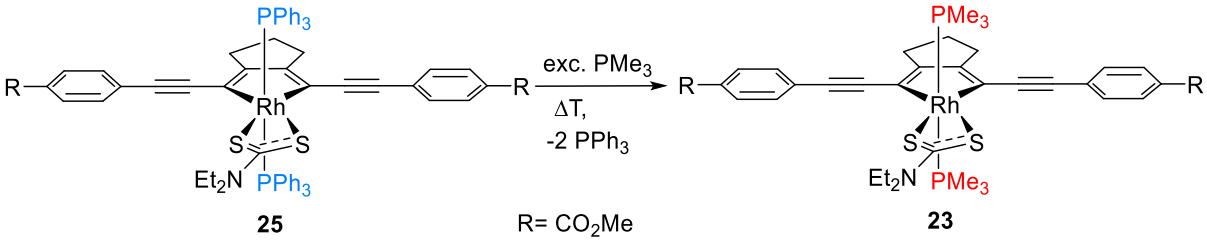


**Scheme 62** Phosphine exchange reaction to obtain rhodacyclopentadiene **23b**.

In a second reaction, it was attempted to determine whether the dibenzorhodacyclopentadiene **24e**, which is only formed to a very small amount during the usual reaction using the Rh-complex **13** with undecatetrayne **5e**, could be obtained, starting from compound **24e-acac** *via* exchange of the bidentate ligand acac by dithiocarbamate. Therefore, **24e-acac** was treated with a threefold excess of sodium dithiocarbamate and heated to 80 °C. Compared to the phosphine exchange, which had reached total conversion within a few days, this exchange reaction took 10 weeks to reach 98% conversion.

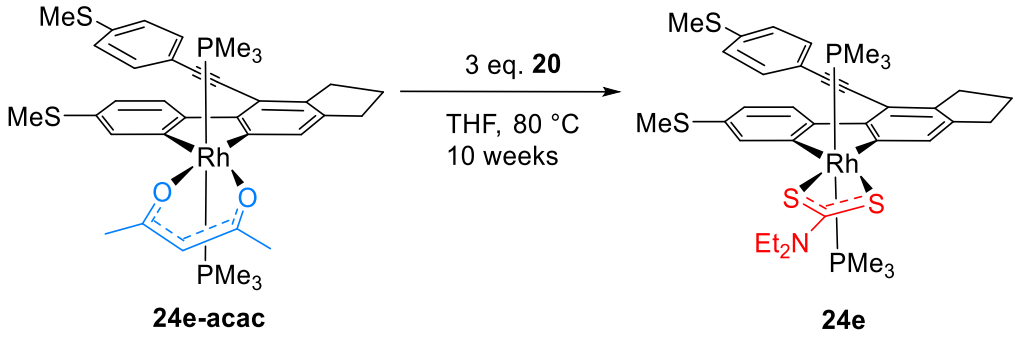


**Scheme 63** Ligand exchange from acac to dithiocarbamate to obtain compound **24e**.

The third exchange reaction was an attempt to obtain a rhodacyclopentadiene bearing two NHC ligands, instead of two triphenylphosphines. The reaction was carried out using an excess of $^{n}Pr$-NHC, which yielded the rhodacyclopentadiene **25b-NHC**, having only one phosphine ligand exchanged, even at elevated temperatures.

The structural motif was confirmed by X-ray diffraction, showing, a *cis* disposition of the NHC ligand to the phosphine ligand (Figure 101).

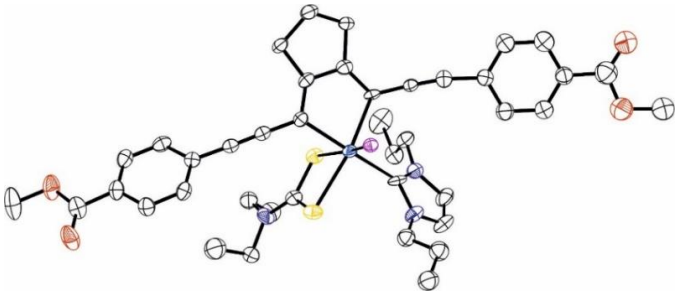

**Figure 101** Molecular structure of compound **25-NHC** to confirm the connectivity of the molecule. ($R_{int}$ = 9.81, due to strong solvent molecule disorder). Hydrogen atoms, solvent molecules and the phenyl groups of $PPh_3$ are omitted for clarity.

*Reactions of [Rh($\kappa^2$-S,S`-$S_2CNEt_2$)($PMe_3$)$_2$] **13** with butadiynes*

During the reaction of [Rh($\kappa^2$-S,S`-$S_2CNEt_2$)($PMe_3$)$_2$] **13** with the butadiynes **4** under ambient or elevated temperature no rhodacyclopentadienes were formed, but the reaction stopped at the step of the *trans* $\pi$-complexes **28**, having only one butadiyne coordinated to the Rh-centre. They have been carried out in a 1:1 as well as a 1:2 ratio (**13** to **4**), which made no difference with respect to the formation of the product. A 1:1 ratio always showed ca. 50 % of unreacted butadiyne **4**, whereas a 1:2 ratio always showed ca. 50 % of the [Rh($\kappa^2$-S,S`-$S_2CNEt_2$)($PMe_3$)$_2$] **13** to be left over. This led to the supposition that the reaction mixture reaches equilibrium, which needs at least a twofold excess of the butadiyne to drive to complete product formation. It was not possible to isolate compounds **28** analytically pure, but the formation of the *trans* $\pi$-complexes **28c** and **g** was confirmed by X-ray diffraction (Figure 102).

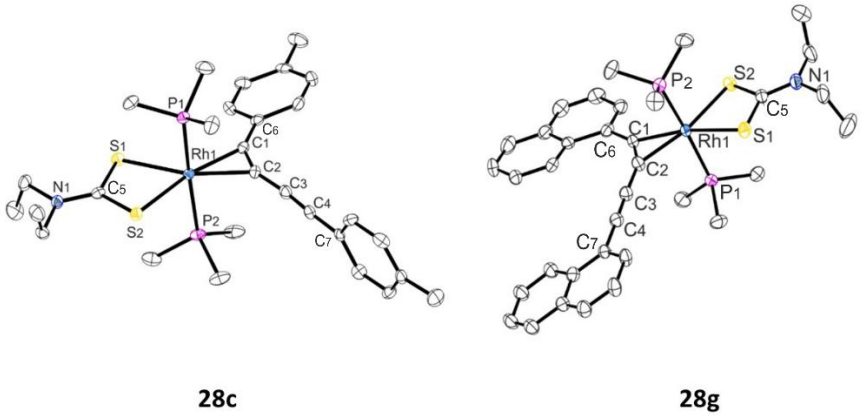


**28c** **28g**

**Figure 102** Molecular structures of *trans* $\pi$-complexes **28c** and **g**.

These results support earlier findings of Marder *et al.* on the reactivity between [Rh($\kappa^2$-O,O`-acac)($PMe_3$)$_2$] **16** and butadiynes **4**, yielding the [3+2] addition product **19** (Scheme 64). It was supposed that during this reaction the analogous *trans* $\pi$-complex is formed, bearing acac as the bidentate ligand.

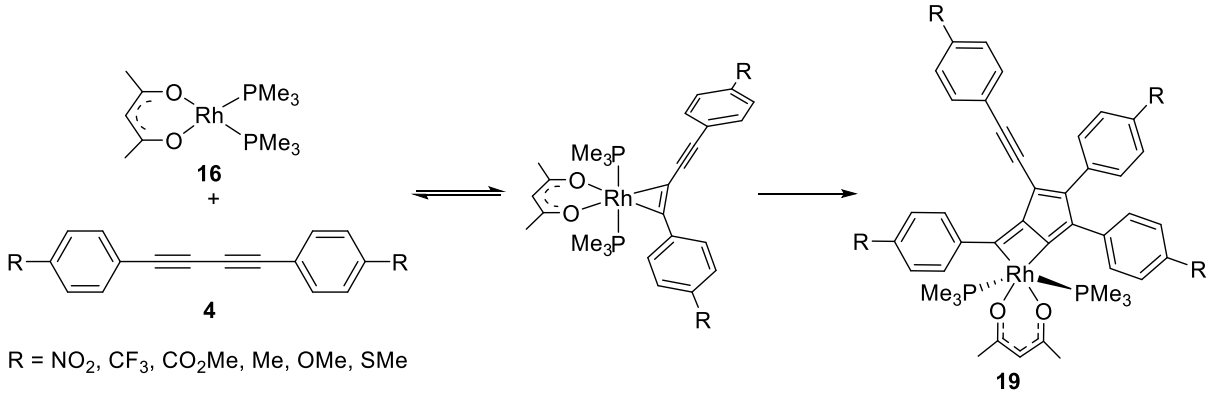


**Scheme 64** Reaction to yield the [3+2] cycloaddition product 19 *via* a *trans* $\pi$-complex intermediate.

Using butadiyne **4b** (R = $CO_2Me$), additionally showed the system with [Rh($\kappa^2$-*S*,*S*`-$S_2CNEt_2$)($PMe_3$)$_2$] **13** to have tendencies to bind a second ligand molecule. However, pushing the reaction to form significant amounts of a species having two ligand molecules bound required very harsh conditions. The reaction took place in the microwave reactor at 80 °C for 75 h, yielding one main product, which may be the [3+2] cycloaddition product **[3+2]-dithio** or an unsymmetric rhodacyclopentadiene **US-dithio** (Figure 103).

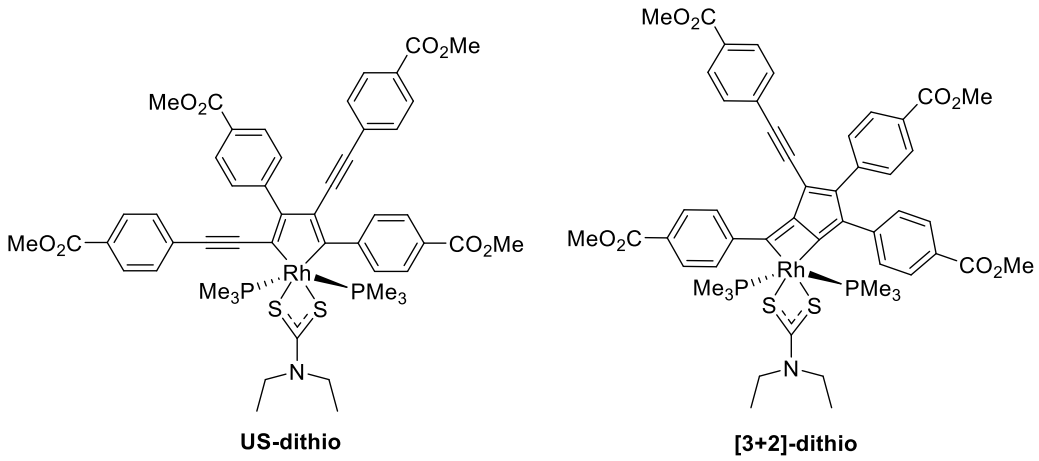


**Figure 103** Possible chemical structures of the unsymmetric Rh-complexes formed from reaction of [Rh($\kappa^2$-*S*,*S*`-$S_2CNEt_2$)($PMe_3$)$_2$] **13** with butadiyne **4b** under microwave radiation.

Characterisation *via* X-ray diffraction of a single crystal, would clarify which product is formed during the reaction of [Rh($\kappa^2$-*S*,*S*`-$S_2CNEt_2$)($PMe_3$)$_2$] **13** and butadiyne **4b** in the microwave. Nevertheless, the formation of **[3+2]-dithio** is likely, as earlier investigations already showed an analogous behaviour to the reactivity of the corresponding Rh-complex **16** bearing acac as the bidentate ligand.

## Chapter Three

*Optical properties of rhodacyclopentadienes **23** and **25***

Rhodacyclopentadienes **23a-f'** absorb in the visible region with $\lambda_{max}$ ranging from 478-594 nm, and large extinction coefficients $\varepsilon$ of 14000-33000 $Lmol^{-1}$. Their emission appears in the visible region with $\lambda_{max}$ ranging from 512-671 nm, showing unusual fluorescence, indicated by the large overlap of the absorption and emission bands and the very short lifetimes, the longest being 1.41 ns. Compounds **23a-f'** have small Stokes shifts with values of 660-1200 $cm^{-1}$. The strongest fluorescence was exhibited by compound **23b**, with a quantum yield of 48% and a typical lifetime $\tau_f$ of 1.4 ns. [71,72,121] With quantum yields of 11 and 28% compounds **23e** and **f'** show moderate fluorescence, that of compounds **23a**, **c** and **d** being weak with only 1-7% quantum yield. The corresponding fluorescence lifetimes of compounds **23c** and **d** are extremely short and therefore were not detectable. Their natural lifetimes $\tau_0$ were obtained from the inverse value of the radiative rate constant $k_r$, using the Strickler-Berg equation.[172]

The absorption spectra of the corresponding compounds **25a**, **b**, **e** and **f**, bearing triphenylphosphine instead of trimethylphosphine ligands, show maxima $\lambda_{max}$ ranging from 495-619 nm with large extinction coefficients $\varepsilon$ of 23000-31000 $Lmol^{-1}$. The absorption maxima are bathochromically shifted of about 20 nm with respect to those of compounds **23**, indicating that the exchange of the phosphine ligand causes a decrease of the energy of the excited states in the rhodacyclopentadienes **25**. They emit in the visible region with maxima $\lambda_{max}$ ranging from 508-686 nm, showing the same trend in the bathochromic shift as in the absorption. The Stokes shifts of 760-1600 $cm^{-1}$ correspond to those of rhodacyclopentadienes **23**. They are very weak emitters ($\phi_f$ = 0.1-4%), rhodacyclopentadiene **25e** not showing any detectable fluorescence at all. In general, the low quantum yields of rhodacyclopentadienes **23a**, **c-f'** and **25** indicated that strong competing processes take place during the relaxation of the excited state, not only being non-radiative decay but also inter system crossing (ISC) to the excited triplet states. The ISC rate of the rhodacyclopentadienes is supposed to be on the same order of magnitude ($10^8$ $s^{-1}$) as radiative relaxation from the $S_1$ state.[71,72]

To prove if ISC occurs in the system after excitation, it was checked if singlet oxygen ($^1O_2$) is generated, when measurements are carried out in an $O_2$-saturated medium. For model compounds **23b** and **25b** $^1O_2$ quantum yields $\Phi_\Delta$ of 27 (**23b**) and 37% (**25b**) were obtained.

Earlier results of the group, showed the quantum yields of **14j** and the singlet oxygen to give an overall quantum yield of 100% ($\Phi_f + \Phi_\Delta \approx 1$; vide supra), meaning that the only relaxation path ways of the singlet excited state are fluorescence and ISC.[71] In contrast,

rhodacyclopentadienes **23** and **25** experience an additional relaxation pathway (vibration, rotation), causing the small quantum yields of the compounds, being more significant for rhodacyclopentadienes **25**.

To further investigate the ISC process, low temperature lifetime measurements were carried out, using rhodacyclopentadienes **23b 25b** (R = $CO_2Me$) as model compounds. The fluorescence lifetimes of compound **23b** were recorded from 175 to 295 K in 10 K steps. A plateau at ca. 2.1 ns appeared from 175 to 225 K, which was referred to as non-thermal activated ISC. Compound **25b**, measured in Me-THF, showed a plateau appearing from 77 to 97 K. The lifetime of 2.49 ns at this state was only slightly shorter than the calculated natural lifetime $\tau_0$, indicating a thermal activated ISC. The exchange of the phosphine ligands at the Rh-centre seems change the character of the non-radiative decay, leading to a significant increase of the activation energy of the ISC.

*Solvatochromic effects of rhodacyclopentadienes **23a** and **25a***

A large solvatochromic effect was observed for rhodacyclopentadienes **23a** and **25a** (R = $NO_2$). Absorption and emission spectra were recorded in hexane, Me-cyclohexane, toluene and THF. The emission data from hexane to THF showed a bathochromic shift of ca.100 nm and an increase in the Stokes shift of 2290-3100 $cm^{-1}$, indicating charge-transfer character in the emissive excited state. This was accompanied by a significant decrease of the quantum yields of compound **23a**, that in hexane and Me-cyclohexane being ca. 20% and 7% in toluene. In THF no data for the quantum yield was obtained. For compound **25a** no trend was observed, the quantum yields being 3-4 %, except for THF, in which no data was obtained.

For comparison, the solvatochromism of compound **23b** was additionally investigated. The bathochromic shift of the emission maxima in the different solvents appeared to be significantly smaller than for compounds **23a** and **25a**, with 10-20 nm. The Stokes shifts of 719-1332 $cm^{-1}$ only showed differences of about 300 $cm^{-1}$. The quantum yields did not show a trend, corresponding to the polarity of the solvent. They gave values of ca. 35%-48%.

The comparison of the emission properties of compounds **23a** and **25a** with those of compounds **23b** clearly indicated that the unusual solvatochromism shown for former two compounds is caused by the strong electron acceptor $NO_2$.

*Optical properties of compounds **24a** and **24b***

Absorption spectra of the dibenzorhodacyclopentadienes **24a** and **b** show maxima $\lambda_{max}$ in the visible region, ranging from 370-379 nm, with large extinction coefficients $\varepsilon$ of 19000-

23000 $Lmol^{-1}$. The emission of compounds **24a** and **b** appears in the visible region with maxima $\lambda_{max}$ ranging from 541-592 nm. The corresponding Stokes shifts of 8500 and 9500 $cm^{-1}$ are large and indicate phosphorescence. The emission leads to moderate quantum yields of 14 and 23% from long lived excited triplet states giving phosphorescence lifetimes of 94 (**24a**) and 185 $\mu$s (**24b**).

*Optical properties of dimers **26** and trimers **27***

Dimers **26** show strong absorption in the UV/visible region with maxima $\lambda_{max}$ 297-332 nm, having large extinction coefficients $\varepsilon$ of 55000-95000 $Lmol^{-1}$. Emission takes place in the visible region with maxima $\lambda_{max}$ ranging from 377-438 nm, leading so small stokes shifts of 2900-5300 $cm^{-1}$, which indicates typical fluorescence for organic emitting compounds.[175] The emission spectra of dimers **26** show, a bathochromic shift of the dimers substituted with electron-withdrawing and -donating groups, compound **26d** showing the strongest bathochromic shift.

Trimers **27** show strong absorption in the visible region with maxima $\lambda_{max}$ ranging from 305-325 nm, having large extinction coefficients $\varepsilon$ of 84000-131000 $Lmol^{-1}$. Depending on the substituent in *para*-position of the phenyl ring a small bathochromic shift appeared with respect to trimer **27**, which bears a rather neutral substituent (R = Me). The emission occurs in the visible region with maxima $\lambda_{max}$ ranging from 378-400 nm with small Stokes shifts of 5300-7800 $cm^{-1}$, indicating fluorescence. The fluorescence quantum yields of both, Dimers **26** ($\phi_f$ = 9-78%) and trimers **27** ($\phi_f$ = 12-72%), are moderate to excellent. The lifetimes are in the typical scope of fluorescent emitters, giving values of 0.83-2.36 ns for dimers **26** and 1.57-1.60 ns for trimers **27**. The radiative and non-radiative rate constants are in the same order of magnitude, the individual rates being consistent with the fluorescence quantum yield.

# 5. Zusammenfassung

Ausgehend von früheren Forschungsergebnissen der Arbeitsgruppe Marder, war das Ziel der vorliegenden Arbeit die Synthese und Charakterisierung neuer lumineszierender Rhodacyclopentadiene, ausgehend von den Rh(I)-Komplexen [Rh($\kappa^2$-*S*,*S*`-$S_2CNEt_2$)($PMe_3$)$_2$] **13** und [Rh($\kappa^2$-*S*,*S*`-$S_2CNEt_2$)($PPh_3$)$_2$] **22**. Beide Komplexe tragen als Liganden, unter Anderem, ein bidentates Dithiocarbamat, das für seine gute $\pi$- und $\sigma$-Donorstärke bekannt ist. Der erste Teil der Arbeit befasst sich mit der Synthese und Charakterisierung der organischen Startmaterialen, wobei es sich um die 1,3-Butadiine **4b-h** und die 1,3,9,11-Undecatetraine **5a-f' 5h** handelt. Der zweite Teil behandelt die Synthese und Charakterisierung der Startkomplexe [Rh($\kappa^2$-*S*,*S*`-$S_2CNEt_2$)($PMe_3$)$_2$] **13** und [Rh($\kappa^2$-*S*,*S*`-$S_2CNEt_2$)($PPh_3$)$_2$] **22**. Deren Reaktivität gegenüber den Butadiinen **4b-d** und **g** sowie den Undecatetrainen **5a-f'** wurde untersucht und die aus den Reaktionen erhaltenen Rhodacyclopentadiene **23a-f'**, **25a-c**, **e** und **f'**, Dibenzorhodacyclopentadiene **24a-c**, organischen Dimere **26b**, **c** und **f'**, Trimere **27b** und **c**, sowie *trans* $\pi$-Komplexe **28c** und **g** wurden charakterisiert. Auch Testreaktionen, die hinsichtlich des Austauschs der Phosphan- sowie der bidentaten Liganden untersucht wurden, sind im zweiten Teil dieser Arbeit aufgeführt. Der dritte Teil der Arbeit beinhaltet die Charakterisierung der optischen Eigenschaften der erhaltenen organo-metallischen sowie organischen Verbindungen.

## Kapitel Eins

Es wurde eine Reihe von 1,3-Butadiinen sowie 1,3,9,11-Undecatetrainen synthetisiert (Verbindungen **4b-h** sowie **5a-f'** und **5h**). Hierzu wurden zunächst die TMS-geschützten Benzylalkine **2a-h** über die Sonogashira Kreuz-Kupplung dargestellt. Anschließend wurde die Schutzgruppe unter basischen Bedingungen entfernt um die entsprechenden terminalen Ethinylarene **3a-h** zu erhalten. Alle dargestellten Substanzen wurde mittels $^1$H, $^{13}$C und $^{19}$F NMR Spektroskopie, sowie GCMS und Massenspektrometrie charakterisiert. Bereits literaturbekannte Verbindungen wurden lediglich zur Überprüfung auf Reinheit mittels $^1$H NMR Spektroskopie und GCMS charakterisiert.

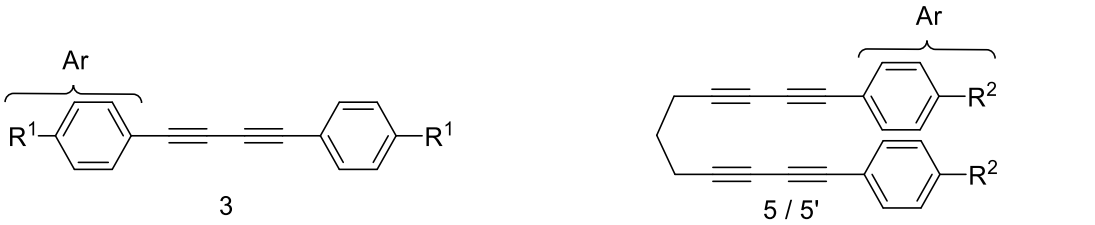


$R^1$ = $NO_2$ (**a**), $CO_2Me$ (**b**), Me (**c**), $NMe_2$ (**d**), SMe (**e**), $CF_3$ (**h**)
Ar = $C_6F_5$ (**f**), naphthyl (**g**)

$R^2$ = $NO_2$ (**a**), $CO_2Me$ (**b**), Me (**c**), $NMe_2$ (**d**), SMe (**e**), $CF_3$ (**h**)
Ar = $C_6F_4$-OMe (**f'**)

**Abbildung 1** Übersicht über die dargestellten Butadiine **4b-h** sowie Undecatetraine **5a-f'** und **5h**.

Die Synthese der Verbindungen **2f**, **3f** sowie **3f'** bereitete einige Probleme. Die Phenylringe aller drei Substanzen sind perfluoriert, was bedeutet, dass diese in Kombination mit der durchgeführten Pd-Katalyse anfällig für Hydro-Dehalogenierungen sind. Zusätzlich erfordert die Sonogashira Kreuzkupplung in diesem Fall den Einsatz von mehr TMSA, welches gleichzeitig die Entstehung von mehr homogekoppeltem TMSA verursacht. Die anschließende Aufarbeitung des Produktes erforderte folglich mehr Aufwand. Eine weitere Herausforderung war die Darstellung von Verbindung **2f**. Diese ist einerseits sehr flüchtig, andererseits ist das Fluoratom am Phenylring in *para*-Stellung zum Alkin anfällig für nukleophile Substitutionen. Folglich wurde während der Entschützung in Methanol Verbindung **2f'** erhalten, bei der das *para*-ständige Fluoratom durch eine OMe-Gruppe ersetzt ist. Diese wurde später zur Darstellung von Verbindung **5f'** verwendet.

Im Gegensatz zur Darstellung der 1,3-Butadiine, die über die Glaser-Kupplung stattfindet, erfolgte die Synthese der Undecatetraine über die Cadiot-Chodkiewicz-Kreuzkupplung. Da sich die Synthese von Verbindung **5f** außerdem als nicht erfolgreich erwies, wurde das alternative Undecatetrain **5f'** synthetisiert und eingesetzt. Ein Grund weshalb sich Verbindung **5f** nicht erfolgreich herstellen ließ, könnte möglicherweise eine Nebenreaktion am Fluoratom in *para*-Position des Phenylrings sein, die durch Triethylamin verursacht wird, das während der Reaktion als Base dient. Das alternativ dargestellte Undecatetrain **5f'** besitzt eine Methoxy-Gruppe in *para*-Position und macht eine derartige Nebenreaktion somit unmöglich.

## Kapitel Zwei

Der zweite Teil dieser Arbeit befasste sich mit der Synthese einer Reihe von lumineszierenden organo-metallischen und organischen Verbindungen. Hierzu wurden im Vorfeld die beiden Komplexe [Rh($\kappa^2$-*S,S`*-$S_2CNEt_2$)($PMe_3$)$_2$] **13** und [Rh($\kappa^2$-*S,S`*-$S_2CNEt_2$)($PPh_3$)$_2$] **22** synthetisiert und charakterisiert. Ihre Struktur wurde mittels Röntgendiffraktometrie bestätigt (Abbildung 2)

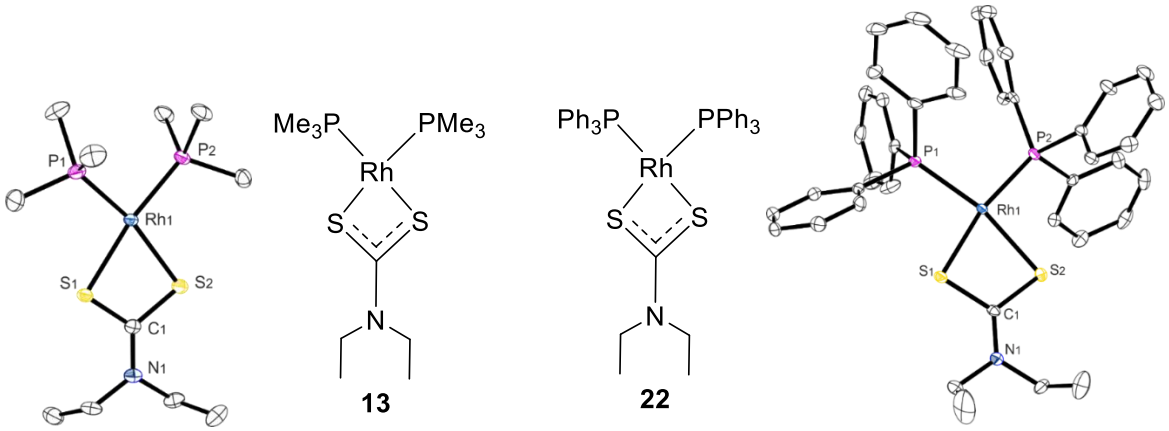


**Abbildung 2** Molekül- sowie Kristallstruktur von [Rh($\kappa^2$-*S,S`*-$S_2CNEt_2$)($PMe_3$)$_2$] **13** und [Rh($\kappa^2$-*S,S`*-$S_2CNEt_2$)($PPh_3$)$_2$] **22**

*Umsetzung von [Rh($\kappa^2$-S,S`-$S_2CNEt_2$)($PMe_3$)$_2$] **13** mit den Undecatetrainen **5***

Es zeigte sich, dass die Umsetzung von [Rh($\kappa^2$-*S,S`*-$S_2CNEt_2$)($PMe_3$)$_2$] **13** mit verschiedenen Undecatetrainen **5** bei Raumtemperatur fast ausschließlich die Rhodacyclopentadiene **23** erzeugt. Dies geschieht mittels einer [2+2+M]-Cycloaddition. Die Reaktionsdauer beträgt, in Abhängigkeit des Substituenten am Phenylring des Undecatetrains **5**, eine bis mehrere Wochen, wobei Reaktionen mit Donor-substituierten Undecatetrainen (R = $NMe_2$, SMe) die längste Reaktionsdauer verursachen. Um diese zu verkürzen wurden die Reaktionen mit Donor-substituierten Undecatetrainen in der Mikrowelle ausgeführt, wodurch diese signifikant beschleunigt wurden. Eine komplette Umsetzung der Edukte wurde durch die Umsetzung in der Mikrowelle nach ca. 24 Stunden erreicht.

Die Rhodacyclopentadiene **23a-f'** wurden erfolgreich isoliert und charakterisiert. Ihre Struktur wurde mittels Röntgendiffraktometrie bestätigt (Abbildung 3).

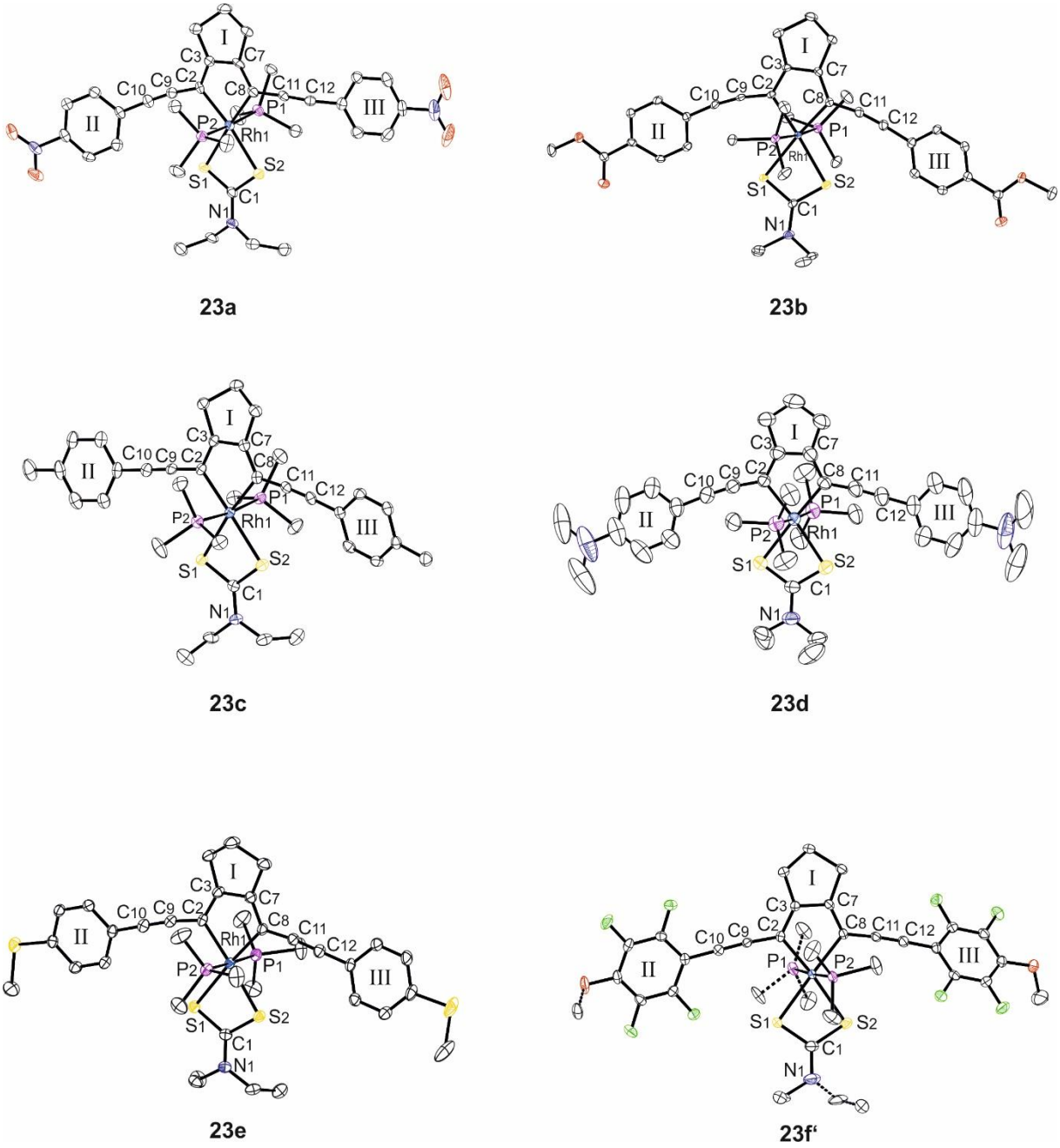


**Abbildung 3** Kristallstrukturen der Rhodacyclopentadiene **23a-f'**.

Entgegen der restlichen Rhodacyclopentadiene wurde eine vollständige Umsetzung zu Verbindung **23f'** nicht durch Reaktion bei Raumtemperatur, sondern bei hohen Temperaturen erreicht.

Die Umsetzung des Startkomplexes **13** mit den Undecatetrainen **5** bei erhöhter Temperatur verändert das Reaktionsverhalten drastisch. Entsprechend vorheriger Untersuchungen zum Reaktionsverhalten dieser Substanzklasse, bei denen vom Rh(I)-Komplex [Rh($\kappa^2$-*O,O`*-acac)($PMe_3$)$_2$] **16** ausgegangen wurde, bildet sich bei hohen Temperaturen ein Produktgemisch, das sich aus dem üblichen analogen Rhodacyclopentadien **23** mit acac sowie dem zusätzlich gebildeten, isomeren Dibenzorhodacyclopentadien **24** mit acac zusammensetzt. Allerdings liegt beim Bildungsverhältnis der Produkte zueinander der umgekehrte Fall vor, als er während den Reaktionen mit Rh(I)-Komplex **13** vorgefunden wurde. Ausgehend von Edukt **16** wurden bei Raumtemperatur vorwiegen die entsprechenden Dibenzorhodacyclopentadiene **24** mit acac als bidentatem Liganden gebildet, während bei hohen Temperaturen die Bildung der Rhodacyclopentadiene **23** mit acac gefördert wurde.

Die Zusammensetzung des Produktgemisches ist jedoch nicht nur von der Reaktionstemperatur abhängig, sondern auch vom Substituenten am Phenylring des Undecatetrains **5**. Elektronen-ziehende Substituenten (z.B. R = $CO_2Me$) fördern die Bildung des isomeren Dibenzorhodacyclopentadienes **24** bei hohen Temperaturen, während die Reaktion mit Elektronen-schiebenden Substituenten nur geringe Mengen des Dibenzorhodacyclopentadienes **24** hervorbringt, so dass eine Isolierung der Produkte deutlich erschwert wird. Nichts desto trotz war es möglich, die Dibenzorhodacyclopentadiene **24a**, **b** und **c** erfolgreich zu isolieren, wobei die Struktur der Verbindungen **24a** und **b** mittels Röntgendiffraktometrie bestätigt werden konnten (Abbildung 4).

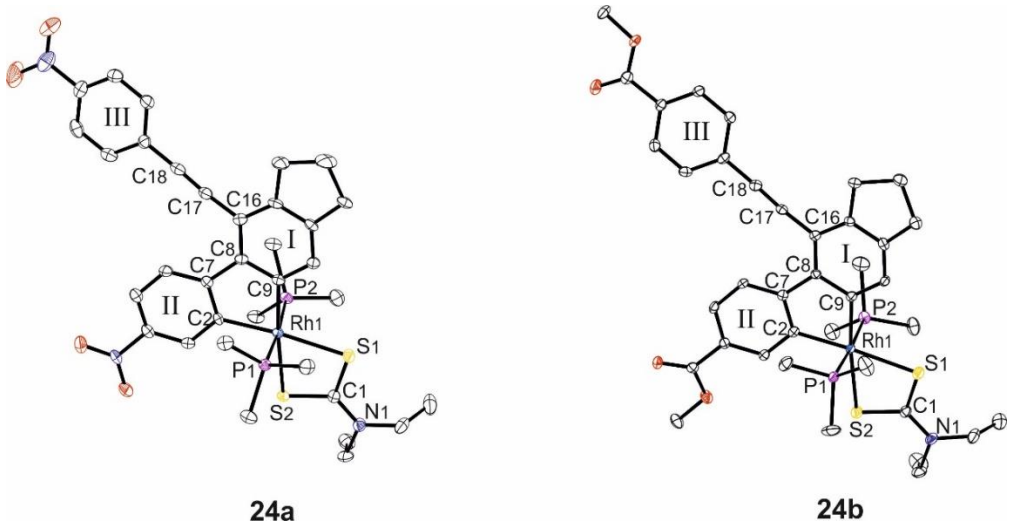


**Abbildung 4** Kristallstrukturen der Dibenzorhodacyclopentadiene **24a** und **b**.

Es wird davon ausgegangen, dass der Schlüsselschritt zur Bildung des Dibenzorhodacyclopentadiens **24** eine CH-Aktivierung ist, auf die eine [4+2] Cycloaddition und ein ß-H Shift folgen. Um dies zu überprüfen, wurden Testreaktionen unter Verwendung

des Undecatetrains **5f'** (Ar = $C_6F_4$-OMe) bei Raumtemperatur, sowie bei erhöhten Temperaturen durchgeführt. Durch die Fluoratome in *ortho* Position am Phenyldring des Tetrains wird eine CH-Aktivierung und somit die Bildung des isomeren Rh(III)-Komplexes **24** unmöglich. Während der Reaktion bei Raumtemperatur wurde das Dibenzorhodacyclopentadien **24**, wie erwartet, nicht gebildet. Es fand eine Umsetzung zum Rhodacyclopentadien **23f'** statt, parallel bildete sich allerdings noch eine zweite Spezies, die sich als der bimetallische Rh(III)-Komplex **24f'-bi** herausstellte (Abbildung 5). Das Produkt konnte erfolgreich isoliert und charakterisiert werden. Die Struktur wurde mittels Röntgendiffraktometrie bestätigt.

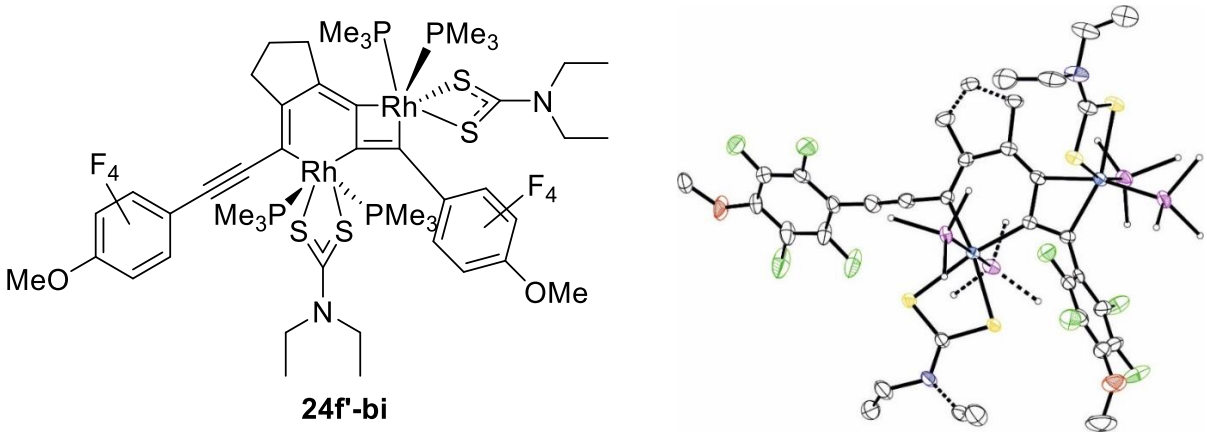


**Abbildung 5** Molekül- sowie Kristallstruktur des bimetallischen Rh[III)-Komplexes **24f'-bi**.[23]

Die Umsetzung von Rh(I)-Komplex **13** mit Undecatetrain **5f'** bei hohen Temperaturen führte, wie schon erwähnt, nicht zur Bildung des isomeren Dibenzorhodacyclopentadienes **24f'**, stattdessen entstand ausschließlich das Rhodacyclopentadien **23f'**.

*Umsetzung von [Rh($\kappa^2$-S,S`-$S_2CNEt_2$)($PPh_3$)$_2$] **22** mit den Undecatetrainen **5***

Der Austausch der Phosphanliganden von Trimethylphosphan gegen Triphenylphosphan hatte einen starken Einfluss auf das Reaktionsverhalten dieser Substanzklasse. Wurde [Rh($\kappa^2$-*S*,*S*`-$S_2CNEt_2$)($PPh_3$)$_2$] **22** mit den verschiedenen Undecatetrainen **5** umgesetzt, bildete sich nach wie vor das erwartete Rhodacyclopentadien **25**, allerdings fungierte dieses als Intermediat in einer katalytischen Cyclotrimerisierungsreaktion, die ein Gemisch aus den stark lumineszierenden, organischen Dimeren **26** und Trimeren **27** hervorbrachte (Abbildung 6). Die Dimere **26b-d**, sowie Trimere **27b**, **c**, und **f'** konnten erfolgreich isoliert und charakterisiert werden. Die Strukturen der Verbindungen **26c**, sowie **27c** und **f'** wurden mittels Röntgendiffraktometrie bestätigt.

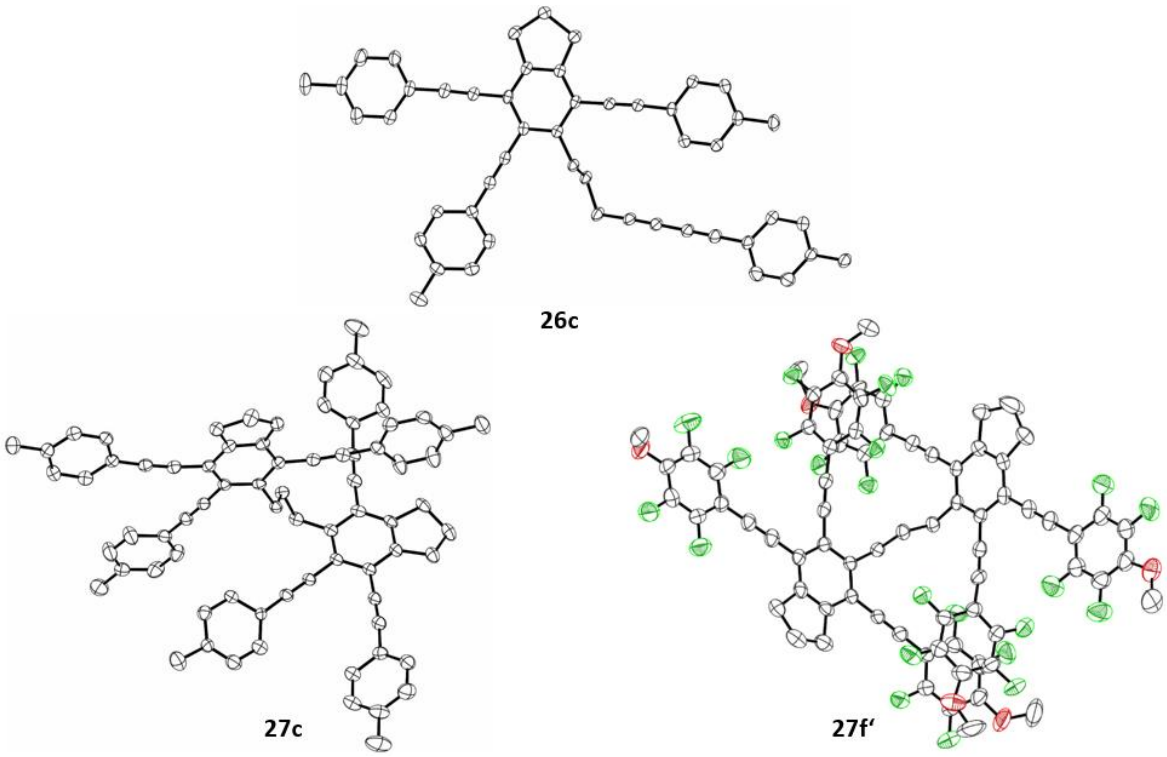


**Abbildung 6** Kristallstrukturen des Dimers **26c** sowie der Trimere **27c** und **f'**.

Das Bildungsverhältnis der Dimere und Trimere in der Reaktionsmischung hängt vom Verhältnis von [Rh($\kappa^2$-*S*,*S*`-$S_2CNEt_2$)($PPh_3$)$_2$] **22** zu den Undecatetrainen **5** ab. Somit führte ein Verhältnis von 100:1 (**5** zu **22**) fast ausschließlich zur Bildung des Dimers **26**, während ein Verhältnis von 10:1 (**5** zu **22**), im Vergleich dazu, die Bildung des Trimers **27** förderte. Zusätzlich ist das Bildungsverhältnis der beiden Benzolderivate **26** und **27** vom Substituenten am Phenylring des Undecatetrains **5** abhängig.

Fand die Umsetzung mit dem Undecatetrain **5b** (R = $CO_2Me$) in einem 10:1 Verhältnis (**5**:**13**) statt, welches mit einem elektronen-ziehenden Rest substituiert ist, wurde die Bildung des

Trimers gefördert, während im Gegensatz dazu bei einem 100:1 Verhältnis fast ausschließlich das Dimer gebildet wurde. Während der Umsetzung mit Undecatetrain **5c** (R = Me), welches sich weitgehend neutral verhält, war ein nur sehr kleiner Unterschied im Verhältnis der gebildeten Produkte zu beobachten. Mit einem 10:1 Verhältnis ließ sich das System nur gering in Richtung des Trimers verschieben und erzeugte hauptsächlich das entsprechende Dimer, welches auch mit einem 100:1 Verhältnis die dominante Spezies darstellte.

Unter Verwendung des Undecatetrains **5d** (R = $NMe_2$) war keine Kontrolle der Produktverhältnisse möglich. Es entstand in beiden Fällen fast ausschließlich das Dimer. Eine Umsetzung mit dem tetra-fluorierten Undecatetrain **5f'** (Ar = $C_6F_4$-OMe) mit einem 10:1 Verhältnis führte zu einer fast 100%igen Umsetzung zum Trimer, wobei ein 100:1 Verhältnis in einem ca. 1:1 Gemisch von Dimer und Trimer führte (Tabelle 1).

**Tabelle 1** Übersicht über die Bildungsverhältnisse der Verbindungen **26** und **27.**

| | **Ratio** | |
|---|---|---|
| **Tetrayne** | **5:22** | **A:B** |
| **5b** | 10:1 | 1:3 |
| | 100:1 | 1:0.05 |
| **5c** | 10:1 | 1:0.5 |
| | 100:1 | 1:0.1 |
| **5d** | 10:1 | 1:0.2 |
| | 100:1 | 1:0.2 |
| **5f'** | 10:1 | 0.05:1 |
| | 100:1 | 1:0.8 |

Die Rhodacyclopentadiene **25a**, **b**, **e** und **f'** konnten während der katalytischen Reaktion angefangen und charakterisiert werden. Ihre Strukturen wurden mittels Röntgendiffraktometrie bestätigt (Abbildung 7). Auch das Rhodacyclopentadien **25c** konnte isoliert werden, es war jedoch nicht möglich die Verbindung analytisch rein zu erhalten.

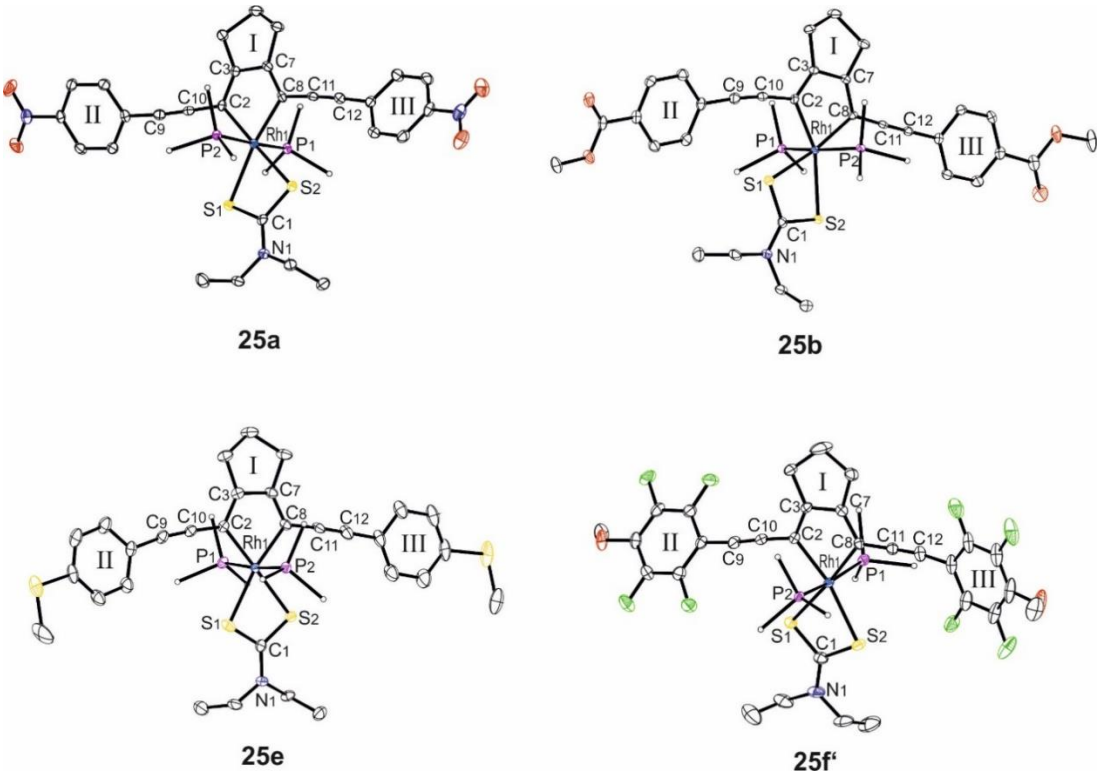


**Abbildung 7** Kristallstrukturen der Rhodacyclopentadiene **25a, b, e** and **f'**.

*Ligand-Austausch-Reaktionen*

Es wurden drei verschiedene Ligand-Austausch-Reaktionen durchgeführt. Zwei dieser Reaktionen sollten als Alternativroute dienen, die Rhodacyclopentadiene **23** und die Dibenzorhodacyclopentadiene **24** unabhängig voneinander darzustellen, um der aufwendigen Trennung der Isomere aus dem Weg zu gehen.

Als erster Ansatz wurde eine Testreaktion, ausgehend vom Rhodacyclopentadien **25b** (R = $CO_2Me$), welches Triphenylphosphan als Liganden trägt, durchgeführt. Mit Hilfe eines Überschusses an Trimethylphosphan war es möglich bei Raumtemperatur einen der beiden Phosphan-Liganden auszutauschen. Der Austausch des zweiten Liganden fand erst bei höheren Temperaturen statt, was zur vollständigen Umsetzung zum erwünschen Rhodacyclopentadien **23b** führte (Schema 1).

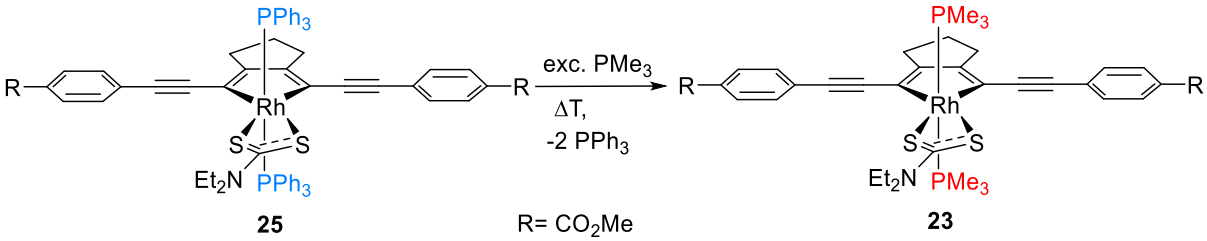


**Schema 1** Umsetzung zum Rhodacyclopentadien **23b** *via* Phosphan-Austausch-Reaktion.

Eine weitere Testreaktion wurde ausgeführt um zu überprüfen ob das Rhodacyclopentadien **24e**, das während der Reaktion von Rh(I)-Komplex **13** mit dem Undecatetrain **5e** lediglich zu einem sehr kleinen Anteil entstand, durch einen Austausch von Acetylacetonat gegen Dithiocarbamat an Verbindung **24e-acac** erhalten werden kann.

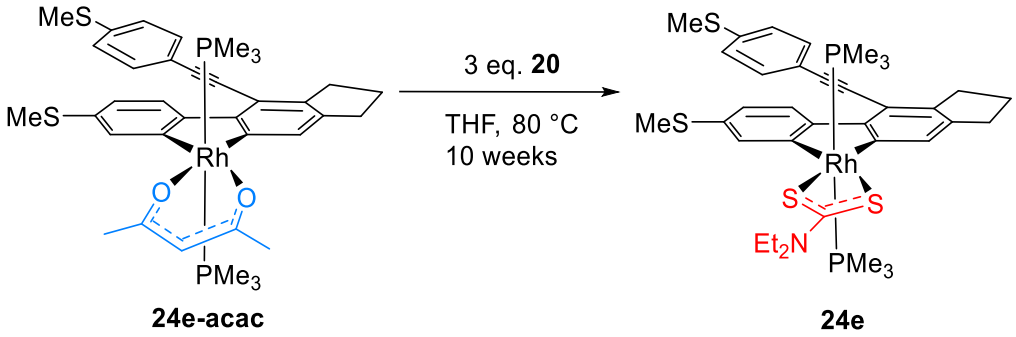


**Schema 2** Austausch von Acetylacetonat gegen Dithiocarbamat um Verbindung **24e** zu erhalten.

Hierfür wurde die Verbindung mit einem dreifachen Überschuss an Natrium-Dithiocarbamat versetzt und das Reaktionsgemisch auf 80 °C erhitzt. Verglichen mit dem Phosphan-Austausch, der innerhalb von einigen Tagen durchgeführt werden konnte, dauerte diese Austausch-Reaktion zehn Wochen.

Ein dritter Ansatz bestand darin, ein Rhodacyclopentadien zu erhalten, das anstelle von zwei Phosphan-Liganden NHC-Liganden trägt. Die Reaktion wurde ausgehend von Rhodacyclopentadien **25b**, welches mit einem Überschuss an $^{n}Pr$-NHC versetzt wurde, ausgeführt. Dabei wurde das Rhodacyclopentadien **25b-NHC** erhalten, welches entgegen der Erwartungen nur einen Ligand-Austausch aufweist. Auch eine Umsetzung bei höheren Temperaturen konnte den Austausch des zweiten Liganden nicht herbeiführen. Das Strukturmotiv von Verbindung **25b-NHC** konnte mittels Röntgendiffraktometrie bestätigt werden. Es zeigt, dass der NHC-Ligand in einer *cis*-Stellung zum Phosphan-Liganden steht.

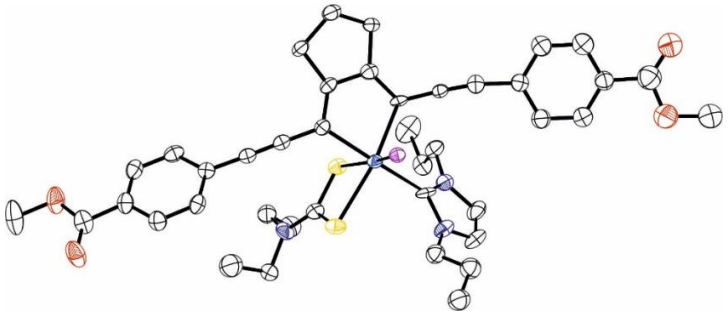

**Abbildung 8** Kristallstruktur von Verbindung **25b-NHC** zur Bestätigung des Strukturmotivs. ($R_{int}$ = 9.81, auf Grund der starken Fehlordnung der Lösungsmittelmoleküle). Die Wasserstoffatome, Lösungsmittelmoleküle sowie die Phenylreste des Triphenylphosphans wurden zur besseren Übersicht entfernt.

*Reaktionen von [Rh($\kappa^2$-S,S`-$S_2CNEt_2$)($PMe_3$)$_2$] 13 mit Diaryl-1,3-Butadiinen*

Während der Umsetzung von [Rh($\kappa^2$-S,S`-$S_2CNEt_2$)($PMe_3$)$_2$] **13** mit den Butadiinen **4** wurde weder bei Raum- noch bei erhöhter Temperatur ein Rhodacyclopentadien geformt. Stattdessen blieb die Reaktion bei einem Zwischenprodukt, dem *trans* $\pi$-Komplex **28**, bei dem nur ein Butadiin zum Rh-Zentrum koordiniert ist, stehen. Die betreffenden Reaktionen wurden sowohl in einem 1:1 als auch einem 1:2 Verhältnis (**13** zu **4**) durchgeführt, wobei diese in Bezug auf die Produktbildung keine Unterschiede aufwiesen. Bei der Reaktion in einem 1:1 Verhältnis blieben während der Umsetzung mit den Butadiinen **4c** und **g** ca. 50% des Startkomplexes übrig, während mit einem 1:2 Verhältnis ca. 50% Prozent des Butadiins **4** übrig blieben. Die Beobachtungen legen nahe, dass das Reaktionsgemisch ein Gleichgewicht ausbildet, das einen mindestens zweifachen Überschuss an Butadiin benötigt, um eine komplette Umsetzung des Startkomplexes **13** zu erreichen.

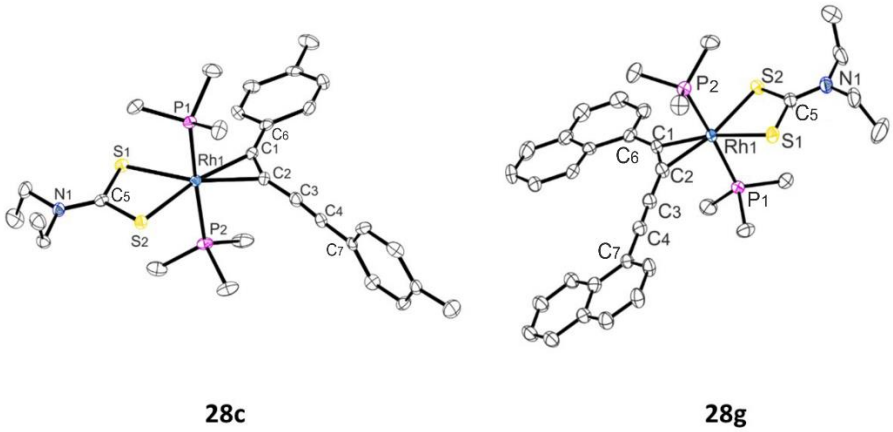


**Abbildung 9** Kristallstrukturen der *trans* $\pi$-Komplexe **28c** und **g**.

Eine vollständige Isolierung der Verbindung **28** war nicht möglich. Allerdings konnte die Struktur der gebildeten *trans* $\pi$-Komplexe **28c** und **g** mittels Röntgendiffraktometrie bestätigt werden.

Reaktionen von [Rh($\kappa^2$-*S*,*S*`-$S_2CNEt_2$)($PMe_3$)$_2$] **13**, die mit dem Butadiin **4b** (R = $CO_2Me$) durchgeführt wurden, zeigten außerdem, dass das Reaktionssystem dazu neigt ein zweites Butadiin an sich zu binden. Allerdings erforderte es sehr harsche Reaktionsbedingungen (80 °C, 75h $\mu$W), um eine signifikante Menge der Spezies mit zwei gebundenen Butadiinen zu erzeugen. Dabei wurde ein Hauptprodukt gebildet, welches dem [3+2]-Cycloadditionsprodukt **[3+2]-dithio** entsprechen könnte. Es könnte sich jedoch auch um ein asymmetrisches Rhodacyclopentadien **US-dithio** handeln (Abbildung 10).

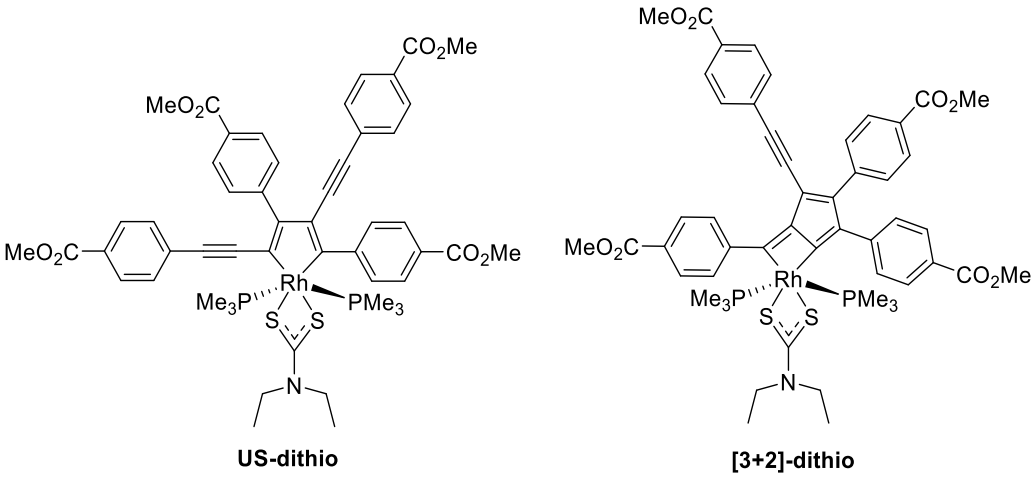


**Abbildung 10** Molekülstrukturen des asymmetrischen Rh-Komplexe **US-dithio** und **[3+2]-dithio**.

Die Charakterisierung eines Einkristalls mittels Röntgendiffraktometrie könnte aufklären welches Produkt bei der Reaktion von [Rh($\kappa^2$-*S*,*S*`-$S_2CNEt_2$)($PMe_3$)$_2$] **13** und Butadiin **4b** in der Mikrowelle geformt wird. Es liegt auf Grund der früheren Ergebnisse der Arbeitsgruppe Marder zur Reaktivität des Rh-Komplexes **16** mit acac als bidentatem Liganden jedoch nahe, dass sich der **[3+2]-dithio** Komplex bildet.

## Kapitel Drei

*Optische Eigenschaften der Rhodacyclopentadiene **23** und **25***

Rhodacyclopentadiene **23a-f'** absorbieren im sichtbaren Bereich mit Maxima $\lambda_{max}$ von 478-594 und Extinktionskoeffizienten $\varepsilon$ von 14000-33000 $Lmol^{-1}$. Die Emission findet im sichtbaren Bereich mit Maxima $\lambda_{max}$ von 512-671 nm, und sehr kleinen Stokes Verschiebungen von 660-1200 $cm^{-1}$. Der starke Überlapp der Absorptions- und Emissionsspektren, sowie die sehr kurzen Lebenszeiten (max. 1.41 ns) weisen auf Emission in Form von Fluoreszenz hin. Die stärkste Emission geht von Verbindung **23b** aus, die eine Quantenausbeute von 48%, sowie eine typische Lebenszeit von 1.41 ns liefert.[71,72,121] Mit Quantenausbeuten von 11 und 28% erreichen die Verbindungen **23e** und **f'** eine durchschnittliche Quantenausbeute, während diese bei den Verbindungen **23a**, **c** und **e** klein ausfiel (1-7%). Die entsprechenden Lebenszeiten für

Verbindungen **23c** und **d** waren zu kurz um Werte zu erhalten. Die natürlichen Lebenszeiten $\tau_0$ dieser Verbindungen wurden alternativ über den Kehrwert der Strahlungsratenkonstante $k_r$, mit Hilfe der Strickler-Berg Beziehung berechnet.[172]

Die Rhodacyclopentadiene **25a**, **b**, **e** und **f'**, die Triphenylphosphan an Stelle von Trimethylphosphan als Liganden tragen, absorbieren im sichtbaren Bereich mit Maxima $\lambda_{max}$ von 495-619 nm statt, mit Extinktionskoeffizienten $\varepsilon$ von 23000-31000 $Lmol^{-1}cm^{-1}$. Die Absorptionsmaxima der Verbindungen **25** sind zu denen von Verbindungen **23** um ca. 20 nm bathochrom verschoben. Dies impliziert, dass der Austausch der Phosphanliganden einen Energieverlust der angeregten Zustände in den Rhodacyclopentadienen **25** verursacht. Die Verbindungen emittieren im sichtbaren Bereich mit Maxima $\lambda_{max}$ von 508-686 nm, wobei die resultierende bathochrome Verschiebung einen zur Absorption vergleichbaren Trend aufweist. Die Stokes Verschiebungen von 760-1600 $cm^{-1}$ liegen im selben Bereich wie die der Verbindungen **23**. Mit Quantenausbeuten $\phi_f$ von 0.1-4% erwiesen sich Verbindungen **25** als sehr schwache Emitter, wobei Rhodacyclopentadien **25e** keinerlei detektierbare Emission aufweist. Im Allgemeinen weißt die niedrige Quantenausbeute der Rhodacyclopentadiene **23a**, **c-f'** und **25** darauf hin, dass während der Relaxation des angeregten Zustandes weitere Relaxationsprozesse stattfinden, die stark in Konkurrenz zur Fluoreszenz stehen. Diese bestehen nicht nur aus strahlungsfreier Desaktivierung sondern auch aus einem Inter System Crossing (ISC) zu den angeregten Triplet Zuständen. Die ISC-Rate der Rhodacyclopentadiene läuft auf der gleichen Geschwindigkeitsskala ab wie die strahlende Desaktivierung aus dem $S_1$-Zustand ($10^8$ $s^{-1}$).[71,72]

Um zu überprüfen ob tatsächlich Inter System Crossing stattfindet, wurde getestet, ob das System Singlet-Sauerstoff ($^1O_2$) generiert. Es wird davon ausgegangen, dass Singlet-Sauerstoff über den $T_1$ Zustand sensitisiert wird. Die Quantenausbeute des generierten Singlet-Sauerstoffs von Verbindungen **23b** und **25b** ergaben Quantenausbeuten $\phi_\Delta$ von 27 (**23b**) und 37% (**25b**).
Bei früheren Untersuchungen im Arbeitskreis Marder zeigte sich, dass die Quantenausbeute von Verbindung **14j** und die Singlet-Sauerstoff Quantenausbeute sich zu einer Gesamt-Quantenausbeute von 100% ergänzen ($\phi_f + \phi_\Delta \approx 1$; vide supra), was bedeutet, dass Fluoreszenz und ISC die einzigen Relaxationsmechanismen aus dem $S_1$-Zustand darstellen .[71] Im Vergleich dazu, laufen bei den Verbindungen **23** und **25** zusätzliche Relaxationsmechanismen ab (Vibration, Rotation), die die Quantenausbeuten drastisch verringern. Dieser Effekt ist bei den Verbindungen **25** deutlich verstärkt.

Um das stattfindende ISC genauer zu untersuchen, wurden die Lebenszeiten bei tiefen Temperaturen bestimmt, wobei die Modellverbindungen **23b** und **25b** (R = $CO_2Me$) vermessen wurden. Die Fluoreszenzlebenszeit von Verbindung **23b** wurde in einem Temperaturbereich von 175-295 K, in 10K Schritten vermessen. Im Bereich von 175-225 K bildete sich bei ca. 2.1 ns ein leichtes Plateau. Da die Lebenszeit bei tiefen Temperaturen deutlich kürzer als die natürliche Lebenszeit ($\tau_0$ = 2.93) ausfällt, wurde dies letztendlich als Hinweis auf ein nicht thermisch aktiviertes ISC interpretiert.
Verbindung **25b**, die in Me-THF vermessen wurde, zeigte ein Plateau im Bereich von 77-97 K mit einer Lebenszeit von 2.49 ns. Die geringe Differenz zur natürlichen Lebenszeit ($\tau_0$ = 2.62) von Verbindung **25**, ist ein deutlicher Hinweis auf ein thermisch aktiviertes ISC. Offensichtlich verursacht der Austausch der Phosphanliganden am Rh-Zentrum zu einer starken Veränderung des Charakters der strahlungsfreien Relaxation, was einen deutlichen Anstieg der Aktivierungsenergie des ISC zur Folge hat.

*Solvatochromie-Effekte der Rhodacyclopentadiene **23a** und **25a***

Im Fall der Rhodacyclopentadiene **23a** und **25a** (R = $NO_2$) zeigte sich ein deutlicher solvatochromer Effekt. Die Absorptions- und Emissionspektren wurden in Hexan, Me-Cyclohexan, Toluol und THF aufgenommen. Das Emissionsmaximum in THF zeigt im Vergleich zu dem in Hexan aufgenommenen eine bathochrome Verschiebung von ca. 100 nm und ein Wachstum der Stokes Verschiebung von 2290 zu 3100 $cm^{-1}$, was auf einen Charge-Transfer Charakter im angeregten Zustand hinweist. Zusätzlich verschlechtert sich mit der starken Verschiebung der Emission die Quantenausbeute. Diese beträgt in Hexan und Me-Cyclohexan ca. 20% und 7% in Toluol. In THF konnte keine Quantenausbeute erhalten werden. Im Fall von Verbindung **25a** ließen die Werte der Quantenausbeute keinen Trend erkennen. Außer für THF, das auch hier keine Quantenausbeute lieferte, beliefen sich alle Werte auf 3-4%. Zum Vergleich wurde außerdem die Solvatochromie von Verbindung **23b** untersucht. Die bathochrome Verschiebung der Emissionsmaxima in den verschiedenen Lösungsmitteln fiel mit 10-20 nm deutlich kleiner als für Verbindungen **23a** und **25a** aus. Die Stokes-Verschiebungen von 719-1332 $cm^{-1}$ unterschieden sich um nur 300 $cm^{-1}$. Für die Quantenausbeuten ließ sich kein Trend hinsichtlich der unterschiedlichen Polarität der Lösungsmittel erkennen. Es ergaben sich Werte von ca. 35%, wobei sich in Toluol eine deutlich größere Quantenausbeute von 48% ergab.

Der Vergleich der Emissionseigenschaften von Verbindungen **23a** und **25a** mit denen von Verbindung **23b** zeigt deutlich, dass die ungewöhnliche Solvatochromie der erstgenannten Verbindungen vom starken elektronenziehenden Substituenten $NO_2$ verursacht wird.

*Optische Eigenschaften der Verbindungen **24a** und **24b***

Die Dibenzorhodacyclopentadiene **24a** und **b** absorbieren im sichtbaren Bereich mit Maxima $\lambda_{max}$ von 370-379 nm, mit hohen Extinktionskoeffizienten $\varepsilon$ von 19000 und 23000 $Lmol^{-1}cm^{-1}$. Die Emission der Verbindungen **24a** und **b** findet im sichtbaren Bereich mit Maxima $\lambda_{max}$ 541-592 nm statt und liefert Stokes Verschiebungen von 8500-9500 $cm^{-1}$, die vergleichsweise groß sind und somit auf Phosphoreszenz hinweisen. Die Bestimmung der Quantenausbeute liefert moderate Werte von 14 und 23%, die aus extrem langlebigen, angeregten Triplett-Zuständen von 94 (**24a**) und 185 $\mu$s (**24b**) resultieren.

*Optische Eigenschaften der Dimere **26** und Trimere **27***

Dimere **26** absorbieren im UV/sichtbaren Bereich mit Maxima $\lambda_{max}$ von 297-332 nm mit hohen Extinktionskoeffizienten $\varepsilon$ von 55000-95000 $Lmol^{-1}cm^{-1}$ auf. Die Emission der Verbindungen findet im sichtbaren Bereich mit Maxima $\lambda_{max}$ von 377-438 nm statt. Die daraus resultierenden Stokes Verschiebungen von 2900-5300 $cm^{-1}$ weisen auf eine, für emittierende organische Verbindungen typische Fluoreszenz hin.[176] Im Gegensatz zur Absorption weist die Emission der Verbindungen **26** eine bathochrome Verschiebung der Dimere auf, die Elektronen-ziehende sowie -schiebende Substituenten tragen, wobei Verbindung **26d** die stärkste bathochrome Verschiebung zeigt.

Trimere **27** absorbieren im UV/sichtbaren Bereich mit Maxima $\lambda_{max}$ von 305-325 nm mit hohen Extinktionskoeffizienten $\varepsilon$ von 84000-131000 $Lmol^{-1}cm^{-1}$. Abhängig vom Subtituenten in *para*-Position am Phenylring zeigte sich, verglichen mit Trimer **27c** (R = Me), eine geringe bathochrome Verschiebung. Die Emission der Trimere **27** findet im sichtbaren Bereich mit Maxima $\lambda_{max}$ von 378-400 nm statt und führt zu geringen Stokes Verschiebungen von 5300-7800 $cm^{-1}$, die auf Fluoreszenz hinweisen. Die Quantenausbeuten der Dimere **26** ($f_f$ = 9-78%) sowie der Trimere **27** ($f_f$ = 12-72%) resultierten in moderaten bis exzellenten Werten. Mit 0.83-2.36 ns lieferen die Dimere **26** Lebenszeiten, die im typischen Bereich für fluoreszente organische Emitter liegen. Die Trimere **27** lieferen entsprechende Lebenszeiten von 1.57-1.60 ns. Die emissiven und strahlungsfreien Ratenkonstanten lagen in der selben Größenordnung, wobei die individuellen Raten mit den Fluoreszenzquantenausbeuten in Einklang stehen.

# 6. Experimental

## 6.1 General

If not mentioned otherwise, the following conditions are valid: All Sonogashira and Cadiot-Chodkiewicz cross-coupling reactions were carried out using standard Schlenk techniques under inert atmosphere (argon or nitrogen). Solvents used ($NEt_3$, THF, MeOH, $Et_2O$, *n*-hexane, DCM, chloroform, toluene) were dried, deoxygenated and argon saturated by an Innovative Technology Inc. Pure Solvent Purification System. *n*$BuNH_2$ was used without drying. For further deoxygenation the freeze-pump-thaw method was used.

Microwave assisted experiments were performed using a Biotage® Initiator+. The reactions were set in a glovebox in standard microwave tubes (0.2-20 mL). Depending on the reaction, the temperature range was set at 40-300° with a power range of 0-400 W at 2.45 GHz with and a maximal pressure of 30 bar.

Deuterated solvents ($C_6D_6$, $CDCl_3$, $CD_2Cl_2$, THF-$_{d8}$ and $D_2O$) used for nuclear magnetic nuclear resonance spectroscopy were purchased from Euroiso-Top. Iodopentafluorobenzene and trimethylsilylacetylene were purchased from Fluorochem and used without further purification. Bis(triphenylphosphine)palladium(II)dichloride and 1,7-dibromopentadiyne were synthesised by the group following known literature methods. Copper(I)chloride was kindly donated by the first year lab-course of the inorganic institute.

Reaction progress was monitored using thin layer chromatography (TLC) plates pre-coated with a layer of silica (Polygram® Sil G/$UV_{254}$) and fluorescent indicator $UV_{254}$ which were purchased from Machery-Nagel. Column chromatography was performed with aluminium oxide ($Al_2O_3$) as the matrix and a solvent system as described. Solvents were removed using a rotary evaporator *in vacuo* at a maximum temperature of 45°C.

$^1H$, $^{13}C\{^1H\}$, $^{19}F\{^1H\}$, $^{31}P\{^1H\}$ NMR spectroscopy data were recorded at ambient temperature either on a Bruker Avance 500, a Bruker Avance 400, a Bruker DRX-300 or a Bruker Avance 200 NMR spectrometer.

All chemical shifts were referenced to solvent peaks as follows: $^1H$ NMR spectra were referenced *via* the residual proton resonances of $D_2O$ (4.79 ppm), THF-$_{d8}$ (1.72, 3.58 ppm), $CD_2Cl_2$ (5.32 ppm), $CDCl_3$ (7.26 ppm) and $C_6D_6$ (7.16 ppm). $^{13}C\{^1H\}$ NMR spectra were referenced to THF-$_{d8}$ (67.21, 25.31 ppm), $CD_2Cl_2$ (53.84 ppm), $CDCl_3$ (77.16 ppm) and $C_6D_6$

(128.06 ppm). The signals are given with one decimal point. If they are not differentiable, they are given with two decimal points.

GC/MS analyses were performed using an Agilent 7890A gas chromatograph (column: HP-5MS 5% phenyl methyl siloxane, 10 m, 0.25 mm, film 0.25 $\mu$m; injector: 250 °C; oven: 40 °C for method A, 80 °C for method B; 40 °C to 180 °C (20 °C / min), 180 °C to 280 °C (50 °C / min) for method A, 80 °C to 180 °C (20 °C / min), 180 °C to 280 °C (50 °C / min) for method B; carrier gas: He (1.2 mL / min) equipped with an Agilent 5975C inert MSD detector operating in EI mode and an Agilent 7693A series liquid handling system functioning as auto sampler. Elemental analyses were performed on an Elementar vario MICRO cube elemental analyser.

Mass spectra were recorded on a Varian 320-MS-GC/MS system operating in the EI method. The Varian MS Workstation 6.9.2. software was used for the calculation of the respective mass values and the corresponding isotopic pattern. MALDI mass spectrometry was performed with a Bruker Daltonics autoflex II in a 2-[(2*E*)-3-(4-tert-butylphenyl)-2-methylprop-2-enylidene]malononitrile (DCTB) matrix. High-resolution ESI-TOF mass spectra were performed with a Bruker Daltonics microTOF focus mass spectrometer equipped with an ESI ion source. The ´Bruker Daltonics Isotope-Pattern´ software from Bruker Daltonics was used for the calculation of the respective mass values of the isotopic distribution.

Also used for mass spectrometry was the Exactive Plus mass spectrometer equipped with an Orbitrap from Thermo Scientific. ESI mass spectrometry was performed using an HESI source with an auxiliary gas temperature of 50 °C. APCI and ASAP spectrometry was performed using an APCI source equipped with a corona needle, under an auxiliary gas temperature of 400 °C, if not noted differently.

Single-crystal Xray diffraction studies were carried out using a Siemens SMART three-circle diffractometer with graphite-monochromated MoKα radiation ($\lambda$ = 0.71073 Å) from a sealed X-ray tube operated at 60 kV and 50 mA, equipped with an Apex II area detector. Subsequently, the structures were solved by direct methods using XS and refined by full-matrix least-squares on $F^2$ using XL, as implemented in the SHELXTL suite of programs. All non-hydrogen atom positions were located from the Fourier maps and refined anisotropically. Hydrogen atom positions were calculated using a riding model and refined isotropically. Molecular structures were depicted using OLEX$^2$ software.

Samples for optical measurements of the rhodacyclopentadienes **23** and **25** as well as their isomers **24** were prepared under argon in the glovebox. Absorption and emission spectra as well as quantum yields and lifetimes were performed at ambient temperature in dry, degassed toluene, or in spectroscopic grade, degassed Me-THF (Alfa Aesar) using standard quartz cuvettes (1 cm x 1 cm cross section). Optical measurements of the organic dimers **26** and trimers **27** were carried out under air, in dichloromethane (dried using an Inert Inc. solvent purification system) in standard quartz cuvettes (1 cm x 1 cm cross section). UV/Vis absorption spectra were recorded using an Agilent 8453 diode array UV/Vis spectrophotometer. Excitation, emission, lifetime and quantum yield measurements were carried out using an Edinburgh Instruments FLSP920 spectrometer equipped with double monochromators. The measurements were made in right-angle geometry mode. All solutions used in photophysical measurements had a concentration lower than $10^{-5}$ M.

Fluorescence quantum yields of the samples were measured using a calibrated integrating sphere (150 mm inner diameter) from Edinburgh Instruments combined with the FLSP920 spectrometer described above. For solution-state measurements, the longest wavelength absorption maximum of the compound in the respective solvent was chosen for the excitation.

Singlet oxygen sensitising was carried out in acetonitrile which was bubbled which $O_2$ for ten minutes. As a standard, perinaphthenone was chosen, as it is known to have a quantum yield for singlet oxygen emission up to unity.[174] To prove the singlet oxygen quantum yield of the standard, it was measured relative to that of $[Ru(bpy)^3]^+$, fitting to literature with a value of 0.59 (Lit.: 0.57(4)).[175]

Lifetime measurements were conducted using the time-correlated single-photon counting method (TCSPC) on the FLSP920 spectrometer equipped with a high speed photomultiplier tube positioned after a double emission monochromator. Solutions were excited with either a 376, 472, 505 nm pulsed diode laser or 508 nm laser LED at repetition rates of 1-5 MHz and the time-dependent emission intensity was recorded at the respective emission maxima. The instrument response functions (IRF) were ca. 950 ps FWHM. Decays were recorded to 10000 - 100000 counts in the peak channel with a record length of 10000 channels. The band-pass of the monochromator was adjusted to give a signal count rate of <250 kHz. Iterative reconvolution of the IRF with multiple decay functions and nonlinear least-squares analysis were used to analyse the data. Alternatively, tail fitting was used. The quality of all decay fits was judged to be satisfactory based on the calculated values of the reduced $\chi^2$ and Durbin-Watson parameters and visual inspection of the weighted and auto correlated residuals.

## 6.2 Synthetic Routes

### Synthesis of Trimethylsilyl-Protected Ethynylbenzenes

*4-(trimethylsilylethynyl)nitrobenzene* (**2a**) [22,31]

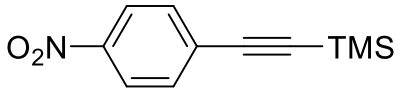


This compound was synthesised according to a typical procedure carried out in this group, for comparable compounds. To a solution of 1-bromo-4-nitrobenzene (5.01 g, 22.2 mmol) in 200 mL of degassed $NEt_3$ were added CuI (0.08 g, 0.44 mmol) and $Pd(PPh_3)_2Cl_2$ (0.15 g, 0.22 mmol). TMSA (3.81 mL, 2.65 g, 27.0 mmol) was added under nitrogen to the rapidly stirred solution. The mixture was stirred for 21 h at 60 °C. Afterwards, the solvent was removed *in vacuo*. The residue was dissolved in hexane and filtered through a 5 cm silica gel column with hexane eluent. After removal of the solvent *in vacuo*, the product was obtained as an off-white solid (4.90 g, 20.0 mmol, 91%).$^1$H NMR (300 MHz, $CDCl_3$): $\delta$ = 8.16 (d, $J_{HH}$ = 9 Hz, 2H, C$H_{arom}$), 7.59 (d, $J_{HH}$ = 9 Hz, 2H, C$H_{arom}$), 0.27 (s, 9H, Si(C$H_3$)$_3$) ppm. GCMS (Method B): $t_R$ = 5.65 min, m/z = 219.

*4-(trimethylsilyl)ethynylbenzoic acid methylester* (**2b**) [31]

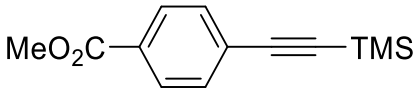


To a solution of 4-iodobenzoic acid methyl ester (6.00 g, 23.0 mmol) in 200 mL of degassed $NEt_3$ were added CuI (0.09 g, 0.45 mmol) and $Pd(PPh_3)_2Cl_2$ (0.16 g, 0.23 mmol). TMSA (3.57 mL, 2.47 g, 25.2 mmol) was added under argon to the rapidly stirred solution. The mixture was stirred overnight at room temperature. Afterwards the solvent was removed *in vacuo*. The residue was dissolved in hexane/diethylether (95:5) and filtered through a 5 cm silica gel column with hexane/diethylether eluent (95:5). After removal of the solvent *in vacuo* the product was obtained as a colourless solid (5.13 g, 22.1 mmol, 96%). $^1$H NMR (300 MHz, $CDCl_3$): $\delta$ = 7.98 (d, $J_{HH}$ = 9 Hz, 2H, C$H_{arom}$), 7.52 (d, $J_{HH}$ = 9 Hz, C$H_{arom}$), 3.91 (s, 3H, OC$H_3$), 0.26 (s, 9H, Si(C$H_3$)$_3$) ppm. GCMS (Method B): $t_R$ = 5.85, m/z = 232.

*4-(trimethylsilylethynyl)toluene* (**2c**) [31]

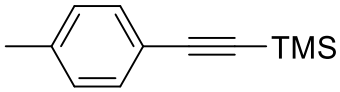


To a solution of 4-iodotoluene (3.00 g, 14.0 mmol) in 100 mL of degassed $NEt_3$ were added CuI (0.13 g, 0.69 mmol) and $Pd(PPh_3)_2Cl_2$ (0.10 g, 0.14 mmol). TMSA (2.12 mL, 1.47 g, 15.0 mmol) was added under nitrogen to the rapidly stirred solution. The mixture was stirred for 2 d at room temperature. The solid was separated from the solution and washed with $Et_2O$. After removal of the solvent *in vacuo*, the residual oil was dissolved in a small amount of hexane and filtered through a short silica gel column with hexane eluent. After removal of the solvent *in vacuo*, the product was obtained as a colourless oil (2.19 g, 11.7 mmol, 84%). $^1$H NMR (200 MHz, $CDCl_3$): $\delta$ = 7.38 (d, $J_{HH}$ = 8 Hz, 2H, C$H_{arom}$), 7.10 (d, $J_{HH}$ = 8 Hz, 2H, C$H_{arom}$), 2.35 (s, 3H, C$H_3$), 0.27 (s, 9H, Si(C$H_3$)$_3$) ppm. GCMS (Method B): $t_R$ = 7.0 min, m/z = 188.

*4-(trimethylsilylethynyl)-N,N'-dimethylaniline* (**2d**) [31]

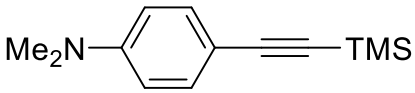


To a solution of 4-iododimethylaniline (15.0 g, 60.7 mmol) in 350 mL of degassed $NEt_3$ were added CuI (0.23 g, 1.20 mmol), $Pd(PPh_3)_2Cl_2$ (0.43 g, 0.61 mmol). TMSA (9.40 mL, 6.56 g, 66.8 mmol) was added under argon to the rapidly stirred solution. The mixture was stirred at 70 °C for 2 h. Afterwards, the solvent was removed *in vacuo*. The residue was dissolved in hexane and filtered through a 2 cm silica gel column with hexane eluent. After removal of the solvent *in vacuo* the product was obtained as a yellow solid (12.4 g, 57.1 mmol, 94 %).$^1$H NMR (200 MHz, $CDCl_3$): $\delta$ = 7.34 (d, $J_{HH}$ = 9 Hz, 2H, C$H_{arom}$), 6.59 (d, $J_{HH}$ = 9 Hz, 2H, C$H_{arom}$), 2.96 (s, 6H, N(C$H_3$)$_2$), 0.23 (s, 9H, Si(C$H_3$)$_3$) ppm. GCMS (Method B): $t_R$ = 6.17 min, m/z = 217.

*4-(trimethylsilylethynyl)thioanisole* (**2e**)[31]

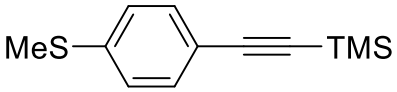


This compound was synthesised according to a typical procedure carried out in this group, for comparable compounds. To a solution of 4-bromothioanisole (10.0 g, 49.3 mmol) in 200 mL of degassed $NEt_3$ were added CuI (0.18 g, 0.98 mmol) and $Pd(PPh_3)_2Cl_2$ (0.34 g, 0.49 mmol). TMSA (7.65 mL, 5.32 g, 54.1 mmol) was added under argon to the rapidly stirred solution. The mixture was stirred for 3 d at RT - 70 °C. Afterwards the solvent was removed *in vacuo*. The residue was dissolved in $Et_2O$ and filtered through a 5 cm silica gel column with $Et_2O$ eluent and trough a second 5 cm silica gel column with hexane eluent. After removal of the solvent *in vacuo*, the product was obtained as a yellowish liquid (11.1 g, 50.2 mmol, 98%). $^1$H NMR (300 MHz, $CDCl_3$). $\delta$ = 7.37 (d, $J_{HH}$ = 9 Hz, 2H, C$H_{arom}$), 7.15 (d, $J_{HH}$ = 9 Hz, 2H, C$H_{arom}$), 2.47 (s, 3H, SC$H_3$), 0.25 (s, 9H, Si(C$H_3$)$_3$) ppm. GCMS (Method B): $t_R$ = 6.0 min, m/z = 220.

*4-(trimethylsilylethynyl)pentafluorobenzene* (**2f**)[176]

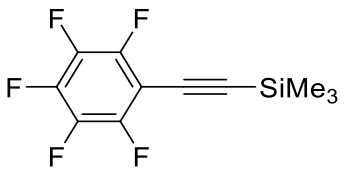


To a solution of iodopentafluorobenzene (5.00 g, 2.26 mL, 17.0 mmol) in 150 mL of degassed $NEt_3$ was added CuI (0.16 mg, 0.85 mmol), $Pd(PPh_3)_2Cl_2$ (0.29 mg, 0.43 mmol) and TMSA (2.51 mL, 1.76 g, 18.0 mmol) under argon to the rapidly stirred solution. The mixture was stirred at 50 °C for 2 d. Afterwards, the solution was separated from the solid *via* filtration and the filtrate was diluted with $Et_2O$ (100 mL) and washed with water (3 x 70 mL) and dilute acetic acid (3 x 60 mL). After the solvent was removed *in vacuo*, the crude product was filtered through a short $Al_2O_3$ column with *n*-hexane eluent. Afterwards, the solvent was removed *in vacuo* and the product was obtained as a yellowish liquid (2.89 g, 10.9 mmol, 64 %). $^1$H NMR (200 MHz, $C_6D_6$): $\delta$ = 0.17 (s, Si(C$H_3$)$_3$, 9H) ppm. $^{19}$F{$^1$H} NMR (200 MHz, $C_6D_6$): $\delta$ = -137.1 (m, 2F), -153.15 (tt, 1F), -162.60 (m, 2F) ppm. GC-MS (Method A): $t_R$ = 4.25 min, m/z = 264.

*4-(trimethylsilylethynyl)naphthalene* (**2g**) [46]

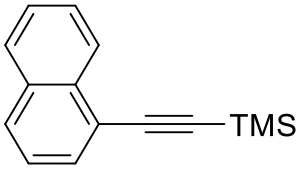


To a solution of 1-iodonaphthalene (25.0 g, 98.4 mmol) in 60 mL of degassed $NEt_3$, were given CuI (0.37 g, 1.96 mmol), $Pd(PPh_3)_2Cl_2$ (0.69 g, 0.98 mmol). TMSA (15.3 mL, 10.6 g, 108 mmol) were added under argon to the rapidly stirred solution. The mixture was stirred for 1 d at 55 °C. Afterwards, the solvent was removed *in vacuo*. The residue was dissolved in hexane and filtered through a 10 cm silica gel column with hexane eluent. After removal of the solvent *in vacuo*, the product was obtained as a yellow liquid (19.7 g, 87.6 mmol, 89%). $^1$H NMR (200 MHz, $CDCl_3$): $\delta$ = 8.29-8.46 (m, 1H, C*H*$_{arom}$), 7.77-7.91 (m, 2H, C*H*$_{arom}$), 7.66-7.76 (m, 1H, C*H*$_{arom}$), 7.46-7.66 (m, 2H, C*H*$_{arom}$), 7.34-7.46 (m, 1H, C*H*$_{arom}$), 0.35 (s, 9H, Si(C*H*$_3$)$_3$) ppm. GCMS (Method B): $t_R$ = 6.4 min, m/z = 224.

*4-(trimethylsilylethynyl)benzotrifluoride* (**2h**) [31]

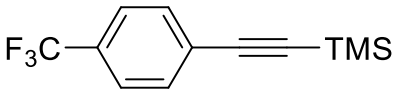


To a solution of 4-bromobenzotrifluoride (20.0 g, 12.2 mL, 89.0 mmol) in 350 mL of degassed $NEt_3$, CuI (0.32 g, 1.70 mmol), $Pd(PPh_3)_2Cl_2$ (0.62 g, 0.89 mmol) and TMSA (14.5 mL, 10.0 g, 102 mmol) were added under nitrogen to the rapidly stirred solution. The mixture was stirred for 2 h at 60 °C. Afterwards, the solvent was removed *in vacuo*. The residue was dissolved in hexane and filtered through a 5 cm silica gel column with hexane eluent. After removal of the solvent *in vacuo*, the product was obtained as a colourless liquid (16.5 g, 68.0 mmol, 76%). $^1$H NMR (300 MHz, $CDCl_3$): $\delta$ = 7.56 (s, 4H, C*H*$_{arom}$), 0.27 (s, 9H, Si(C*H*$_3$)$_3$) ppm. $^{19}$F{$^1$H} NMR (200 MHz, $CDCl_3$): $\delta$ = -63.3 (s, 3F, C*F*$_3$) ppm. GCMS (Method B): $t_R$ = 6.03 min, m/z = 242.

**Synthesis of Ethynylbenzenes**

*4-ethynyl-nitrobenzol* (**3a**)[31]

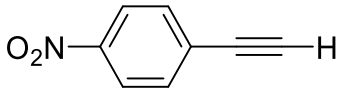

This compound was synthesised according to a typical procedure carried out in this group, for comparable compounds. Compound **2a** (9.20 g, 42.0 mmol) was added to a stirred suspension of $Na_2CO_3$ (19.4 g, 183 mmol) in 300 mL of MeOH. The mixture was stirred for 2.5 h before the solution was separated from the solid *via* filtration. The solvent was removed *in vacuo* and the crude product was diluted with 100 mL of DCM and extracted (3 x 200 mL) and then washed with water (2 x 200 mL). The organic fraction was separated, dried over $Na_2SO_4$ and the solvent was removed *in vacuo*. The product was obtained as an off-white solid (3.10 g, 21.4 mmol 51 %). $^1$H NMR (300 MHz, $CDCl_3$): $\delta$ = 7.38 (d, $J_{HH}$ = 8 Hz, 2H, C$H_{arom}$), 7.11 (d, $J_{HH}$ = 8 Hz, 2H, C$H_{arom}$), 2.35 (s, 1H, C*H*) ppm. GCMS (Method B): $t_R$ = 4.4 min, m/z = 152.

*4-ethynylbenzoic acid methyl ester* (**3b**)[31]

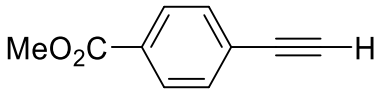

The compound **2b** (5.00 g, 21.5 mmol) was added to a stirred suspension of $Na_2CO_3$ (9.10 g, 85.8 mmol) in 250 mL of MeOH and 40 mL of $H_2O$. After stirring for 24 h, the solution was separated from the solid *via* filtration and was diluted with 250 mL of DCM. The organic fraction was separated, washed with water (2 x 100 mL), dried over $Na_2SO_4$ and the solvent was removed *in vacuo*. The product was obtained as an off-white solid (2.70 g, 16.9 mmol, 73%). $^1$H NMR (300 MHz, $CDCl_3$): $\delta$ = 7.27 (d, $J_{HH}$ = 7 Hz, 2H, C$H_{arom}$), 6.98 (d, $J_{HH}$ = 7 Hz, 2H, C$H_{arom}$), 2.90 (s, 1H, C*H*), 2.20 (s, 3H, C$H_3$) ppm. GCMS (Method B): $t_R$ = 3.6 min, m/z = 160.

*4-ethynyl-toluene* (**3c**)[31]

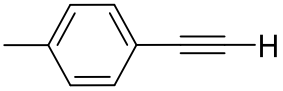

The compound **2c** (2.19 g, 11.7 mmol) was added to a stirred suspension of $Na_2CO_3$ (4.00 g, 38.4 mmol) in 100 mL of MeOH and 10 mL of water. The mixture was stirred overnight before being diluted with 200 mL of $Et_2O$ and then washed with water (2 x 200 mL). The organic

fraction was separated, dried over $MgSO_4$ and the solvent was removed *in vacuo*. The oil obtained was re-dissolved in hexane and filtered through a 5 cm silica gel column. Removal of the solvent *in vacuo* gave the product as brown oil (2.36 g, 20.3 mmol, 95%). $^1$H NMR (300 MHz, $CDCl_3$): $\delta$= 7.27 (d, $J_{HH}$ = 7 Hz, 2H, C$H_{arom}$), 6.98 (d, $J_{HH}$ = 7 Hz, 2H, C$H_{arom}$), 2.90 (s, 1H, C*H*), 2.20 (s, 3H, C$H_3$) ppm. GCMS (Method A): $t_R$ = 3.2 min, m/z = 115.

*4-ethynyl-N,N-dimethylaniline* (**3d**) [31]

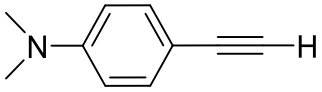


The compound **2d** (3.00 g, 13.8 mmol) was added to a stirred suspension of $Na_2CO_3$ (5.50 g, 52.8 mmol) in 100 mL of MeOH and 10 mL of $H_2O$. After stirring for 24 h, the reaction was diluted with 250 mL of DCM. The organic fraction was separated, washed with water (3 x 100 mL), dried over $Na_2SO_4$ and the solvent was removed *in vacuo*. The product was obtained as a colourless solid (1.50 g, 10.3 mmol, 75%). $^1$H NMR (300 MHz, $CDCl_3$): $\delta$ = 7.38 (d, $J_{HH}$ = 9 Hz, 2H, C$H_{arom}$), 6.62 (d, $J_{HH}$ = 9 Hz, 2H, C$H_{arom}$), 2.85 (s, 7H, N(C$H_3$)$_2$ and C*H*) ppm. GCMS (Method A): $t_R$ = 4.1 min, m/z = 145.

*4-ethynyl-thioanisole* (**3e**) [31]

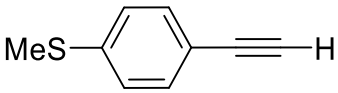


Compound **2e** (5.00 g, 22.7 mmol) was added to a stirred suspension of $Na_2CO_3$ (4.50 g, 42.5 mmol) in 150 mL of MeOH. The mixture was stirred over night before the solution was separated from the solid *via* filtration. The solvent was removed *in vacuo* and the crude product was diluted with 200 mL of $Et_2O$ and then washed with water (2 x 200 mL). The organic fraction was separated, dried over $MgSO_4$ and the solvent was removed *in vacuo*. The product was obtained as an off-white solid (2.50 g, 16.8 mmol, 74%). Compound **3e** was only characterised *via* GCMS. GCMS (Method A): $t_R$ = 5.65 min, m/z = 148.

*4-ethynyl-pentafluorobenzene* (**3f**)[177]

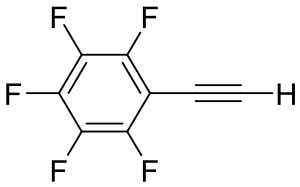


To a stirred solution of **2f** (1.30 g, 4.92 mmol) in 35 mL of $Et_2O$ was added a 1 M solution of TBAF in THF (4.92 mL, 1.29 g. 4.29 mmol) at 0°C. The colour of the mixture subsequently changed from colourless to black. After stirring for 18 h at ambient temperature, the reaction mixture was filtered and the filtrate was carefully concentrated *in vacuo*. A clear, dark liquid was obtained (501 mg, 2.45 mmol, 43%). $^1$H NMR (500 MHz, $CDCl_3$): $\delta$ = 3.61 (s, C*H*, 1H) ppm. $^{19}$F{$^1$H} NMR (188 MHz, $CDCl_3$): $\delta$ = -135.9 -136.0 (m, 2F, C$F_{arom}$), -151.5 -151.8 (m 1F, C$F_{arom}$), -161.6 -161.9 (m, 2F, C$F_{arom}$) ppm. GCMS (Method A): $t_R$ = 1.0 min, m/z = 192.

*4-ethynyl-p-methoxy-tetrafluorobenzene* (**3f'**)[178]

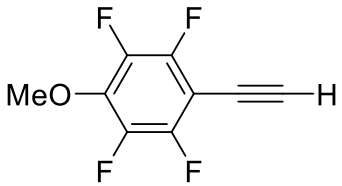


Compound **2f** (2.89 g, 10.5 mmol) was added to a stirred suspension of $Na_2CO_3$ (1.32 g, 12.50 mmol) in 50 mL of MeOH. The mixture was stirred 3 d before the solution was separated from the solid *via* filtration. The solvent was removed *in vacuo* and the crude product was diluted with 50 mL of DCM, extracted 3 times and then washed with water (2 x 50 mL). The organic fraction was separated, dried over $Na_2SO_4$ and the solvent was removed *in vacuo*. The product was obtained as a white crystalline solid (1.79 g, 8.82 mmol, 84%). $^1$H NMR (500 MHz, $CDCl_3$): $\delta$ = 4.11 (t, $J_{HF}$ = 1.6 Hz, 3H, OC$H_3$), 3.54 (t, C*H*, 1H) ppm. $^{19}$F{$^1$H} NMR (500 MHz, $CDCl_3$): $\delta$ = -157.86 (m, 2F), -137.69 (m, 2F) ppm. GCMS (Method A): $t_R$ = 4.0 min, m/z = 204.

*4-ethynyl-naphthalene* (**3g**)[31]

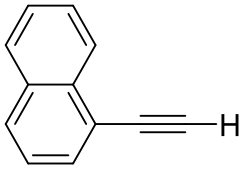

Compound **2g** (5.60 g, 25.0 mmol) was added to a stirred solution of KOH (1.40 g, 25.0 mmol) in 100 mL of MeOH. The mixture was stirred at RT for 1 h before the solution was separated from the solid *via* filtration. The solvent was removed *in vacuo* and the crude product was diluted with 50 mL of pentane and extracted (3 x 50 mL) and washed with water (2 x 50 mL). The organic fraction was separated, dried over $Na_2SO_4$ and the solvent was removed *in vacuo*. The product was obtained as a pale yellow oil (3.20 g, 84%, 21.0 mmol). $^1$H NMR (500 MHz, $CDCl_3$): $\delta$ = 8.31 (d, $J_{HH}$ = 8 Hz, 1H, C*H*$_{arom}$), 7.81 (d, $J_{HH}$ = 8 Hz, 2H, C*H*$_{arom}$), 7.69 (d, $J_{HH}$ = 8 Hz, 1H, C*H*$_{arom}$), 7.51-7.56 (m, 1H, C*H*$_{arom}$), 7.45-7.50 (m, 1H, C*H*$_{arom}$), 7.36-7.40 (m, 1H, C*H*$_{arom}$), 3.45 (s, 3H, C*H*) ppm. GCMS (Method B): $t_R$ = 4.4 min, m/z = 152.

*4-ethynylbenzo-trifluoromethane* (**3h**) [31]

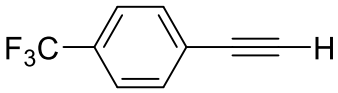

Compound **2h** (3.69 g, 15.2 mmol) was added to a stirred suspension of $Na_2CO_3$ (4.40 g, 42.3 mmol) in 90 mL of MeOH and 40 mL of water. After stirring for 24 h, the reaction mixture was diluted with 250 mL of $Et_2O$. The organic fraction was separated, washed with water (3 x 100 mL), dried over $Na_2SO_4$ and the solvent was slightly removed *in vacuo*. Due to its high volatility, **3h** was not detectable *via* GCMS and was used directly as a solution in $Et_2O$. *In situ*-$^1$H NMR (300 MHz, $Et_2O/CDCl_3$): $\delta$ = 7.52 (s, 4H, C*H*$_{arom}$), 3.16 (s, 1H, C*H*) ppm.

**Synthesis of 1,4-Bis(*p*-R-phenyl)buta-1,3-Diynes and Related Compounds**

*1,4-bis(p-carbomethoxyphenyl)buta-1,3-diyne* (**4b**) [6]

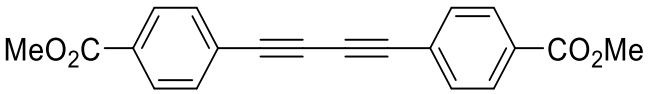


Compounds **3b** (6.87 mmol, 1.10 g), CuI (0.29 mmol, 0.06 g), $Pd(PPh_3)_2Cl_2$ (0.12 mmol, 0.09 g) and $I_2$ (3.70 mmol, 0.95 g) were slurred in 100 mL of $NEt_3$ and the mixture was stirred for 36 h. The solvent was removed *in vacuo* and the residue was dissolved in DCM (10 ml). The organic fraction was washed with a saturated solution of $Na_2S_2O_3$, dried over $Na_2SO_4$, and the solvent was removed *in vacuo* to give a brown solid. The solid was dissolved in a small amount of DCM, crystallised in the refrigerator and afterwards washed with cold DCM. The product was obtained as colourless solid (0.50 g, 31.6 mmol, 46%). $^1$H NMR (300 MHz, $CDCl_3$): $\delta$ = 7.95 (d, $J_{HH}$ = 8 Hz, 4H, C$H_{arom}$), 7.52 (d, $J_{HH}$ = 8 Hz, 4H, C$H_{arom}$), 3.87 (s, 6H, OC$H_3$) ppm. GCMS (Method B): $t_R$ = 9.3 min, m/z = 318.

*1,4-bis(p-tolyl)buta-1,3-diyne* (**4c**) [6]

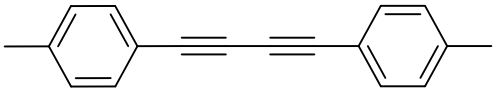

Compounds **3c** (1.00 g, 8.61 mmol), CuI (0.08 g, 0.43 mmol), $Pd(PPh_3)_2Cl_2$ (0.12 g, 0.17 mmol) and $I_2$ (1.09 g, 4.29 mmol) were slurred in 150 mL of $NEt_3$ and the mixture was stirred overnight. The solvent was removed *in vacuo* and then the resulting solid was applied to the top of a 10 cm silica gel column, which was diluted with hexane until no further product was obtained. Removal of the solvent *in vacuo* yielded a colourless solid, which was washed with MeOH to remove any residual starting material and dried *in vacuo* (0.52 g, 2.25 mmol, 52%). $^1$H NMR (300 MHz, $CDCl_3$): $\delta$ = 7.43 (d, $J_{HH}$ = 8 Hz, 4H, C$H_{arom}$), 7.15 (d, $J$ = 8 Hz, 4H, C$H_{arom}$), 2.37 (s, 6H, C$H_3$) ppm. GCMS (Method B): $t_R$ = 12.4 min, m/z = 230.

*1,4-bis(p-N,N'-dimethylaniline)buta-1,3-diyne* (**4d**) [6]

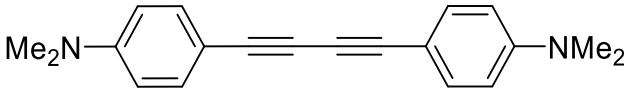


Compound **3d** (1.50 g, 10.3 mmol) was dissolved in 50 mL of MeOH and heated to 50 °C. $Cu(OAc)_2$ (1.87 g, 10.3 mmol) was dissolved in 20 mL of pyridine and added to the MeOH solution. The mixture was stirred at 60 °C for 2 d. The solvent was removed *in vacuo* and the crude product was diluted in hot toluene and washed 3 times with $H_2O$. The organic phase was separated and applied to the top of a 2 cm silica gel column and filtered with hot toluene eluent. After the solvent was removed *in vacuo*, the product was obtained as a yellow powder (1.2 g, 4.2 mmol, 81%). $^1$H NMR (200 MHz, $CDCl_3$): $\delta$ = 7.39 (d, $J_{HH}$ = 9 Hz, 4H, C$H_{arom}$), 6.61 (d, $J$ = 9 Hz, 4H, C$H_{arom}$), 2.99 (s, 12H, N(C$H_3$)$_2$) ppm. GCMS (Method B): $t_R$ = 9.2 min, m/z = 288.

*1,4-bis(p-(methylthiophenyl)buta-1,3-diyne* (**4e**) [6]

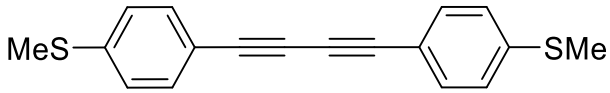


Compound **3e** (2.50 g, 16.8 mmol) was dissolved in 50 mL of MeOH. $Cu(OAc)_2$ (3.05 g, 16.8 mmol) was dissolved in 20 mL of pyridine and added to the MeOH solution. The mixture was stirred at RT for 4 d. The precipitated product was collected *via* filtration and washed with MeOH. The product was dried *in vacuo* and obtained as beige solid (2.30 mg, 7.80 mmol, 93%). $^1$H NMR (200 MHz, $CD_2Cl_2$) $\delta$: 7.44 (d, $J_{HH}$ = 8 Hz, 4H, C$H_{arom}$), 7.22 (d, $J_{HH}$ = 8 Hz, 4H, C$H_{arom}$), 2.53 (s, 6H, SC$H_3$) ppm. GCMS (Method B): $t_R$ = 9.9 min, m/z = 294.

*1,4-bis(pentafluorophenyl)buta-1,3-diyne* (**4f**)[6]

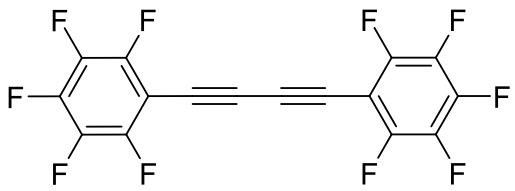


This compound was synthesised according to a typical procedure carried out in this group, for comparable compounds. Compound **3f** diluted in $Et_2O$/THF, CuI (0.04 g 0.20 mmol), $Pd(PPh_3)_2Cl_2$ (0.07 g, 0.10 mmol) and $I_2$ (0.95 g, 3.70 mmol) were suspended in 40 mL of $NEt_3$

and the reaction mixture was stirred for 5 h at RT. The solvent was removed *in vacuo* and the residue was dissolved in 100 mL of DCM. The organic fraction was washed with a saturated $Na_2S_2O_3$ solution (3 x 75 mL) and water (2 x 75 mL), dried over $Na_2SO_4$ and the solvent was subsequently removed *in vacuo*. The product was obtained as a colourless powder (251 mg, 2.7 mmol, 27%). $^{19}F\{^1H\}$ NMR (188 MHz, $CDCl_3$): $\delta$ = -133.8 − -134.0 ppm (m, 4F, C$F_{arom}$), -148.4 − -148.7 (m, 2 F, C$F_{arom}$), -160.2 − -160.5 (m, 4F, C$F_{arom}$) ppm. GCMS(Method A): $t_R$ = 8.1 min, m/z = 382.

*1,4-bis(1-naphthyl)buta-1,3-diyne* (**4g**) [31]

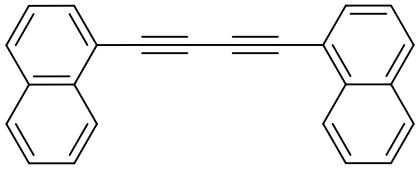

Compound **3g** (3.20 g, 21.0 mmol) was dissolved in 50 mL of MeOH. $Cu(OAc)_2$ (3.80 g, 21.0 mmol) was dissolved in 20 mL of pyridine and added to the MeOH solution. The mixture was stirred at RT for 4 d. The precipitated product was filtered off and washed with MeOH. The product was dried *in vacuo* and the product was obtained as a beige solid (2.76 g, 9.12 mmol, 87%). $^1H$ NMR (200 MHz, $CD_2Cl_2$): $\delta$ = 8.32-8.53 (m, 2H, C$H_{arom}$), 7.78-8.01 (m, 6H, C$H_{arom}$), 7.39-7.73 (m, 6H, C$H_{arom}$) ppm. GCMS (Method B): $t_R$ = 10.7 min, m/z = 302.

*1,4-bis(p-trifluoromethylphenyl)buta-1,3-diyne* (**4h**)[6]

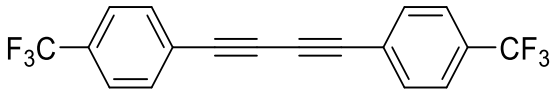


Compound **3h** (2.33 g, 13.6 mmol), CuI (0.06 g, 0.29 mmol), and $Pd(PPh_3)_2Cl_2$ (0.09 g, 0.13 mmol) were slurred in 150 mL of $NEt_3$ and the mixture was stirred for 7 d. After the reaction was finished, the solvent was removed *in vacuo*. The residue was dissolved in hexane and filtered over a short silica column. The product was obtained as an off-white solid (1.53 g, 4.5 mmol, 66%). $^1H$ NMR (300 MHz): $\delta$ = 7.60 (m, 8H, C$H_{arom}$) ppm. $^{19}F\{^1H\}$ NMR (200 MHz,):$\delta$ = -63.03 (s, 6F, C$F_3$) ppm. GCMS (Method B): $t_R$ = 7.24 min, m/z = 338.

**Synthesis of 1,11-Bis(4-(*p*-R-phenyl))Undeca-1,3,8,10-Tetraynes**

*1,11-bis(4-(p-nitrophenyl))undeca-1,3,8,10-tetrayne* (**5a)**

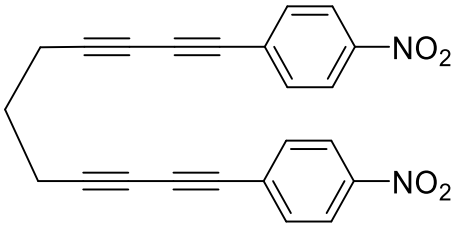


A degassed solution of CuCl (0.02 g, 0.20 mmol) in 115 mL of *n*BuNH$_2$/MeOH (1:6) was charged with a small amount of crystals of NH$_2$OH·HCl (0.1 g, 1.43 mmol). The solution went from blue to colourless immediately. After 10 min **3a** (3.14 g, 21.4 mmol) was added to the solution, which turned to a red suspension subsequently. After 5 more minutes 1,7-dibromo-hepta-1,6.diyne (2.50 g, 10.00 mmol) was added. The reaction mixture was stirred at RT overnight. After the reaction was finished the solvent was removed *in vacuo*, the residue was washed with MeOH and THF. As some of the product was dissolved in THF, the solvent of the mother liquid was removed *in vacuo* again and washed with small portions of THF until residual Cu(II) was removed. The product was obtained as a beige solid (2.30 g, 6.01 mmol, 60%). $^1$H-NMR (500 MHz, C$_6$D$_6$): $\delta$ = 8.26 (d, $J_{HH}$ = 9 Hz, 4H, C$H_{arom}$), 7.74 (d, $J_{HH}$ = 9 Hz, 4H, C$H_{arom}$), 3.49 (m, 2H, C$H_2$), 1.26 (m, 4H, (C$H_2$)$_2$) ppm.

*1,11-bis(4-(p-carbomethoxy-phenyl))undeca-1,3,8,10-tetrayne* (**5b**) [121]

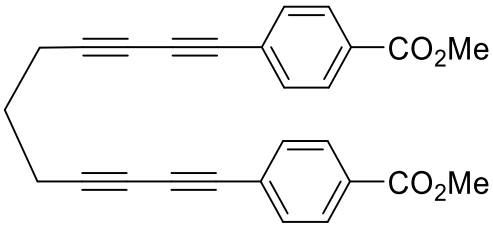


A degassed solution of CuCl (0.05 g, 0.51 mmol) in 100 mL of *n*BuNH$_2$/MeOH (1:2) was charged with a small amount of crystals of NH$_2$OH·HCl (0.5 g, 7.19 mmol). The blue solution subsequently became colourless. After 10 min, **3b** (3.91 g, 24.4 mmol) was added to the solution. After 5 more minutes, 1,7-dibromo-hepta-1,6.diyne (3.05g, 12.2 mmol) was added and a yellow solution formed. The reaction mixture was stirred over night at RT. After the reaction was finished, the solvent was removed *in vacuo* and the residue was diluted in CH$_2$Cl$_2$ and precipitated in MeOH. The precipitate was collected *via* filtration and washed with MeOH. The product was obtained as a white solid (3.65 g, 8.9 mmol, 72%). $^1$H-NMR (500 MHz, C$_6$D$_6$): $\delta$ = 7.83 (d, $J_{HH}$ = 9 Hz, 4H, C$H_{arom}$), 7.23 (d, $J_{HH}$ = 9 Hz, 4H, C$H_{arom}$), 3.42 (s, 6H, OC$H_3$), 1.96 (t, $J_{HH}$ = 7 Hz, 4H, C$H_2$), 1.26 (quint, $J_{HH}$ = 7 Hz, 2H, C$H_2$) ppm.

*1,11-bis(4-(p-tolyl))undeca-1,3,8,10-tetrayne* (**5c**)

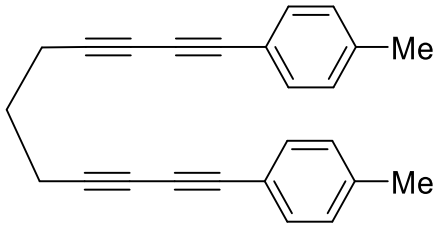


A degassed solution of CuI (0.02 g, 0.19 mmol) in 60 mL of *n*BuNH$_2$/MeOH (1:2) was charged with a small amount of crystals of NH$_2$OH·HCl (0.20 g, 2.87 mmol). The solution subsequently became colourless. After 10 min, **3c** (1.60 g, 10.0 mmol) was added to the solution. After 5 more minutes, 1,7-dibromo-hepta-1,6.diyne (1.25 g, 5.00 mmol) was added and a yellow solution formed. The reaction mixture was stirred at RT for 2 h. After the reaction was finished, the product was collected *via* filtration, diluted in hot hexane, applied on the top of a 5 cm silica gel column and filtered with hot hexane. The product was obtained as an off-white solid (1.00 g, 6.24 mmol, 62%). $^1$H NMR (200 MHz, C$_6$D$_6$): $\delta$ = 7.32 (d, $J_{HH}$ = 8 Hz, 4H, C$H_{arom}$), 7.23 (d, $J_{HH}$ = 8 Hz, 4H, C$H_{arom}$), 1.97 (t, $J_{HH}$ = 7 Hz, 4H, (C$H_2$)$_2$), 1.90 (s, 6H, C$H_3$), 1.27 (quint, $J_{HH}$ = 7 Hz, 2H, C$H_2$) ppm. $^{13}$C{$^1$H} NMR (125 MHz, CDCl$_3$): $\delta$ = 139.34, 132.51, 129.24, 118.85, 82.78, 75.52, 73.67, 66.26, 27.11, 21.65, 18.85 ppm.

Elemental analysis calcd (%) for C$_{25}$H$_{20}$: C 93.71, H 6.29; found: C 93.45, H 6.35.

MS (ESI) *m/z*: calcd: 321.15986 [M]$^+$; found: 321.16363 [M]$^+$.

*1,11-bis(4-(p- N,N-dimethylaniline)undeca-1,3,8,10-tetrayne* (**5d**)

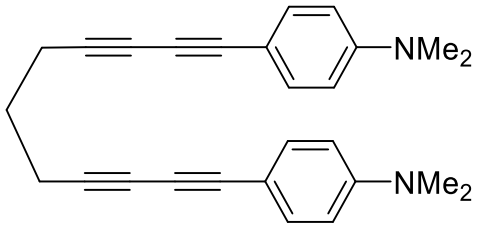


A degassed solution of CuI (0.06 g, 0.38 mmol) in 150 mL of *n*BuNH$_2$/MeOH (1:20) was charged with a small amount of crystals of NH$_2$OH·HCl (0.50 g, 7.19 mmol). The solution subsequently became colourless. After 10 min, **3d** (2.49 g, 17.2 mmol) was added to the solution. After 5 more minutes, 1,7-dibromo-hepta-1,6.diyne (2.03 g, 8.14 mmol) was added and the solution changed to yellow. The reaction mixture was stirred for 1 h and became a yellow suspension. After the reaction was finished the solvent was removed *in vacuo* and the residue was diluted in MeOH and put into the refrigerator for 2 h. Afterwards, the product was collected *via* filtration, recrystallised from MeOH/DCM and dried *in vacuo*. The product was obtained as an orange solid (1.29 g, 3.41 mmol, 40%). $^1$H NMR (500 MHz, C$_6$D$_6$): $\delta$ = 7.36 (d,

$J_{HH}$ = 9 Hz, 4H, C$H_{arom}$), 6.62 (d, $J_{HH}$ = 9 Hz, 4H, C$H_{arom}$), 2.97 (s, 12H, N(C$H_3$)$_2$), 2.51 (t, $J_{HH}$ = 7 Hz, 4H, (C$H_2$)$_2$), 1.81 (quint, $J_{HH}$ = 7 Hz, 2H, C$H_2$) ppm. $^{13}$C{$^1$H} (125 MHz, $CDCl_3$) $\delta$ = 149.36, 132.76, 110.64, 107.13, 81.06, 71.21, 65.47, 39.08, 26.25, 17.83 ppm.

Elemental analysis calcd (%) for $C_{27}H_{26}N_2$: C 85.68, H 6.92, N 7.40; found: C 85.71, H 6.91, N 7.18.

MS (ESI) *m/z*: calcd: 379.21295 $[M]^+$; found: 379.21754 $[M]^+$.

*1,11-bis(4-(p-thioanisole)undeca-1,3,8,10-tetrayne*( **5e**) [121]

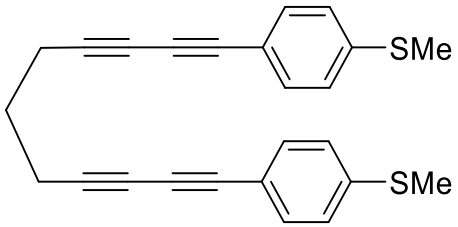


A degassed solution of CuI (0.06 g, 0.68 mmol) in 100 mL of *n*Bu$NH_2$/MeOH (1:2) was charged with a small amount of crystals of $NH_2OH$·HCl (0.50 g, 7.19 mmol). The solution went from blue to colourless subsequently. After 10 min **3e** (3.36 g, 22.7 mmol) was added to the solution. After 5 more minutes the yellow solution 1,7-dibromo-hepta-1,6-diyne (2.81 g, 11.3 mmol) was added and a yellow suspension formed. The reaction mixture was stirred over night at RT. After the reaction was finished, the solvent was removed *in vacuo*, the residue was slurried in MeOH, the product was collected *via* filtration and washed with Methanol. The product was obtained as an off-white solid (1.52 g, 3.95 mmol, 30%). $^1$H NMR (500 MHz, $C_6D_6$): $\delta$ = 7.38 (d, $J_{HH}$ = 9 Hz, 4H, C$H_{arom}$), 7.15 (d, $J_{HH}$ = 9 Hz, 4H, C$H_{arom}$), 2.54 (t, $J_{HH}$ = 7 Hz, 4H, (C$H_2$)$_2$), 2.48 (s, 6H, SC$H_3$), 1.84 (quint, $J_{HH}$ = 7 Hz, 2H, C$H_2$) ppm.

*1,11-bis(4-(p-methoxy-tetrafluorophenyl))undeca-1,3,8,10-tetrayne* (**5f'**)[23]

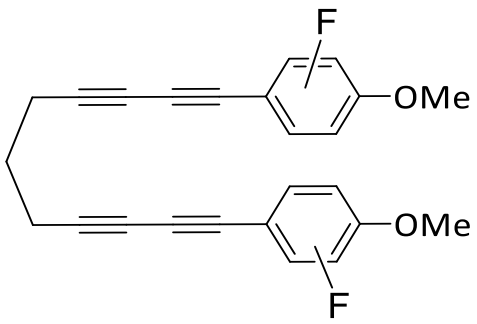


A degassed solution of CuI (0.02 g, 0.20 mmol) in 84 mL of *n*Bu$NH_2$/MeOH (1:20) was charged with a small amount of crystals of $NH_2OH$·HCl (0.50 g, 7.19 mmol). The solution became colourless subsequently. After 10 minutes, **3f'** (1.04 g, 5.08 mmol) was added to the solution,

which turned yellow subsequently. After 5 more minutes, 1,7-dibromo-hepta-1,6.diyne (0.57 g, 2.31 mmol) was added and a yellow suspension formed. The reaction mixture was stirred at 60 °C for 1 h. After the reaction was finished, the solvent was removed *in vacuo*, the residue was washed with cold MeOH and then further purified *via* recrystallisation from a mixture of hot DCM and MeOH. The solution was cooled in a freezer to -30 °C. Colourless crystals could be obtained from the solution (0.57 g, 1.15 mmol, 50 %). $^{1}$H NMR (500 MHz, $C_6D_6$): $\delta$ = 3.32 (t, $J_{HF}$ =1 Hz, 6H; OMe), 1.81 (t, $J_{HH}$ = 7 Hz, 4H; $CH_2$), 1.17 (q, $J_{HH}$ = 7 Hz, 2H; $CH_2$); $^{19}$F{$^{1}$H} NMR (471 MHz, $C_6D_6$): $\delta$ = -158.04 ppm (m, 4F), -137.76 ppm (m, 4F); $^{13}$C NMR (50.3 MHz, $C_6D_6$) = 149.67, 147.67, 141.42, 139.42, 86.52, 84.95, 65.82, 61.06, 60.01, 25.93, 18.16.
Elemental analysis calcd (%) for $C_{27}H_{26}F_8O_2$: C 60.50, H 2.44; found: C 60.52, H 2.21.

*1,11-bis(4-(p-trifluoromethyl-phenyl))undeca-1,3,8,10-tetrayne* (**5h**)

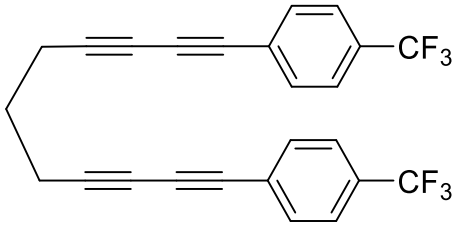


A degassed solution of CuCl (0.08 g, 0.76 mmol) in 70 mL of *n*$BuNH_2$/MeOH (1:2) was charged with a small amount of crystals of $NH_2OH{\cdot}HCl$ (0.5 g, 7.19 mmol). The solution became colourless subsequently. After 10 minutes, **3h** (3.21 g, 18.9 mmol) was added to the solution. After 5 more minutes, 1,7-dibromo-hepta-1,6.diyne (2.36 g, 9.45 mmol) was added and a yellow solution formed. The reaction mixture was stirred for 72 h at RT. After the reaction was finished, the solvent was removed *in vacuo* and the residue was extracted with 150 mL of DCM and washed with a saturated $NH_4Cl$ solution (3 x 100 mL). The organic phase was dried over $Na_2SO_4$, the drying agent was filtered off and the solvent was removed *in vacuo*. The resulting solid was recrystallised from a small amount of acetonitrile and the crystallised product was washed with cold acetonitrile. The product was obtained as an off-white solid (1.64 g, 3.83 mmol, 41%). $^{1}$H NMR (300 MHz, $CDCl_3$): $\delta$ = 7.57 (m, 8H, C$H_{arom}$), 2.56 (t, $J_{HH}$ = 7 Hz, 3H, C$H_2$), 1.87 (quint, $J_{HH}$ = 7 Hz, 2H, C$H_2$) ppm. $^{13}$C {$^{1}$H} NMR (75 MHz, $CDCl_3$): $\delta$ = 132.7, 130.6, 125.8, 125.6, 125.3, 121.9, 84.4, 73.6, 65.8, 26.7, 18.8 ppm. $^{19}$F{$^{1}$H} NMR (188 MHz, $CDCl_3$): $\delta$ = -63.0 (s, 6F, C$F_3$) ppm.
Elemental analysis calcd (%) for $C_{25}H_{14}F_6$: C 70.10, H 3.29; found: C 70.47, H 3.24.
MS (APCI) *m/z*: calcd: 427.0916 $[M]^-$; found: 427.0928 $[M]^-$.

## Synthesis of Metal Complex Starting Materials

*Bis-(triphenylphosphine)-palladium dichloride* **1**

A suspension of $PdCl_2$ (4.0 g, 22.5 mmol) and $PPh_3$ (13.0 g, 49.5 mmol) in 120 mL of degassed benzonitrile was stirred at 180°C for 30 min and at RT overnight. During the reaction, the solution became deep red and the product precipitated as a yellow solid. The product was collected *via* filtration and washed three times with $Et_2O$ (14.5 g, 20.7 mmol, 92%). Elemental analysis calcd (%) for $C_{36}H_{30}Cl_2P_2Pd$: C: 61.60, H: 4.31, found: C: 61.55, H: 4.20.

*Sodium N,N-diethyl-dithiocarbamate* (**20**)[118]

A solution of NaOH (2.0 g, 50 mmol) in 9 mL of $H_2O$ was cooled to 0 °C and charged with $Et_2NH$ (2.49 g, 3.56 mL, 34.0 mmol). $CS_2$ (2.59 g, 34.0 mmol, 2.05 mL) was added dropwise to the solution. The solution subsequently turned yellow and a white precipitate appeared. The reaction mixture was allowed to warm to RT and was stirred for 2 h. When the reaction was finished the product was collected *via* filtration and washed with EtOAc and hexane. The product was obtained as a colourless crystalline solid (4.90 g, 29.0 mmol, 84%). $^1$H NMR (200 MHz): $\delta$ = 4.03 (q, $J_{HH}$ = 7 Hz, 4 H C$H_2$), 1.23 (t, $J_{HH}$ = 7 Hz, 6 H, C$H_3$) ppm.

*Tetrakis-trimethylphosphine-rhodium(I)-chloride* (**6-Cl**)[117]

[Rh(COE)$_2$]Cl (4.00 g, 11.1 mmol) was suspended in 150 mL of THF and heated to 35 °C. Afterwards, 10 eq. of $PMe_3$ (8.66 g, 11.7 mL, 111 mmol) were added dropwise. The solution became deep red and subsequently an orange precipitate appeared. The reaction was stirred at RT overnight, the product was collected *via* filtration and washed with dry $Et_2O$. The product was obtained as a fine orange powder. (4.00 g, 9.04 mmol, 81%). $^1$H NMR (500 MHz): $\delta$ = 1.51 (s, P(C$H_3$)$_3$) ppm. $^{31}$P{$^1$H} NMR(202 MHz): $\delta$ = -16.49 (d, $J_{Rh\text{-}P}$ = 125 Hz) ppm.

*Tris-triphenylphosphine-rhodium(I)-chloride* (**21**, Wilkinson's catalyst)[120]

$RhCl_3 \cdot 3H_2O$ (2.00 g, 7.59 mmol) was dissolved in 70 mL of degassed EtOH and added *via* cannula to a solution of $PPh_3$ (12.0 g, 45.6 mmol, 6.1 eq.) in 350 mL of degassed, hot EtOH (50 °C). The reaction mixture was heated to reflux and stirred for 30 min. After the reaction was finished the hot mixture was filtered, the solid product collected and washed with dry $Et_2O$. The product was obtained as a dark red powder. The NMR showed that the product exists as dimeric species, to a certain amount. (4.80 g, 5.19 mmol, 68%). NMR-data of monomeric species: $^1$H NMR (500 MHz, $CD_2Cl_2$): $\delta$ = 6.7-7.2 (m, $P(C_6H_5)_3$) ppm. $^{31}$P NMR (202 MHz, $CD_2Cl_2$): $\delta$ = -48.10 (dt, $J_{PP}$ = 39 Hz, $J_{RhP}$ = 188 Hz, 1P), 31.38 (dd, $J_{PP}$ = 39 Hz, $J_{RhP}$ = 142 Hz, 2P) ppm.

*Bis-trimethylphosphine-$\kappa^2$-S,S`-dithiocarbamate-rhodium(I)* (**13**)[72]

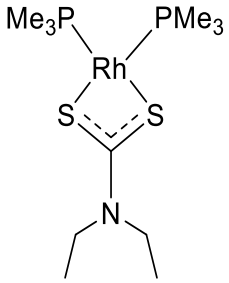


The reaction was carried out in a 20 mL vial under an argon atmosphere in the glovebox. Compound **20** (810 mg, 4.51 mmol) and **6-Cl** (2.00 g, 4.51 mmol) were suspended in 8 mL of THF and stirred overnight at RT. The solution became dark red and a yellow precipitate appeared subsequently. When the reaction was finished, the solution was separated *via* filtration from the solid and the solvent was removed *in vacuo*. The product was obtained as a yellow powder (1.3 g, 3.22 mmol, 72%). $^1$H NMR (300 MHz): $\delta$ = 3.47 (q, $J_{HH}$ = 7 Hz, 4 H C$H_2$), 1.19 (d, $J_{HH}$ = 8 Hz, 9 H, P(C$H_3$)$_3$), 0.90 (t, $J_{HH}$ = 7 Hz, 6 H, C$H_3$) ppm. $^{31}$P{$^1$H} NMR (300 MHz): $\delta$ = - 5.45 (d, $J_{Rh\text{-}P}$ = 172 Hz, 2P, *P*$(CH_3)_3$) ppm.

*Bis-triphenylphosphine-$\kappa^2$-S,S`-dithiocarbamate-rhodium(I)* (**22**)[119]

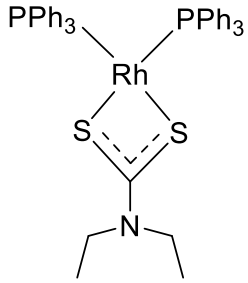


The reaction was carried out in a 100 mL vial under an argon atmosphere in the glovebox. Compounds **21** (1.00 g, 1.08 mmol) and **20** (200 mg, 1.17 mmol) were dissolved in 20 mL of THF and stirred overnight at room temperature. The colour of the solution changed from deep red to orange-red and NaCl precipitated. After the reaction was finished, the reaction mixture was filtered through celite and the solvent was removed *in vacuo*. The solid residue was recrystallised from THF/hexane at -30 °C. The product was obtained as a dark orange, crystalline solid (694 mg, 0.90 mmol, 83%). $^1$H NMR (500 MHz, $C_6D_6$): $\delta$ = 7.86 (m, 12H, C*H*$_{arom}$), 6.94 (m, 18H, C*H*$_{arom}$), 3.12 (q, $J_{HH}$ = 7 Hz, 4H, (C*H*$_2$)$_2$), 0.66 (t, 6H, $J_{HH}$ = 7 Hz, (C*H*$_3$)$_2$) ppm. $^{31}$P{$^1$H} NMR (202 MHz, $C_6D_6$): $\delta$ = 49.31 (d, $J_{Rh\text{-}P}$ = 179 Hz, 2P, *P*(CH$_3$)$_3$) ppm.

Elemental analysis calcd for $C_{41}H_{40}NP_2RhS_2$: C 63.48, H 5.20, N 1.81, S 8.27; found: C63.77, H 5.27, N 1.79, S 8.32.

**Synthesis of Rhodacyclopentadiene and Dibenzorhodacyclopentadiene Complexes**

*Trans-[bis-(trimethylphosphine)-κ²-S,S`-dithiocarbamate-2,5-bis-(4-(p-nitrophenylethynyl))-3,4-μ-trimethylenerhodacyclopenta-2,4-diene]* (**23a**)

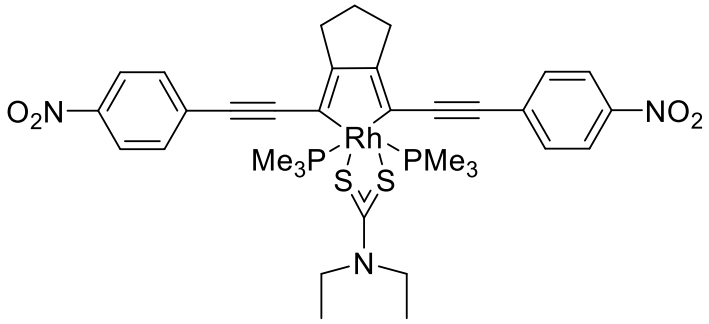


The reaction was prepared in a 20 mL vial under an argon atmosphere in the glovebox. Compounds **13** (0.16 g, 0.39 mmol) and 1 eq. of **5a** (0.15 g, 0.39 mmol) were dissolved in 12 mL of toluene and reacted in the microwave for 24 h at 40 °C. The solvent was removed *in vacuo* and the deep blue residue was washed with hot hexane five times (ultrasonic bath). The solvent of the washing solution was removed *in vacuo* and the residue was recrystallised with THF/hexane at -30 °C. A deep blue solid was obtained. (26 mg, 0.03 mmol, 8%). $^{1}$H NMR (500 MHz, $C_6D_6$): $\delta$ = 7.73 (d, $J_{HH}$ = 9 Hz, 4H, C$H_{arom}$), 7.28 (d, $J_{HH}$ = 9 Hz, 4H, C$H_{arom}$), 3.49 (q, $J_{HH}$ = 7 Hz, 4H, C$H_2$), 2.68 (m, 4H, C$H_2$), 2.20 (quint., $J_{HH}$ = 7 Hz, 2H, C$H_2$), 1.23 (t, $J_{HH}$ = 3 Hz, 18H, P(C$H_3$)$_3$), 0.98 (t, $J_{HH}$ = 7 Hz, 6H, C$H_3$). $^{13}$C{$^{1}$H} NMR (125 MHz, $C_6D_6$) $\delta$ = 210.3, 169.4, 145.6, 137.0, 132.6, 131.1, 106.6, 102.1, 44.4, 30.8, 30.1, 12.8, 12.3 ppm. $^{31}$P{$^{1}$H} NMR (202 MHz, $C_6D_6$): $\delta$ = -7.34 (d, $J_{Rh\text{-}P}$ = 106 Hz, 2P, *P*Me$_3$).

Elemental analysis calcd (%) for $C_{34}H_{42}N_3O_4P_2RhS_2$: C 51.92, H 5.39, N 5.35, S 8.16; found: C 51.92, H 5.51, N 5.47, S 8.16.

MS (APCI) *m/z*: calcd: 786.1220 $[M+H]^+$, 710.0778 $[MH - PMe_3]^+$; found: 786.1199 $[M + H]^+$, 710.0767 $[MH - PMe_3]^+$.

*Trans-[bis(trimethylphosphine)-κ²-S,S`-dithiocarbamate-2,5-bis(4-(p-nitro-phenylethynyl))-dibenzorhodacyclopenta-2,4-diene]* (**24a**)

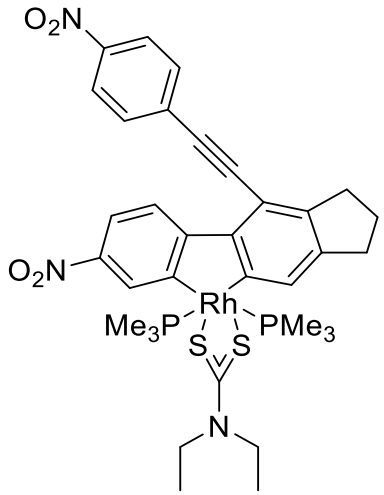


In the glovebox compound **13** (0.16 g, 0.39 mmol) and 1 eq. of **5a** (0.15 g, 0.39 mmol) were dissolved in toluene and stirred in a young's tube at 110 °C for 12 days to get a mixture of compound **23a** and **24a** (3:2). The solvent was removed *in vacuo* and the deep blue residue was washed with hot hexane several times (ultrasonic bath). The solvent of the washing solution was removed *in vacuo* and the residue was recrystallised with THF/hexane at -30 °C. A red crystalline solid was obtained. (2 mg, 2.5 $\mu$mol, 0.7%). $^{1}$H NMR (500 MHz, $C_6D_6$): $\delta$ = 9.27 (d, $J_{HH}$ = 9 Hz, 1H, C$H_{\text{arom}}$), 8.69 (m, 1H, C$H_{arom}$), 8.33 (m, 1H, C$H_{arom}$), 7.78 (d, $J_{HH}$ = 9 Hz, 2H, C$H_{arom}$), 7.64 (s, 1H, C$H_{arom}$), 7.20 (d, $J_{HH}$ = 9 Hz, 2H, C$H_{arom}$), 3.50 (q, $J_{HH}$ = 7 Hz, 4H, $CH_2$), 3.16 (t, $J_{HH}$ = 7 Hz, 2H, C$H_2$), 2.89 (t, $J_{HH}$ =7 Hz, 2H, C$H_2$), 1.98 (quint., $J_{HH}$ = 7 Hz, 2H, C$H_2$), 1.02 (dt, $J_{HH}$ = 7 Hz, 6H, C$H_3$), 0.69 (t, $J_{HH}$ = 3 Hz, 18H, P(C$H_3$)$_3$). $^{13}$C{$^{1}$H} NMR (125 MHz, $C_6D_6$): $\delta$ = 160.1, 147.8, 146.8, 144.7, 143.7, 141.7, 133.0, 131.4, 130.1, 129.0, 123.6, 122.7, 118.1, 113.4, 96.0, 94.8, 44.9, 44.8, 33.2, 33.0, 24.5, 12.5, 12.22, 12.19, one signal could not be detected, due to low intensity. $^{31}$P{$^{1}$H}NMR (202 MHz, $C_6D_6$): $\delta$ = -7.89 (d, $J_{Rh\text{-}P}$ = 104 Hz, 2P, *P*Me$_3$).

Due to the low yield of product, it was not possible to characterise **24a** *via* elemental analysis.

MS (APCI) *m/z*: calcd: 785.1142 [M]$^+$, 709.0708 [M – PMe$_3$]$^+$; found: 785.1119 [M]$^+$, 709.0685 [M – PMe$_3$]$^+$.

*Trans-[bis-(trimethylphosphine)-κ²-S,S`-dithiocarbamate-2,5-bis-(4-(p-carbomethoxy-phenylethynyl))-3,4-μ-trimethylenerhodacyclopenta-2,4-diene]* (**23b**)

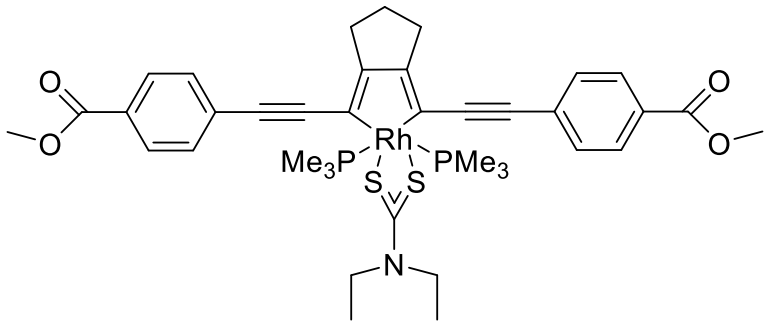


The reaction was prepared in a 20 mL vial under an argon atmosphere in the glovebox. Compounds **13** (0.30 g, 0.74 mmol) and 1eq. of **5b** (0.30 g, 0.74 mmol) were dissolved in THF and stirred at room temperature for 7 d. After the reaction was finished, the solvent was removed *in vacuo* and the deep red residue was dissolved in THF and purified *via* flash chromatography with a THF/hexane eluent (gradient). The solvent was removed *in vacuo* and the crude product was recrystallised from THF/hexane at -30 °C and washed with hot hexane and MeOH five times (ultrasonic bath). The product was obtained as a dark red, crystalline solid (2.00 mg, 2.5 μmol, 0.3%). $^{1}$H NMR (500 MHz, $C_6D_6$): $\delta$ = 8.01 (d, $J_{HH}$ = 9 Hz, 4H; C$H_{arom}$), 7.61 (d, $J_{HH}$ = 9 Hz, 4H; C$H_{arom}$), 3.48 (q, $J_{HH}$ = 7 Hz, 4H, 2 x C$H_2$), 3.42 (s, 6H, 2 x OC$H_3$), 2.72 (sept, $J_{HH}$ = 7 Hz, 4H, 2 x C$H_2$), 2.22 (quint, $J_{HH}$ = 7 Hz, 4H, C$H_2$), 1.26 (t, $J_{HH}$ = 3 Hz, 18H, P(C$H_3$)$_3$), 0.96 (t, $J_{HH}$ = 7 Hz, 6H, 2 x C$H_3$) ppm. $^{13}$C{$^{1}$H} NMR (125 MHz, $C_6D_6$): $\delta$ = 168.2, 166.1, 136.5, 131.4, 131.1, 129.6, 106.9, 99.9, 51.1, 44.4, 30.8, 30.3, 13.1, 12.4 ppm. $^{31}$P{$^{1}$H} NMR (202 MHz, $C_6D_6$): $\delta$ = -7.22 (d, $J_{PP}$ = 107 Hz, 2P, *P*Me$_3$) ppm.

Elemental analysis calcd (%) for $C_{38}H_{48}NO_4P_2RhS_2$: C 56.22, H 5.96, N 1.73, S 7.90 ; found: C 56.45, H 6.10, N 1.98, S 7.88.

MS (APCI) *m/z*: calcd: 812.1628 $[M + H]^+$, 736.1186 $[MH - PMe_3]^+$; found: 812.1609 $[M + H]^+$, 736.1169 $[MH - PMe_3]^+$.

Compound **23b** was alternatively synthesised *via* phosphine exchange starting from compound **25b** (Chap. 2.2.4)

*Trans-[bis(trimethylphosphine)-κ²-S,S`-dithiocarbamate-2,5-bis(4-(p-carbomethoxy-phenylethynyl))-dibenzorhodacyclopenta-2,4-diene]* (**24b**)

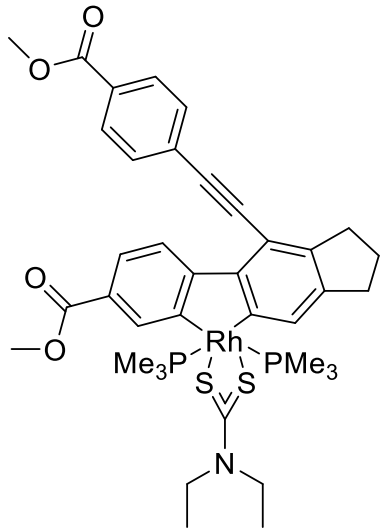


In the glovebox compound **13** (0.30 g, 0.74 mmol) and 1eq of **5b** (0.30 g, 0.74 mmol) were dissolved in 10 mL of THF and stirred in a Young's tube at 90 °C for 7 d to give a 2:1 mixture of **23b** and **24b**. The solvent was removed *in vacuo* and the deep red residue was dissolved in THF and purified *via* flash chromatography with a THF/hexane eluent (gradient). The solvent was removed *in vacuo* and the crude product was recrystallised from THF/hexane at -30 °C and washed with hot hexane and MeOH several times (ultrasonic bath). A pale yellow, crystalline solid was obtained (4 mg, 4.9 µmol, 0.7%). $^{1}$H NMR (500 MHz, $C_6D_6$): $\delta$ = 9.55 (d, $J_{HH}$ = 8 Hz, 1H, C$H_{arom}$), 8.65 (s, 1H, C$H_{arom}$), 8.41 (m, 1H, C$H_{arom}$), 8.04 (d, $J_{HH}$ = 9 Hz, 2H, C$H_{arom}$), 7.69 (s, 1H, C$H_{arom}$), 7.57 (d, $J_{HH}$ = 9 Hz, 2H, C$H_{arom}$), 3.60 (s, 3H, OC$H_3$), 3.55 (m, 4H, C$H_2$), 3.49 (s, 3H, OC$H_3$), 3.24 (t, $J_{HH}$ = 7 Hz, 2H, C$H_2$), 2.94 (t, $J_{HH}$ =7 Hz, 2H, C$H_2$), 1.99 (quint, $J_{HH}$ = 7 Hz, 2H, C$H_2$), 1.03 (t, $J_{HH}$ = 7 Hz, 6H, 2 x C$H_3$), 0.77 (t, $J_{HH}$ = 3 Hz, 18H, P(C$H_3$)$_3$). $^{13}$C{$^{1}$H} NMR (125 MHz): $\delta$ = 167.7, 167.1, 166.9, 165.9, 158.7, 149.1, 143.3, 140.7, 136.0, 132.5, 131.2, 129.8, 129.5, 129.1, 126.5, 124.5, 123.4, 113.5, 96.9, 93.7, 51.3, 51.0, 44.9, 33.4, 33.2, 31.7, 24.7, 22.8, 14.1, 12.7, 12.4. $^{31}$P{$^{1}$H} NMR (202 MHz, $C_6D_6$): $\delta$ = -7.48 (d, $J_{Rh\text{-}P}$ = 106 Hz, 2P, *P*Me$_3$).

Elemental analysis calcd (%) for $C_{38}H_{48}NO_4P_2RhS_2$: C 56.22, H 5.96, N 1.73, S 7.90 ; found: C 56.49, H 6.09, N 1.94, S 7.60.

MS (APCI) *m/z*: calcd: 812.1628 $[M + H]^+$, 736.1186 $[MH - PMe_3]^+$; found: 812.1623 $[M + H]^+$, 736.1184 $[MH - PMe_3]^+$.

*Trans-[bis-(trimethylphosphine)-κ²-S,S`-dithiocarbamate-2,5-bis-(4-(p-tolylethynyl))-3,4-μ-trimethylenerhodacyclopenta-2,4-diene]* (**23c**)

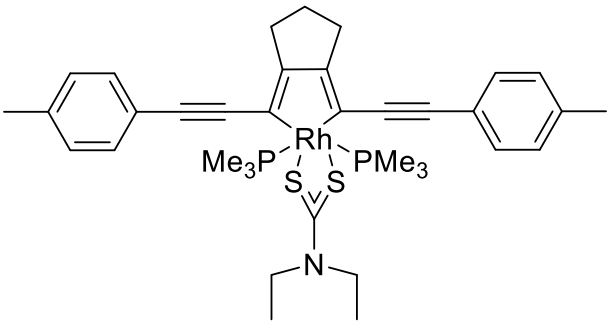


The reaction was prepared in a 20 mL microwave vial under an argon atmosphere in the glovebox. Compound **13** (0.46 g, 1.14 mmol) and 1 eq. of **5c** (0.37 g, 1.15 mmol) were dissolved in 15 mL of THF and stirred for 15 h at 80°C in the microwave reactor. The solvent was removed *in vacuo* and the orange brownish residue washed with hot hexane five times (ultrasonic bath). The solvent was removed and the product was recrystallised from THF/hexane at -30 °C three times and the crystals were again washed with hexane. A dark orange brownish, crystalline product was obtained (60 mg, 83 µmol, 6%). $^{1}$H NMR (500 MHz, $C_6D_6$): $\delta$ = 7.63 (d, $J_{HH}$ = 8 Hz, 4H, C$H_{arom}$), 6.86 (d, $J_{HH}$ = 8 Hz, 4H, C$H_{arom}$), 3.53 (q, $J_{HH}$ = 7 Hz, 4H, 2 x C$H_2$), 2.76 (tt, $J_{HH}$ = 7 Hz, $J$ = 3 Hz 4H, 2 x C$H_2$), 2.24 (quint., $J_{HH}$ = 7 Hz, 2H, C$H_2$), 1.98 (s, 6H, 2 x C$H_3$), 1.32 (t, $J_{HH}$ = 3 Hz, 18H, P(C$H_3$)$_3$), 0.98(t, $J_{HH}$ =7 Hz, 6H, C$H_3$),. $^{13}$C{$^{1}$H} NMR (125 MHz, $C_6D_6$): $\delta$ = 211.0, 165.9, 135.8, 135.5, 131.3, 128.9, 124.2, 106.9, 95.7, 44.3, 30.7, 30.4, 21.0, 13.2, 12.5. $^{31}$P{$^{1}$H} NMR (500 MHz, $C_6D_6$): $\delta$ = -6.97 (d, $J_{Rh\text{-}P}$ = 108 Hz, 2P, *P*Me$_3$).

Elemental analysis calcd (%) for $C_{38}H_{54}N_3P_2RhS_2$: C 59.89, H 6.86, N 1.79, S 8.69; found: C 59.74, H 6.69, N 1.94, S 8.86.

MS (APCI) *m/z*: calcd: 724.1831 $[M + H]^+$, 648.1389 $[MH - PMe_3]^+$; found: 724.1819 $[M + H]^+$, 648.1379 $[MH - PMe_3]^+$.

*Trans-[bis(trimethylphosphine)-κ²-S,S`-dithiocarbamate-2,5-bis(4-(p-tolylethynyl))-dibenzorhodacyclopenta-2,4-diene]* (**24c**)

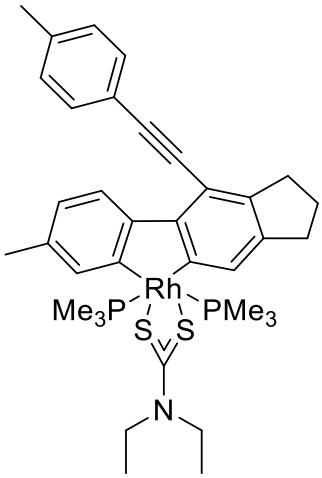


In the glovebox compounds **13** (0.46 g, 1.14 mmol) and 1eq. of **5c** (0.37 g, 1.15 mmol) were dissolved in toluene and stirred in a Young's tube at 110 °C for 16 d to obtain a 2:1 mixture of **23c** and **24c**. The solvent was removed *in vacuo* and the dark brown residue was washed with hot hexane (ultrasonic bath) to separate the product from its isomer. The solvent was removed *in vacuo* and the crude product was recrystallised from THF/hexane at -30 °C and washed with hot hexane. A beige solid was obtained ( 8 mg, 11 µmol, 7%). $^{1}$H NMR (500 MHz, $C_6D_6$): $\delta$ = 9.52 (d, $J_{HH}$ = 8 Hz, 1H, C$H_{arom}$), 7.69 (s, 1H, C$H_{arom}$), 7.67 (d, $J_{HH}$ = 8 Hz, 2H, C$H_{arom}$), 7.59 (s, 1H, C$H_{arom}$), 7.14 (s, 1H, C$H_{arom}$), 6.92 (d, $J_{HH}$ = 8 Hz, 2H, C$H_{arom}$), 3.60 (q, $J_{HH}$ = 7 Hz, 4H, 2 x C$H_2$), 3.35 (t, $J_{HH}$ = 7 Hz, 2H, C$H_2$), 3.00 (t, $J_{HH}$ = 7 Hz, 2H, C$H_2$), 2.40 (s, 3H, C$H_3$), 2.03 (s, 3H, C$H_3$), 2.03 (quint, $J_{HH}$ = 7 Hz, 2H, C$H_2$), 1.06 (t, $J_{HH}$ = 7 Hz, 6H, 2 x C$H_3$), 0.85 (t, $J_{HH}$ = 3 Hz, 18H, P(C$H_3$)$_3$)ppm. $^{13}$C{$^{1}$H} NMR (125 MHz, $C_6D_6$): $\delta$ = 211.1, 166.7, 164.3, 151.4, 150.3, 142.5, 138.9, 137.3, 135.7, 133.9, 131.7, 131.4, 129.2, 124.1, 123.1, 122.3, 112.8, 97.1, 90.7, 45.0, 33.4, 24.8, 21.5, 21.07, 12.8, 12.4 ppm. $^{31}$P{$^{1}$H} NMR (202 MHz, $C_6D_6$): $\delta$ = -7.27 (d, $J_{Rh\text{-}P}$ = 107 Hz, 2P, *P*Me$_3$) ppm.

Due to the low yield of product, it was not possible to characterise **24c** *via* elemental analysis.

MS (LIFDI) *m/z*: calcd: 723.1753 $[M]^+$, 647.1311 $[M - PMe_3]^+$; found: 723.1740 $[M]^+$, 647.1303 $[M - PMe_3]^+$.

*Trans-[bis-(trimethylphosphine)-κ²-S,S`-dithiocarbamate-2,5-bis-(4-(p-N,N'-dimethylamine-phenylethynyl))-3,4-μ-trimethylenerhodacyclopenta-2,4-diene]* (**23d**)

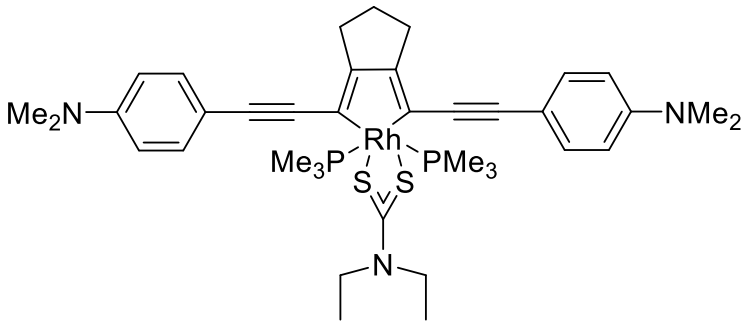


The reaction was prepared in a 20 mL microwave vial under an argon atmosphere in the glovebox. Compounds **13** (0.35 g, 0.87 mmol) and 1eq. of **5d** (0.33 g, 0.87 mmol) were dissolved in THF and stirred in the microwave at 80 °C for 20 h. The solvent was removed *in vacuo* and the brownish residue was dissolved in THF and Hexane (1:4) and precipitated at -30 °C. The solvent was removed and the crude product was washed with hot hexane and MeOH seven times (ultrasonic bath). A brownish solid was obtained (39 mg, 49.8 µmol, 6%). $^{1}$H NMR (500 MHz, $C_6D_6$): $\delta$ = 7.69 (d, $J_{HH}$ = 9 Hz, 4H, C$H_{arom}$), 6.43 (d, $J_{HH}$ = 9 Hz, 4H, C$H_{arom}$), 3.60 (q, $J_{HH}$ = 7 Hz, 4H, C$H_{arom}$), 2.81 (t, $J_{HH}$ = 7 Hz, 2 x C$H_2$), 2.38 (s, 12H, 2 x N(C$H_3$)$_2$), 2.28 (quint, $J_{HH}$ = 7 Hz, 2H, C$H_2$), 1.38 (t, $J_{HH}$ = 4 Hz, 18H, P(C$H_3$)$_3$, 1.03 (t, $J_{HH}$ = 7 Hz, 6H, 2 x C$H_3$) ppm. $^{13}$C{$^{1}$H} NMR (125 MHz, $C_6D_6$): $\delta$ = 211.5, 164.2, 148.9, 135.1, 132.5, 115.2, 112.4, 107.8, 54.2, 44.3, 39.7, 30.5, 13.1, 12.5 ppm. $^{31}$P{$^{1}$H} NMR (500 MHz, $C_6D_6$): $\delta$ = -6.08 (d, $J_{Rh\text{-}P}$ = 110 Hz, 2P, *P*Me$_3$) ppm.

Elemental analysis calcd (%) for $C_{38}H_{54}N_3P_2RhS_2$: C 58.38, H 6.96, N 5.37, S 8.20; found: C 57.93, H 7.05, N 5.42, S 7.82.

MS (APCI) *m/z*: calcd: 782.2362 [M + H]$^+$, 706.1920 [MH – PMe$_3$]$^+$; found: 782.2350 [M + H]$^+$, 706.1913 [MH – PMe$_3$]$^+$.

*Trans-[bis-(trimethylphosphine)-κ²-S,S`-dithiocarbamate-2,5-bis-(4-(p-methylsulfanyl-phenylethynyl))-3,4-μ-trimethylenerhodacyclopenta-2,4-diene]* (**23e**)

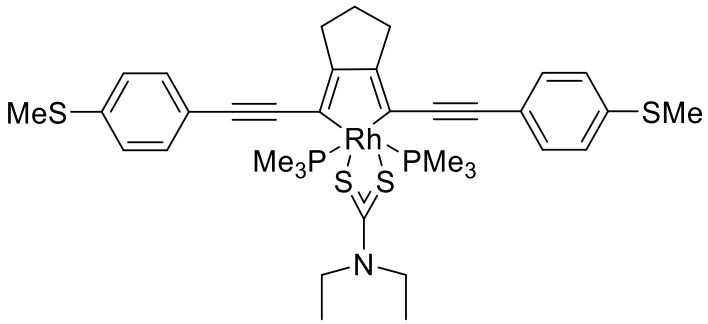


The reaction was prepared in a 20 mL microwave vial under an argon atmosphere in the glovebox. Compound **13** (0.30 g, 0.74 mmol) and 1 eq. of **5e** (0.385 g, 0.74 mmol) were dissolved in 12 mL of THF and stirred for 24 h at 80°C in the microwave reactor. The solvent was removed *in vacuo* and the brownish orange residue was washed with hot hexane several times. The solvent was removed *in vacuo* and the crude product was recrystallised from THF/hexane at -30 °C and washed with hot hexane seven times. An orange powder was obtained (20 mg, 0.025 mmol, 3%). $^{1}$H NMR (300 MHz, $C_6D_6$): $\delta$ = 7.54 (d, $J_{HH}$ = 8 Hz, 4H, C$H_{arom}$), 6.95 (d, $J_{HH}$ = 8 Hz, 4H, C$H_{arom}$), 3.54 (q, $J_{HH}$ = 7 Hz, 4H, C$H_2$), 2.75 (m, 4H, C$H_2$), 2.24 (quint, $J_{HH}$ = 6 Hz, 2H, C$H_2$), 1.88 (s, 6H, SC$H_3$), 1.32 (t, $J_{HH}$ = 4 Hz, 18H, P(C$H_3$)$_3$), 0.99 (t, $J_{HH}$ = 7 Hz, 6H, C$H_3$). $^{13}$C{$^{1}$H} NMR (125 MHz, $C_6D_6$): $\delta$ = 211.1, 166.3, 136.9, 135.6, 131.7, 126.4, 125.6, 123.5, 106.8, 96.6, 44.3, 36.7, 30.4, 15.1, 13.1, 12.4. $^{31}$P{$^{1}$H} NMR (202 MHz, $C_6D_6$): $\delta$ = -7.05 (d, $J_{Rh\text{-}P}$ = 108 Hz, 2P, *P*Me$_3$).

Elemental analysis calcd (%) for $C_{36}H_{48}NP_2RhS_4$: C 54.88, H 6.14, N 1.78, S 16.28; found: C 54.93, H .175, N 1.97, S 16.28.

MS (APCI) *m/z*: calcd. 788.1273 $[M + H]^+$, 712.0813 $[MH - PMe_3]^+$; found: 788.1251 $[M + H]^+$, 712.0809 $[MH - PMe_3]^+$.

*Trans-[bis(trimethylphosphine)-κ²-S,S`-dithiocarbamate-2,5-bis(4-(p-trifluoromethylethynyl))-dibenzorhodacyclopenta-2,4-diene]* (**24e**)

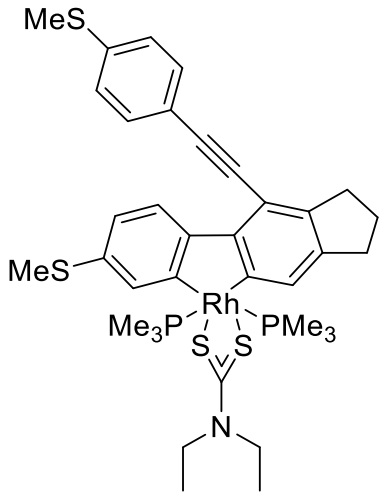


Compound **24e** was obtained *via* exchange of acac by dithiocarbamate. Rh(acac) **16** (100 mg, 0.28 mmol) and 1 eq. of **5e** (109 mg, 0.28 mmol) were dissolved in 3 mL of THF and stirred over 1 w at RT. After the reaction had reached completion, the solvent was removed *in vacuo* and the crude product was washed with hot hexane several times. In the second step compound **24e-acac** (30 mg, 0.04 mmol) and 3 eq. of sodium dithiocarbamate (18 mg, 0.12 mmol) were dissolved in THF and stirred for 10 weeks at 80 °C. After no more change in the reaction could be obtained *via* $^{31}P\{^{1}H\}$ NMR the solvent was removed *in vacuo* and the crude product was washed several times with hot hexane and with hexane in the ultra sonic bath. A beige powder was obtained (15 mg, 0.02 mmol, 50%).Compound **24e** was only characterised *via* NMR-spectroscopy and HRMS, showing 2% of residual **24e-acac**. $^{1}H$ NMR (500 MHz, $C_6D_6$): $\delta$ = 9.50 (d, $J_{HH}$ = 8 Hz, 1H, C$H_{arom}$), 7.80 (s, 1H, C$H_{arom}$), 7.66 (s, 1H, C$H_{arom}$), 7.56 (d, $J_{HH}$ = 8 Hz, 2H, C$H_{arom}$), 7.34 (m, 1H, C$H_{arom}$), 6.99 (d, $J_{HH}$ = 8 Hz, 2H, C$H_{arom}$), 3.56 (q, $J_{HH}$ = 7 Hz, 4H, 2 x C$H_2$), 3.32 (t, $J_{HH}$ = 7 Hz, 2H, C$H_2$), 2.97 (t, $J_{HH}$ = 7 Hz, 2H, C$H_2$), 2.28 (s, 3H, C$H_3$), 2.03 (quint, $J_{HH}$ = 7 Hz, 2H, C$H_2$), 1.90 (s, 3H, C$H_3$), 1.04 (t, $J_{HH}$ = 7 Hz, 6H, 2 x C$H_3$), 0.82 (t, $J_{HH}$ = 3 Hz, 18H, P(C$H_3$)$_3$) ppm. $^{31}P\{^{1}H\}$ NMR (202 MHz, $C_6D_6$): $\delta$ = -7.38 (d, $J_{Rh\text{-}P}$ = 107 Hz, 2P, *P*Me$_3$).

MS (APCI) *m/z*: calcd: 787.1194 $[M]^+$, 711.0753 $[M - PMe_3]^+$; found: 787.11894 $[M]^+$, 711.0746 $[M - PMe_3]^+$.

*Trans-[bis-(trimethylphosphine)-κ²-S,S`-dithiocarbamate-2,5-bis-(4-(p-methoxy-perfluorophenylethynyl))-3,4-μ-trimethylenerhodacyclopenta-2,4-diene]* (**23f'**)

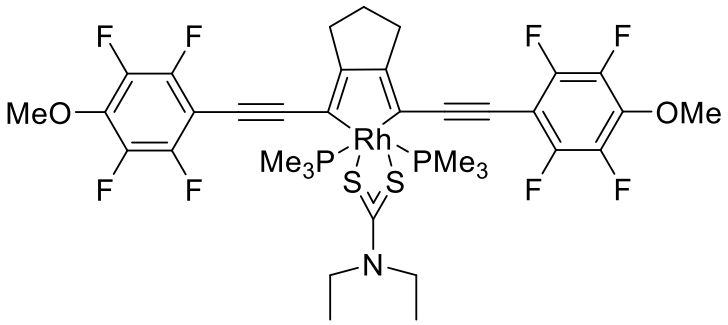


Compound **13** (0.27 g, 0.67 mmol) and 0.5 eq. of **5f'** (0.17 g, 0.34 mmol) were dissolved in 10 mL of toluene and stirred in a Young's tube for 7 d at 60 °C. The solvent was removed *in vacuo* and crude product was washed with hot hexane several times (also ultrasonic bath). The yellow solution was separated from the brownish residue by pipette and the solvent was removed *in vacuo*. The dark orange solid was recrystallised from EtOH at 10 °C several times and washed with pentane several times. An orange, crystalline product was obtained (17 mg, 19 µmol, 5%). $^{1}$H NMR (500 MHz, $C_6D_6$): $\delta$ = 3.41 (q, $J_{HH}$ = 7 Hz, 4H, 2 x C$H_2$), 3.34 (s, 6H, OC$H_3$), 2.68 (sept, $J_{HH}$ = 7 Hz, 4H, 2 x C$H_2$), 2.15 (quint, $J_{HH}$ = 7 Hz, 2H, C$H_2$), 1.34 (t, $J_{HH}$ = 3 Hz, 18H, P(C$H_3$)$_3$), 0.89 (t, $J_{HH}$ = 7 Hz, 6H, C$H_3$) ppm. $^{13}$C{$^{1}$H} NMR (125 MHz, $C_6D_6$): $\delta$ = 210.9, 169.4, 146.9, 144.9, 142.2, 140.2, 136.3, 107.6, 88.6, 61.3, 44.1, 30.8, 30.2, 12.9, 12.3 ppm. $^{31}$P{$^{1}$H} NMR (202 MHz, $C_6D_6$): $\delta$ = -7.37 (d, $J_{Rh\text{-}P}$ = 105 Hz, 2P, *P*Me$_3$). $^{19}$F{$^{1}$H} NMR (500 MHz, $C_6D_6$): $\delta$ = -139.15 − -139.08 (m, 4F, OMe-C$_6F_4$), -159.48 − -159.42 (m, 4F, OMe-C$_6F_4$) ppm.

Elemental analysis calcd (%) $C_{36}H_{40}F_8NO_2P_2RhS_2$: C 48.43, H 4.65, N 1.69, S 6.83; found: C 48.06, H 4.65, N 1.69, S 6.83.

MS (LIFDI) *m/z*: calcd: 899.0897 $[M]^+$; found: 899.0870 $[M]^+$.

*Bimetallic complex* (**24f'-bi**)

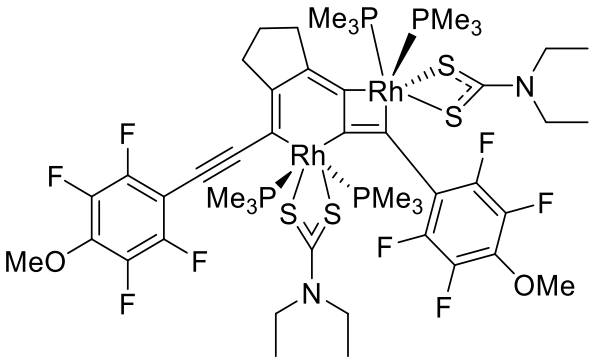


The reaction was prepared in a 20 mL vial under an argon atmosphere in the glovebox. Compounds **13** (0.20 g, 0.46 mmol) and **5f'** (0.25 g, 0.50 mmol) were dissolved in 5 mL of THF and stirred at RT for 24 h. After reaction was finished, the solvent was removed *in vacuo* and the residue was washed with hot hexane several times. The solvent of the mother liquor was removed under vacuum and the remaining solid was recrystallised from a THF/hexane (1:4) mixture at -30 °C. The product was obtained as an orange, crystalline solid (80 mg, 0.06 mmol, 12%). $^{1}$H NMR (500 MHz, $C_6D_6$): $\delta$ = 3.79 (s, 3H, OC$H_3$), 3.65-3.31 (m, 7H, C$H_2$), 3.34 (s, 3H, OC$H_3$), 3.30-3.13 (m, 5H, C$H_2$), 3.07-3.01 (m, 1H, C$H_2$), 2.02-1.85 (m, 2H, C$H_2$), 1.63 (d, $J_{HH}$ = 8 Hz, 9H, P(C$H_3$)$_3$), 1.51 (d, $J_{HH}$ = 8 Hz, 9H, P(C$H_3$)$_3$), 1.32 (d, $J_{HH}$ = 9 Hz, 9H, P(C$H_3$)$_3$), 1.02 (dt, $J_{HH}$ =7 Hz, 6H, C$H_3$), 0.93 (d, $J_{HH}$ = 6 Hz, 9H, P(C$H_3$)$_3$), 0.91 (dt, $J_{HH}$ =7 Hz, 6H, C$H_3$) ppm. $^{13}$C{$^{1}$H} NMR ( 125 MHz, $C_6D_6$) : $\delta$ = 210.6, 207.8, 150.6, 147.2, 145.3, 144.9, 143.2, 142.4, 140.4, 137.7, 135.6, 134.5, 124.0, 115.3, 113.2, 103.1, 82.1, 61.9, 61.3, 44.7, 43.7, 43.6, 42.9, 37.7, 35.5, 25.1, 19.2, 18.9, 17.8, 15.4, 14.7, 14.6, 12.6, 12.4, 12.1 ppm. $^{31}$P NMR (202 MHz, $C_6D_6$): $\delta$ = 0.60 (dd, $J_{Rh\text{-}Rh}$ = 3 Hz, $J_{P\text{-}P}$ = 24 Hz, $J_{Rh\text{-}P}$ = 153 Hz, 1P, *P*Me$_3$), -9.5, -12.04, -13.94, -16.49 (2 dd, $J_{P\text{-}P}$ = 508 Hz, $J_{Rh\text{-}P}$ = 108 Hz and 112 Hz, 2P, *P*Me$_3$), -29.99 (dd, $J_{P\text{-}P}$ = 24 Hz, $J_{Rh\text{-}P}$ = 85 Hz, 1P, *P*Me$_3$) ppm. $^{19}$F{$^{1}$H} NMR (500 MHz, $C_6D_6$): $\delta$ = -133.98 − -134.19 (m, 1F, OMe-C$_6F_4$), -138.55− -138.74 (m, 1F, OMe-C$_6F_4$), -139.23 − -139.38 (m, 2F, OMe-C$_6F_4$), -159.99 − -160.18 (m, 2F, OMe-C$_6F_4$), -160.61 − -160.76 (m, 1F, OMe-C$_6F_4$) -161.80 − -161.98 (m, 1F, OMe-C$_6F_4$) ppm.

Elemental analysis calcd (%) for $C_{49}H_{82}F_8N_2O_2P_4Rh_2S_4$: C 43.32, H 5.26, N 2.15, S 9.84; found: C 43.55, H 5.35, N 2.39, S 9.77.

MS (LIFDI) *m/z*: calcd: 1302.1091 [M]$^+$, 1226.0649 [M – PMe$_3$]$^+$, 1150.0207 [M – 2 PMe$_3$]$^+$, 1073.9765 [M – 3 PMe$_3$]$^+$; found: 1302.1075 [M]$^+$, 1226.0616 [M – PMe$_3$]$^+$, 1150.0178 [M – 2 PMe$_3$]$^+$, 1073.9740 [M – 3 PMe$_3$]$^+$.

*Trans-[bis-(triphenylphosphine)-κ²-S,S`-dithiocarbamate-2,5-bis-(4-(p-nitrophenylethynyl))-3,4-μ-trimethylenerhodacyclopenta-2,4-diene]* (**25a**)

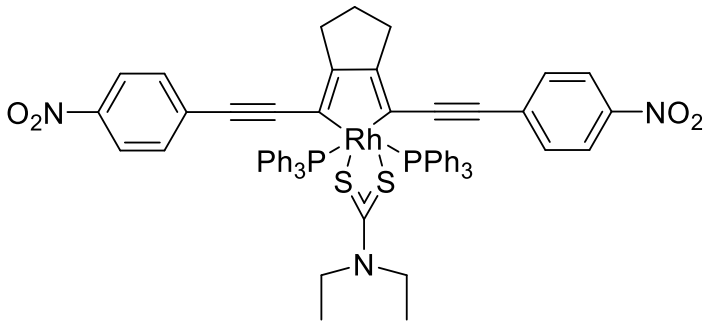


The reaction was prepared in a 20 mL vial under an argon atmosphere in the glovebox. Compounds **22** (0.20 g, 0.26 mmol) and 1 eq. of **5a** (0.10 g, 0.26 mmol) were dissolved in 5 mL of THF and stirred at RT for 24 h. The solvent was removed *in vacuo* and the deep blue residue was washed with hot hexane seven times (ultrasonic bath). The solvent of the washing solution was removed *in vacuo* and the residue was recrystallised with THF/hexane at -30 °C and again washed with hexane six times. A deep blue solid was obtained (16 mg, 13.8 µmol, 5%). $^{1}$H NMR (300 MHz, $C_6D_6$): $\delta$ = 7.86-7.99,6.93-7.08 (m, 30H, 2 x P($C_6H_5$)$_3$), 7.88 (d, $J_{HH}$ = 9 Hz, 4H, C$H_{arom}$), 7.50 (d, $J_{HH}$ = 9 Hz, 4H, C$H_{arom}$), 2.76 (q, $J_{HH}$ = 7 Hz, 4H, 2 x C$H_2$), 1.90 (m, 4H, 2 x C$H_2$), 1.25 (quint, $J_{HH}$ =7 Hz, 2H, C$H_2$), 0.48 (t, $J_{HH}$ = 7 Hz, 6H, 2 x C$H_3$)ppm. $^{13}$C NMR (125 MHz, $C_6D_6$): $\delta$ = 175.5, 145.8, 135.5, 133.8, 131.2, 129.1, 126.7, 123.9, 108.4, 105.6, 43.6, 30.5, 27.9, 11.8 ppm, due to low intensity, one signal could not be detected. $^{31}$P{$^{1}$H} NMR (300 MHz, $C_6D_6$): $\delta$ = 32.18 (d, $J_{Rh\text{-}P}$ = 109 Hz, 2P, *P*Ph$_3$) ppm.

Elemental analysis calcd (%) for $C_{64}H_{54}N_3O_4P_2RhS_2$: C 66.53, H 4.77, N 3.67, S 5.33; found: C 66.37, H 4.70, N 3.63, S 5.54.

MS (APCI) *m/z*: calcd: 896.1247 [MH – PPh$_3$]$^+$; found: 896.1226 [MH – PPh$_3$]$^+$.

*Trans-[bis-(triphenylphosphine)-κ²-S,S`-dithiocarbamate-2,5-bis-(4-(p-carbomethoxy-phenylethynyl))-3,4-μ-trimethylenerhodacyclopenta-2,4-diene]* (**25b**)

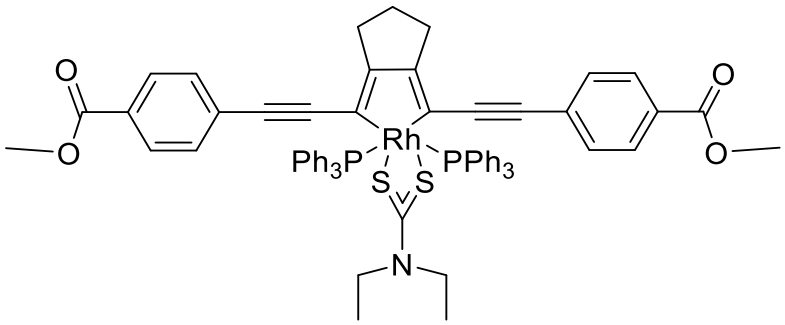


The reaction was prepared in a 20 mL vial under an argon atmosphere in the glovebox. Compounds **22** (0.30 g, 0.39 mmol) and 1 eq. of **5b** (0.16 g, 0.39 mmol) were dissolved in 10 mL of THF and stirred at RT for 1 day. The solvent was removed *in vacuo* and the violet residue was recrystallised from THF/hexane (1:4) at -30 °C and washed with hot hexane several times (ultrasonic bath). A violet, crystalline product was obtained (200 mg, 0.17 mmol, 43%). $^{1}$H NMR (500 MHz, $C_6D_6$): $\delta$ = 7.99-8.00, 6.97-7.05 (m, 30H, 2 x P($C_6H_6$)$_3$), 8.15 (d, $J_{HH}$ = 9 Hz, 4H, C$H_{arom}$), 7.79 (d, $J_{HH}$ = 9 Hz, 4H, C$H_{arom}$), 3.52 (s, 6H, OC$H_3$), 2.76 (q, $J_{HH}$ = 7 Hz, 4H, 2 x C$H_2$), 1.92 (m, 4H, 2 x C$H_2$), 1.52 (quint, $J_{HH}$ =7 Hz, 2H, C$H_2$), 0.46 (t., $J_{HH}$ = 7 Hz, 6H, 2 x C$H_3$) $^{13}$C{$^{1}$H} NMR (125 MHz, $C_6D_6$): $\delta$ = 174.1, 166.3, 135.0, 134.9, 134.1, 131.5, 131.1, 129.9,128.8, 126.7, 108.7, 103.3, 67.5, 51.3, 43.6, 30.4, 27.9, 25.5, 11.8 ppm. $^{31}$P{$^{1}$H} NMR (500 MHz, $C_6D_6$): $\delta$ = 32.58 (d, $J_{Rh\text{-}P}$ = 109 Hz, 2P, *P*$Ph_3$) ppm.

Elemental analysis calcd (%) for $C_{68}H_{60}NO_4P_2RhS_2$: C 68.90, H 5.30, N 1.37, S 5.04; found: C 68.97, H 5.11, N 1.18, S 5.41.

MS (APCI) *m/z*: calcd: 922.1655 [MH – $PPh_3$]$^+$; found: 922.1635 [MH – $PPh_3$]$^+$.

.

*Trans-[bis-(triphenylphosphine)-κ²-S,S`-dithiocarbamate-2,5-bis-(4-(p-tolylethynyl))-3,4-μ-trimethylenerhodacyclopenta-2,4-diene]* (**25c**)

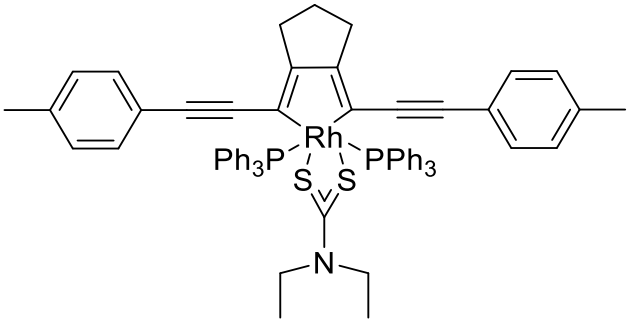


The reaction was prepared in a 20 mL vial under an argon atmosphere in the glovebox. Compound **22** (0.40 g, 0.5 mmol) and **5c** (0.17 g, 0.5 mmol) were dissolved in 10 mL of THF and stirred at RT for 1 d to obtain a 1:1 mixture of **22** and **25c** and organic trimer **27**. The solvent was removed *in vacuo* and the orange residue diluted with THF and hexane to precipitate the organic product. The mother liquor was concentrated and stored in the freezer to crystallise the starting compound **22**. Afterwards, the mother liquor was separated and the solvent was removed *in vacuo*. The brownish residue was washed with pentane seven times and dried *in vacuo*. It was not possible to obtain **25c** without phosphine oxide, due to this characterisation was only carried out via $^{1}$H, $^{13}$C and $^{31}$P{$^{1}$H} NMR and high resolution mass spectroscopy. $^{1}$H NMR (300 MHz, $C_6D_6$): $\delta$ = 8.14-8.05 (m, 12H, P($C_6H_5$)$_3$), 7.81 (d, $J_{HH}$ = 8 Hz, 4H, C$H_{arom}$), 7.11-6.95 (m, 18H, P($C_6H_5$)$_3$), 4H, C$H_{arom}$), 2.80 (q, $J_{HH}$ = 7 Hz, 4H, 2xC$H_2$), 2.12 (s, 6H, 2xC$H_3$), 1.95 (m, 4H, 2xC$H_2$), 1.54 (quint., $J_{HH}$ = 7., 2H, C$H_2$), 0.47 (t, $J_{HH}$ = 7 Hz, 6H, C$H_3$) ppm. $^{13}$C (125 MHz, $C_6D_6$) ): $\delta$ = 205.1, 171.5, 136.0, 135.7, 134.5, 133.6, 131.3, 129.2, 128.5, 126.5, 124.3, 108.5, 99.1, 43.4, 30.3, 27.9, 21.0, 11.8 ppm. $^{31}$P NMR (202 MHz, $C_6D_6$): $\delta$ = 32.86 (d, $J_{Rh-P}$ = 111 Hz, 2P, *P*Ph$_3$) ppm.

MS (LIFDI) *m/z*: calcd: 1095.2692 $[M]^+$, 833.1781 $[M - PPh_3]^+$; found: 1095.2679 $[M]^+$, 833.1769 $[M - PPh_3]^+$.

*Trans-[bis-(triphenylphosphine)-κ²-S,S`-dithiocarbamate-2,5-bis-(4-(p-thioanisole-ethynyl))-3,4-μ-trimethylenerhodacyclopenta-2,4-diene]* (**25e**)

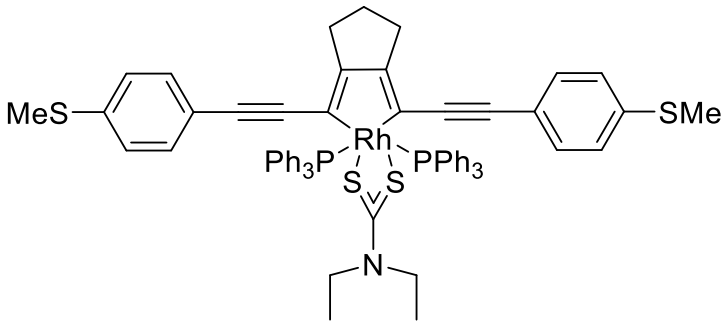


The reaction was prepared in a 20 mL vial under an argon atmosphere in the glovebox. Compound **22** (0.20 g, 0.25 mmol) and 1 eq. of **5e** (0.10 g, 0.25 mmol) were dissolved in 10 ml of THF and stirred at RT for 1 day. The solvent was removed *in vacuo* and the red residue was washed with hot hexane and MeOH several times. The product was obtained as a red powder (6 mg, 0.005 mmol, 2%). $^{1}$H NMR (500 MHz, $C_6D_6$): $\delta$ = 8.10-8.02 (m, 12H, P($C_6H_6$)$_3$), 7.75 (d, $J_{HH}$ = 8 Hz, 4H, C$H_{arom}$), 7.09 (d, $J_{HH}$ = 8 Hz, 4H, C$H_{arom}$), 7.08-6.98 (m, 18H, P($C_6H_6$)$_3$), 2.80 (q, $J_{HH}$ = 7 Hz, 4H, 2 x C$H_2$), 1.99 (s, 6H, 2xC$H_3$), 1.94 (m, 4H, 2 x C$H_2$), 1.55 (quint, $J_{HH}$ =7 Hz, 2H, C$H_2$), 0.49 (t, $J_{HH}$ = 7 Hz, 6H, 2xC$H_3$) ppm. $^{31}$C{$^{1}$H} NMR (125 MHz, $C_6D_6$): $\delta$ = 205.0, 172.0, 137.2, 135.7, 134.4, 133.8, 131.7, 128.6, 126.5, 126.4, 123.5, 108.4, 99.9, 43.4, 30.3, 28.0, 14.9, 11.8 ppm. $^{31}$P{$^{1}$H} NMR (121 MHz, $C_6D_6$): $\delta$ = 32.70 (d, $J_{Rh\text{-}P}$ = 111 Hz, 2P, *P*$Ph_3$) ppm.

Elemental analysis calcd (%) for $C_{66}H_{60}NP_2RhS_4$: C 68.32, H 5.21, N 1.21, S 11.05; found: C 68.32, H 5.51, N 1.40, S 10.88.

MS (LIFDI) *m/z*: calcd: 1159.2133 $[M]^+$, 897.1222 $[M - PPh_3]^+$; found: 1159.2113 $[M]^+$, 897.1204 $[M - PPh_3]^+$.

*Trans-[bis-(triphenylphosphine)-κ²-S,S`-dithiocarbamate-2,5-bis-(4-(p-methoxy-perfluorophenylethynyl))-3,4-μ-trimethylenerhodacyclopenta-2,4-diene]* (**25f'**)

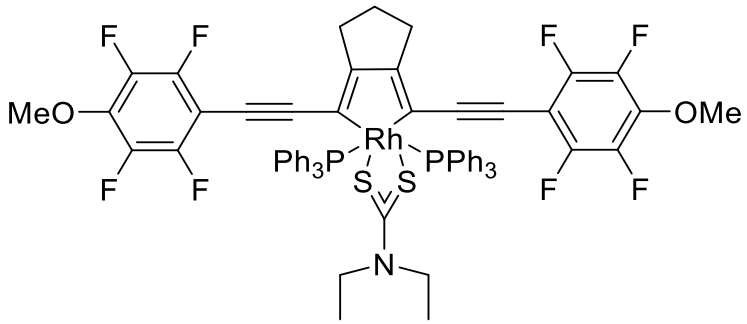


The reaction was prepared in a 20 mL vial under an argon atmosphere in the glovebox. Compounds **22** (0.40 g, 0.51 mmol) and of **5f'** (0.25 g, 0.51 mmol) were dissolved in THF and stirred at RT for 3 days to obtain a 7:1 mixture of **25f** and **22** and organic trimer **27f'**. The solvent was removed *in vacuo* and the orange residue was recrystallised from THF/hexane (1:4) at -30 °C to remove the starting material and washed with hot hexane several times (ultrasonic bath). The product was obtained as a red, amorphous powder (90 mg, 0.07 mmol, 20%). $^{1}$H NMR (500 MHz, $C_6D_6$): $\delta$ = 8.03-8.07, 7.13-7.16, 7.01-7.03 (m, 30H, 2xP($C_6H_5$)$_3$), 3.43 (s, 6H, OC$H_3$), 2.71 (q, $J_{HH}$ = 7 Hz, 4H, 2 x C$H_2$), 1.96 (sept, $J_{HH}$ = 8 Hz, 4H, 2 x C$H_2$), 1.44 (quint, $J_{HH}$ =8 Hz, 2H, C$H_2$), 0.40 (t., $J_{HH}$ = 7 Hz, 6H, 2 x C$H_3$) ppm. $^{13}$C{$^{1}$H} (125 MHz, $C_6D_6$): $\delta$ = 147.0, 145.1, 142.4, 140.4, 136.8, 135.8, 134.3, 133.7, 128.9, 126.6, 110.9, 102.1, 90.1, 61.4, 43.3, 30.63, 27.8, 11.8 ppm. $^{31}$P{$^{1}$H} NMR (500 MHz, $C_6D_6$): $\delta$ = 33.21 (d, $J_{Rh\text{-}P}$ = 107 Hz, 2P, *P*Ph$_3$) ppm.

Elemental analysis calcd (%) for $C_{66}H_{52}F_8NO_2P_2RhS_2$: C 62.41, H 4.05, N 1.35, S 4.57; found: C 62.32, H 4.12, N 1.10, S 5.04.

MS (APCI) *m/z*: calcd: 1010.1003 [MH – PPh$_3$]$^+$; found: 1010.0972 [MH – PPh$_3$]$^+$.

**Synthesis of Benzene Derivatives**

*Dimer* (**26b**)

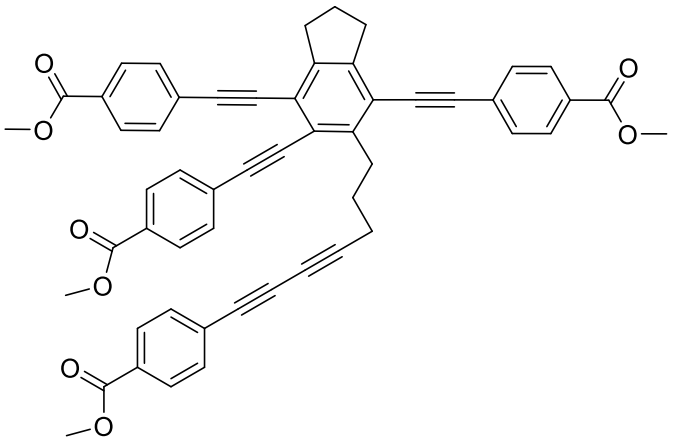

The reaction was prepared in a 20 mL vial under an argon atmosphere in the glovebox. Compound **22** (3 mg, 0.004 mmol) and 100 eq. of compound **5b** (0.16 g, 0.39 mmol) were dissolved in 10 mL of THF and stirred at RT for 8 days. A white solid precipitated from the solution, which turned out to be a 20:1 mixture of dimeric and trimeric species. The solid was filtrated from the solution, washed with hexane and recrystallised from hot toluene to separate the two species. A white amorphous solid was obtained (35 mg, 0.04 mmol, 11%). $^{1}$H NMR (500 MHz, $C_6D_6$): $\delta$ = 8.03 (d, $J_{HH}$ = 8 Hz, 2H, C$H_{arom}$), 8.01 (d, $J_{HH}$ = 8 Hz, 2H, C$H_{arom}$), 8.00 (d, $J_{HH}$ = 8 Hz, 2H, C$H_{arom}$), 7.96 (d, $J_{HH}$ = 8 Hz, 2H, C$H_{arom}$), 7.64 (d, $J_{HH}$ = 8 Hz, 2H, C$H_{arom}$), 7.63 (d, $J_{HH}$ = 8 Hz, 2H, C$H_{arom}$), 7.60 (d, $J_{HH}$ = 8 Hz, 2H, C$H_{arom}$), 7.46 (d, $J_{HH}$ = 8 Hz, 2H, C$H_{arom}$), 3.94 (s, 3H, OC$H_3$), 3.92 (s, 3H, OC$H_3$), 3.90 (s, 3H, OC$H_3$), 3.89 (s, 3H, OC$H_3$), 3.30-3.33 (m, 2H, C$H_2$), 3.13-3.18 (m, 4H, 2 x C$H_2$), 2.58 (t, $J_{HH}$ = 7 Hz, 2H, C$H_2$), 2.19 (quint, $J_{HH}$ = 7 Hz, 2H, C$H_2$), 2.07 (quint., $J_{HH}$ = 7 Hz, 2H, C$H_2$). $^{13}$C (125 MHz, $CD_2Cl_2$): $\delta$ = 166.2, 166.17, 166.15, 166.13, 148.3, 145.3, 144.1, 132.4, 131.5, 131.47, 131.41, 130.2, 130.0, 129.9, 129.8, 129.54, 129.53, 129.5, 129.3, 127.8, 127.7, 127.6, 126.5, 122.75, 121.9, 119.6, 96.9, 96.8, 95.8, 89.9, 89.7, 88.7, 86.2, 77.1, 73.9, 65.3, 52.2, 52.13, 52.07, 33.8, 33.3, 32.8, 28.4, 23.9, 19.9 ppm.

Elemental analysis calcd (%) for $C_{54}H_{40}O_8$: C 79.40, H 4.94; found: C 79.02, H 5.00.

MS (APCI) *m/z*: calcd: 817.2796 $[M + H]^+$; found: 817.2787 $[M + H]^+$.

*Dimer* (**26c**)

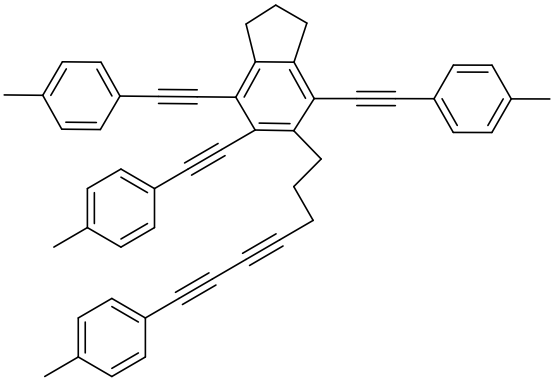

The reaction was prepared in a 20 mL vial under an argon atmosphere in the glovebox. Compound **22** (4 mg, 0.0054 mmol) and 100 eq. of compound **5c** (0.17 g, 0.54 mmol) were dissolved in 10 mL of THF and stirred at RT for 7 days. After the reaction was finished, the solvent was removed *in vacuo*. The obtained solid was dissolved in $CHCl_3$ and precipitated with hexane. The solvent was separated from the solid *via* pipette and washed several times with hot methanol and hexane. Afterwards the solid was recrystallised from a $CD_2Cl_2$/ hexane mixture. A crystalline, beige solid was obtained (7 mg, 0.01 mmol, 2%). $^1$H NMR (500 MHz, $CDCl_3$): $\delta$ = 7.50 (d, $J_{HH}$ = 8 Hz, 2H, C$H_{arom}$), 7.47 (d, $J_{HH}$ = 8 Hz, 4H, 2 x C$H_{arom}$), 7.37 (d, $J_{HH}$ = 8 Hz, 2H, C$H_{arom}$), 7.16 (d, $J_{HH}$ = 8 Hz, 2H, C$H_{arom}$), 7.15 (d, $J_{HH}$ = 8 Hz, 2H, C$H_{arom}$), 7.14 (d, $J_{HH}$ = 8 Hz, 2H, C$H_{arom}$), 7.10 (d, $J_{HH}$ = 8 Hz, 2H, C$H_{arom}$), 3.28-3.31 (m, 2H, C$H_2$), 3.12 (q, $J_{HH}$ = 8 Hz, 4H, 2 x C$H_2$), 2.55 (t, $J_{HH}$ = 7 Hz, 2H, C$H_2$), 2.38 (s, 3H, C$H_3$), 2.35 (s, 3H, C$H_3$), 2.34 (s, 6H, 2 x C$H_3$), 2.15 (quint, $J_{HH}$ = 8 Hz, 2H, C$H_2$), 2.06 (quint, $J_{HH}$ = 8 Hz, 2H, C$H_2$). $^{13}$C (125 MHz, $CDCl_3$): $\delta$ = 146.9, 144.6, 143.5, 139.1, 138.7 138.6, 138.4, 132.6, 131.70, 131.66, 131.6, 129.4, 129.31, 129.28, 129.2, 123.4, 122.0, 120.7, 120.68, 120.4, 119.6, 119.3, 97.7, 97.6, 96.7, 87.2. 86.8, 95.9, 84.5, 75.2, 74.2, 65.8, 33.9, 33.5, 33.1, 28.7, 24.1, 21.7, 21.6, 20.1 ppm, one signal was not detected, due to low intensity.

Elemental analysis calcd (%) for $C_{50}H_{40}$: C 93.71, H 6.29; found: C 93.43, H 6.64.

MS (APCI) *m/z*: calcd: 641.3203 $[M + H]^+$; found: 641.3191 $[M + H]^+$.

*Dimer* (**26d**)

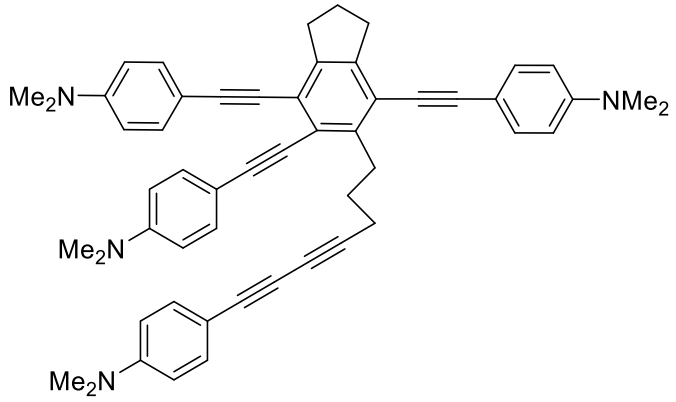


The reaction was prepared in a 20 mL vial under an argon atmosphere in the glovebox. Compounds **22** (83 mg, 0.11 mmol) and 50 eq. of **5d** (2.0 g, 5.2 mmol) were dissolved in 10 mL of THF and stirred at RT for 14 d. After the reaction was finished, the solvent concentrated *in vacuo* and the crude product was precipitated in hexane. The solvent was separated from the solid *via* pipette and the solid was washed with hot hexane and dried *in vacuo*. Afterwards the crude product was filtered over a short alumina column, which was deactivated with 10 mol % of distilled $H_2O$, with $CH_2Cl_2$/hexane eluent (1:3). The product was obtained as a beige, powder (148 mg, 0.20 mmol, 4%). $^1$H NMR (500 MHz, $CD_6D_6$): $\delta$ = 7.89 (d, $J_{HH}$ = 9 Hz, 2H, C$H_{arom}$), 7.80 (d, $J_{HH}$ = 9 Hz, 2H, C$H_{arom}$), 7.76 (d, $J_{HH}$ = 9 Hz, 2H, C$H_{arom}$), 7.40 (d, $J_{HH}$ = 9 Hz, 2H, C$H_{arom}$), 6.53 (d, $J_{HH}$ = 9 Hz, 2H, C$H_{arom}$), 6.51 (d, $J_{HH}$ = 9 Hz, 2H, C$H_{arom}$), 6.45 (d, $J_{HH}$ = 9 Hz, 2H, C$H_{arom}$), 6.21 (d, $J_{HH}$ = 9 Hz, 2H, C$H_{arom}$) 3.69-3.72 (m, 2H, C$H_2$), 3.10-3.15 (m, 4H, 2 x C$H_2$), 2.52 (t, $J_{HH}$ = 8 Hz, 2H, C$H_2$), 2.40 (s, 6H, N(C$H_3$)$_2$), 2.38 (s, 6H, N(C$H_3$)$_2$), 2.37 (s, 6H, N(C$H_3$)$_2$), 2.31 (s, 6H, N(C$H_3$)$_2$), 2.27 (quint, $J_{HH}$ = 8 Hz, 2H, C$H_2$), 1.84 (quint, $J_{HH}$ = 8 Hz, 2H, C$H_2$). $^{13}$C(125 MHz, $CDCl_3$): $\delta$ = 150.4, 150.22, 150.19, 150.1, 145.5, 143.8, 142.7, 133.9, 132.9, 132.88, 132.87, 123.5, 121.5, 119.5, 112.2, 112.1, 112.0, 111.8, 111.0, 110.6, 108.9, 98.42, 98.39, 97.5, 86.4, 85.9, 85.0, 84.0, 76.3, 73.1, 66.1, 40.4, 40.3, 40.2, 33.9, 33.5, 33.2, 28.8, 24.1, 20.3 ppm, one signal was not detected, due to low intensity.

Elemental analysis calcd (%) for $C_{54}H_{52}N_4$: C 85.68, H 6.92, N 7.40; found: C 84.72, H 6.74, N 7.93.

MS (APCI) *m/z*: calcd: 757.4265 $[M + H]^+$; found: 757.4251 $[M + H]^+$.

*Dimer* (**26f'**)

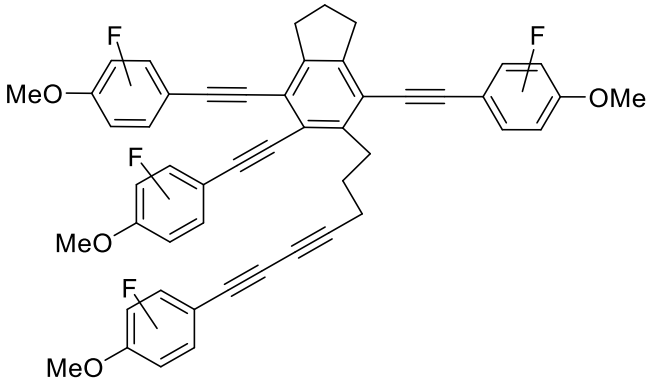


The reaction was prepared in a 20 mL vial under an argon atmosphere in the glovebox. Compounds **22** (3.50 mg, 4.5 $\mu$mol) and 100 eq. of **5f'** (0.224 g, 0.45 mmol) were dissolved in 10 mL of THF and stirred at RT for 14 days. A white solid precipitated from the solution, which was a 20:1 mixture of dimeric and trimeric species. The solid was separated from the solution by filtration, washed with hexane and recrystallised from hot toluene three times to separate the two species. A white amorphous solid was obtained (40 mg, 0.04 mmol, 9%). $^{1}$H NMR (500 MHz, $CDCl_3$): $\delta$ = 4.13 (t, $J_{HF}$ = 1 Hz, 3H, OC$H_3$), 4.12 (t, $J_{HF}$ = 1 Hz, 3H, OC$H_3$), 4.11 (t, $J_{HF}$ = 2 Hz, 3H, OC$H_3$), 4.10 (t, $J_{HF}$ = 2 Hz, 3H, OC$H_3$), 3.23-3.26 (m, 2H, C$H_2$), 3.10-3.16 (m, 4H, 2 x C$H_2$), 2.53 (t, $J_{HH}$ = 7.15 Hz, 2H, C$H_2$), 2.19 (quint, $J_{HH}$ = 8 Hz, 2H, C$H_2$), 2.03 (quint., $J_{HH}$ = 7 Hz, 2H, C$H_2$) $^{19}$F NMR (500 MHz, $CDCl_3$): $\delta$ = -137.25 − -137.36 (m, 4H, C$F_{arom}$), -137.42 − -137.59 (m, 4H, C$F_{arom}$), -157.89 − -158.03 (m, 4H, C$F_{arom}$), -158.16 − -158.27 (m, 4H, C$F_{arom}$) $^{13}$C(125 MHz, $CDCl_3$): $\delta$ = 148.8, 148.4, 148.3, 146.4, 146.3, 145.6, 145.4, 141.7, 139.8, 139.2, 139.9, 129.2, 128.4, 125.4, 122.1, 121.7, 119.7, 98.1, 97.9, 97.8, 97.5, 97.3, 97.2, 82.3, 92.2, 81.3, 62.34, 62.27, 62.2, 33.8, 33.2, 29.8, 24.9 ppm, eight signals could not be detected.

Elemental analysis calcd (%) for $C_{50}H_{24}F_{16}O_4$: C 60.50, H 2.44; found: C 60.94, H 2.37.

MS (APCI) *m/z*: calcd: 993.1492 $[M + H]^+$; found: 993.1481 $[M + H]^+$.

*Trimer* (**27b**)

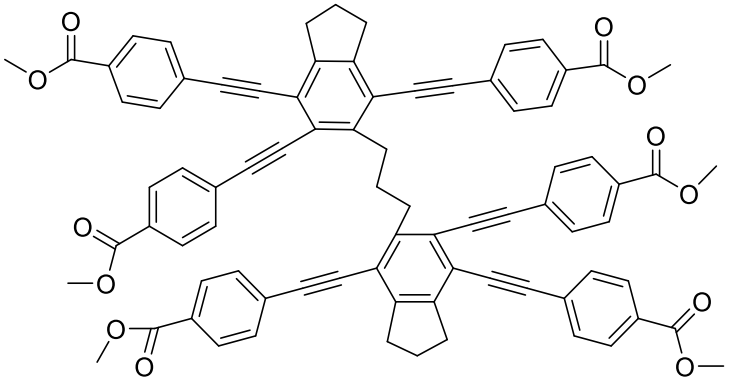

The reaction was prepared in a 20 mL vial under an argon atmosphere in the glovebox. Compounds **22** (0.15 g, 0.19 mmol) and 4 eq. of **5b** (0.316 g, 0.36 mmol) were dissolved in 10 mL of THF and stirred at RT for 8 days. A white solid precipitated from the solution. The solid was collected *via* filtration, washed with hexane four times and recrystallised from hot toluene. A colourless amorphous solid was obtained (7 mg, 0.006 mmol, 2%). $^{1}$H NMR (500 MHz, $CDCl_3$): $\delta$ = 8.01 (d, $J_{HH}$ = 9 Hz, 4H, C$H_{arom}$), 7.88 (d, $J_{HH}$ = 9 Hz, 4H, C$H_{arom}$), 7.87 (d, $J_{HH}$ = 9 Hz, 4H, C$H_{arom}$), 7.57 (d, $J_{HH}$ = 9 Hz, 4H, C$H_{arom}$), 7.44 (d, $J_{HH}$ = 9 Hz, 4H, C$H_{arom}$), 7.41 (d, $J_{HH}$ = 9 Hz, 4H, C$H_{arom}$), 3.93 (s, 6H, 2 x OC$H_3$), 3.90 (s, 6H, 2xOC$H_3$), 3.89 (s, 6H, 2 x OC$H_3$), 3.39 (t, $J_{HH}$ = 7, 4H, 2 x C$H_2$), 3.10 (q, $J_{HH}$ = 7, 4H, 2 x C$H_2$), 2.36 (quint, $J_{HH}$ = 7 Hz, 2H, C$H_2$), 2.13 (quint, $J_{HH}$ = 7, 4H, 2 x C$H_2$), ppm. $^{13}$C NMR (125 MHz, $CDCl_3$): $\delta$ = 166.5, 166.4, 166.3, 147.9, 144.9, 144.8, 131.5, 131.3, 131.2, 129.7, 129.6, 129.5, 129.5, 129.4, 129.4, 128.0, 127.9, 127.7, 122.9, 122.1, 119.7, 96.9, 96.8, 95.8, 90.2, 90.1, 89.2, 52.3, 52.2, 33.8, 33.3, 23.8 ppm.

MS (APCI) *m/z*: calcd: 1225.4158 $[M + H]^+$; found: 1225.4133 $[M + H]^+$.

*Trimer* (**27c**)

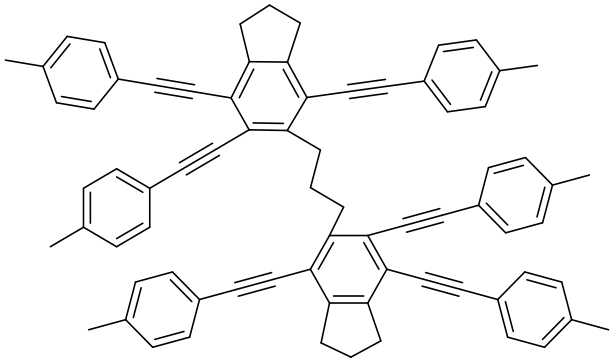

Compound **27c** was collected as by-product from the synthesis of rhodacyclopentadiene **25c**. The reaction was prepared in a 20 mL microwave vial under an argon atmosphere in the glovebox. Compounds **22** (0.2 g, 0.261 mmol) and 1 eq. of **5c** (83 mg, 0.26 mmol) were dissolved in 5 ml of THF and stirred in the microwave at 50 °C for 23 h. A 10:1 mixture of **25c** and **22** and the organic trimer **27c** were obtained. The solvent was removed *in vacuo* and the orange residue was recrystallised from THF/hexane (1:4) at -30 °C to separate the organic product from the starting material and compound **25c**. It was washed with hot hexane several times (ultrasonic bath). The product was obtained as a beige, crystalline solid (8 mg, 0.008 mmol, 3%). $^{1}$H NMR (500 MHz, $C_6D_6$): $\delta$ = 7.63 (d, $J_{HH}$ = 8 Hz, 4H, C$H_{arom}$), 7.62 (d, $J_{HH}$ = 8 Hz, 4H, C$H_{arom}$), 7.52 (d, $J_{HH}$ = 8 Hz, 4H, C$H_{arom}$), 6.88 (d, $J_{HH}$ = 8 Hz, 8H, C$H_{arom}$), 6.83 (d, $J_{HH}$ = 8 Hz, 4H, C$H_{arom}$), 3.96 (t, $J_{HH}$ = 7, 4H, 2 x C$H_2$), 3.04 (t, $J_{HH}$ = 7, 4H, 2 x C$H_2$), 2.96 (quint, $J_{HH}$ = 7 Hz, 2H, C$H_2$), 2.95 (t, $J_{HH}$ = 7, 4H, 2 x C$H_2$), 2.01 (s, 6H, 2 x C$H_3$), 1.99 (s, 6H, 2 x C$H_3$), 1.96 (s, 6H, 2 x C$H_3$), 1.77 (quint, $J_{HH}$ = 7 Hz, 4H, 2 x C$H_2$) ppm. $^{13}$C NMR (125 MHz, $C_6D_6$): $\delta$ = 146.8, 144.9, 144.1, 138.1, 137.9, 137.7, 131.7, 131.7, 131.7, 129.2, 129.1, 129.1, 124.1, 122.4, 121.2, 121.2, 120.9, 120.2, 97.8, 97.6, 97.1, 88.2, 87.7, 86.7, 34.1, 33.7, 33.3, 31.1, 23.7, 21.0, 21.0 ppm, due to low intensity one carbon atom is not visible.

Elemental analysis calcd (%) for $C_{75}H_{60}$: C 93.71, H 6.29; found: C 93.76, H 6.52.

MS (APCI) *m/z*: calcd: 961.4768 $[M + H]^+$; found: 961.4753 $[M + H]^+$.

*Trimer* (**27f'**)

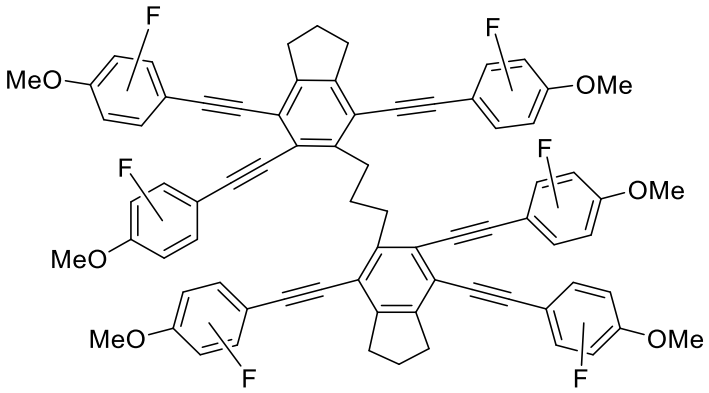


The reaction was prepared in a 20 mL vial under an argon atmosphere in the glovebox. Compound **22** (0.035 g, 0.045 mmol) and 10 eq. of compound **5f'** (0.224 g, 0.45 mmol) were dissolved in 10 mL of THF and stirred at RT for 14 days. A white solid precipitated from the solution. The solid was filtrated from the solution, washed with hexane and recrystallised from hot toluene. A white amorphous solid was obtained (20 mg, 0.01 mmol, 3%). $^{1}$H NMR (500 MHz, $CDCl_3$): $\delta$ = 4.12 (s, 6H, 2 x OC$H_3$), 4.10 (s, 6H, 2 x OC$H_3$), 4.09 (s, 6H, 2 x OC$H_3$), 3.30 (t, $J_{HH}$ = 7 Hz, 4H, 2 x C$H_2$), 3.08 (q, $J_{HH}$ = 7 Hz, 8H, 4 x C$H_2$), 2.31 (quint, $J_{HH}$ = 7 Hz, 2H, C$H_2$), 2.15 (quint., $J_{HH}$ = 7 Hz, 4H, 2 x C$H_2$) ppm. $^{13}$C NMR (125 MHz, $CDCl_3$): $\delta$ = 148.7, 148.2, 146.2, 145.5, 145.2, 141.6, 139.6, 138.9, 121.9, 121.6, 119.5, 107.6, 106.4, 97.9, 97.8, 97.4, 97.2, 97.1, 82.2, 82.1, 81.1, 68.0, 67.5, 62.2 62.1, 33.6, 33.1, 29.7, 29.6, 29.5, 23.9, 23.8 ppm. $^{19}$F (470 MHz, $CDCl_3$) : $\delta$ = -137.42 (m, 8F, C*F*), -137.65 (m, 4F, C*F*), 158.35 (m, 8F, C*F*), 158.71 (m, 4F, C*F*) ppm.

Elemental analysis calcd (%) for $C_{75}H_{36}F_{24}O_6$: C 60.50, H 2.44; found: C 60.33, H 2.35.

MS (APCI) *m/z*: calcd: 1489.2201 $[M + H]^+$; found: 1489.2189 $[M + H]^+$.

**Synthesis of *trans* $\pi$-Complexes**

*Trans-[bis-(trimethylphosphine)-$\kappa^2$-S,S`-dithiocarbamate-$\eta^2$-1-tolyl-2-p-tolylethynyl-ethenyl-Rh(III)* (**28c**)

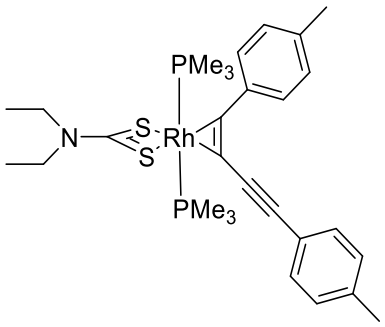


The reaction was prepared in a 20 mL vial under an argon atmosphere in the glovebox. Compounds **13** (0.30 g, 0.75 mmol) and 2 eq. of **4c** (0.34 g, 1.4 mmol) were dissolved in 10 mL of THF and stirred at RT for 14 d. After the reaction had reached completion, the solvent was removed *in vacuo* and the yellow residue was extracted with hot hexane several times. The solvent of the hexane solution was removed *in vacuo* and the yellow residue was then dissolved in THF and layered with hexane. The mixture was stored in the freezer at -30 °C to give a yellow crystalline solid, which turned out to be a 10:1.5 mixture of **28c** and **4c** (30 mg, 0.5 mmol, 3%). Compound **28c** seems to dissociate at -10 °C and forms an equilibrium with the starting compounds **13** and **4c**. $^1$H NMR (500 MHz, -40 °C, toluene-$d_8$): $\delta$ = 8.03 (d, $J_{HH}$ = 8 Hz, 2H, C$H_{arom}$), 7.46 (d, $J_{HH}$ = 8 Hz, 2H, C$H_{arom}$), 7.00 (d, $J_{HH}$ = 8 Hz, 2H, C$H_{arom}$), 6.73 (d, $J_{HH}$ = 8 Hz, 2H, C$H_{arom}$), 3.93 (q, $J_{HH}$ = 7 Hz, 4H, C$H_2$), 2.07 (s, 3H, C$H_3$), 1.93 (s, 3H, C$H_3$), 1.15 (t, $J_{HH}$ = 3 Hz, 18H, P(C$H_3$)$_3$), 3.24 (dt, $J_{HH}$ = 7 Hz, 6H, C$H_3$). $^{31}$P {$^1$H} NMR (202 MHz, $THF_{d8}$): $\delta$ = -5.74 (d, $J_{Rh-P}$ = 104 Hz, 2P, *P*Me$_3$).

*Trans-[bis-(trimethylphosphine)-$\kappa^2$-S,S`-dithiocarbamate-$\eta^2$-1-naphthyl-2-p-naphthylethynyl-ethenyl-Rh(III)* (**28g**)

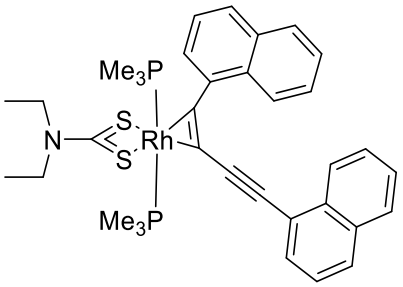


The reaction was prepared in a 20 mL vial under an argon atmosphere in the glovebox. Compounds **13** (0.56 g, 1.4 mmol) and 2 eq. of **4g** (0.42 g, 1.4 mmol) were dissolved in 10 mL of THF and stirred at RT for 14 d. After no more change in the $^{31}P\{^1H\}$ NMR could be observed, the solvent was removed *in vacuo* and the deep red residue was washed with hot hexane six times. The solvent of the hexane solution was removed *in vacuo* and the red residue was dissolved in THF and layered with hexane. The mixture was stored in the freezer at -30 °C to give red crystals, which could be characterised *via* X-ray diffraction. Compound **28g** seems to form an equilibrium with the starting compounds **13** and **4g**. The following $^{31}P\{^1H\}$ NMR-data were depicted from the mixture. The signals of the $^1H$ NMR spectrum were not assigned as they are shifted into the signals of the starting material. $^{31}P\{^1H\}$ NMR (121 MHz, $C_6D_6$): $\delta$ = -6.33 (d, $J_{Rh\text{-}P}$ = 104 Hz, 2P, *P*Me$_3$).

# 7. Crystallographic Data

| | **13** |
|---|---|
| Chemical formula | $C_{11}H_{28}NP_2RhS_2$ |
| Formula mass | 403.31 |
| Crystal system | Monoclinic |
| Space group, Z | $P2_1/c$, 8 |
| $a$ /Å | 11.0733(7) |
| $b$ /Å | 10.6764(6) |
| $c$ /Å | 30.7281(19) |
| $\alpha$ | 90 |
| $\beta$ | 93.7420(14) |
| $\gamma$ | 90 |
| Volume /Å$^3$ | 3625.0(4) |
| $\rho_{calcd}$ /g · cm$^{-3}$ | 1.478 |
| $T$ /K | 100(2) |
| $\mu$ /mm$^{-1}$, Radiation | $Mo_{K\alpha}$ 0.71073 |
| Measured reflns | 49236 |
| Indep. reflns | 7705 |
| param./restraints | 354/285 |
| $\theta$ range | 1.328 - 26.739° |
| GoF on $F^2$ | 1.256 |
| $R_{int}$ | 0.0206 |
| $R_1$ [$I > 2\sigma(I)$] | 0.0242 |
| $wR_2$ (all data) | 0.0527 |

| | **22** |
|---|---|
| Chemical formula | $C_{47}H_{46}NP_2RhS_2$ |
| Formula mass | 853.82 |
| Crystal system | Monoclinic |
| Space group, Z | $P2_1/c$, 4 |
| $a$ /Å | 21.0759(10) |
| $b$ /Å | 11.0408(5) |
| $c$ /Å | 17.4932(8) |
| $\alpha$ | 90 |
| $\beta$ | 94.2420(12) |
| $\gamma$ | 90 |
| Volume /Å$^3$ | 4059.4(3) |
| $\rho_{calcd}$ /g · cm$^{-3}$ | 1.397 |
| $T$ /K | 100 |
| $\mu$ /mm$^{-1}$, Radiation | $Mo_{K\alpha}$ 0.71073 |
| Measured reflns | 47909 |
| Indep. reflns | 8569 |
| param./restraints | 480 / 399 |
| $\theta$ range | 3.143 - 26.749° |
| GoF on $F^2$ | 1.033 |
| $R_{int}$ | 0.0688 |
| $R_1$ [$I > 2\sigma(I)$] | 0.0410 |
| $wR_2$ (all data) | 0.0965 |

| | **23a** |
|---|---|
| Chemical formula | $C_{34}H_{42}N_3O_4P_2RhS_2$ |
| Formula mass | 785.67 |
| Crystal system | Monoclinic |
| Space group, Z | *Pn* |
| *a* /Å | 9.131(4) |
| *b* /Å | 9.720(4) |
| *c* /Å | 21.075(9) |
| $\alpha$ | 90 |
| $\beta$ | 101.685(13) |
| $\gamma$ | 90 |
| Volume /Å$^3$ | 1831.8(13) |
| $\rho_{calcd}$ /g · cm$^{-3}$ | 1.424 |
| *T* /K | 100(2) |
| $\mu$ /mm$^{-1}$, Radiation | $Mo_{K\alpha}$ 0.71073 |
| Measured reflns | 37759 |
| Indep. reflns | 7234 |
| param./restraints | 424 / 2 |
| $\theta$ range | 1.973 - 26.022° |
| GoF on $F^2$ | 1.086 |
| $R_{int}$ | 0.0418 |
| $R_1$ [$I > 2\sigma(I)$] | 0.0338 |
| $wR_2$ (all data) | 0.0867 |

| | **23b** |
|---|---|
| Chemical formula | $C_{38}H_{48}NO_4P_2RhS_2$ |
| Formula mass | 811.74 |
| Crystal system | Monoclinic |
| Space group, Z | $P2_1/c$, 4 |
| $a$ /Å | 14.0532(17) |
| $b$ /Å | 15.506(2) |
| $c$ /Å | 17.749(2) |
| $\alpha$ | 90 |
| $\beta$ | 95.415(3) |
| $\gamma$ | 90 |
| Volume /Å$^3$ | 3850.5(8) |
| $\rho_{calcd}$ /g · cm$^{-3}$ | 1.400 |
| $T$ /K | 100 |
| $\mu$ /mm$^{-1}$, Radiation | $Mo_{K\alpha}$ 0.71073 |
| Measured reflns | 25037 |
| Indep. reflns | 8175 |
| param./restraints | 443 / 402 |
| $\theta$ range | 1.455 - 26.753° |
| GoF on $F^2$ | 0.997 |
| $R_{int}$ | 0.0685 |
| $R_1$ [$I > 2\sigma(I)$] | 0.0441 |
| $wR_2$ (all data) | 0.1009 |

| | **23c** |
|---|---|
| Chemical formula | $C_{39}H_{51}NP_2RhS_2$ |
| Formula mass | 762.78 |
| Crystal system | Monoclinic |
| Space group, Z | P 1 21/n 1, 4 |
| *a* /Å | 9.9882(7) |
| *b* /Å | 23.1345(14) |
| *c* /Å | 16.8134(10) |
| $\alpha$ | 90 |
| $\beta$ | 96.301(2) |
| $\gamma$ | 90 |
| Volume /Å$^3$ | 3861.6(4) |
| $\rho_{calcd}$ /g · cm$^{-3}$ | 1.312 |
| *T* /K | 100 |
| $\mu$ /mm$^{-1}$, Radiation | $Mo_{K\alpha}$ 0.71073 |
| Measured reflns | 43884 |
| Indep. reflns | 8222 |
| param./restraints | 416 / 369 |
| $\theta$ range | 1.503 - 26.767° |
| GoF on $F^2$ | 1.036 |
| $R_{int}$ | 0.0724 |
| $R_1$ [$I > 2\sigma(I)$] | 0.0404 |
| $wR_2$ (all data) | 0.0914 |

| | **23d** |
|---|---|
| Chemical formula | $C_{42.67}H_{61.33}N_3O_{0.67}P_2RhS_2$ |
| Formula mass | 855.91 |
| Crystal system | Monoclinic |
| Space group, Z | *C*2/c, 12 |
| *a* /Å | 30.618(13) |
| *b* /Å | 17.498(8) |
| *c* /Å | 28.543(18) |
| $\alpha$ | 90 |
| $\beta$ | 118.480(9) |
| $\gamma$ | 90 |
| Volume /Å$^3$ | 13442(12) |
| $\rho_{calcd}$ /g · cm$^{-3}$ | 1.269 |
| *T* /K | 120 |
| $\mu$ /mm$^{-1}$, Radiation | $Mo_{K\alpha}$ 0.71073 |
| Measured reflns | 70911 |
| Indep. reflns | 14266 |
| param./restraints | 720 / 630 |
| $\theta$ range | 1.388 - 26.774° |
| GoF on $F^2$ | 1.024 |
| $R_{int}$ | 0.0733 |
| $R_1$ [$I > 2\sigma(I)$] | 0.0458 |
| $wR_2$ (all data) | 0.1325 |

| | **23e** |
|---|---|
| Chemical formula | $C_{36}H_{48}NP_2RhS_4$ |
| Formula mass | 787.84 |
| Crystal system | Triclinic |
| Space group, Z | *P -1*, 2 |
| *a* /Å | 13.143(2) |
| 17.536(3) | 17.536(3) |
| *c* /Å | 18.225(3) |
| $\alpha$ | 68.615(7) |
| $\beta$ | 77.460(7) |
| $\gamma$ | 83.525(7) |
| Volume /Å$^3$ | 3815.4(12) |
| $\rho_{calcd}$ /g · cm$^{-3}$ | 1.269 |
| *T* /K | 100(2) |
| $\mu$ /mm$^{-1}$, Radiation | $Mo_{K\alpha}$ 0.71073 |
| Measured reflns | 31092 |
| Indep. reflns | 22289 |
| param./restraints | 813 / 0 |
| $\theta$ range | 1.222 - 33.999° |
| GoF on $F^2$ | 1.044 |
| $R_{int}$ | 0.0668 |
| $R_1$ [$I > 2\sigma(I)$] | 0.0377 |
| $wR_2$ (all data) | 0.0962 |

| | **23f'** |
|---|---|
| Chemical formula | $C_{36}$ $H_{40}$ $F_8$ N $O_2$ $P_2$ Rh $S_2$ |
| Formula mass | 899.66 |
| Crystal system | Monoclinic |
| Space group, Z | $P2_1/n$ , 4 |
| $a$ /Å | 11.5749(14) |
| $b$ /Å | 13.2608(16) |
| $c$ /Å | 24.884(3) |
| $\alpha$ | 90 |
| $\beta$ | 92.043(5) |
| $\gamma$ | 90 |
| Volume /Å$^3$ | 3817.0(8) |
| $\rho_{calcd}$ /g · cm$^{-3}$ | 1.566 |
| $T$ /K | 100(2) |
| $\mu$ /mm$^{-1}$, Radiation | $Mo_{K\alpha}$ 0.71073 |
| Measured reflns | 42977 |
| Indep. reflns | 7518 |
| param./restraints | 540 / 15 |
| $\theta$ range | 1.638 - 25.999 |
| GoF on $F^2$ | 1.047 |
| $R_{int}$ | 0.0390 |
| $R_1$ [$I > 2\sigma(I)$] | 0.0276 |
| $wR_2$ (all data) | 0.0679 |

| | **24a** |
|---|---|
| Chemical formula | $C_{34}H_{42}N_3O_4P_2RhS_2$ |
| Formula mass | 785.67 |
| Crystal system | Monoclinic |
| Space group, Z | $P2_1/c$ |
| $a$ /Å | 10.998(6) |
| $b$ /Å | 12.184(7) |
| $c$ /Å | 26.206(12) |
| $\alpha$ | 90 |
| $\beta$ | 97.75(2) |
| $\gamma$ | 90 |
| Volume /Å$^3$ | 3480(3) |
| $\rho_{calcd}$ /g · cm$^{-3}$ | 1.500 |
| $T$ /K | 100(2) |
| $\mu$ /mm$^{-1}$, Radiation | $Mo_{K\alpha}$ 0.71073 |
| Measured reflns | 25251 |
| Indep. reflns | 6859 |
| param./restraints | 423 / 0 |
| $\theta$ range | 1.568 - 26.021° |
| GoF on $F^2$ | 1.116 |
| $R_{int}$ | 0.0619 |
| $R_1$ [$I > 2\sigma(I)$] | 0.0526 |
| $wR_2$ (all data) | 0.1174 |

| | **24b** |
|---|---|
| Chemical formula | $C_{44}H_{62}NO_4P_2RhS_2$ |
| Formula mass | 897.91 |
| Crystal system | Triclinic |
| Space group, Z | P-1. 2 |
| *a* /Å | 11.4756(7) |
| *b* /Å | 13.4655(8) |
| *c* /Å | 16.1303(9) |
| $\alpha$ | 107.1424(18) |
| $\beta$ | 90.3406(19) |
| $\gamma$ | 112.1548(18) |
| Volume /Å$^3$ | 2186.6(2) |
| $\rho_{calcd}$ /g · cm$^{-3}$ | 1.364 |
| *T* /K | 100(2) |
| $\mu$ /mm$^{-1}$, Radiation | $Mo_{K\alpha}$ 0.71073 |
| Measured reflns | 29143 |
| Indep. reflns | 9301 |
| param./restraints | 499 / 0 |
| $\theta$ range | 1.333 - 26.755° |
| GoF on $F^2$ | 1.098 |
| $R_{int}$ | 0.0411 |
| $R_1$ [$I > 2\sigma(I)$] | 0.0337 |
| $wR_2$ (all data) | 0.1030 |

| | **25a** |
|---|---|
| Chemical formula | $C_{64}H_{54}N_3O_4P_2RhS_2$ |
| Formula mass | 1158.07 |
| Crystal system | Triclinic |
| Space group, Z | P-1 |
| *a* /Å | 13.682(7) |
| *b* /Å | 19.535(9) |
| *c* /Å | 21.554(10) |
| $\alpha$ | 106.43(3) |
| $\beta$ | 95.353(14) |
| $\gamma$ | 91.08(2) |
| Volume /Å$^3$ | 5496(5) |
| $\rho_{calcd}$ /g · cm$^{-3}$ | 1.400 |
| *T* /K | 100(2) |
| $\mu$ /mm$^{-1}$, Radiation | $Mo_{K\alpha}$ 0.71073 |
| Measured reflns | 21602 |
| Indep. reflns | 16434 |
| param./restraints | 1383 , 36 |
| $\theta$ range | 1.667 – 26.000° |
| GoF on $F^2$ | 1.030 |
| $R_{int}$ | 0.0540 |
| $R_1$ [$I > 2\sigma(I)$] | 0.0344 |
| $wR_2$ (all data) | 0.0726 |

| | **25b** |
|---|---|
| Chemical formula | $C_{68}H_{60}NO_4P_2RhS_2$ |
| Formula mass | 1184.14 |
| Crystal system | Triclinic |
| Space group, Z | P-1, 2 |
| *a* /Å | 11.6808(8) |
| *b* /Å | 13.6031(9) |
| *c* /Å | 18.1131(11) |
| $\alpha$ | 89.240(2) |
| $\beta$ | 81.631(2) |
| $\gamma$ | 81.457(2) |
| Volume /Å$^3$ | 2815.7(3) |
| $\rho_{calcd}$ /g · cm$^{-3}$ | 1.397 |
| *T* /K | 100(2) |
| $\mu$ /mm$^{-1}$, Radiation | $Mo_{K\alpha}$ 0.71073 |
| Measured reflns | 45159 |
| Indep. reflns | 13789 |
| param./restraints | 707 , 0 |
| $\theta$ range | 2.953 - 28.242° |
| GoF on $F^2$ | 0.963 |
| $R_{int}$ | 0.0623 |
| $R_1$ [$I > 2\sigma(I)$] | 0.0350 |
| $wR_2$ (all data) | 0.0740 |

| | **25e** |
|---|---|
| Chemical formula | $C_{66}H_{60}NP_2RhS_4$ |
| Formula mass | 1160.24 |
| Crystal system | Monoclinic |
| Space group, Z | P2(1)/c |
| *a* /Å | 17.5344(5) |
| *b* /Å | 16.5106(4) |
| *c* /Å | 20.3795(5) |
| $\alpha$ | 90 |
| $\beta$ | 106.5900(10) |
| $\gamma$ | 90 |
| Volume /Å$^3$ | 5654.3(3) |
| $\rho_{calcd}$ /g · cm$^{-3}$ | 1.363 |
| *T* /K | 100(2) |
| $\mu$ /mm$^{-1}$, Radiation | $Mo_{K\alpha}$ 0.71073 |
| Measured reflns | 61807 |
| Indep. reflns | 11124 |
| param./restraints | 691 / 0 |
| $\theta$ range | 1.615 - 26.000° |
| GoF on $F^2$ | 1.046 |
| $R_{int}$ | 0.0371 |
| $R_1$ [$I > 2\sigma(I)$] | 0.0282 |
| $wR_2$ (all data) | 0.0725 |

| | **25f'** |
|---|---|
| Chemical formula | $C_{72}H_{61}F_8NO_{3.5}P_2RhS_2$ |
| Formula mass | 1377.18 |
| Crystal system | Triclinic |
| Space group, Z | P-1, 2 |
| *a* /Å | 11.2331(7) |
| *b* /Å | 15.5381(10) |
| *c* /Å | 20.1541(14) |
| $\alpha$ | 95.598(2) |
| $\beta$ | 97.760(2) |
| $\gamma$ | 107.630(2) |
| Volume /Å$^3$ | 3285.9(4) |
| $\rho_{calcd}$ /g · cm$^{-3}$ | 1.392 |
| *T* /K | 100(2) |
| $\mu$ /mm$^{-1}$, Radiation | 0.443, 0.71073 A |
| Measured reflns | 73569 |
| Indep. reflns | 12890 |
| param./restraints | 920/ 140 |
| $\theta$ range | 1.848 - 26.000 |
| GoF on $F^2$ | 0.993 |
| $R_{int}$ | 0.0398 |
| $R_1$ [$I > 2\sigma(I)$] | 0.0420 |
| $wR_2$ (all data) | 0.0535 |

| | **26c** |
|---|---|
| Chemical formula | $C_{50}H_{40}$ |
| Formula mass | 640.82 |
| Crystal system | Triclinic |
| Space group, Z | P-1 |
| *a* /Å | 8.7451(3) |
| *b* /Å | 11.7926(3) |
| *c* /Å | 18.3329(6) |
| $\alpha$ | 102.4120(10) |
| $\beta$ | 97.2340(10) |
| $\gamma$ | 96.0440(10) |
| Volume /Å$^3$ | 1814.57(10) |
| $\rho_{calcd}$ /g · cm$^{-3}$ | 1.173 |
| *T* /K | 100(2) |
| $\mu$ /mm$^{-1}$, Radiation | $Mo_{K\alpha}$ 0.71073 |
| Measured reflns | 29739 |
| Indep. reflns | 7131 |
| param./restraints | 455 / 0 |
| $\theta$ range | 1.785 - 26.000° |
| GoF on $F^2$ | 1.032 |
| $R_{int}$ | 0.0246 |
| $R_1$ [$I > 2\sigma(I)$] | 0.0466 |
| $wR_2$ (all data) | 0.1292 |

| | **27c** |
|---|---|
| Chemical formula | $C_{75}H_{60}$, $OC_4H_8$ |
| Formula mass | 1033.33 |
| Crystal system | Triclinic |
| Space group, Z | P-1 |
| *a* /Å | 13.009(4) |
| *b* /Å | 15.174(6) |
| *c* /Å | 16.337(6) |
| $\alpha$ | 78.07(3) |
| $\beta$ | 71.43(2) |
| $\gamma$ | 76.39(3) |
| Volume /Å$^3$ | 2940.6(19) |
| $\rho_{calcd}$ /g · cm$^{-3}$ | 1.167 |
| *T* /K | 100(2) |
| $\mu$ /mm$^{-1}$, Radiation | $Mo_{K\alpha}$ 0.71073 |
| Measured reflns | 11547 |
| Indep. reflns | 7679 |
| param./restraints | 820 / 120 |
| $\theta$ range | 2.420 - 26.232° |
| GoF on $F^2$ | 1.042 |
| $R_{int}$ | 0.0321 |
| $R_1$ [$I > 2\sigma(I)$] | 0.0566 |
| $wR_2$ (all data) | 0.1765 |

| | **27f'*** |
|---|---|
| Chemical formula | $C_{75}H_{36}F_{24}O6$ |
| Formula mass | 1488.21 |
| Crystal system | Triclinic |
| Space group, Z | P-1 |
| *a* /Å | 13.8942(17) |
| *b* /Å | 16.356(2) |
| *c* /Å | 20.143(3) |
| $\alpha$ | 73.303(3) |
| $\beta$ | 76.173(3) |
| $\gamma$ | 73.568(3) |
| Volume /Å$^3$ | 4142.9(9) |
| $\rho_{calcd}$ /g · cm$^{-3}$ | 1.553 |
| *T* /K | 168(2) |
| $\mu$ /mm$^{-1}$, Radiation | $Mo_{K\alpha}$ 0.71073 |
| Measured reflns | 16904 |
| Indep. reflns | 10078 |
| param./restraints | 1151 / 0 |
| $\theta$ range | 1.727-26.948 |
| GoF on $F^2$ | 1.150 |
| $R_{int}$ | 0.0368 |
| $R_1$ [$I > 2\sigma(I)$] | 0.1150 |
| $wR_2$ (all data) | 0.3196 |

* The obtained structure is not publishable. The data is only given for orientation.

| | **28c** |
|---|---|
| Chemical formula | $C_{29}H_{42}NP_2RhS_2$ |
| Formula mass | 633.60 |
| Crystal system | Orthorhombic |
| Space group, Z | $P2_12_12_1$ |
| *a* /Å | 9.1177(6) |
| *b* /Å | 11.9603(6) |
| *c* /Å | 28.6216(16) |
| $\alpha$ | 90 |
| $\beta$ | 90 |
| $\gamma$ | 90 |
| Volume /Å$^3$ | 3121.2(3) |
| $\rho_{calcd}$ /g · cm$^{-3}$ | 1.348 |
| *T* /K | 100(2) |
| $\mu$ /mm$^{-1}$, Radiation | $Mo_{K\alpha}$ 0.71073 |
| Measured reflns | 16708 |
| Indep. reflns | 6127 |
| param./restraints | 326 / 0 |
| $\theta$ range | 1.845 - 25.999 |
| GoF on $F^2$ | 0.994 |
| $R_{int}$ | 0.0326 |
| $R_1$ [$I > 2\sigma(I)$] | 0.0277 |
| $wR_2$ (all data) | 0.0544 |

| | **28g** |
|---|---|
| Chemical formula | $C_{35}$ $H_{42}$ N $P_2$ Rh $S_2$ |
| Formula mass | 705.66 |
| Crystal system | Monoclinic |
| Space group, Z | *Pc* , 4 |
| *a* /Å | 16.1014(9) |
| *b* /Å | 12.6068(6) |
| *c* /Å | 17.8262(9) |
| $\alpha$ | 90 |
| $\beta$ | 105.693(3) |
| $\gamma$ | 90 |
| Volume /Å$^3$ | 3483.6(3) |
| $\rho_{calcd}$ /g · cm$^{-3}$ | 1.345 |
| *T* /K | 100(2) |
| $\mu$ /mm$^{-1}$, Radiation | $Mo_{K\alpha}$ 0.71073 |
| Measured reflns | 36628 |
| Indep. reflns | 12086 |
| param./restraints | 918 / 218 |
| $\theta$ range | 1.615 - 25.998 |
| GoF on $F^2$ | 1.047 |
| $R_{int}$ | 0.0258 |
| $R_1$ [$I > 2\sigma(I)$] | 0.0305 |
| $wR_2$ (all data) | 0.0722 |

# 8. Appendix

## 8.1 Abbreviations

| | |
|---|---|
| Å | Angstrom |
| Abs. | Absorption |
| acac | Acetylacetonate |
| Bmim | 1-Butyl-3-methyl-imidazolium |
| BPET | 1,2-bis(4-pyridyl)ethane |
| bph | Biphenyl |
| bpy | Bipyridine |
| cm | Centimetre |
| COD | Cyclo-octadiene |
| Cp | Cyclopentadiene/ Cyclopentadienyl |
| CP* | Methylcyclopentadiene/ Methylcyclopentadienyl |
| $\delta$ | Delta |
| d | Doublet |
| DFT | Density functional theory |
| dt | Doublet of triplets |
| dppe | (Diphenylphosphino)ethane |
| dppf | (Diphenylphosphino)ferrocene |
| dppm | (Diphenylphosphino)methane |
| dppn | Benzo[I]dipyrido-[3, 2-a:2',3'-c]phenazine |
| $\varepsilon$ | Extinction coefficient |
| Em. | Emission |
| eV | Electron volt |
| $\phi$ | Quantum yield |
| F | Fluorescence |
| GCMS | Gas chromatography mass spectrometry |
| h | Hour |
| hbph | $\eta^1$-biphenyl monoanion |
| HDDA | Hexadehydro Diels-Alder |
| HOMO | Highest Occupied Molecular Orbital |

| | |
|---|---|
| HRMS | High-resolution mass spectrometry |
| Hz | Hertz |
| IC | Internal conversion |
| IL | Intra Ligand |
| IR | Infrared |
| IRF | Instrument response factor |
| ISC | Inter System Crossing |
| *J* | Coupling constant |
| K | Kelvin |
| OLED | Organic Light Emitting Diode |
| Ox | Oxidation |
| LUMO | Lowest Unoccupied Molecular Orbital |
| m | Multiplet |
| MHz | Mega Hertz |
| min | Minutes |
| MLCT | Metal to Ligand Charge Transfer |
| µs | Microseconds |
| µw | Microwave |
| NHC | N-heterocyclic carbene |
| nm | Nanometre |
| NMR | Nuclear Magnetic Resonance |
| ns | Nanosecond |
| OLED | Organic light emitting diode |
| $^{n}Pr$ | n-propyl |
| *p* | *para* |
| P | Phosphorescence |
| ppm | Parts per million |
| ppy | Phenyl pyridine |
| ps | Picoseconds |
| psi | Pound-force per square inch (pressure) |
| q | Quartet |
| quint | Quintet |
| Red | Reduction |
| RT | Room Temperature |

| | |
|---|---|
| s | second |
| S | Singlet |
| sept | Septet |
| SOC | Spin Orbit Coupling |
| $\tau$ | Lifetime |
| t | Triplet |
| TBAF | Tetrabutyl-ammoniumfluoride |
| THF | Tetrahydrofuran |
| TMSA | Trimethylsilylacetylene |
| TMS | Trimethylsilane |
| UV/Vis | Ultra Violet/ Visible |
| ν | Wavelength |
| $\tilde{\nu}$ | Wavenumber |

## 8.2 List of Compounds

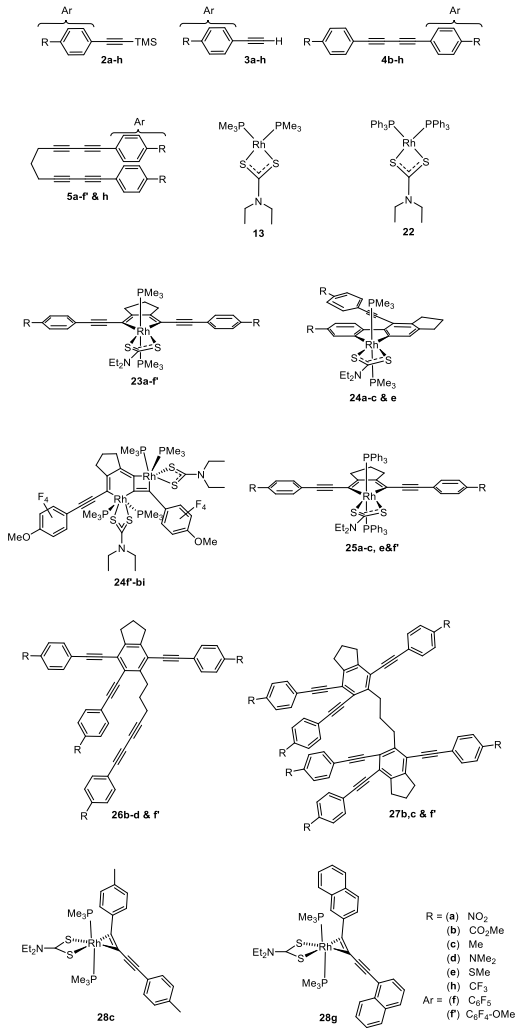

## 8.3 Additional Spectra

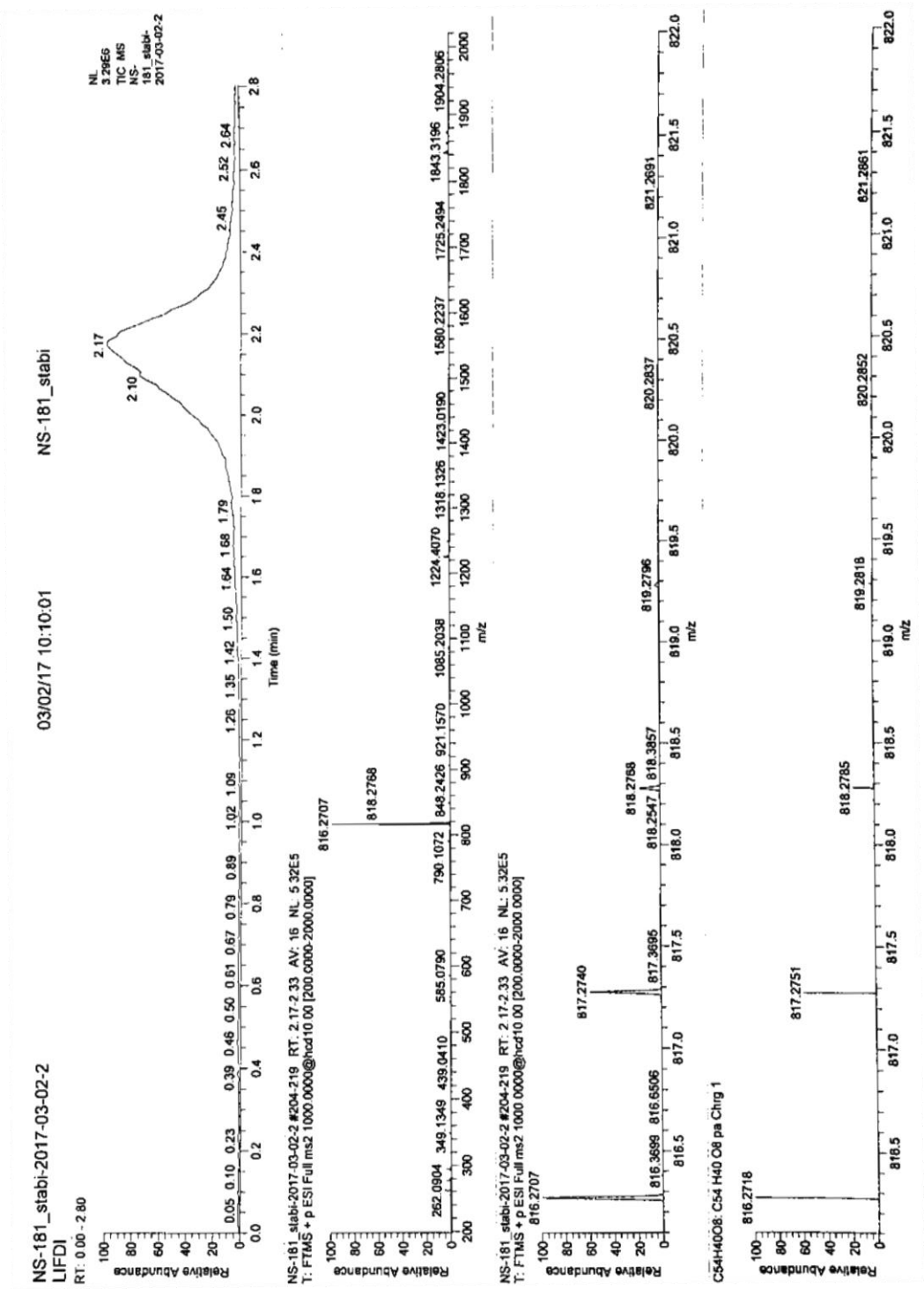


**Figure 104** High resolution mass spectrum of compound **25b** in $C_6D_6$ after heating to 90 °C for two weeks.

## References


[1] L. Cassar, *J. Organomet. Chem.* **1975**, *93*, 253-257.
[2] K. Sonogashira, Y. Tohda, N. Hagihara, *Tetrahedron Lett.* **1975**, *16*, 4467-4470.
[3] P. Fitton, E. A. Rick, *J. Organomet. Chem.* **1971**, *28*, 287-291.
[4] C. Glaser, *Ber. Dtsch. Chem. Ges.* **1869**, *2*, 422-424.
[5] G. Eglinton, A. R. Galbraith, *J. Chem. Soc.* **1959**, 889-896.
[6] A. S. Batsanov, J. C. Collings, I. J. S. Fairlamb, J. P. Holland, J. A. K. Howard, Z. Lin, T. B. Marder, A. C. Parsons, R. M. Ward, J. Zhu, *J. Org. Chem.* **2005**, *70*, 703-706.
[7] E. Shirakawa, Y. Nakao, Y. Murota, T. Hiyama, *J. Organomet. Chem.* **2003**, *670*, 132-136.
[8] M. Ochiai, Y. Nishi, S. Goto, H. J. Frohn, *Angew. Chem. Int. Ed.* **2005**, *44*, 406-409; *Angew. Chem.* **2005**, *117*, 410-413.
[9] A. S. Hay, *J. Org. Chem.* **1962**, *27*, 3320-3321.
[10] A. Sharifi, M. Mirzaei, M. Reza Naimi-Jamal, *Monatsh. Chem. - Chem. Mon.* **2006**, *137*, 213-217.
[11] G. W. Kabalka, L. Wang, R. M. Pagni, *Green Chem.* **2001**, *3*, 261-262.
[12] C. Schweitzer, R. Schmidt, *Chem. Rev.* **2003**, *103*, 1685-1758.
[13] J. S. Yadav, B. V. S. Reddy, K. B. Reddy, K. U. Gayathri, A. R. Prasad, *Tetrahedron Lett.* **2003**, *44*, 6493-6496.
[14] S.-K. Kang, T.-H. Kim, S.-J. Pyun, *J. Chem. Soc., Perkin Trans. 1* **1997**, 797-798.
[15] E. H. Smith, J. Whittall, *Organometallics* **1994**, *13*, 5169-5172.
[16] I. Rhee, M. Ryang, S. Tsutsumi, *Tetrahedron Lett.* **1969**, *10*, 4593-4596.
[17] S. V. Damle, D. Seomoon, P. H. Lee, *J. Org. Chem.* **2003**, *68*, 7085-7087.
[18] C. C. C. Johansson Seechurn, M. O. Kitching, T. J. Colacot, V. Snieckus, *Angew. Chem. Int. Ed.* **2012**, *51*, 5062-5085.
[19] M. Alami, F. Ferri, *Tetrahedron Lett.* **1996**, *37*, 2763-2766.
[20] Y. Nishihara, K. Ikegashira, A. Mori, T. Hiyama, *Tetrahedron Lett.* **1998**, *39*, 4075-4078.
[21] V. Fiandanese, D. Bottalico, G. Marchese, A. Punzi, *Tetrahedron Lett.* **2003**, *44*, 9087-9090.
[22] P. Nguyen, Z. Yuan, L. Agocs, G. Lesley, T. B. Marder, *Inorg. Chim. Acta* **1994**, *220*, 289-296.
[23] S. McKnight, *M. Sc. Thesis, Herriot-Watt University*, **2015**.
[24] E. O. Greaves, C. J. L. Lock, P. M. Maitlis, *Can. J. Chem.* **1968**, *46*, 3879-3891.
[25] T. L. Cairns, V. A. Engelhardt, H. L. Jackson, G. H. Kalb, J. C. Sauer, *J. Am. Chem. Soc.* **1952**, *74*, 5636-5640.
[26] P. M. Maitlis, *Cyclobutadiene-Metal Complexes* in *Adv. Organomet. Chem., Vol. 4*, Eds. F. G. A. Stone, R. West, Academic Press, **1966**, 95-143.
[27] L. S. Meriwether, M. F. Leto, E. C. Colthup, G. W. Kennerly, *J. Org. Chem.* **1962**, *27*, 3930-3941.
[28] J. H. Nelson, H. B. Jonassen, *Coord. Chem. Rev.* **1971**, *6*, 27-63.
[29] J. P. Collman, J. W. Kang, *J. Am. Chem. Soc.* **1967**, *89*, 844-851.
[30] S. Kenkichi, H. Nobue, *Bull. Chem. Soc. Jpn.* **1966**, *39*, 1178-1182.
[31] R. M. Ward, *Ph. D. Thesis, Durham University*, **2007**.
[32] F. M. Brewer, *Proc. Chem. Soc.* **1957**, 185-216.
[33] H. Braunschweig, A. Damme, R. D. Dewhurst, A. Vargas, *Nat. Chem.* **2013**, *5*, 115-121.
[34] K. P. C. Vollhardt, *Angew. Chem. Int. Ed. Engl.* **1984**, *23*, 539-556.

[35] H. Shinokubo, K. Oshima, *Eur. J. Org. Chem.* **2004**, *2004*, 2081-2091.
[36] J. P. Collman, J. W. Kang, W. F. Little, M. F. Sullivan, *Inorg. Chem.* **1968**, *7*, 1298-1303.
[37] M. Lautens, W. Klute, W. Tam, *Chem. Rev.* **1996**, *96*, 49-92.
[38] I. Ojima, M. Tzamarioudaki, Z. Li, R. J. Donovan, *Chem. Rev.* **1996**, *96*, 635-662.
[39] Y. Wakatsuki, H. Yamazaki, *J. Chem. Soc., Chem. Commun.* **1973**, 280a.
[40] Y. Wakatsuki, T. Kuramitsu, H. Yamazaki, *Tetrahedron Lett.* **1974**, *15*, 4549-4552.
[41] V. Gandon, C. Aubert, M. Malacria, *Chem. Commun.* **2006**, 2209-2217.
[42] A. T. Blomquist, P. M. Maitlis, *J. Am. Chem. Soc.* **1962**, *84*, 2329-2334.
[43] P. J. Low, M. I. Bruce, *Transition Metal Chemistry of 1,3-Diynes, Poly-ynes, and Related Compounds* in *Adv. Organomet. Chem., Vol. 48*, Eds. R. West, A. F. Hill, Academic Press, **2001**, 71-288.
[44] P. J. Low, N. J. Brown, *J. Cluster Sci.* **2010**, *21*, 235-278.
[45] S. B. Falloon, S. Szafert, A. M. Arif, J. A. Gladysz, *Chem. Eur. J.* **1998**, *4*, 1033-1042.
[46] R. M. Ward, A. S. Batsanov, J. A. K. Howard, T. B. Marder, *Inorg. Chim. Acta* **2006**, *359*, 3671-3676.
[47] T. Rappert, O. Nuernberg, H. Werner, *Organometallics* **1993**, *12*, 1359-1364.
[48] P. Schwab, H. Werner, *J. Chem. Soc., Dalton Trans.* **1994**, 3415-3425.
[49] H. Werner, O. Gevert, P. Haquette, *Organometallics* **1997**, *16*, 803-806.
[50] H. Werner, O. Gevert, P. Steinert, J. Wolf, *Organometallics* **1995**, *14*, 1786-1791.
[51] H. Werner, R. W. Lass, O. Gevert, J. Wolf, *Organometallics* **1997**, *16*, 4077-4088.
[52] H. Werner, M. Schäfer, J. Wolf, K. Peters, H. G. von Schnering, *Angew. Chem. Int. Ed. Engl.* **1995**, *34*, 191-194.
[53] N. W. Alcock, A. F. Hill, R. P. Melling, A. R. Thompsett, *Organometallics* **1993**, *12*, 641-648.
[54] A. Werth, K. Dehnicke, D. Fenske, G. Baum, *Z. Anorg. Allg. Chem.* **1990**, *591*, 125-136.
[55] K. Stahl, F. Weller, K. Dehnicke, *Z. Anorg. Allg. Chem.* **1984**, *518*, 175-186.
[56] C. P. Casey, S. Chung, Y. Ha, D. R. Powell, *Inorg. Chim. Acta* **1997**, *265*, 127-138.
[57] M. I. Bruce, P. J. Low, A. Werth, B. W. Skelton, A. H. White, *J. Chem. Soc., Dalton Trans.* **1996**, 1551-1566.
[58] S. Yamazaki, A. J. Deeming, D. M. Speel, *Organometallics* **1998**, *17*, 775-778.
[59] J. K. D. Surette, M.-A. MacDonald, M. J. Zaworotko, R. D. Singer, *J. Chem. Crystallogr.* **1994**, *24*, 715-717.
[60] S. Yamazaki, Z. Taira, T. Yonemura, A. J. Deeming, *Organometallics* **2005**, *24*, 20-27.
[61] H. S. Huh, Y. K. Lee, S. W. Lee, *J. Mol. Struct.* **2006**, *789*, 209-219.
[62] C. V. Ursini, G. H. M. Dias, M. Hörner, A. J. Bortoluzzi, M. K. Morigaki, *Polyhedron* **2000**, *19*, 2261-2268.
[63] S. Pulst, P. Arndt, B. Heller, W. Baumann, R. Kempe, U. Rosenthal, *Angew. Chem. Int. Ed. Engl.* **1996**, *35*, 1112-1115.
[64] C. J. Adams, M. I. Bruce, E. Horn, E. R. T. Tiekink, *J. Chem. Soc., Dalton Trans.* **1992**, 1157-1164.
[65] C. Gauss, D. Veghini, H. Berke, *Chem. Ber.* **1997**, *130*, 183-194.
[66] T. Shimura, A. Ohkubo, K. Aramaki, H. Uekusa, T. Fujita, S. Ohba, H. Nishihara, *Inorg. Chim. Acta* **1995**, *230*, 215-218.
[67] Y. Wakatsuki, O. Nomura, K. Kitaura, K. Morokuma, H. Yamazaki, *J. Am. Chem. Soc.* **1983**, *105*, 1907-1912.
[68] J. P. Rourke, A. S. Batsanov, J. A. K. Howard, T. B. Marder, *Chem. Commun.* **2001**, 2626-2627.

[69] A. Steffen, R. M. Ward, M. G. Tay, R. M. Edkins, F. Seeler, M. van Leeuwen, L.-O. Pålsson, A. Beeby, A. S. Batsanov, J. A. K. Howard, T. B. Marder, *Chem. Eur. J.* **2014**, *20*, 3652-3666.
[70] A. F. Hill, A. D. Rae, M. Schultz, A. C. Willis, *Organometallics* **2007**, *26*, 1325-1338.
[71] A. Steffen, M. G. Tay, A. S. Batsanov, J. A. K. Howard, A. Beeby, K. Q. Vuong, X.-Z. Sun, M. W. George, T. B. Marder, *Angew. Chem.* **2010**, *122*, 2399-2403.
[72] A. Steffen, K. Costuas, A. Boucekkine, M. H. Thibault, A. Beeby, A. S. Batsanov, A. Charaf-Eddin, D. Jacquemin, J. F. Halet, T. B. Marder, *Inorg. Chem.* **2014**, *53*, 7055-7069.
[73] M. G. Tay, *Ph. D. Thesis, Durham University*, **2010**.
[74] A. Morneau, B. T. Donovan-Merkert, W. E. Geiger, *Inorg. Chim. Acta* **2000**, *300–302*, 96-101.
[75] J. J. Eisch, A. M. Piotrowski, K. I. Han, C. Kruger, Y. H. Tsay, *Organometallics* **1985**, *4*, 224-231.
[76] X. Zhang, G. B. Carpenter, D. A. Sweigart, *Organometallics* **1999**, *18*, 4887-4888.
[77] M. Retbøll, A. J. Edwards, A. D. Rae, A. C. Willis, M. A. Bennett, E. Wenger, *J. Am. Chem. Soc.* **2002**, *124*, 8348-8360.
[78] Z. Hou, A. Fujita, T.-a. Koizumi, H. Yamazaki, Y. Wakatsuki, *Organometallics* **1999**, *18*, 1979-1985.
[79] Z. Lu, C.-H. Jun, S. R. de Gala, M. P. Sigalas, O. Eisenstein, R. H. Crabtree, *Organometallics* **1995**, *14*, 1168-1175.
[80] Z. Lu, C.-H. Jun, S. R. de Gala, M. Sigalas, O. Eisenstein, R. H. Crabtree, *J. Chem. Soc., Chem. Commun.* **1993**, 1877-1880.
[81] C. Perthuisot, W. D. Jones, *J. Am. Chem. Soc.* **1994**, *116*, 3647-3648.
[82] C. Perthuisot, B. L. Edelbach, D. L. Zubris, W. D. Jones, *Organometallics* **1997**, *16*, 2016-2023.
[83] W.-Y. Yeh, S. C. N. Hsu, S.-M. Peng, G.-H. Lee, *Organometallics* **1998**, *17*, 2477-2483.
[84] S. A. Gardner, H. B. Gordon, M. D. Rausch, *J. Organomet. Chem.* **1973**, *60*, 179-188.
[85] C. L. Hilton, B. T. King, *Organometallics* **2006**, *25*, 4058-4061.
[86] M. R. Plutino, L. M. Scolaro, A. Albinati, R. Romeo, *J. Am. Chem. Soc.* **2004**, *126*, 6470-6484.
[87] Y.-H. Chen, J. W. Merkert, Z. Murtaza, C. Woods, D. P. Rillema, *Inorg. Chim. Acta* **1995**, *240*, 41-47.
[88] S. C. Cohen, A. G. Massey, *J. Organomet. Chem.* **1967**, *10*, 471-481.
[89] M. D. Rausch, L. P. Klemann, *J. Chem. Soc. D: Chem. Commun.* **1971**, 354-354.
[90] P. Buchalski, I. Grabowska, E. Kamińska, K. Suwińska, *Organometallics* **2008**, *27*, 2346-2349.
[91] C. N. Iverson, R. J. Lachicotte, C. Müller, W. D. Jones, *Organometallics* **2002**, *21*, 5320-5333.
[92] S. Yamaguchi, K. Tamao, *J. Organomet. Chem.* **2002**, *653*, 223-228.
[93] K. Tamao, S. Yamaguchi, M. Shiro, *J. Am. Chem. Soc.* **1994**, *116*, 11715-11722.
[94] A. J. Boydston, Y. Yin, B. L. Pagenkopf, *J. Am. Chem. Soc.* **2004**, *126*, 3724-3725.
[95] P. Nguyen, G. Lesley, T. B. Marder, I. Ledoux, J. Zyss, *Chem. Mater.* **1997**, *9*, 406-408.
[96] M. Biswas, P. Nguyen, T. B. Marder, L. R. Khundkar, *J. Phys. Chem. A* **1997**, *101*, 1689-1695.
[97] J. G. Rodríguez, A. Lafuente, L. Rubio, J. Esquivias, *Tetrahedron Lett.* **2004**, *45*, 7061-7064.
[98] J. G. Rodriguez, J. Esquivias, A. Lafuente, L. Rubio, *Tetrahedron* **2006**, *62*, 3112-3122.
[99] S.-S. Sun, A. J. Lees, *J. Am. Chem. Soc.* **2000**, *122*, 8956-8967.

[100] T. S. Jung, J. H. Kim, E. K. Jang, D. H. Kim, Y.-B. Shim, B. Park, S. C. Shin, *J. Organomet. Chem.* **2000**, *599*, 232-237.
[101] J. S. Siddle, R. M. Ward, J. C. Collings, S. R. Rutter, L. Porres, L. Applegarth, A. Beeby, A. S. Batsanov, A. L. Thompson, J. A. K. Howard, A. Boucekkine, K. Costuas, J.-F. Halet, T. B. Marder, *New J. Chem.* **2007**, *31*, 841-851.
[102] S. Kenichi, Y. Takakazu, Y. Akio, *Bull. Chem. Soc. Jpn.* **1984**, *57*, 752-755.
[103] M. A. Pena, I. Perez, J. P. Sestelo, L. A. Sarandeses, *Chem. Commun.* **2002**, 2246-2247.
[104] A. Orita, F. Ye, G. Babu, T. Ikemoto, J. Otera, *Can. J. Chem.* **2005**, *83*, 716-727.
[105] A. Beeby, K. S. Findlay, P. J. Low, T. B. Marder, P. Matousek, A. W. Parker, S. R. Rutter, M. Towrie, *Chem. Commun.* **2003**, 2406-2407.
[106] P. Lind, C. Lopes, K. Öberg, B. Eliasson, *Chem. Phys. Lett.* **2004**, *387*, 238-242.
[107] P. Lind, A. Eriksson, C. Lopes, B. Eliasson, *J. Phys. Org. Chem.* **2005**, *18*, 426-433.
[108] R. Vestberg, C. Nilsson, C. Lopes, P. Lind, B. Eliasson, E. Malmström, *J. Polym. Sci. Part A: Pol. Chem.* **2005**, *43*, 1177-1187.
[109] G. Heppke, D. Moro, *Science* **1998**, *279*, 1872-1873.
[110] S. H. Eichhorn, A. J. Paraskos, K. Kishikawa, T. M. Swager, *J. Am. Chem. Soc.* **2002**, *124*, 12742-12751.
[111] H.-F. Hsu, C.-H. Kuo, C.-F. Chen, Y.-H. Lin, L.-Y. Huang, C.-H. Chen, K.-C. Cheng, H.-H. Chen, *Chem. Mater.* **2004**, *16*, 2379-2385.
[112] K. Kishikawa, M. C. Harris, T. M. Swager, *Chem. Mater.* **1999**, *11*, 867-871.
[113] P. Lind, M. Carlsson, B. Eliasson, E. Glimsdal, M. Lindgren, C. Lopes, L. Boman, P. Norman, *Mol. Phys.* **2009**, *107*, 629-641.
[114] S. Holand, F. Gandolfo, L. Ricard, F. Mathey, *Bull. Soc. Chim. Fr.* **1996**, *133*, 33-37.
[115] Y. Matano, M. Nakashima, H. Imahori, *Angew. Chem. Int. Ed. Engl.* **2009**, *48*, 4002-4005.
[116] A. Van Der Ent, A. L. Onderdelinden, R. A. Schunn, *Inorg. Synth.* **2007**, *28*, 90-92.
[117] R. T. Price, R. A. Andersen, E. L. Muetterties, *J. Organomet. Chem.* **1989**, *376*, 407-417.
[118] R. M. Golding, P. C. Healy, P. W. G. Newman, E. Sinn, A. H. White, *Inorg. Chem.* **1972**, *11*, 2435-2440.
[119] D. H. W. Thewissen, H. L. M. Van Gaal, *J. Organomet. Chem.* **1979**, *172*, 69-79.
[120] J. A. Osborn, G. Wilkinson, J. J. Mrowca, *Inorg. Synth.* **2007**, *10*, 67-71.
[121] C. Sieck, M. G. Tay, M.-H. Thibault, R. M. Edkins, K. Costuas, J.-F. Halet, A. S. Batsanov, M. Haehnel, K. Edkins, A. Lorbach, A. Steffen, T. B. Marder, *Chem. Eur. J.* **2016**, *22*, 10523-10532.
[122] C. Sieck, *unpublished results*.
[123] U. Rosenthal, V. V. Burlakov, M. A. Bach, T. Beweries, *Chem. Soc. Rev.* **2007**, *36*, 719-728.
[124] M. Lautens, W. Klute, W. Tam, *Chem. Rev.* **1996**, *96*, 49-92.
[125] B. Heller, M. Hapke, *Chem. Soc. Rev.* **2007**, *36*, 1085-1094.
[126] H. Bönnemann, *Angew. Chem. Int. Ed. Engl.* **1985**, *24*, 248-262.
[127] M.-H. Thibault, *unpublished results*.
[128] F. Kerner, *Unpublished results*.
[129] D. P. Allen, C. M. Crudden, L. A. Calhoun, R. Wang, A. Decken, *J. Organomet. Chem.* **2005**, *690*, 5736-5746.
[130] C. Sieck, D. Sieh, M. Sapotta, M. Haehnel, K. Edkins, A. Lorbach, A. Steffen, T. B. Marder, *J. Organomet. Chem.* **2017**, *accepted*.
[131] K. Murata, *unpublished results*.
[132] A. C. M. Montalti, L. Prodi, M. T. Gandolfi, *Handbook of Photochemistry, Vol. 3rd ed., CRC Tylor & Francis: Boca Raton*, **2006**.
[133] H. Saigusa, T. Azumi, M. Sumitani, K. Yoshihara, *J. Chem. Phys.* **1980**, *72*, 1713-1715.

[134] H. Yersin, *Triplet Emitters for OLED Applications. Mechanisms of Exciton Trapping and Control of Emission Properties* in *Transition Metal and Rare Earth Compounds: Excited States, Transitions, Interactions III*, Springer, Berlin, **2004**, 1-26.
[135] R. C. Evans, P. Douglas, C. J. Winscom, *Coord. Chem. Rev.* **2006**, *250*, 2093-2126.
[136] A. Hagfeldt, M. Grätzel, *Acc. Chem. Res.* **2000**, *33*, 269-277.
[137] A. M. Blanco-Rodríguez, M. Busby, C. Grădinaru, B. R. Crane, A. J. Di Bilio, P. Matousek, M. Towrie, B. S. Leigh, J. H. Richards, A. Vlček, H. B. Gray, *J. Am. Chem. Soc.* **2006**, *128*, 4365-4370.
[138] G. S. He, L. S. Tan, Q. Zheng, P. N. Prasad, *Chem. Rev.* **2008**, *108*, 1245-1330.
[139] S. Bonnet, J.-P. Collin, *Chem. Soc. Rev.* **2008**, *37*, 1207-1217.
[140] P.-T. Chou, Y. Chi, *Eur. J. Inorg. Chem.* **2006**, *2006*, 3319-3332.
[141] N. Robertson, *Angew. Chem. Int. Ed.* **2006**, *45*, 2338-2345.
[142] S. Chakraborty, T. J. Wadas, H. Hester, R. Schmehl, R. Eisenberg, *Inorg. Chem.* **2005**, *44*, 6865-6878.
[143] C. Kaes, A. Katz, M. W. Hosseini, *Chem. Rev.* **2000**, *100*, 3553-3590.
[144] D. J. Stufkens, A. Vlček Jr, *Coord. Chem. Rev.* **1998**, *177*, 127-179.
[145] L. De Cola, P. Belser, *Coord. Chem. Rev.* **1998**, *177*, 301-346.
[146] S. I. Gorelsky, E. S. Dodsworth, A. B. P. Lever, A. A. Vlcek, *Coord. Chem. Rev.* **1998**, *174*, 469-494.
[147] H. J. Bolink, F. De Angelis, E. Baranoff, C. Klein, S. Fantacci, E. Coronado, M. Sessolo, K. Kalyanasundaram, M. Gratzel, M. K. Nazeeruddin, *Chem. Commun.* **2009**, 4672-4674.
[148] Y. You, S. Y. Park, *Dalton Trans.* **2009**, 1267-1282.
[149] C. F. Chang, Y. M. Cheng, Y. Chi, Y. C. Chiu, C. C. Lin, G. H. Lee, P. T. Chou, C. C. Chen, C. H. Chang, C. C. Wu, *Angew. Chem. Int. Ed. Engl.* **2008**, *47*, 4542-4545.
[150] L. Flamigni, A. Barbieri, C. Sabatini, B. Ventura, F. Barigelletti, *Photochemistry and Photophysics of Coordination Compounds: Iridium* in *Photochemistry and Photophysics of Coordination Compounds II*, Eds. V. Balzani, S. Campagna, Springer, Berlin, **2007**, 143-203.
[151] R. Ragni, E. A. Plummer, K. Brunner, J. W. Hofstraat, F. Babudri, G. M. Farinola, F. Naso, L. De Cola, *J. Mater. Chem.* **2006**, *16*, 1161-1170.
[152] M. S. Lowry, S. Bernhard, *Chem. Eur. J.* **2006**, *12*, 7970-7977.
[153] P. G. Bomben, K. C. D. Robson, B. D. Koivisto, C. P. Berlinguette, *Coord. Chem. Rev.* **2012**, *256*, 1438-1450.
[154] F. P. S. Campagna, F. Nastasi, G. Bergamini, V. Balzani, *Top. Curr. Chem.* **2007**, *280*, 117-214.
[155] D. N. Kozhevnikov, V. N. Kozhevnikov, M. Z. Shafikov, A. M. Prokhorov, D. W. Bruce, J. A. Gareth Williams, *Inorg. Chem.* **2011**, *50*, 3804-3815.
[156] D. Ramlot, M. Rebarz, L. Volker, M. Ovaere, D. Beljonne, W. Dehaen, L. Van Meervelt, C. Moucheron, A. Kirsch-De Mesmaeker, *Eur. J. Inorg. Chem.* **2013**, *2013*, 2031-2040.
[157] M. Chergui, *Dalton Trans.* **2012**, *41*, 13022-13029.
[158] H. Yersin, *Transition Metal and Rare Earth Compounds III, Vol. 241*, Springer, Berlin, **2004**, 1, 1-26.
[159] R. A. Kirgan, B. P. Sullivan, D. P. Rillema, *Photochemistry and Photophysics of Coordination Compounds: Rhenium*, Eds. V. Balzani, S. Campagna, Springer, Berlin, **2007**, 45-100.
[160] M. T. Indelli, C. Chiorboli, F. Scandola, *Photochemistry and Photophysics of Coordination Compounds: Rhodium*, Eds. V. Balzani, S. Campagna, Springer, Berlin, **2007**, 215-255.
[161] J. J. Wilson, S. J. Lippard, *Inorg. Chim. Acta* **2012**, *389*, 77-84.

[162] V. Prusakova, C. E. McCusker, F. N. Castellano, *Inorg. Chem.* **2012**, *51*, 8589-8598.
[163] G. J. Zhao, F. Yu, M. X. Zhang, B. H. Northrop, H. Yang, K. L. Han, P. J. Stang, *J. Phys. Chem. A* **2011**, *115*, 6390-6393.
[164] B. Zhang, Y. Li, W. Sun, *Eur. J. Inorg. Chem.* **2011**, *2011*, 4964-4969.
[165] C. Cornioley-Deuschel, A. Von Zelewsky, *Inorg. Chem.* **1987**, *26*, 3354-3358.
[166] C. B. Blanton, Z. Murtaza, R. J. Shaver, D. P. Rillema, *Inorg. Chem.* **1992**, *31*, 3230-3235.
[167] S. R. Stoyanov, J. M. Villegas, D. P. Rillema, *Inorg. Chem.* **2003**, *42*, 7852-7860.
[168] G. Y. Zheng, D. P. Rillema, J. DePriest, C. Woods, *Inorg. Chem.* **1998**, *37*, 3588-3592.
[169] J. DePriest, G. Y. Zheng, N. Goswami, D. M. Eichhorn, C. Woods, D. P. Rillema, *Inorg. Chem.* **2000**, *39*, 1955-1963.
[170] G. Y. Zheng, D. P. Rillema, *Inorg. Chem.* **1998**, *37*, 1392-1397.
[171] G. Y. Zheng, D. P. Rillema, J. H. Reibenspies, *Inorg. Chem.* **1999**, *38*, 794-797.
[172] S. J. Strickler, R. A. Berg, *J. Chem. Phys.* **1962**, *37*, 814-822.
[173] C. Würth, M. Grabolle, J. Pauli, M. Spieles, U. Resch-Genger, *Nat. Protocols* **2013**, *8*, 1535-1550.
[174] E. Oliveros, S. H. Bossmann, S. Nonell, C. Marti, G. Heit, G. Troscher, A. Neuner, C. Martinez, A. M. Braun, *New J. Chem.* **1999**, *23*, 85-93.
[175] M. Zhu, C. Yang, *Chem. Soc. Rev.* **2013**, *42*, 4963-4976.
[176] Z. Yadong, W. Jianxun, *J. Fluorine Chem.* **1990**, *47*, 533-535.
[177] L. A. Paquette, A. M. Doherty, C. M. Rayner, *J. Am. Chem. Soc.* **1992**, *114*, 3910-3926.
[178] C. Dai, Z. Yuan, J. C. Collings, T. M. Fasina, R. L. Thomas, K. P. Roscoe, L. M. Stimson, D. S. Yufit, A. S. Batsanov, J. A. K. Howard, T. B. Marder, *CrystEngComm* **2004**, *6*, 184-188.

# Copyright

| | |
|---|---|
| Figure 13<br>Figure 76<br>Figure 83 | Reprinted (adapted) with permission from A. Steffen, K. Costuas, A. Boucekkine, M. H. Thibault, A. Beeby, A. S. Batsanov, A. Charaf-Eddin, D. Jacquemin, J. F. Halet, T. B. Marder, *Inorg. Chem.* **2014**, *53*, 7055-7069. Copyright 2017 American Chemical Society. |
| Figure 78 | Reprinted (adapted) with permission from A. Steffen, M. G. Tay, A. S. Batsanov, J. A. K. Howard, A. Beeby, K. Q. Vuong, X.-Z. Sun, M. W. George, T. B. Marder, *Angew. Chem.* **2010**, *122*, 2399-2403. Copyright 2017 Wiley and Sons. |

Declaration

I hereby declare, that in the thesis with the title "Seeing the Light: Synthesis of Luminescent Rhodacyclopentadienes and Investigations of their Optical Properties and Catalytic Activity" for figures taken from journals the copyright of the publisher or author was secured. Figures taken from the internet are marked with the corresponding link.

Würzburg, _____ _____

Signature

Erklärung

Hiermit erkläre ich, dass ich in meiner Doktorarbeit mit dem Titel „Seeing the Light: Synthesis of Luminescent Rhodacyclopentadienes and Investigations of their Optical Properties and Catalytic Activity" bei Abbildungen aus Journalen das Copyright von den Verlagen bzw. vom Autor eingeholt habe. Bei Abbildungen aus dem Internet habe ich den entsprechenden Link angegeben.

Würzburg, den _____ _____

Unterschrift

## Acknowledgement

First of all, thanks so much to you Todd, for trusting in that I am smart enough to do a Ph. D., right from the start. Thanks for all the patience, support, discussions, help and time you offered to me. I think I really developed throughout the years and I enjoyed being a member of the "Marder Family" a lot! Thanks to you and your awesome wife Anne, that you are who you are.
Big thanks also goes to Dr Andreas Steffen. Thanks for answering all the questions about photophysics throughout the years and for always giving me new and exciting input.
I also want to thank the whole group for the good time, the support and help and funny working days, parties and widening of my cultural horizon. Special thanks goes to the "Rhodacycle-subgroup", Caro, Flo K., Martin H., Hashem, Daniel, Qing, Jan, Tim, Sarah, Bob, Marie-Luise and Kei, for helping me with problems and giving me inspiration and starting material. ☺ At this point, thanks also to the office 407. Many times, you made my day. Time passes by so fast, when you are having fun and I do not want to miss a second of it (even the sometimes-questionable background music, feat. DJ Cordula). Thanks also for the great time with my favourite grumpy teddy bear Flo in lab 403 and all the help and support from Caro to keep me from going crazy with getting my stuff clean!
Big thank you to Martin E., Benni, Markus and Steffi for introducing me to our equipment and helping me to solve problems, no matter how busy you were.
Thanks also to my internship students, bachelor and master students Peter Demirel, Natalia Wolf, Benjamin Kiendl, Sarah McKnight, Niklas Noll and Florian Kerner for all the results and persistence. Sarah, you are amazing and I am happy to have been your supervisor!
I also want to appreciate the energy and time Charlotte, Sabine and Christoph spent on feeding the "Rhodacycle Group" with inexhaustible amounts of starting material, thanks for that! Thanks, also Andreas L., Martin H., Alexandra and Daniel for giving a chance to every single of my more or less beautiful crystals and delighting me with new and surprising structures.
Also thank you, Christoph and Dr Stephan Wagner for measuring numerous high-resolution mass spectra for me.
Many thanks also go to the NMR-service, Dr Rüdiger Berterman and Marie-Luise Schäfer, thank you for recording hundreds of NMR spectra and special measurements for me.
A big thank you to the ladies of the elemental analysis, Lieselotte Michels and Sabine Timmroth, for patiently weighing tons of tiny amounts of substance and preparing so many elemental analyses for me. I also want to thank Mrs Wunderling who cares for keeping the representability of our institute every day.

Acknowledgement

Thanks to our secretaries Patricia Schmidt, Bianca Putz, Stefanie Ziegler and especially Ellen Klaus and Conny Walter for handling all the administrative tasks, always being helpful to solve any problem and especially for the nice little chats that always make me smile.

Thanks to our glassblower Berthold Fertig, it was always nice visiting you and thanks for repairing all my NMR tubes. At this point, also many thanks to the whole workshop crew (Alois Ruf, Wolfgang Obert, Manfred Reinhardt and Michael Ramold), Alfred Schertzer and the technical service to solve all technical problems, any time.

Thanks to my buddies from the weakly "Thursday-canteen-crew", Pietschi, Sarah, Lisa, Christoph, Fede, Fabian and Michael and also to Julia Gmeiner. It was always fun and I enjoyed having you by my side during the studies. Actually, I am happy to at least have some of you still there. At this point, also thanks to Dominik "The Batchman" Gehrig, you always explained the world to me and I am lucky to call you one of my best friends.

Girls, girls, girls! Caro, Juli, Steffi, Julia, Ulli, no matter what we do, I love having you by my side and I hope it will last until and even beyond the time we're spread all over Germany, or the world.

Pietschi, thanks for always being there! The best things happen unexpectedly and I am happy to have found a soulmate here! Proverb Great minds think alike! <3

Special thanks also to my ladies from home: Kathy, Anna, Vicky, Nora, Miri, Milli (meine Herde), thanks for always supporting me in every future dream I had and for being by my side for at least half of my life now! Stick together, friends forever!

Thanks also to my "Gnodstadt-girls-connection", Fulli, Britta, Linda, Ellen and Betty, who always give an ear to me. You are great and I am lucky to call you my friends!

Mom and Dad, thanks for being there for me from the first second of my life and never questioning any decision I made. Thanks for all the support you gave and give to me! You are the best parents I could imagine and I love you!

Big thanks also to Margit und Günter for all your support and accepting me as a member of your family. I am looking forward to the next step in my life, being your "neighbour".

Christoph, thanks for everything and the warmth you give to me. I love that you understand me without saying any word and I cannot imagine having anyone but you as my companion. I love you.

## Affidavit

I hereby confirm that the thesis entitled “Seeing the Light: Synthesis of Luminescent Rhodacyclopentadienes and Investigations of their Optical Properties and Catalytic Activity” is the result of my own work. I did not receive any help or support from commercial consultants. All sources and / or materials applied are listed and specified in the thesis.

Furthermore, I confirm, that this thesis has not yet been submitted as part of another examination process, neither in identical nor in similar form.

Würzburg, _____ _____

Signature

## Eidesstattliche Erklärung

Hiermit erkläre ich an Eides statt, dass ich die Dissertation mit dem Titel „Seeing the Light: Synthesis of Luminescent Rhodacyclopentadienes and Investigations of their Optical Properties and Catalytic Activity“ selbständig angefertigt und keine anderen als die von mir angegebenen Quellen und Hilfsmittel benutzt habe.

Ich erkläre außerdem, dass diese Dissertation weder in gleicher oder in anderer Form bereits in einem anderen Prüfungsverfahren vorgelegen hat. Ich habe früher außer den mit dem Zulassungsgesuch urkundlich vorgelegten Graden keine weiteren akademischen Grade erworben oder zu erwerben versucht.

Würzburg, den _____ _____

Unterschrift